MAGNETO-VISCOUS EFFECTS IN COMBUSTION PLASMA

by

D.E. Fussey, M.A.

A Ph.D. Thesis submitted to the University of Warwick.

CONTAINS PULLOUTS

DAMAGED TEXT IN ORIGINAL

ABSTRACT

This thesis presents a theoretical and experimental study of magneto-viscous effects in laminar fluid flows.

The fully developed M.H.D. flow past a semi-infinite plate (semi-infinite perpendicular to flow) in an unbounded fluid, with a magnetic field perpendicular to the plate, is analysed by a simple similarity method to demonstrate the characteristic transverse wakes which are produced in such situations. The analysis shows that the wakes emanate from the edge of the plate along the direction of the applied magnetic field - a more complete analysis is, however, given by Hasimoto (1960).

The flow past plates is investigated in the more complex situation, when the flow is bounded by rectangular ducts. A computerised numerical study of ordinary hydrodynamic and M.H.D. flows (at moderate Hartmann Number) explores the effects of (a) inserting plates into rectangular ducts, (b) of imposing pressure gradients, and (c) of moving sections of the duct walls or the inserted plates. In each case, the fully developed flow (2-D variation across the duct cross-section) is presented.

The experimental investigation employs a combustion plasma as a working fluid. Magneto-viscous interactions are produced by inserting refractory plates into a refractory-lined duct. The experiments include internal (pitot) measurements of velocity distributions for both ordinary hydrodynamic flow and M.H.D. flow. Two configurations of the inserted plate are adopted; firstly, a plate long in the flow direction, but only half duct height, and, secondly, a plate which extends across the full width of the duct, but which is 'semi-infinite' in the flow direction. For both configurations in the M.H.D. case, the applied magnetic field is perpendicular to the plate.

In the M.H.D. flows, the first plate configuration produces transverse wakes, similar in form to those found theoretically. In the second configuration where the developing boundary layer is investigated, the Hartmann effect is demonstrated.

A water-cooled pitot-static probe, and an R.F. conductivity probe, which were developed for these experiments, are described.

The theoretical solutions which relate to uniform property flows do not show close agreement with the experimental results, and it is suggested that non-uniformity of electrical conductivity in the combustion plasma is the main cause for incompatibility. However, the same trends can be seen.

The magnitude of the interactions produced in this small scale experiment suggest that highly significant magneto-viscous effects could be produced in combustion M.H.D. generators, which operate at much higher values of the Hartmann Number.

CONTENTS

APPENDIX

LIST OF FIGURES

LIST OF PLATES

NOMENCLATURE

$\underline{A}$ Matrix of coefficients for finite difference equation.

a Sonic velocity.

$\underline{b}$ Vector in matrix equation.

$\underline{B}$ Magnetic Flux Density Vector.

B_{x_0} Applied (constant) Magnetic Flux Density in x -direction.

$C, C_1 \to C_4$ Constants.

d Typical length scale - duct $\frac{1}{2}$ width.

d_1, d_2 Duct $\frac{1}{2}$ widths in x and y directions.

d_p Diameter of Probe.

$\underline{E}$ Electric Field Vector.

h Velocity Head ($= \frac{1}{2}\rho v^2$), x-spacing of finite difference mesh, Planck's constant.

h_c Convective Heat Transfer Coefficient.

H Hartmann Number ($= Bd\sqrt{\frac{\sigma}{\eta}}$)

$\underline{j}$ Current Density Vector

J Total current flow.

k Modulus of complex elliptic function, y-spacing of finite difference mesh.

K, K_1, K_2 Constants.

m, m_1, m_2 Variables used in section 4.3.

M Mach Number (v/a)

N Interaction Parameter ($= \frac{\sigma B^2 d}{\rho v}$)

N_H Hall Parameter ($\omega\tau$)

p Pressure.

$p_{\pm} = \frac{\partial \phi_{\pm}}{\partial x}$ (used in section 3.1).

q_r Radiative Heat Flux Density.

R Reynolds Number ($= \frac{vd}{\nu}$).

S	Shape factor for rectangular duct ($= h/k$)
T	Characteristic time, temperature.
u / v	(real) / (imaginary) coordinates of complex plane.
$\underline{v}$	Velocity
$\bar{v}$	Mean Velocity
V_0	Velocity of moving wall or plate.
W_0	S.T.P. Velocity
x,y,z	Right-handed set of Cartesian Coordinates.
z	Complex coordinate.
α	Thermal Diffusivity.
Δ,δ	Overall Difference, width of boundary layer.
ε	Emissivity.
ϵ	Permittivity.
ξ	Similarity Variable.
η	Kinetic Viscosity.
λ	Diffusivity of Magnetic Field = $(\frac{1}{\mu\sigma})$, wavelength of light.
μ	Permeability of free space.
ν	kinematic viscosity
ρ	density
σ	electrical conductivity.
τ	Collision Time.
$\phi_\pm$	Combined variable defined in Section 2.
ϕ	Real part of complex function.
$\underline{\phi}$	Vector of ϕ.
ψ	Imaginary part of complex function.
χ	Similarity variable.
ω	Cyclotron frequency; frequency of R.F. signal.

ACKNOWLEDGEMENTS

I should like to thank all those who, in many ways, have contributed to this project.

In particular, I thank Professor J.A. Shercliff who first introduced me to this subject and who has guided the project throughout. Also my thanks are due to Dr. C.J.N. Alty, Dr. D.T. Swift-Hook and Dr. G.J. Womack, for their advice and encouragement.

Mr. M.K. Bevir gave valuable assistance which enabled me to carry out the work described in section 4.3.4.

Mr. B.E. Cunio and Mrs. H.B. Winch of the C.E.G.B. Computing Department gave me most helpful advice and assistance during the development and execution of the computational work described in Chapter 4. I am particularly grateful to Mr. Cunio for instructing me in the use of 'Fortran'.

Mr. G.F. Trim and Mr. G.E. Minett both assisted me during the experimental programme and Mr. J.C. Pulford made a substantial contribution to the development of the pitot-static probe.

I should like to thank Mrs. Irene Buxey, who willingly undertook the typing of this thesis.

The C.E.G.B. were most generous in providing the facilities for this research and in supporting me with a salary during the period in which I did the work. I should particularly like to thank Mr. H.R. Johnson, Director, and Mr. H.F.J. Hadrill, Assistant Director, Marchwood Engineering Laboratories, for their co-operation and support.

Finally, I should like to thank my wife for her patience when she was being neglected in favour of M.H.D.

1. INTRODUCTION

1.1. The Conception of the Project

The work described in this thesis was carried out at the Marchwood Engineering Laboratories of the Central Electricity Generating Board (C.E.G.B.) while I was registered as a full-time non-resident student of the University of Warwick. At the time when the work was initiated, the Marchwood Laboratories were engaged in a large scale investigation of the feasibility of open-cycle Magnetohydrodynamic (M.H.D.) Power Generation. The conception of this project was inspired by the need to provide a better fundamental understanding of some basic fluid-mechanic aspects of M.H.D. flows in open-cycle generators, which employed high temperature, seeded gases as the working fluid. In fact, very little investigation of magneto-viscous effects in combustion plasmas had been done anywhere. Also, there was a need to develop instrumentation for detailed investigations of the internal behaviour of such generators.

There is a considerable fund of knowledge in the field of M.H.D. flows using electrically conducting liquids such as mercury, and the School of Engineering Science at Warwick University, who were actively engaged in advanced studies of such flows, inspired the fundamental approach to these studies. The Marchwood Laboratories were able to provide the complementary background of practical expertise in the technology of high temperature gas flows.

1.2. Open-Cycle M.H.D. Generation - Background Discussion

A few comments on the background of the C.E.G.B.'s open-cycle M.H.D. Generation research programme, which influenced many practical aspects of this project, will give a useful introduction to the work. (Heywood and Womack (1969) give a full account of the research programme

carried out by the C.E.G.B. together with the National Coal Board, and the British Manufacturers of Power Station Plant).

The M.H.D Generator was conceived as a 'topping' unit to be used in open cycle mode, together with a Rankine-cycle steam plant. The M.H.D. Generator would be fired by a combustion chamber, using heavy fuel-oil or coal, and pre-heated air (exit temperature 2700°C). The exhaust gases leaving the generator at about 2000°C would pass directly into a radiant boiler and thence through a chain of heat exchangers comprising a high temperature air heater, steam superheater and reheater, low temperature air heater and economiser, before rejection to atmosphere.

Several successful experiments had been completed by the C.E.G.B. (e.g. Bugden et al(1964))using a small oxygen/kerosene fired duct of ~ 2 MW thermal input and these led to a pilot-plant of 25 MW electrical output to be built at Marchwood. Unfortunately, the project was cancelled for economic reasons before this experiment had been completed.

The use of oxygen in the 25 MW experiment would have eliminated the need for the complications of introducing air heaters to provide the high temperatures required for satisfactory electrical conductivity. There was to be no waste-heat utilisation in steam generation plant, and for experimental purposes, the exhaust from the M.H.D. duct was to be merely quenched and wasted. The main purpose of the experiments was to prove the stability of large-scale direct generation by M.H.D., to investigate various designs of duct, to produce duct walls and electrodes which had satisfactory lifetime and to optimise the gas-dynamic and electrodynamic design of the ducts for the generation process.

Experiments were to be limited to overall measurements of generated voltages, bulk gas conductivity and bulk fluid-mechanic properties - no internal duct measurements were to be attempted.

1.3. M.H.D. Effects in Duct Flows

A problem which had not been investigated was the effect of applying a transverse magnetic field on the detailed fluid flow patterns within combustion plasma flows. The experimental work on mercury flows, and also a vast amount of theoretical work, suggested that substantial interactions could be produced, which may dominate the flow in some circumstances. These interactions include:-

(a) the suppression of fluid-mechanic turbulence,

(b) the flattening of velocity profiles (i.e. suppression of vorticity by transverse field) and the related creation of wall boundary layers,

(c) the production of transverse "wakes" in mid-stream which follow the lines of the imposed magnetic field from discontinuities at the boundary.

Investigations of effects (b) and (c) are described in this thesis.

1.4. Layout of Thesis

The thesis comprises two self-contained exercises; a theoretical study of a particular class of M.H.D. flow problems which involve transverse wakes, and an experimental study of the same type of problem, together with some other flow configurations.

In Chapter 2, the governing equations and basic properties of ordinary hydrodynamic and magnetohydrodynamic flows, which are useful in this study, are developed. Some methods which have been used previously for solving M.H.D. flow problems are also described. In Chapters 3 and 4, the use of two particular methods to provide original solutions of M.H.D. duct flows and flows past plates (under the action of a transverse

magnetic field) are described. The similarity solutions described in Chapter 3 give an immediate understanding of the qualitative nature of the transverse wakes, although the solution is limited to rather simple physical conditions which could not be achieved in practice. Chapter 4 describes a much more detailed study of the flows which occur in physically realistic geometrical arrangements, although this study is limited to fully-developed flows of fluid with uniform properties and scalar conductivity. The results of Chapter 4 were obtained using a computer, which enabled particularly lengthy calculations to be completed. The results of the computer study were compared with previous analytical solutions for some simple cases and the study was then extended to provide solutions to configurations which had not previously been tackled.

In Chapter 5, the basis for the experimental programme is discussed, and previous relevant experimental work is described. The overall design philosophy of the experiment is then developed.

A description of the design and construction of the experimental apparatus and instrumentation is given in Chapter 6, and in Chapter 7, the experimental results are presented. The results include some measurements of gas temperature and electrical conductivity, and a large number of measurements of velocity profiles in the experimental M.H.D. duct, which demonstrate the existence of magneto-viscous interactions in the flow in the case of transverse magnetic fields with inserted plates in the flow.

Chapter 8 presents a discussion of some aspects of the experimental results and a comparison between the theoretical and experimental results. Some indications of the qualitative effect of

non-uniformity of electrical conductivity on M.H.D. flows are given.

Finally in Chapter 9, overall conclusions are presented, and in Chapter 10, suggestions for future work are enumerated.

The Appendix contains a more detailed description of the computer program developed for Chapter 4 and the calibration of some of the items of experimental apparatus.

The order of presentation of work follows closely the chronological order in which it was carried out, although some of the preliminary experiments and the rig construction were carried out concurrently with the computer study. A review of previous relevant work is included in Chapters 2 and 4 (theoretical work) and Chapter 5 (experimental work).

The units which are used in this study do not correspond to the latest S.I. Standard, but follow, in general, the practice which was accepted within the Engineering Departments of the C.E.G.B. at the time when the project was started, i.e. the old British system of Units (with temperatures in degrees Centigrade).

2. M.H.D. DUCT FLOWS AND FLOWS PAST PLATES WITH A TRANSVERSE MAGNETIC FIELD

2.1. Ordinary Hydrodynamic Flows.(Laminar)

2.1.1 Formulation of Flow Equations

Since the solutions to some ordinary hydrodynamic (O.H.D.) flows will be considered later, and their properties will be compared with M.H.D. flows, this section briefly formulates the equations governing O.H.D. flows and discusses some of their relevant properties.

Consider a viscous fluid with uniform properties, which is incompressible; then the continuity equation and the equation of motion may be written as

$$div\ \underline{v} = 0 \qquad \ldots.2.1.1.$$

$$\rho \frac{D\underline{v}}{Dt} + \nabla p = \eta \nabla^2 \underline{v} \qquad \ldots.2.1.2.$$

In the steady state, equation 2.1.2 reduces to

$$\rho(\underline{v}.\nabla)\underline{v} + \nabla p = \eta \nabla^2 \underline{v} \qquad \ldots.2.1.3.$$

If the flow is further limited to rectilinear flow, i.e. $\underline{v} = v_z$ only, with no variation in the flow direction, except $\frac{\partial p}{\partial z}$ (which is independent of x and y),

then, since $\rho v_z \frac{\partial v_z}{\partial z} = 0$

$$\frac{\partial p}{\partial z} = \eta \nabla^2 v_z \qquad \ldots.2.1.4.$$

Such flows can occur as fully developed, steady state, pressure driven duct flows (e.g. the classical Poiseuille Pipe flow). They also occur in certain flows in ducts, when the flow occurs without pressure gradients (i.e. with $\frac{\partial p}{\partial z} = 0$), but with part of the bounding surface or an immersed object moving, (for these cases, the exciting wall or object must be infinite in the z -direction). For the latter case, the solution to the

flow situation is simply $\nabla^2 v_z = 0$ ....2.1.5.

Usually, flows will be considered which have a 2-D variation perpendicular to the flow direction and thus

$$\nabla^2 = \frac{\partial^2}{\partial x^2} + \frac{\partial^2}{\partial y^2} \quad \text{....2.1.6.}$$

(Couette flow and Poiseuille flow are examples of flows with one dimensional variation).

2.1.2 Discussion

If un-bounded flows are considered, e.g. the flow excited by moving a semi-infinite flat plate along its length in an un-bounded fluid, then a developing boundary layer is established on the plate which increases in thickness from the tip of the plate. This flow never reaches a fully developed situation, since the only force which is able to balance the viscous force in this layer is the inertia force, and the thickness of the layer tends to infinity at large distances from the tip. (This is the classical Blasius Flow situation which has a similarity solution in terms of $\zeta = \frac{1}{2}\sqrt{\frac{V_0}{\nu x}}$, where V_0 is the velocity of the plate and x is distance from tip of plate). Equations 2.1.4. and 2.1.5. can therefore only be applied to bounded flows.

2.2 Magneto-Hydrodynamic Flows. (Laminar, 2-D, fully developed)

2.2.1 Formulation of Flow Equations

The ordinary hydrodynamic equations formulated in section 2.1 can be extended to treat magneto-hydrodynamic flows by combining them with the steady state form of Maxwell's equations and Ohm's Law. The equation of motion is also modified by the addition of the magnetic body force $\underline{j} \times \underline{B}$.

Thus for the steady state, for uniform fluid properties and for scalar conductivity,

$$\text{curl } \underline{E} = 0 \qquad \ldots.2.2.1.$$

$$\text{curl } \underline{B} = \mu \underline{j} \qquad \ldots.2.2.2.$$

$$\text{div } \underline{B} = 0 \qquad \ldots.2.2.3.$$

and $$\underline{j} = \sigma(\underline{E} + \underline{v} \times \underline{B}) \qquad \ldots.2.2.4.$$

Also:- $$\text{div } \underline{v} = 0 \qquad \ldots.2.2.5.$$

and $$\rho(\underline{v}.\nabla)\underline{v} + \nabla p = \eta \nabla^2 \underline{v} + \underline{j} \times \underline{B} \qquad \ldots.2.2.6.$$

Taking the curl of 2.2.2. gives,

$$\text{curl } \underline{j} \left[= \sigma \, \text{curl}(\underline{v} \times \underline{B}) \right] = \frac{1}{\mu} \text{curl curl } \underline{B}.$$

and using vector identities gives,

$$\lambda \nabla^2 \underline{B} + (\underline{B}.\nabla)\underline{v} = (\underline{v}.\nabla)\underline{B}. \qquad \ldots.2.2.7.$$

$$\left(\lambda = \frac{1}{\mu\sigma} \right).$$

Combining equation 2.2.2. with 2.2.6. gives,

$$\eta \nabla^2 \underline{v} + \frac{1}{\mu}(\text{curl } \underline{B}) \times \underline{B} = \rho(\underline{v}.\nabla)\underline{v} + \nabla p$$

or $$\eta \nabla^2 \underline{v} + \frac{1}{\mu}(\underline{B}.\nabla)\underline{B} = \rho(\underline{v}.\nabla)\underline{v} + \nabla p^* \qquad \ldots.2.2.8.$$

where $p^* = p + \frac{|B|^2}{2\mu}$

If the flows are restricted again to (2-D) fully developed rectilinear flows then the z-component of equation 2.2.8 becomes:

$$\eta \left[\frac{\partial^2 v_z}{\partial x^2} + \frac{\partial^2 v_z}{\partial y^2} \right] + \frac{B_{xo}}{\mu} \frac{\partial B_z}{\partial x} = \frac{\partial p^*}{\partial z} = \frac{\partial p}{\partial z} \qquad \ldots.2.2.9$$

(only p varies in the flow direction and $\frac{\partial p}{\partial z}$ must be constant - this can be verified by taking $\partial/\partial z$ of equation 2.2.8).

The z-component of equation 2.2.7 gives

$$\lambda \left[\frac{\partial^2 B_z}{\partial x^2} + \frac{\partial^2 B_z}{\partial y^2} \right] + B_{xo} \frac{\partial v_z}{\partial x} = 0 \qquad \ldots.2.2.10.$$

For these rectilinear flows it is assumed that $B_x = B_{xo}$, an applied (external) magnetic field, and that B_y is zero. ($j_z = 0$ also, since $v_y = 0$).

B_z, the induced magnetic field, will be very much smaller than the applied magnetic field and $(B.\nabla) \approx B_{xo} \frac{\partial}{\partial x}$, since $\frac{\partial}{\partial z} = 0$ and $B_y = 0$.

Thus to solve 2-D, fully developed rectilinear M.H.D. flows equations 2.2.9 and 2.2.10 must be solved simultaneously. Shercliff (1953) adopted the technique of adding and subtracting these two equations to give (taking (2.2.9) $\pm \frac{1}{\mu\sqrt{\sigma\eta}}$ × (2.2.10)).

$$\left[\frac{\partial^2\phi_\pm}{\partial x^2} + \frac{\partial^2\phi_\pm}{\partial y^2}\right] \pm B_{xo}\sqrt{\frac{\sigma}{\eta}}\frac{\partial\phi_\pm}{\partial x} = \frac{1}{\eta}\frac{\partial\phi}{\partial x} \qquad \text{....2.2.11.}$$

where, $\phi_\pm = v_z \pm \frac{B_z}{\mu\sqrt{\sigma\eta}}$

and the $\pm$ signs are taken in order.

An alternative approach is to combine the equations to give a fourth order equation - Braginskii (1960).

For dynamically driven flows it is convenient to normalise in terms of a fixed velocity V_o, which may be the velocity of a moving wall or plate.

i.e. $v' = \frac{v_z}{V_o}$

and $B' = \frac{B_z}{V_o\mu\sqrt{\sigma\eta}}$

(N.B. in the case of pressure driven flows, it is automatically assumed that $V_o = 1$.)

Equation 2.2.11 can also be normalised with respect to the spatial variables when

$$x' = \frac{x}{d} \quad , \quad y' = \frac{y}{d} \quad ,$$

where 'd' is a reference length. (Typically, the half width of a rectangular duct in the x-direction).

Thus equation 2.2.11 finally becomes:-

$$\left[\nabla'^2 \pm H\frac{\partial}{\partial x'}\right]\phi'_{\pm} = \frac{\partial p'}{\partial z} \qquad \text{....2.2.12.}$$

where $H = Bd\sqrt{\frac{\sigma}{\eta}}$ = Hartmann Number based on the chosen reference length.

$\frac{\partial p'}{\partial z} = \frac{d^2}{\eta}\cdot\frac{\partial p}{\partial z}$ = Normalised Pressure Gradient.

and ∇'^2 is interpreted as $\left(\frac{\partial^2}{\partial x'^2} + \frac{\partial^2}{\partial y'^2}\right)$ & $\phi'_{\pm} = v' \pm B'$.

2.2.2. Discussion

In contrast to ordinary hydrodynamic flows, it is possible to have fully developed M.H.D. flows in un-bounded regions. Although the inertia terms in the fluid equation of motion tend to zero, there can be balance between the viscous force and the magnetic body force at every point in the field. (The superposition of a uniform pressure gradient merely introduces the equivalent of an additional uniform current distribution). For the case of the semi-infinite plate (non-conducting) dragged through an infinite fluid, with an imposed magnetic field normal to the plate, the boundary layer develops for a distance referred to as the interaction length and then reaches a steady state thickness.

The interaction length is $\frac{\rho v}{\sigma B_{x_0}^2}$, and the interaction parameter, $N = \frac{\sigma B_{x_0}^2 d}{\rho v}$, measures the relative size of the magnetic forces $(\sigma v B^2)$ and the inertia forces $\left(\frac{\rho v^2}{d}\right)$ where d is a characteristic length.

The thickness of the fully developed layer is characterised by the Hartmann distance, $\delta_{HART} = \frac{1}{B_{x_0}}\sqrt{\frac{\eta}{\sigma}}$

The Hartmann Number, H, $\left(= d/\delta_{HART}\right)$ measures the relative size of the magnetic forces $(\sigma v B^2)$ and viscous forces $\left(\frac{\eta v}{d^2}\right)$ where d is a characteristic length perpendicular to the plate.

Hartmann's classical experiments (Hartmann and Lazarus (1937)) on 1-D duct flows first demonstrated the existence of the wall boundary layer with characteristic width δ_{HART} which contained current flow and encompassed the region of changing velocity. Subsequently Shercliff (1953) investigated theoretically the 2-D problem of rectangular duct flow, showing the existence of this same layer on walls perpendicular to the magnetic field, but a different layer on the walls which were parallel to the magnetic field. This layer has characteristic thickness $d/H^{\frac{1}{2}}$. (See Shercliff (1956) for experimental investigation of 2-D M.H.D. circular duct flow).

Hasimoto (1960) investigated theoretically the dynamically excited flow produced by dragging a semi-infinite plate along its own length for cases when the plate was non-conducting and perfectly conducting. (The plate was semi-infinite in the direction perpendicular to the flow direction and the magnetic field was perpendicular to the plate. He established the existence of transverse wakes (mid-stream boundary layers), which contained current flow and encompassed the region of changing velocity between two regions of more uniform flow. Since this flow configuration is particularly relevant to the work described later in Chapters 3, 4, and 7, and since it is not so well discussed elsewhere, it is useful to describe his work a little further. (In section 3 the mechanism producing the effect is described in more detail).

Hasimoto considered firstly the motion of an infinitely long cylinder parallel to its length in a conducting fluid and established that when a uniform magnetic field was imposed, perpendicular to the axis of the cylinder, two current wakes were formed which emanated from the cylinder and were parallel to the applied magnetic field. These wakes are the residual stationary current flow which results from the passage of

transverse Alfvén waves along the field lines. With infinite Hartmann Number, the solution demonstrates that, for a perfectly conducting cylinder, the fluid enveloped by the two magnetic field lines which are tangential to the cylinder is frozen to the cylinder and the whole moves as a solid body. For an insulating cylinder, the same volume of fluid moves with half the velocity of the cylinder. The case of the moving cylinder has been dealt with in more detail by Waechter (1966) who produced solutions for velocity and current distributions for large finite Hartmann Number. The phenomenon of "freezing" the fluid to a perfectly conducting plate has been demonstrated experimentally by Alpher et al (1960), in an open channel mercury flow experiment. A copper disc was inserted into the base of the channel and a magnetic field was applied (perpendicular to the disc). The cylindrical column of mercury above the disc behaved as a solid body and the flow past the disturbance closely resembled the hydrodynamic flow past a solid cylinder.

Figure 2.2.1 shows the details of Hasimoto's solution for a semi-infinite plate. The parabolic nature of the wakes which was established in the theory is clearly seen in the plots of constant velocity lines and constant induced magnetic field lines.

In the conducting plate case, the current flowing in the transverse wake all flows up the plate. If the plate had a finite length, it would have entered the plate from a similar wake at the other end. There is no current flow in the core region adjacent to the plate for a semi-infinite plate, but for a finite length plate at finite Hartmann Number, the two wakes would merge to form a finite volume of "frozen" fluid.

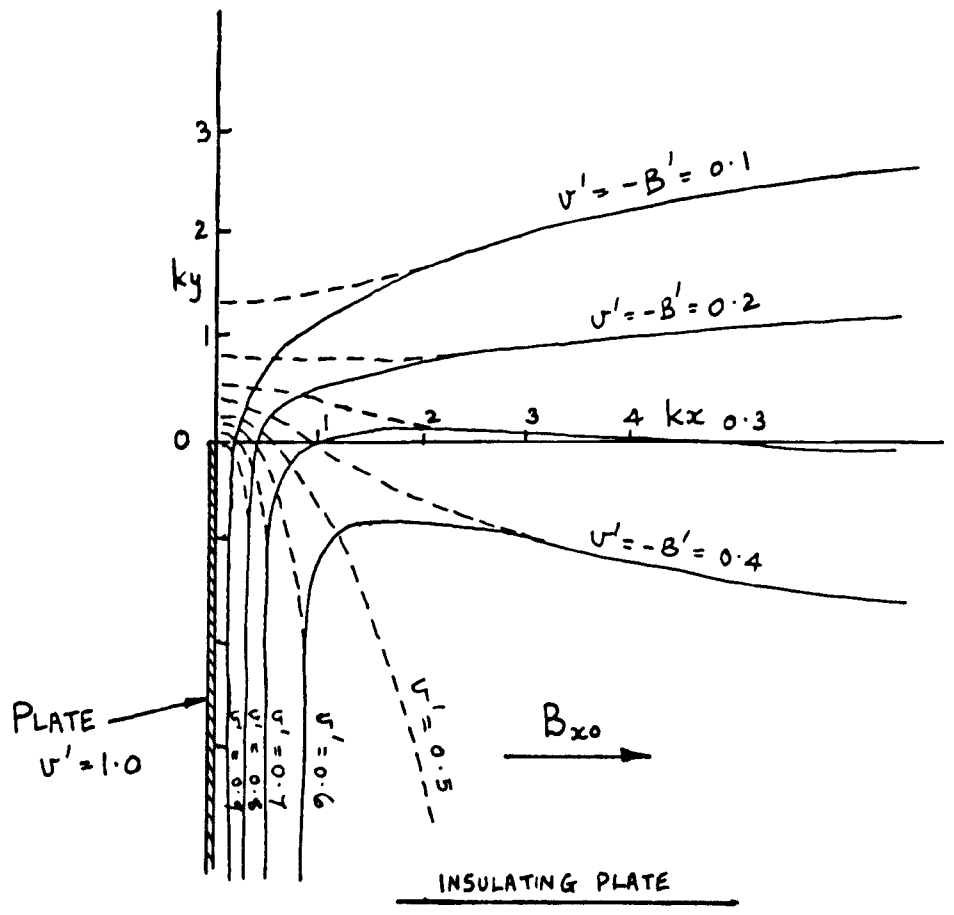

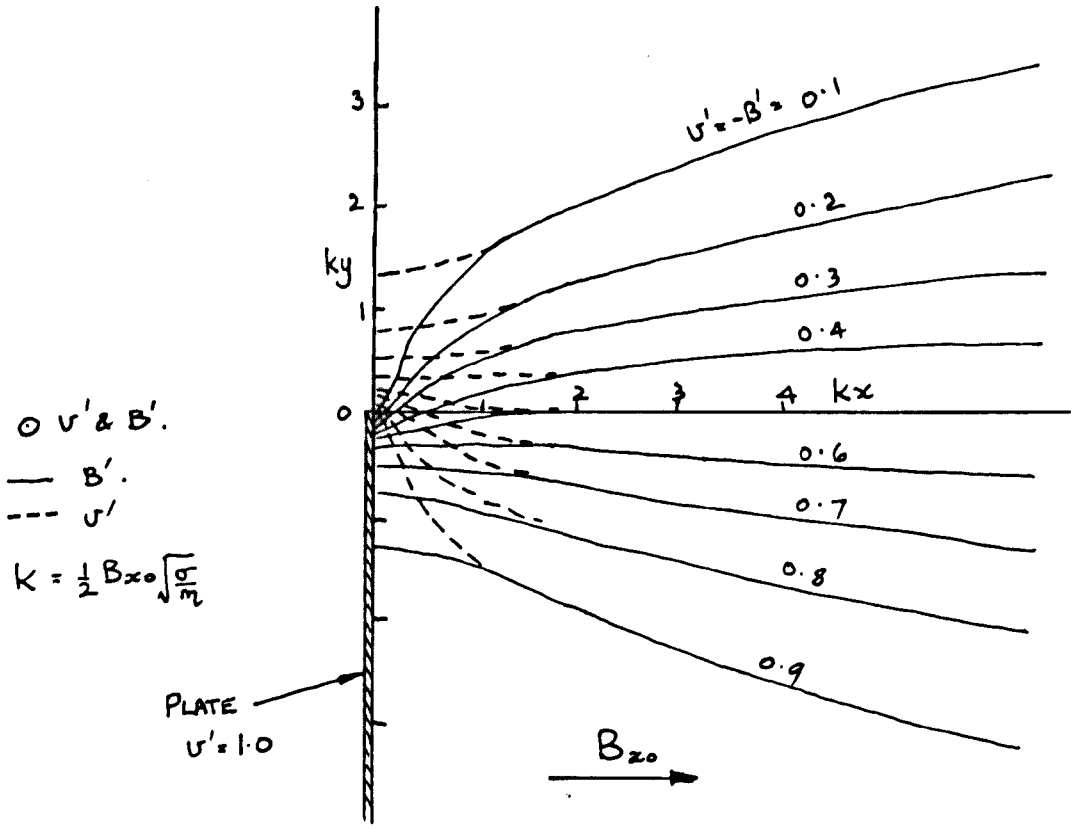

HASIMOTO'S SOLUTION FOR SEMI-INFINITE PLATES MOVING IN INFINITE FLUIDS - FIGURE 2.2.1.

In the insulating plate case, there obviously can no longer be current flow in the plate and in fact there is current continuity between the current flowing in the Hartmann layer on the plate and in the transverse wake. Similar conclusions may be drawn for an insulating plate of finite length.

Hunt and Ludford (1968) have recently analysed the M.H.D. flow past obstacles in constant area channels, and their analysis includes 3-D considerations. They show that Hasimoto's solution is only valid for thin plates which are long in the flow direction and for $N \gg 1$. (N based on duct width). For thick bodies in ducts, a solution of very different character was found.

Todd (1967) in studying the pressure driven M.H.D. flow in non-conducting annular channels also produced solutions which contained transverse wakes (similar to Hasimoto's cylinder solution) which emanated from the edge of the inner wall and followed the magnetic field lines. At high Hartmann Number, the solution demonstrated the existence of curved Hartmann type layers on both the inside and outside walls of the duct and diffuse current return paths through the core of the flow. In this case, the wake consists again of a region of abrupt change in velocity, but doesnot contain all the current flowing in the Hartmann layers (as in Hasimoto's configuration). The wake covers a region where the main core current streamlines are deflected in the direction of the imposed magnetic field. (This result can be compared with the results for pressure driven flows in rectangular ducts with thin plates - see section 4.4.) The diffuse core current flow divides into two to return along the two Hartmann layers. Todd (1968) also demonstrated that transverse wakes can

follow the field lines when they are curved.

Braginskii (1960), H.K. Moffatt (1964), and Hunt and Williams (1968) have also studied M.H.D. flows excited by current flows parallel to the magnetic field, in which layers of discontinuity, which followed the field lines, were produced at the edge of the region of current flow.

It can be seen that M.H.D. flows can exhibit many phenomena quite foreign to O.H.D. flows - including the mid-stream boundary layer. Some of these effects are investigated theoretically in more detail in Chapters 3 and 4, and experiments are described in Chapter 7, which demonstrate the existence of some of the effects in combustion plasma.

2.3. Some Methods for Solving M.H.D. Flow Situations

In this section some of the more important methods which are useful for solving M.H.D. flow situations are described, and the reasons for the selection of two of the methods for use later are outlined.

2.3.1. Exact Analytical Solutions

Some of the simpler configurations can be solved by exact analytical methods to produce solutions in terms of infinite series. (Typically, rectangular duct flow with insulating walls e.g. Shercliff (1953)). These solutions can often be simplified when the assumption $H \gg 1$ is applicable. Alternatively, Weiner-Hopf techniques have been used with the 4th order M.H.D. equation to produce exact solutions (e.g. Yakubenko (1963), Waechter (1968)).

2.3.2. Approximate Analytical Solutions

Hunt and co-authors have applied an approximate analytical technique to a great variety of more complicated situations (e.g. rectangular duct flow with conducting walls parallel to the magnetic field (Hunt and Stewartson (1966)), variable-area channel flow (Hunt and Leibovitch (1967)),

steady electrically driven flows (Hunt and Williams, (1968)). This technique, which is useful for $H \gg 1$, involves splitting the flow into regions, boundary layers and cores, in which plausible assumptions can be made corresponding to $H \to \infty$ - e.g. no viscous forces in core regions - which simplify the analysis. Solutions are then found for each region, which are made to match at the interfaces between regions.

W.C. Moffatt (1964) used the approach of integral momentum methods in the study of M.H.D. boundary layers. Although these methods are useful for studying overall properties such as skin friction and heat transfer, they do not give much detailed information about the flow.

2.3.3. Similarity Solutions

Similarity solutions have found extensive application in O.H.D. flow situations, e.g. developing boundary layers on plates, (see Blasius flow mentioned in section 2.1). In general, a similarity solution is of the form $v' = f(\zeta)$ only, where $\zeta = f(x,y)$. No M.H.D. analogy to the developing Blasius boundary layer flow is possible for reasons described in section 2.2., but similarity solutions are possible for the steady state transverse wakes which are peculiar to M.H.D. flows, (see Shercliff (1965)) and which display the parabolic nature of the Blasius flow.

In Chapter 3 this method is adopted for a study of the semi-infinite moving plate problem. Although the method is limited to $H \gg 1$, it has the advantage that it provides relatively simple solutions which illustrate many of the physical properties of the flow. It gives a good approximation to the wakes at some distance from the tip of the plate for the semi-infinite plate case, (i.e. when $\frac{\partial^2}{\partial y^2} \gg \frac{\partial^2}{\partial x^2}$).

2.3.4. Numerical Solutions

Numerical methods based on finite difference techniques have had extensive application in all types of field problems, including magnetic and electric field problems, temperature and stress distributions and many ordinary hydrodynamic flows. Applications in M.H.D. flows have been somewhat limited, one of the few examples is Dix (1962), who used the technique to solve the M.H.D. flow through a cascade of non-conducting plates (semi-infinite in the flow direction).

The advantage of the method is that any complicated geometrical situation may be modelled with a finite-difference mesh. The size of the region and the degree of detail which can be incorporated into the solution are only limited by the size of the computer which is available to solve the numerical equations. For high Hartmann Numbers, when large variations in velocity and induced magnetic field occur in narrow boundary layers, the method is not ideal, unless a variation in grid spacing is incorporated and this can limit the flexibility of the method. However, for reasons described in Chapter 5, it was not possible to attain high Hartmann Numbers in the experimental situation and so this was not a significant disadvantage.

The method is ideally suited to a comprehensive study of duct flows with and without inserted plates, with pressure gradients or with excitation by moving inserted plates or part of the duct walls, when the Hartmann Number is in the range 0 - 10. This study (presented in Chapter 4) extends the present knowledge of this class of M.H.D. flows and could not be made without recourse to numerical methods since other methods (2.3.1, 2.3.2 and 2.3.3), cannot solve these configurations at this range of Hartmann Number.

3. SIMILARITY SOLUTIONS TO SOME M.H.D. FLOW SITUATIONS

3.1. Simplification of Equations

It is possible to simplify the analysis of fully developed M.H.D. flows induced by a semi-infinite moving plate in an un-bounded electrically conducting fluid by adopting a boundary layer approach.

The general equations for the steady state are (see section 2.2.)

$$\eta\left[\frac{\partial^2 v_z}{\partial x^2} + \frac{\partial^2 v_z}{\partial y^2}\right] + \frac{B_{x_0}}{\mu}\frac{\partial B_z}{\partial x} = \frac{\partial p^*}{\partial z} \qquad \ldots.3.1.1.$$

and

$$\lambda\left[\frac{\partial^2 B_z}{\partial x^2} + \frac{\partial^2 B_z}{\partial y^2}\right] + B_{x_0}\frac{\partial v_z}{\partial x} = 0 \qquad \ldots.3.1.2.$$

which can be reduced to a simpler form in the case of $H \gg 1$ by the assumption that $\partial^2/\partial x^2 \ll \partial^2/\partial y^2$. This situation corresponds to that in which a boundary layer (not however at a solid boundary) extends in the x- direction (direction of applied field) and separates two core regions of fluid with a transition distance which is small compared with the typical length scale of the problem.

The equations 3.1.1. and 3.1.2. then become:-

$$\eta\frac{\partial^2 v_z}{\partial y^2} + \frac{B_{x_0}}{\mu}\cdot\frac{\partial B_z}{\partial x} = \frac{\partial p^*}{\partial z} \qquad \ldots.3.1.3.$$

and

$$\lambda\frac{\partial^2 B_z}{\partial y^2} + B_{x_0}\cdot\frac{\partial v_z}{\partial x} = 0 \qquad \ldots.3.1.4.$$

The known parabolic shape of the layers (see Hasimoto (1960)) suggest a solution of the equations using a similarity variable $\chi = y/x^{\frac{1}{2}}$. (This similarity solution was suggested by Shercliff (1965)). - see Figure 3.1.1.

Then $\frac{\partial \chi}{\partial x} = -\frac{1}{2}\, y/x^{3/2}$ & $\frac{\partial \chi}{\partial y} = 1/x^{\frac{1}{2}}$

Thus equations 3.1.3 and 3.1.4 become:-

$$\frac{\partial^2 v_z}{\partial \chi^2}\cdot\frac{1}{x} - \frac{B_{x_0}}{\mu\eta}\cdot\frac{\partial B_z}{\partial \chi}\cdot\frac{y}{2x^{3/2}} = \frac{1}{\eta}\frac{\partial p^*}{\partial z} \qquad \ldots.3.1.5.$$

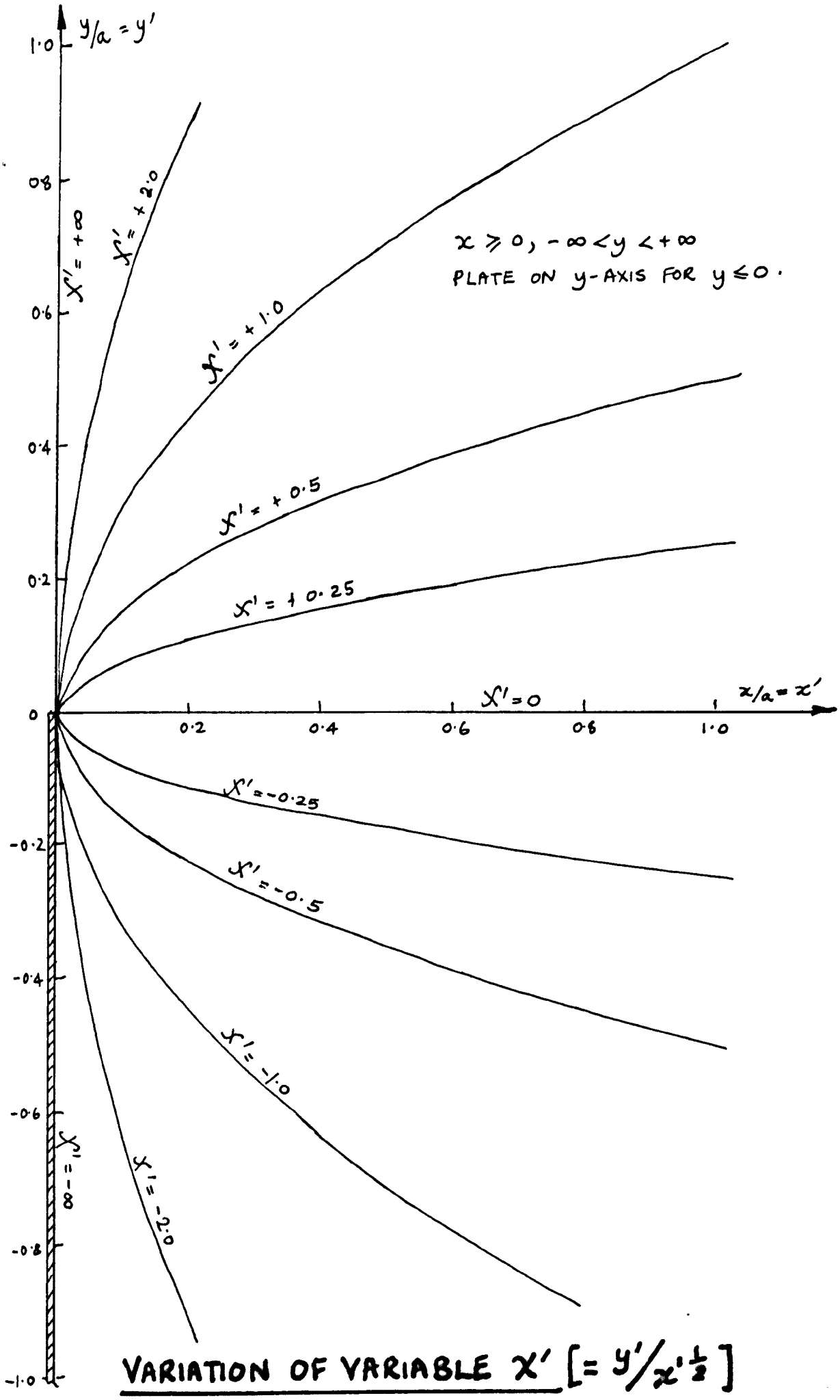

VARIATION OF VARIABLE $\chi' \left[= y'/x'^{\frac{1}{2}}\right]$ OVER SEMI-INFINITE SPACE. FIGURE 3.1.1.

and $$\frac{\partial^2 B_z}{\partial \chi^2} \cdot \frac{1}{\chi} - \frac{B_{x0}}{\lambda} \cdot \frac{\partial v_z}{\partial \chi} \cdot \frac{y}{2x^{3/2}} = 0 \qquad \ldots.3.1.6.$$

As before, B_z and v_z can be de-coupled by adding and subtracting these two equations. The solution for zero pressure gradient is then:-

$$\left[\frac{\partial^2}{\partial \chi^2} \mp \frac{H\chi}{2d} \frac{\partial}{\partial \chi} \right] \phi_\pm = 0 \qquad \ldots.3.1.7.$$

where $\phi_\pm = v_z \pm \frac{B_z}{\mu\sqrt{\rho\eta}}$ (as in section 2).

If this equation is normalised in terms of

$$v' = \frac{v_z}{V_0} \quad \& \quad B' = \frac{B_z}{\mu\sqrt{\rho\eta}\, V_0},$$

and $\chi' = \chi / d^{1/2}$, where d is a characteristic length scale and V_0 is the velocity of the plate, then

$$\left[\frac{\partial^2}{\partial \chi'^2} \mp \frac{H\chi'}{2} \frac{\partial}{\partial \chi'} \right] \phi'_\pm = 0 \qquad \ldots.3.1.8.$$

Equation 3.1.8. may be integrated directly by separating the variables,

thus: $$\frac{\partial^2 \phi'_\pm}{\partial \chi'^2} = \pm \frac{H\chi'}{2} \cdot \frac{\partial \phi'_\pm}{\partial \chi'}$$

or $$\frac{\partial p_\pm}{\partial \chi'} = \pm \frac{H\chi'}{2} \cdot p_\pm \quad \text{where} \quad p_\pm = \frac{\partial \phi'_\pm}{\partial \chi'}$$

$$\therefore \frac{dp_\pm}{p_\pm} = \pm \frac{H\chi' d\chi'}{2}$$

$$\therefore \ln p_\pm = \pm \frac{H\chi'^2}{4} + C_\pm \quad [\text{where } C_\pm \text{ are constants of integration}]$$

$$\therefore p_\pm = C_{1\pm} \exp\left(\pm \frac{H\chi'^2}{4} \right) \qquad \ldots.3.1.9.$$

$$\& \therefore \phi'_\pm = C_{1\pm} \int \exp\left(\pm \frac{H\chi'^2}{4} \right) d\chi + C_{2\pm} \qquad \ldots.3.1.10.$$

$\phi'_\pm$ (and thence v' and B') may be found as functions of χ'. ($C_{1\pm}$ and $C_{2\pm}$ being determined from boundary conditions).

The sets of boundary conditions to be considered are:-

(i) Semi-infinite perfectly conducting plate being dragged at velocity V_0 through conducting fluid experiencing no pressure gradient.

(ii) Semi-infinite insulating plate being dragged at velocity V_o through conducting fluid experiencing no pressure gradient.

3.2. Discussion of general properties of solution

From an examination of equation 3.1.9, it can be seen that

$$\phi_+ = C_{1+} \exp\left(\frac{H\chi'^2}{4}\right)$$

Therefore $\frac{\partial \phi'_+}{\partial \chi'}$ diverges rapidly as $|\chi|$ increases. This would be quite inconsistent with the required solution, since ϕ'_+ must converge for large χ. Thus the only possible solution for ϕ'_+ is that it should be constant i.e. $\phi_+ = C_{1+} = 0$ and therefore $v' + B'$ is constant across these layers.

Before the boundary conditions for equation 3.1.10 can be determined, however, a more detailed physical discussion is necessary. For this purpose cases (i) and (ii) will be considered in more detail.

Case (i) Perfectly conducting plate being dragged through a conducting fluid which is stationary at large distances from the plate.

From Ohm's Law, for a conductor with $\sigma \to \infty$, it follows that $(\underline{E} + \underline{v} \times \underline{B}) \to 0$ for finite $\underline{j}$. Therefore, in the perfectly conducting plate, $E_y \sim -V_o B_{xo}$. Since curl $\underline{E} = -\frac{\partial \underline{B}}{\partial t} = 0$ in the steady state, (also approximately true for constant applied magnetic field and small induced field) and because there can be no discontinuity in $\underline{E}$ across the boundary between the plate and the fluid, (i.e. $\frac{\partial E_y}{\partial x} = 0$, for $E_x = 0$) the electric field in the fluid adjacent to the plate (E_y) must be $\sim -V_o B_{xo}$. Immediately adjacent to the plate, the fluid must be moving with the velocity of the plate, and thus there can be no current flowing. (Since $j_y = \sigma_{fluid}(-V_o B_{xo} + V_o B_{xo})$). But a little further away from the plate, it can be assumed that the fluid is moving at velocity $v_z [\neq V_o]$

which may take any value between V_0 and zero. Then a current will flow in the fluid determined by $j_y = \sigma_{fluid}(-V_0 B_{x0} + v_z B_{x0})$ and will return through the plate. However, this current will produce a body force on the fluid equal to $j_y B_{x0}$ which will act in the opposite direction to $(v_z - V_0)$ and will reduce $|v_z - V_0|$ until no current flows and $v_z = V_0$. This process progresses in a wave-like form (Alfvén propagation - during the starting process) in the direction of x, with the current returning along the x-axis. The current return would form a current sheet for a perfectly conducting fluid, but for σ_{fluid} finite, Hasimoto (1960) has shown that the layers diffuse in a parabolic fashion. So the existence of 3 zones in the flow can be postulated, see Figure 3.2.1 (a); zone A, of undisturbed fluid; zone C, of fluid which is dragged along by the plate; zone B, which is a transition zone from disturbed to undisturbed regions and also the region of current flow, in which $\frac{\partial^2}{\partial y^2} \gg \frac{\partial^2}{\partial x^2}$.

It has been found that the region B has a parabolic shape as mentioned above, and it is in this region that the solution in terms of the parameter χ is useful, although this solution is only valid for the case when the layer is thin in the y-direction. It can be shown that this corresponds to high values of the Hartmann Number H.

This simplified analysis takes no account of the complex flow near the tip of the plate (since it is assumed that $\partial^2/\partial y^2 \gg \partial^2/\partial x^2$ throughout) and the region where the return current actually passes into the conducting plate. Hasimoto's solution shows that the current passes into the plate within a distance $O\left(\frac{1}{H}\right)$ from the tip, and so in the limit $H \to \infty$, it can be considered that all the current flows in at the tip. For the purposes of this simple analysis, it is assumed that B_z is constant along the whole length of the plate; this is equivalent to the case of a perfectly conducting plate with a thin insulating layer over its surface which restricts current entry to the plate to the tip. (Exact boundary condition is; $\frac{\partial B'}{\partial n} = 0$).

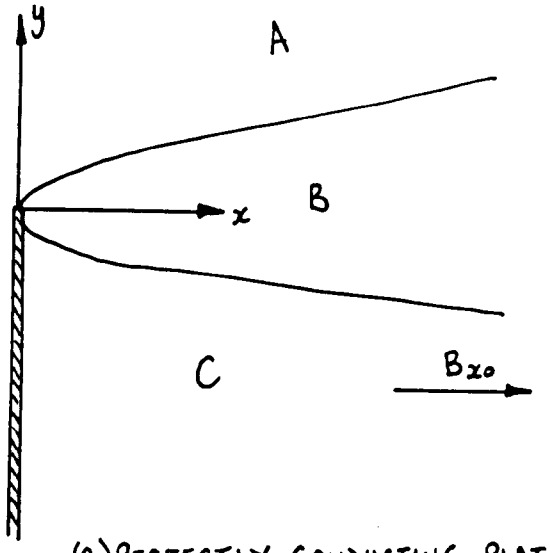

(a) PERFECTLY CONDUCTING PLATE

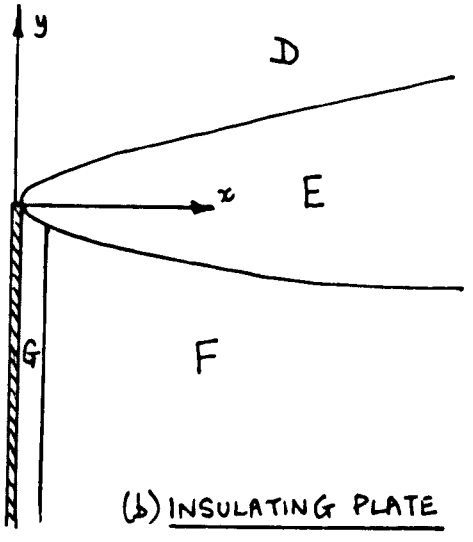

(b) INSULATING PLATE

REGIONS OF FLOW PRODUCED BY MOVING A SEMI-INFINITE PLATE IN AN INFINITE FLUID WITH A TRANSVERSE MAGNETIC FIELD - FIGURE 3.2.1.

Case (ii) Insulating plate being dragged through a conducting fluid - stationary at large distances from the plate. (Figure 3.2.1 (b)

In this case, it would be expected that a Hartmann type boundary layer would exist on the plate, so it would be advisable to split the flow into 4 zones, where G is a Hartmann Boundary layer, in which the fluid velocity changes abruptly from the velocity of the plate to an intermediate velocity V_1 (yet to be determined) in the region F. Zone D is the undisturbed zone and zone E consists of a transition region similar to zone B of 3(a) in which $\partial^2/\partial y^2 \gg \partial^2/\partial x^2$. The Hartmann layer can be analysed quite simply by putting the restriction $\partial^2/\partial x^2 \gg \partial^2/\partial y^2$ into the equations developed earlier.

Thus: $$\eta \frac{\partial^2 v_z}{\partial x^2} + \frac{B_{xo}}{\mu} \frac{\partial B_z}{\partial x} = \frac{\partial p^*}{\partial z}$$

and $$\lambda \frac{\partial^2 B_z}{\partial x^2} + B_{xo} \frac{\partial v_z}{\partial x} = 0$$

or with no pressure gradient, more simply

$$\eta \frac{\partial^2 v_z}{\partial x^2} + \frac{B_{xo}}{\mu} \frac{\partial B_z}{\partial x} = 0 \qquad \ldots.3.2.1.$$

and $$\lambda \frac{\partial^2 B_z}{\partial x^2} + B_{xo} \frac{\partial v_z}{\partial x} = 0 \qquad \ldots.3.2.2.$$

which can be solved by adding and subtracting as before to give

$$\left[\frac{\partial^2}{\partial x'^2} \pm H \frac{\partial}{\partial x'} \right] \phi'_{\pm} = 0 \qquad \ldots.3.2.3.$$

where $\phi'_{\pm} = v' \pm B'$

and $x' = \frac{x}{d}$

Thus $\frac{\partial p_{\pm}}{\partial x'} \pm H p_{\pm} = 0$ where $p_{\pm} = \frac{\partial \phi_{\pm}}{\partial x'}$

$$\therefore \frac{\partial p_-}{\partial x'} = + H p_-$$

or $p_- = C_{3-} \exp(H x)$ which would cause ϕ_- to diverge rapidly as x increases. Thus the only solution for ϕ_- is for it to be constant and thus $p_- = C_{3-} = 0$.

i.e. $v' - B'$ = constant across the Hartmann boundary layer (see Shercliff (1965)). This result may be used to find the mean velocity in region F. (v_1) and the induced field (B_1).

Since, on the plate; $v' = 1$, $B' = 0$

& in region D; $v' = 0$, $B' = 0$,

and since ϕ_+ = constant across E

and ϕ_- = constant across G ,

if $v_1' = \frac{v_1}{V_0}$ and $B_1' = \frac{B_1}{\mu\sqrt{\sigma\eta}\,V_0}$, then, $v_1' + B_1' = 0$ and $v_1' - B_1' = 1$,

and therefore $\underline{v_1' = \frac{1}{2} \;\&\; B_1' = -\frac{1}{2}}$

Thus there is a large region adjacent to the plate (zone F) where the fluid is moving at one half of the plate velocity and the region is bounded by a Hartmann boundary layer and a transverse boundary layer, whose current contents are equal. This solution was confirmed by Hunt and Ludford (1968) for the case of long elliptical plate.

3.2.1. Characteristic thicknesses of layers

The characteristic thicknesses of the various layers sketched in Figure 3.2.1 can be determined for $H \gg 1$. For the Hartmann layer,

$$\left[\frac{\partial^2}{\partial x^2} \pm \frac{H}{d} \frac{\partial}{\partial x} \right] \phi_\pm = 0$$

$\therefore \frac{\partial^2}{\partial x^2} \sim \frac{H}{d} \cdot \frac{\partial}{\partial x}$ across the layer, and so if the characteristic thickness of the layer is δ_{HART}

then $\frac{1}{\delta_{HART}^2} \sim \frac{H}{d} \cdot \frac{1}{\delta_{HART}}$ or $\underline{\delta_{HART} = O\left(\frac{d}{H}\right)}$.

For the transverse (Hasimoto) layers, however,

$$\left[\frac{\partial^2}{\partial y^2} \pm \frac{H}{d}\frac{\partial}{\partial x}\right]\phi_{\pm} = 0$$

$$\therefore \quad \frac{\partial^2}{\partial y^2} \sim \frac{H}{d}\frac{\partial}{\partial x}$$

$$\therefore \frac{1}{\delta^2_{HASIMOTO}} \sim \frac{H}{d}\cdot\frac{1}{x} \qquad \text{or} \quad \delta_{HASIMOTO} = O\left(\sqrt{\frac{dx}{H}}\right).$$

So for $H>1$, the Hartmann layer is thinner than the Hasimoto layer. This fact can be illustrated by an order of magnitude argument based on current flow:-

In the Hasimoto layer, current flows in the x and y directions and obeys $\mathrm{div}\, j = 0$, whereas in the Hartmann layer, $j = j_y$ only (see Figure 3.2.1.(b)) and $j_y B_{x_0} \sim \eta \frac{\partial^2 v_z}{\partial x^2}$.

For case (ii), Figure 3b, the total current in the Hartmann layer can be equated to that in the Hasimoto layer. In the Hasimoto layer, j is predominantly j_x and the j_y component (which produces the body force $j_y B_{x_0}$) is only the diffusing component of the current; so the body force $j_y B_{x_0}$ is weaker in this layer than in the Hartmann layer where j_y is the predominant current component. Consequently, $\eta \frac{\partial^2 v_z}{\partial y^2}$ is smaller in the Hasimoto layer than $\eta \frac{\partial^2 v_z}{\partial x^2}$ in the Hartmann layer, and thus the Hasimoto layer is broader than the Hartmann layer.

For Case (i) The total current in the plate can be found from $\mathrm{curl}\, \underline{B} = \mu j$; thus $J = \frac{1}{\mu}\Delta B$ where Δ signifies the difference from the centre line of the plate to the boundary.

Thus $J = \frac{1}{\mu}\cdot\mu\sqrt{\sigma\eta}\cdot V_0 = \sqrt{\sigma\eta}\, V_0$.

Thus the current density in the Hasimoto layer is $j_x \sim \frac{J}{\delta_{HASIMOTO}}$ per unit distance in the Z-direction, if $j_x \gg j_y$. But since we also have $\frac{j_x}{x} \sim \frac{j_y}{y}$ in this layer, ($\because \mathrm{div}\, j = 0$) $j_y \sim \frac{\sqrt{\sigma\eta}\, V_0}{x}$ and since $j_y B_{x_0} \sim \eta \frac{\partial^2 v_z}{\partial y^2}$ in the layer, $\delta_{HASIMOTO} = O\left(\sqrt{\frac{dx}{H}}\right)^x$ as before.

For Case (ii) The total current content of the Hartmann layer (no current flows in the plate in this case) is given by $J = \frac{1}{\mu}\Delta B$ where Δ signifies now the difference from the edge of the plate to zone F.

Thus $J = \frac{1}{\mu} \cdot \mu\sqrt{\sigma\eta}\,\frac{V_0}{2}$, and so j_y in the Hartmann layer is given by $j_y B_{x_0} \sim \eta \frac{\partial^2 v_z}{\partial x^2}$.

Thus $\sqrt{\sigma\eta}\,\frac{V_0}{2\delta} \sim \eta \frac{V_0}{2\delta^2} \cdot \frac{1}{B_{x_0}}$ i.e. $\underline{\delta_{HART} = O\left(\frac{d}{H}\right)}$

and since the total current content of the Hasimoto layer is equal also to $\sqrt{\sigma\eta} \cdot \frac{V_0}{2}$, again using $div\, j = 0$,

$$j_y \sim \frac{\sqrt{\sigma\eta}\,V_0}{2x} \quad , \qquad \text{and since } j_y B_{x_0} \sim \eta \frac{V_0}{2\delta^2} \, ,$$

$$\therefore \quad \underline{\delta_{HASIMOTO} = O\left(\sqrt{\frac{dx}{H}}\right)}$$

These physical arguments agree with the deductions made earlier from the form of the equations, as would be expected.

3.2.2. Boundary Conditions for determining constants in Equation 3.1.10.

(i) Perfectly Conducting plate

$\chi' \to +\infty$, $v' \to 0$, $B' \to 0$

$\chi' \to -\infty$, $v' \to 1$, $B' \to -1$ (since $v' + B'$ = const)

(ii) Insulating plate

$\chi' \to +\infty$, $v' \to 0$, $B' \to 0$

$\chi' \to -\infty$, $v' \to \frac{1}{2}$, $B' \to -\frac{1}{2}$ (since $v' + B'$ = const for Hasimoto layer)

on plate $(x \to 0)$ $v' \to 1$, $B' \to 0$ (since $v' - B'$ = const for Hartmann layer).

3.3. Solutions to flows with semi-infinite plates in an infinite fluid

Equation 3.1.10. can be rewritten in the form (for ϕ_-')

$$\phi_-' = C_{4-}\, \mathrm{erfc}\left(\frac{\sqrt{H}\chi'}{2}\right) + C_{2-} \qquad \ldots 3.3.1.$$

where $\mathrm{erfc}(z) = \frac{2}{\pi}\int_z^\infty e^{-t^2} dt$. - see Figure 3.3.1.

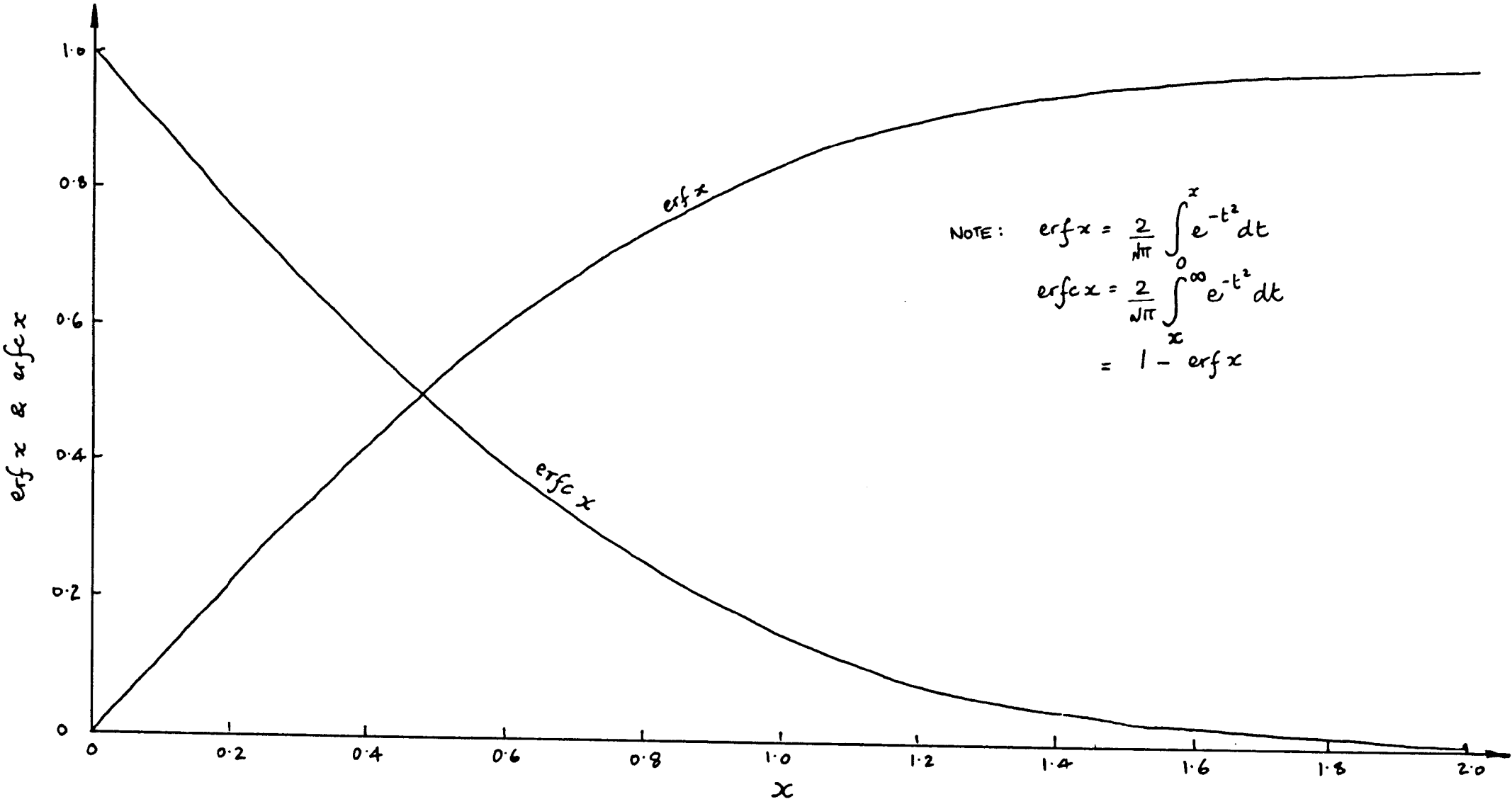

THE ERROR FUNCTION & THE COMPLEMENTARY ERROR FUNCTION

FIGURE 3.3.1

For Case (i) As $\chi' \to +\infty$, $\phi_\pm \to 0$ and $\operatorname{erfc}\chi'' \to 0$

(where $\chi'' = \frac{\sqrt{H}}{2}.\chi'$.) $\therefore C_{2-} = 0$

As $\chi' \to -\infty$, $\phi_- \to +2$ & $\operatorname{erfc}\chi'' \to +2$ $\therefore C_{4-} = +1$

But $\phi_+' = C_{1+}\int_{\chi''}^{\infty} \exp\left(+\frac{H}{4}\chi'^2\right)d\chi + C_{2+}$

so as $\chi' \to +\infty$, $\phi_+ \to 0$ & $\int_{\chi''}^{\infty} \exp\left(+\frac{H}{4}\chi'^2\right)d\chi \to 0$ $\therefore C_{2+} = 0$.

and as $\chi' \to -\infty$, $\phi_+ \to 0$ & " " " $\to \infty$. $\therefore C_{1+} = 0$

$$\therefore \underline{\phi_+' = 0} \quad \& \quad \underline{\phi_-' = \operatorname{erfc}\chi''} \qquad \text{....3.3.2.}$$

For Case (ii) As $\chi' \to +\infty$, again $\phi_\pm \to 0$ and $\operatorname{erfc}\chi'' \to 0$

$\therefore C_{2-} = 0$, as before.

As $\chi' \to -\infty$, $\phi_+ \to 0$, $\phi_- \to +1$ & $\operatorname{erfc}\chi'' \to +2$

$\therefore C_{4-} = \frac{1}{2}$.

As before $C_{2+} = 0$, & $C_{1+} = 0$

$$\therefore \underline{\phi_+' = 0} \quad \& \quad \underline{\phi_-' = \tfrac{1}{2}.\operatorname{erfc}\chi''} \qquad \text{....3.3.3.}$$

or, in terms of v' and B':—

Case (i) $v' = \frac{1}{2}\operatorname{erfc}\chi''$, and $B' = -\frac{1}{2}\operatorname{erfc}\chi''$.

Case (ii) $v' = \frac{1}{4}\operatorname{erfc}\chi''$, and $B' = -\frac{1}{4}\operatorname{erfc}\chi''$

Typical examples of these solutions are shown in Figure 3.3.2 in the form of isovels (lines of constant velocity). The axes are chosen to be Hx' and Hy', so that a solution for all H can be displayed.

This follows since, if $y^* = y'.H$ & $x^* = x'.H$, $\chi^* = \sqrt{H}.\chi'$ and solutions are all of the form $\phi = f(\sqrt{H}.\chi') = f(\chi^*)$. So this simple transformation produces a unique solution for all H in the case of a semi-infinite plate. This was also found by Hasimoto for his exact solutions, which are also shown on Figure 3.3.2, for comparison.

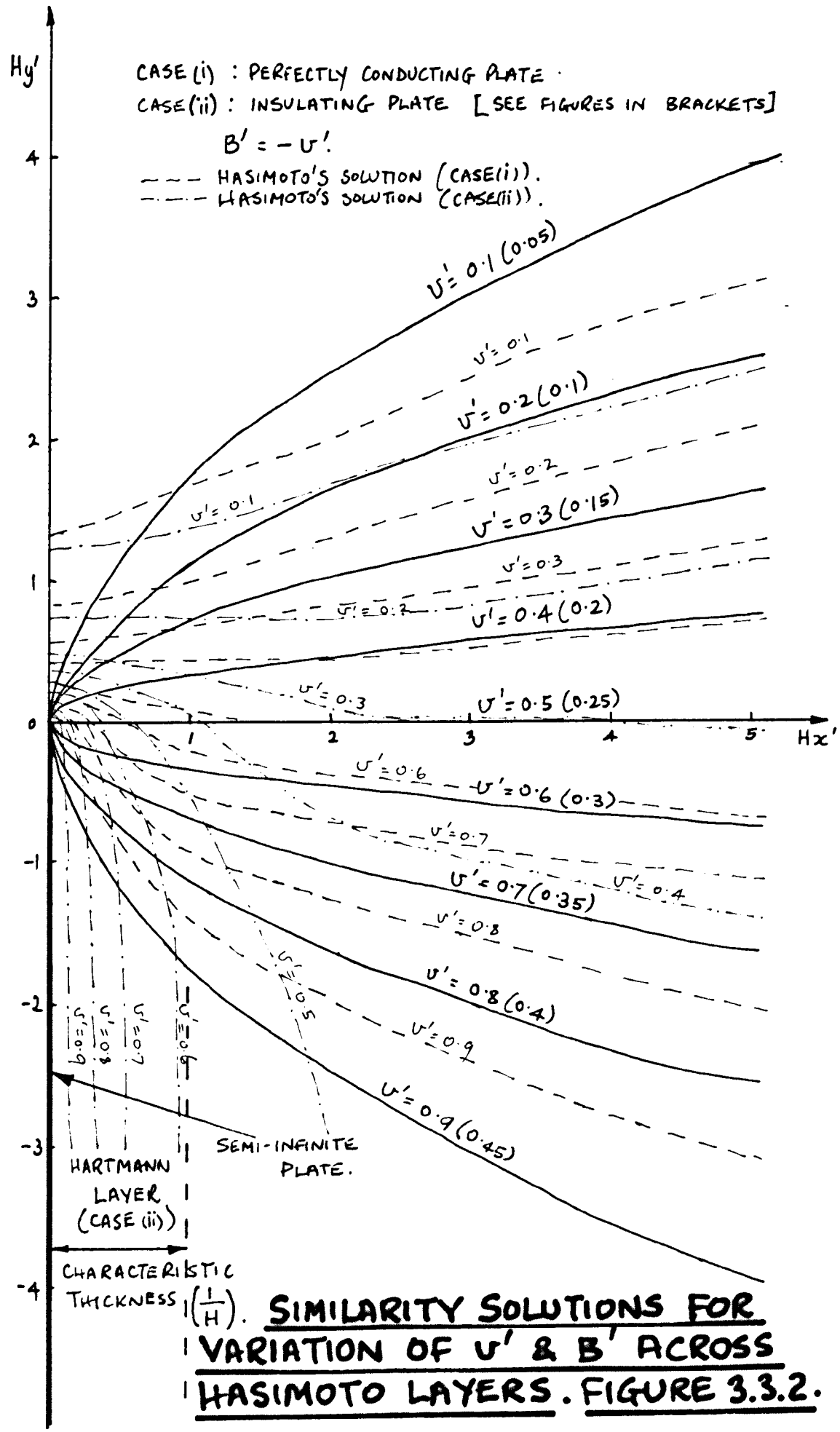

SIMILARITY SOLUTIONS FOR VARIATION OF U' & B' ACROSS HASIMOTO LAYERS. FIGURE 3.3.2.

3.3.1. Conclusions

The results displayed in Figure 3.3.1 give an indication of the qualitative behaviour of Hasimoto effects and demonstrate the usefulness of the boundary layer approach.

The diffusive character of the wakes is at once evident, and likewise the large area adjacent to the plates in which there is a major flow disturbance, although the solution is not valid near the tip of the plate, where $\partial^2/\partial y^2 \sim \partial^2/\partial x^2$. (cf. Hasimoto's exact solution).

However, for a complete study of the flow, for regions in which the boundary layer approach is not possible and for moderate Hartmann Number flow, either Hasimoto's approach must be used, or a numerical solution attempted. The latter has the advantage that it is more flexible and will allow the study of situations with finite dimensions of the plate and fluid.

4. NUMERICAL SOLUTION OF SOME M.H.D. FLOW SITUATIONS

4.1 Description of problem and necessity for numerical work

In order to make a theoretical investigation of M.H.D. flows in more complex configurations, e.g. flows past plates which are bounded by ducts, a numerical method must be adopted. Similarity solutions and asymptotic methods are usually only useful for high Hartmann Number situations and analytical solutions can only be found for the simplest configurations.

Numerical methods based on the finite-difference technique are useful for moderate Hartmann numbers. (e.g. within the range $0-10$). The size of the finite-difference mesh and the computer storage capacity will decide the maximum Hartmann Number.

To incorporate all the physical phenomena, which will be encountered in the experiments described later, into the numerical solution would be most difficult. The experiments involved the use of a fluid with non-uniform electrical conductivity (which is highly dependent on temperature) and with non-scalar electrical conductivity (Hall Effect). These two effects have been ignored in order to reduce the complexity of the numerical solution and so that the particular effects under examination, viz. magneto-viscous interactions, will be clearly visible in the solutions. The qualitative effects of non-uniform and non-scalar electrical conductivity and compressibility on the numerical solutions can be suggested by referring to the available information on these effects in simpler flow situations.

For example, Cramer (1965) and Kieffer (1965) studied the effect of spatially non-uniform electrical conductivity in M.H.D. Couette and Duct Flows. Heywood (1965) studied the temperature dependence of electrical conductivity in M.H.D. duct flows. Fay (1959) studied the effect of non-scalar conductivity on M.H.D. boundary layers. Sato (1961) and Tani (1962)

have studied the Hall effect in M.H.D. duct flows. Yen (1964) used a system of complex parameters to study Hall current flows in M.H.D. channel flows. Kerrebrock (1961) and Hale and Kerrebrock (1964) investigated the boundary layers on the electrodes and insulator walls of M.H.D. accelerators, making allowance for temperature dependent conductivity and in the latter case, non-scalar conductivity. Oliver and Mitchner (1967) studied various effects caused by non-uniformity in cases with non-scalar conductivity. Finally, Bleviss (1960) studied some effects of introducing compressibility into a simple M.H.D. configuration.

The numerical work which is described in this chapter provides solutions for steady state, fully developed, rectangular duct flows. The two dimensional variation of the flow parameters will be studied in the plane perpendicular to the flow direction. Ordinary viscous hydrodynamic solutions (O.H.D.) and magnetohydrodynamic solutions (M.H.D.) will be found for

(a) rectangular ducts with no obstacles

(b) rectangular ducts with thin plates

immersed in the flow. (The plates are long in the flow direction).

As before, only transverse magnetic fields will be considered.

In common with the approach in sections 2 and 3 the flow parameters U' and B' will be used in these numerical solutions.

Two classes of flow excitation will be examined,

(a) Excitation by moving a duct wall or an immersed plate.

(b) Pressure gradient excitation.

Only (b) is comparable with experiment, but (a) provides useful comparisons with other analytical solutions and shows many of the same general

characteristics as (b).

4.2. Computational Method (See Appendix A for fuller details of computer program).

The equation which has to be satisfied at every node on the finite-difference mesh is (from section 2.2 and equation 2.2.12)

$$\left[\nabla'^2 \pm H \frac{\partial}{\partial x'} \right] \phi'_{\pm} = \frac{\partial p'}{\partial z} \qquad \ldots.4.2.1$$

In order to solve this equation over any finite region, it must always be possible to define $\phi'_{\pm}$ or $\frac{\partial \phi'_{\pm}}{\partial n}$ at all points on the boundary of the region (This limitation also occurred in Chapter 3, when it restricted the use of the perfectly conducting plate boundary conditions, $v'=1$, $\frac{\partial B'}{\partial n}=0$).

Although it may seem more economical to cover only one quadrant of a rectangular duct with the finite-difference mesh (i.e. using two axes of symmetry - see Figure 4.1 (a)), the symmetric nature of the v' variable and the antisymmetric nature of B' would produce a boundary condition $\frac{\partial v'}{\partial n}=0$, $B'=0$ on the $x=0$ axis. Hence the finite-difference mesh must be used to cover the upper half of the rectangular duct (above the $y=0$ axis - see Figure 4.1 (b)).

However, the symmetry conditions about the $x=0$ axis can be used to reduce the amount of numerical work. Instead of solving equation 4.2.1 (which is really two equations) the following symmetry condition can be applied. (Shercliff 1953).

$$\phi'_{+}(x,y) = \phi'_{-}(-x,y) \qquad \ldots.4.2.2.$$

(where $\phi'_{\pm} = v' \pm B'$) as long as the boundary conditions also have symmetry about the $x=0$ axis. And then the problem is reduced to satisfying

$$\left[\nabla'^2 + H \frac{\partial}{\partial x} \right] \phi'_{+} = \frac{\partial p'}{\partial z} \qquad \ldots.4.2.3.$$

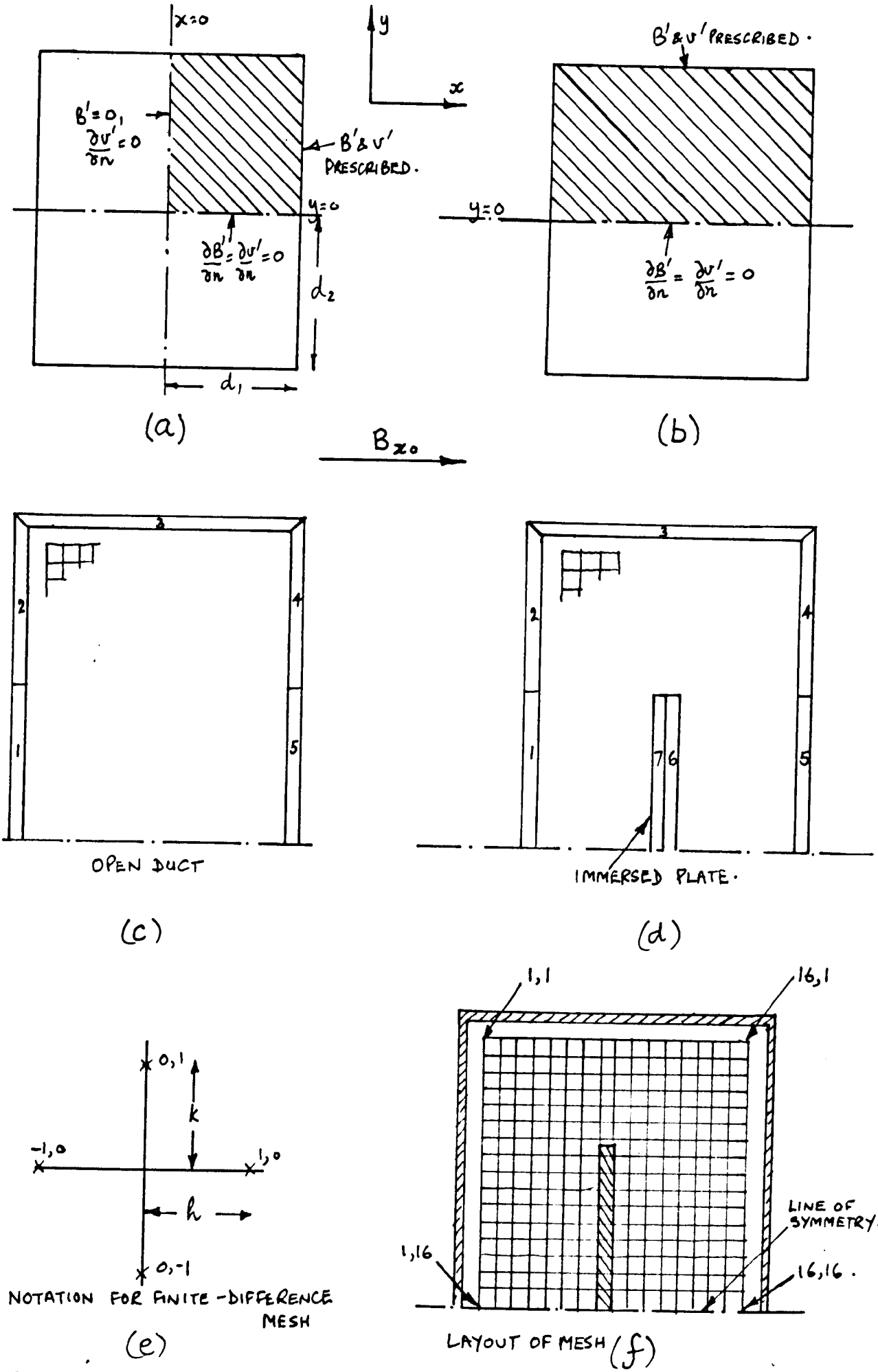

DETAILS OF FINITE-DIFFERENCE MESH.

FIGURE 4.1.1.

at each node on the mesh, and applying a suitable substitution to find ϕ'_- and hence v' and B'.

Equation (4.2.3) can be represented in finite difference form (with $\phi'_+ = \phi$) using the notation of Figure 4.1 (e):-

$$\frac{\phi_{1,0} - 2\phi_{0,0} + \phi_{-1,0}}{h^2/d^2} + \frac{\phi_{0,1} - 2\phi_{0,0} + \phi_{0,-1}}{k^2/d^2}$$

$$+ \frac{H}{2h/d}\left(\phi_{1,0} - \phi_{-1,0}\right) = \frac{\partial p'}{\partial z}. \qquad \ldots.4.2.4.$$

or if $H' = H\frac{l}{d}$, $\frac{\partial p''}{\partial z} = \frac{l^2}{d^2}\cdot\frac{\partial p'}{\partial z}$ & $S = \frac{k}{h}$,

then,

$$\phi_{1,0}\left(1 + \frac{H'}{2}\right) + \phi_{-1,0}\left(1 - \frac{H'}{2}\right) + \phi_{0,1}\cdot\frac{1}{S^2} + \phi_{0,-1}\cdot\frac{1}{S^2}$$

$$- 2\phi_{0,0}\left(1 + \frac{1}{S^2}\right) = \frac{\partial p''}{\partial z} \qquad \ldots.4.2.5.$$

Equation 4.2.5 defines the coefficients of the nodal values of ϕ for use in the numerical solution. The equation can be written for each nodal point on the mesh and then a matrix equation of the form

$$\underline{A}\cdot\underline{\phi} = \underline{b}. \qquad \ldots.4.2.6.$$

can be written; where $\underline{A}$ is the matrix of coefficients of the nodal values, $\underline{\phi}$ is the vector of nodal values, and $\underline{b}$ is the vector containing the pressure gradient term and the boundary conditions.

The matrix is actually of band form and the equation is suitable for solution using the C.E.G.B. Library program 'BAND'. (See Appendix A for further details). The size of the finite-difference mesh is determined by the core-storage capacity of the computer used; with the I.B.M. 360 system in the C.E.G.B. computing center, the program BAND limits the mesh to approximately 16 x 16 nodes. (An alternative program using tape and disk storage would permit larger meshes, but the execution time would be excessively long).

A 16 x 16 mesh is acceptable for Hartmann Numbers up to about 10 (based on the duct $\frac{1}{2}$ width), when the mesh size will be of the same order as the Hartmann boundary layer thickness.

As in section 3, the numerical solutions are limited to non-conducting walls. However, the program accommodates a large variety of spatial distributions of the boundary value of velocity. For the open rectangular duct (no obstacles in the flow), the boundary is divided into five regions as shown in Figure 4.1 (c) and with the immersed plate option, there are two extra regions on the plate. (Figure 4.1 (d)).

The solution to the flow situations is completely defined by specifying the parameters (a) Hartmann Number

(b) Pressure Gradient

(c) Shape Factor,

and the boundary conditions on all regions. (An initial specification is made to choose between the open duct and the immersed plate configurations).

An additional facility is incorporated into the program to replace the bottom line symmetry condition by the same boundary condition as the upper wall. This is useful for investigating the case of an immersed plate attached to the bottom wall, rather than suspended across the $y=0$ axis, which is more easily achieved in practice.

Flows which are excited by pressure gradients may be solved with or without non-zero velocities on the boundary regions, although because the equation is linear, solutions are additive.

The time taken to produce one solution on the computer is 0.25 min. Computer time can be saved if more than one set of boundary conditions and pressure gradient parameter values are required for one set of Hartmann

Number and Shape Factor. In these cases, the program arranges for one reduction of the matrix A to be used with the required number of right-hand side vectors b, corresponding to the different combinations of boundary conditions and/or pressure gradient.

4.3. Testing of Program; comparison with analytical solutions

4.3.1. Finite Difference Approximations

The error involved by taking only the pivotal values in the finite difference equations (4.2.5) was estimated using the finite difference correction terms. (See Goodwin (1960)). For the case of O.H.D. pressure driven flow down a rectangular duct (Figure 4.4.1), the error was estimated to be $\sim 0.1\%$ for points greater than two mesh spacings from a wall and $\sim 1\%$ for points adjacent to the wall. This accuracy is quite acceptable, although a somewhat larger error is produced in the case of M.H.D. flows which exhibit large changes in velocity gradient near the walls.

4.3.2. Comparison with Analytical Solution to Hydrodynamic Rectangular Duct Flow

The solution to viscous hydrodynamic flow in rectangular ducts presented by Langlois (1964), was used to check the equivalent numerical solution (displayed fully in Figure 4.4.1). Langlois transformed the degenerate (ordinary hydrodynamic) form of equation 4.2.1:-

$$\nabla'^2 v' = \frac{\partial p'}{\partial z} \qquad \ldots.4.3.1.$$

into a Laplace equation and produced an infinite series solution:-

$$v' = \frac{-1}{2d_1^2}\frac{\partial p'}{\partial z}\left[d_2^2 - y^2 + \frac{32 d_2^2}{\pi^3}\sum_{n=0}^{\infty}\frac{(-1)^{n+1}\cosh\left\{(2n+1)\frac{\pi x}{2d_2}\right\}\cdot\cos\left\{(2n+1)\frac{\pi y}{2d_2}\right\}}{(2n+1)^3\cosh\left\{(2n+1)\frac{\pi d_1}{2d_2}\right\}}\right] \qquad \ldots.4.3.2.$$

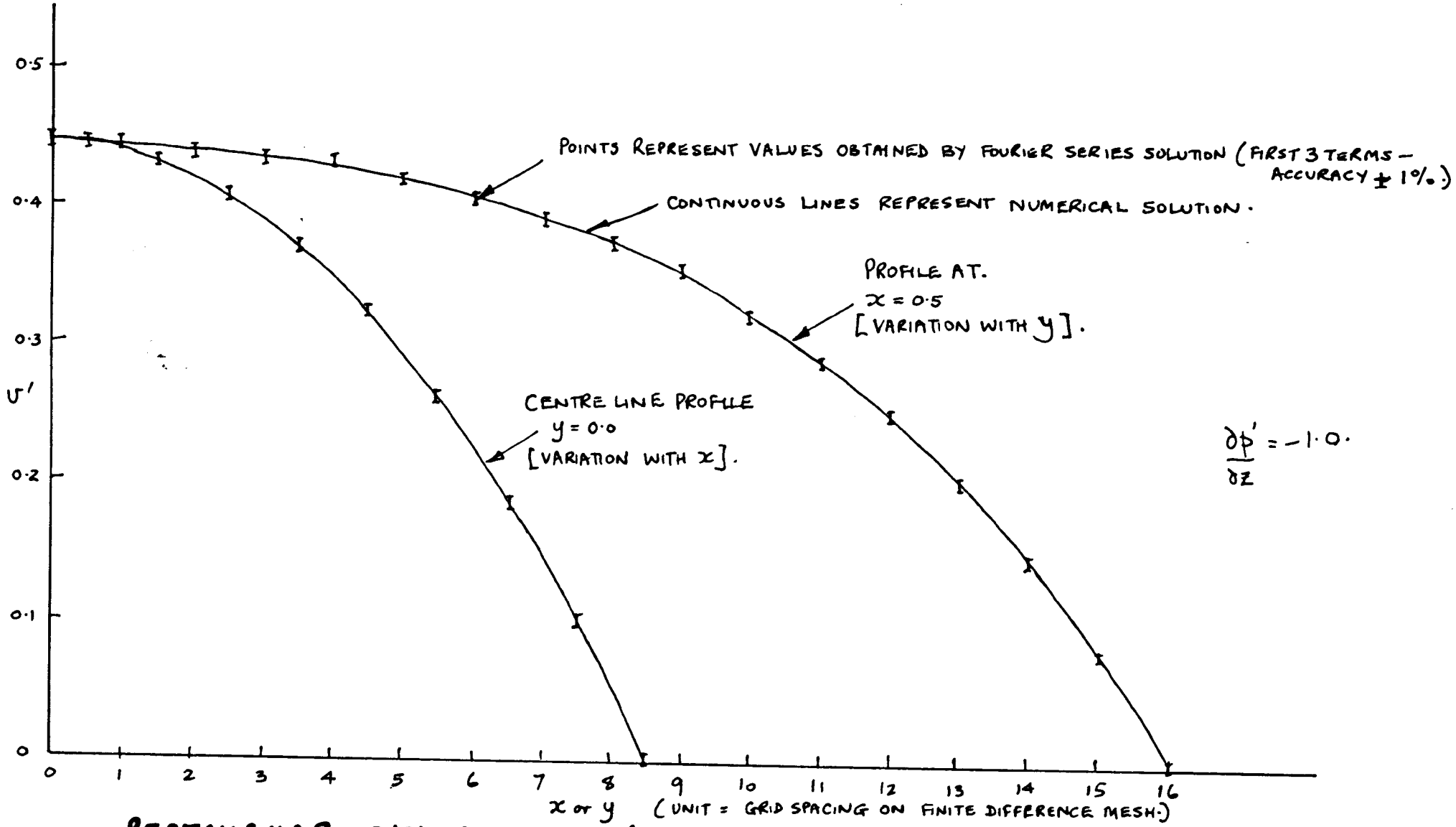

RECTANGULAR O.H.D. DUCT FLOW - COMPARISON OF SOLUTIONS OBTAINED BY NUMERICAL METHOD & FOURIER SERIES METHOD.

FIGURE 4.3.1.

where d_1 and d_2 are the $\frac{1}{2}$-widths of the duct in the x and y directions respectively. (See Figure 4.1.1(a)). Figure 4.3.1 shows the excellent agreement found between this solution (the first 3 terms only were needed to give an accuracy of $\pm$ 0.1%, since the series converged quickly) and the numerical solution, on the centre line y = 0 and on the line x = 0.5 (mesh line nearest to $x = 0$).

4.3.3. Comparison with Analytical Solutions to M.H.D. Rectangular Duct Flow

Two analytical solutions of M.H.D. Rectangular Duct Flows given by Shercliff (1953) were used to check the numerical solution (displayed in Figure 4.4.2), at the Hartmann Number of 10 (based on duct half-width, d_1).

The first (exact) solution to equation 4.2.1 is:-

$$v' + B' = \frac{16 \frac{\partial p'}{\partial z} d_2^2}{d_1^2 \pi^3} \cdot \sum_{n=0}^{\infty} \frac{(-1)^n}{(2n+1)^3} \left\{ 1 + \frac{(\exp m_1 x) \sinh m_2 d_1 - (\exp m_2 x) \sinh m_1 d_2}{\sinh (m_1 - m_2) d_1} \right\} \cos \left[\frac{(2n+1)\pi y}{2 d_2} \right] \quad \ldots.4.3.3.$$

where m_1 and m_2 are the roots of the quadratic equation:-

$$m^2 + \frac{H m}{d_1} - \frac{(2n+1)^2 \pi^2}{4 d_2^2} = 0 \quad \ldots.4.3.4.$$

It was found that 6 terms were required to produce $\pm$ 2% accuracy in the solution, and v' was found using the symmetry conditions described in section 4.2. (A computer program would be required to produce an 'exact' solution by taking a large number of terms - this was not considered necessary since the numerical results are only to be used to provide graphical contour plots in order to produce semi-quantitative results).

The second (approximate) solution, valid for $H \gg 1$, is:-

$$v' + B' = \frac{\partial p'}{\partial z} \cdot \frac{1}{H} \left\{ 1 - \frac{x}{d} - 2 \exp \left[-H \left(1 + \frac{x}{d} \right) \right] \right\} \quad \ldots.4.3.5.$$

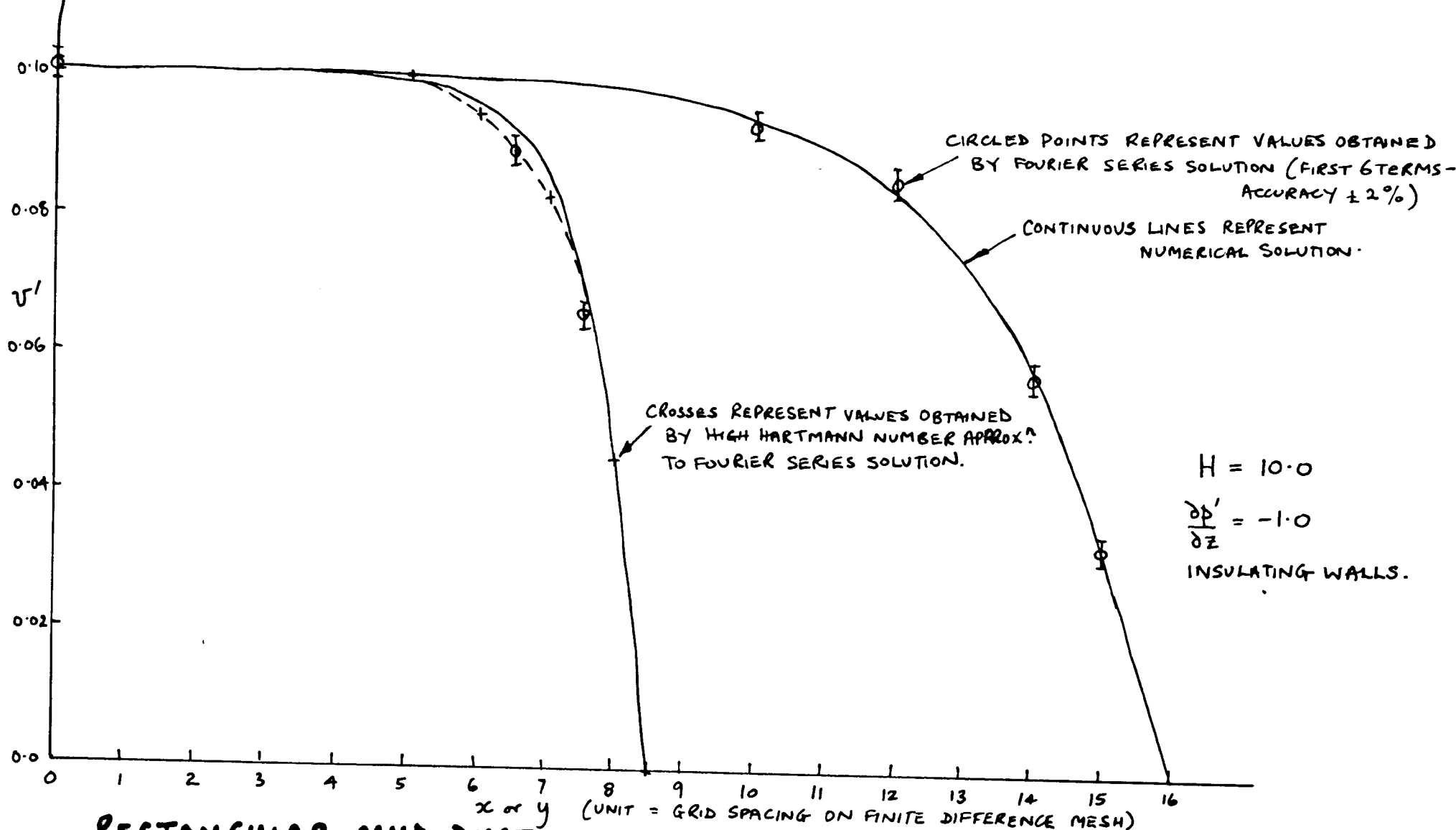

RECTANGULAR M.H.D. DUCT FLOW - COMPARISON OF SOLUTIONS OBTAINED BY NUMERICAL METHOD & FOURIER SERIES METHOD.

FIGURE 4.3.2.

which gives a solution at large distances from the top and bottom walls of the duct.

Again, the numerical solution was compared with the analytical solutions on the lines $x = 0{\cdot}5$ and $y = 0$. Figure 4.3.2 shows all three solutions. The only place where any discrepancy occurs in the $y = 0$ profile is at the maximum value of $\frac{\partial^2 v'}{\partial x^2}$, which may be expected; however this discrepancy is only $\sim 1\%$ and is tolerable.

4.3.4. Comparison with Analytical Solution for flow with moving boundaries

Elliptic functions with complex arguments are useful in checking certain cases of hydrodynamic flows which are excited by moving parts of the duct walls. A particular case which can be handled is that of moving top and bottom duct walls.

Consider a complex elliptic function

$$f(z) = \phi + i\psi \qquad \ldots.4.3.6.$$

where $z = u + iv$

Then $\frac{\partial \phi}{\partial u} + i\frac{\partial \psi}{\partial u} = f'(z)$

and $\frac{\partial \phi}{\partial v} + i\frac{\partial \psi}{\partial v} = if'(z)$ $\qquad \ldots.4.3.7.$

and also $\frac{\partial \phi}{\partial u} = \frac{\partial \psi}{\partial v}$ & $\frac{\partial \psi}{\partial u} = -\frac{\partial \phi}{\partial v}$ $\qquad \ldots.4.3.8.$

Elliptic Function tables (Henderson 1960) give x and y as functions of u and v, for $f'(z) = sn(z)$, $cn(z)$ & $dn(z)$

where $x = \frac{\partial \phi}{\partial u} = \frac{\partial \psi}{\partial v}$

and $y = -\frac{\partial \phi}{\partial v} = \frac{\partial \psi}{\partial u}$ $\qquad \ldots.4.3.9.$

and $x + iy = f'(z)$

It is required to find $\phi + i\psi = \int f'(z)dz = \int (x+iy)dz$ from which either ϕ or ψ may be determined.

Consider the Cn function;

This has the following properties:-

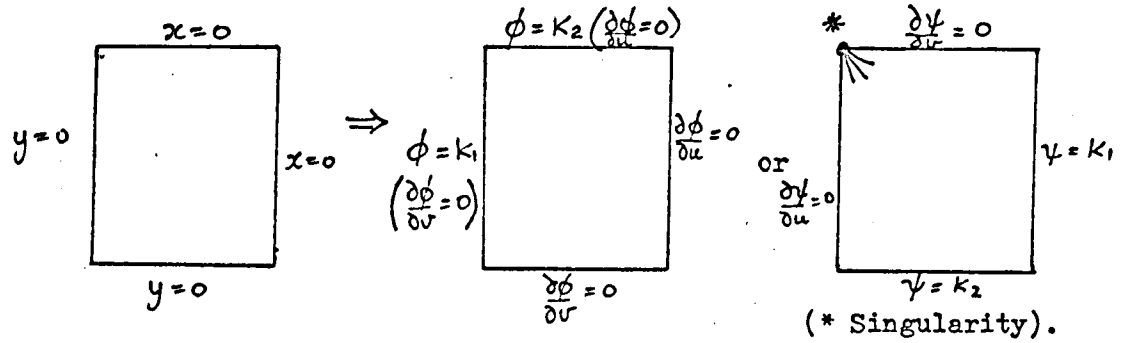

(* Singularity).

(a) Real and imag. parts of Cn.

(b) Real part of $f(z)$ $= Re\left\{\int Cn(z)dz\right\}$

(c) Imag. part of $f(z)$ $= \mathcal{I}\left\{\int Cn(z)dz\right\}$

The function ϕ (Real part of $f(z)$) can be matched to v' in the numerical solution if the region in (b) above is used to cover a quadrant of the rectangular duct and it is arranged that the arbitrary constants K_1 and K_2 are 0 and 1 respectively.

The integration of Cn may be carried out analytically since

$$\int Cn(z)dz = \frac{i}{k} \ln\left| dn(z) - ik\,sn(z)\right| \qquad \ldots.4.3.10.$$

$$\therefore \phi = Re\left\{\int Cn(z)dz\right\}$$

$$= -\frac{1}{k} \arg\left[dn(z) - ik\,sn(z)\right] \qquad \ldots.4.3.11.$$

where k is the modulus of the function and corresponds to the shape factor of the rectangular region. (For this case $k = \sin 12°$).

Figure 4.3.3. shows the velocity profiles obtained by the numerical solution with superimposed point values calculated using the complex elliptic functions. It can be seen that again, excellent agreement was obtained between the numerical and analytical solutions, both along the $\bar{x}=0$ line and along the $\frac{\bar{x}}{d_1} = 0.3$ and 0.5 lines.

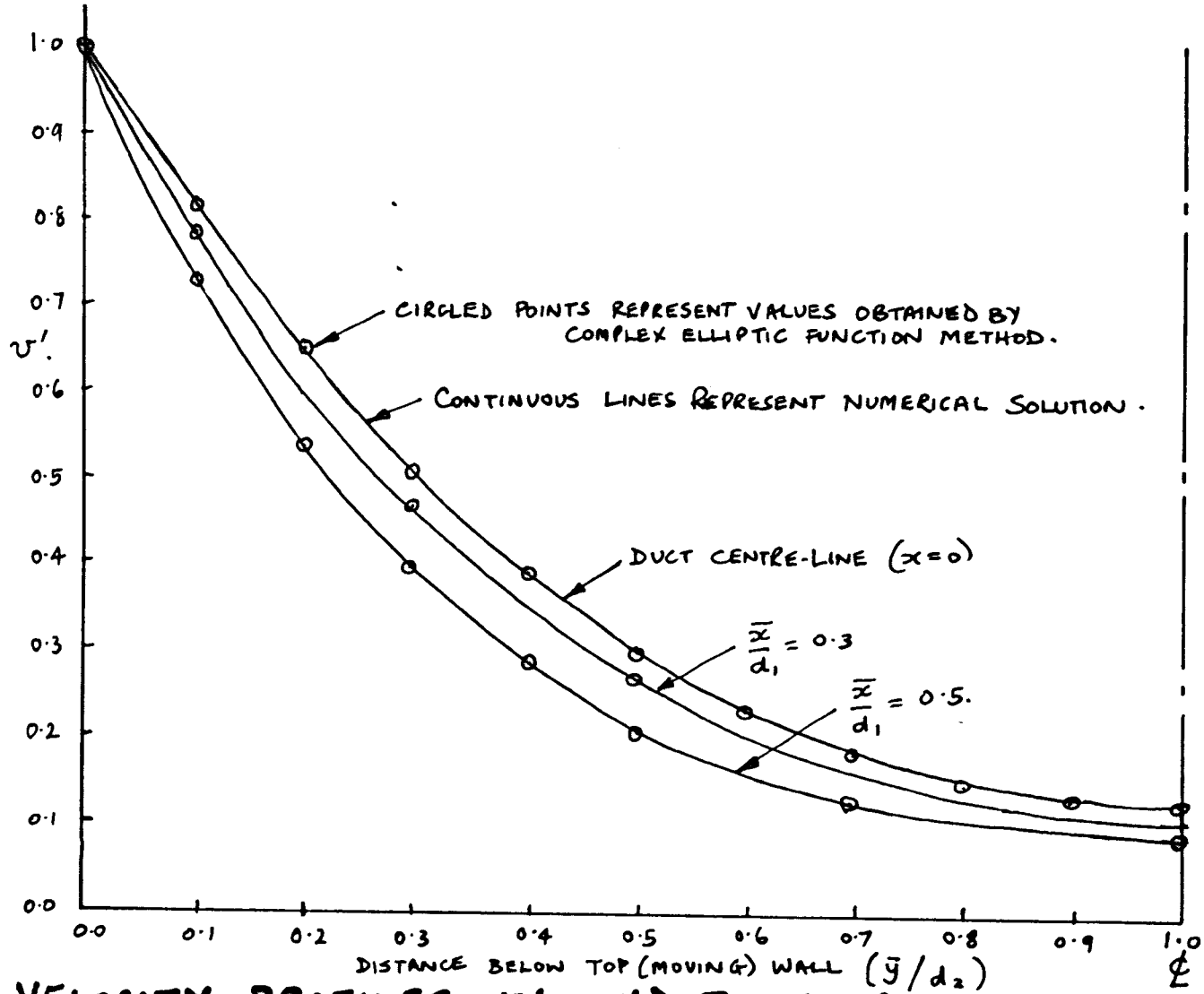

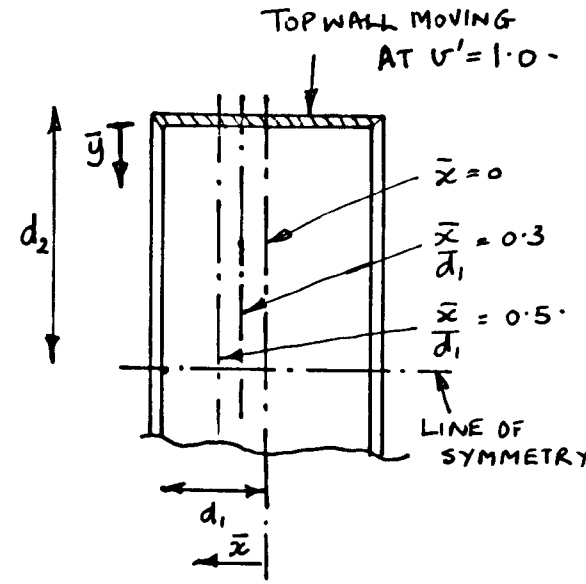

CONFIGURATION USED TO PRODUCE PROFILES — TOP & BOTTOM WALLS MOVING.

VELOCITY PROFILES IN O.H.D. FLOW - COMPARISON OF RESULTS OBTAINED BY NUMERICAL METHOD & COMPLEX INTEGRAL METHOD.

FIGURE 4.3.3.

4.4. Results for Pressure Driven Flows

4.4.1. Rectangular Duct Flow

The classical case of flow through a rectangular duct with no obstructions in the flow and with stationary, non-conducting walls was solved first. The O.H.D. case is shown in Figure 4.4.1 and the M.H.D. case at the Hartmann Number of 10 (based on the duct half-width) is shown in Figure 4.4.2.

In these two Figures and in all subsequent 2-D solutions presented in this Chapter, v' and B' are shown as contours over the 2-D fully developed cross-section of the flow. For economy, the contours are only drawn for one quadrant of the duct cross-section and in all cases, the v'-contours take the left-hand upper quadrant, and the B'-contours the right-hand upper quadrant.

The solutions to all the pressure driven flows are presented for $\frac{\partial p'}{\partial z} = -1$ and so the mean velocity decreases with increasing Hartmann Number. (See Shercliff (1953)). The contours are plotted in any one case with equal intervals, although the size of interval varies from case to case. Initially the mesh is used with the grid shape factor, S = 1.

The Hartmann Number of 10 was chosen as the standard value for most M.H.D. cases which are displayed in this Chapter, since it represented the approximate value expected in practice (see section 5.2) and since this was the highest value which the numerical method could handle with proven accuracy. Some solutions were obtained for H = 20 and H = 50; at H = 20, there was an overshoot on the mesh points adjacent to the wall of $\sim 10\%$, but this error did not propagate into the core of the flow. At H = 50, there was a serious overshoot which did propagate into the core and which invalidated the solution. If the overshoot was ignored for H = 20, a

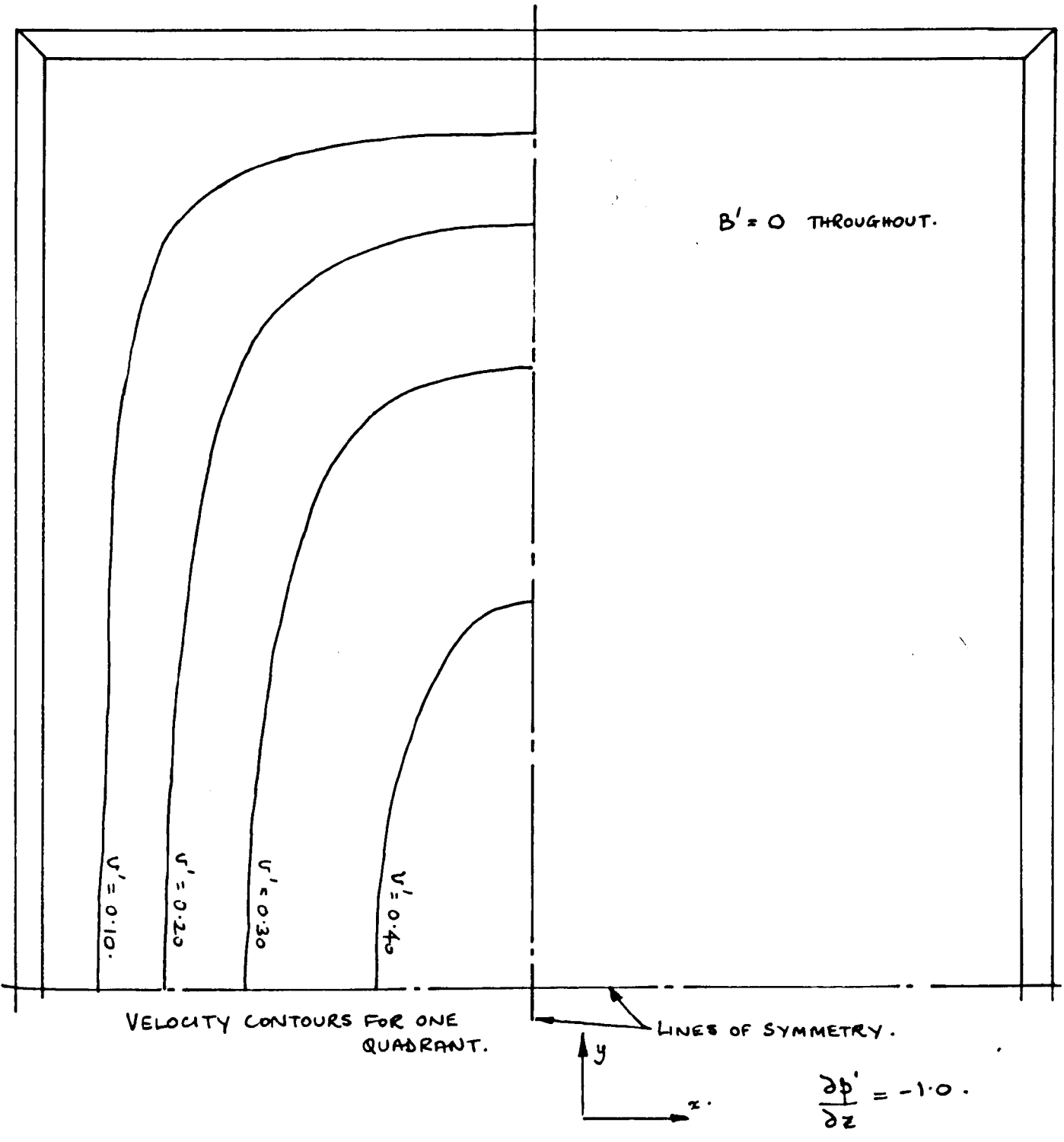

PRESSURE DRIVEN O.H.D. FLOW - STATIONARY WALLS. (COMPUTER SOLUTION)

FIGURE 4.4.1.

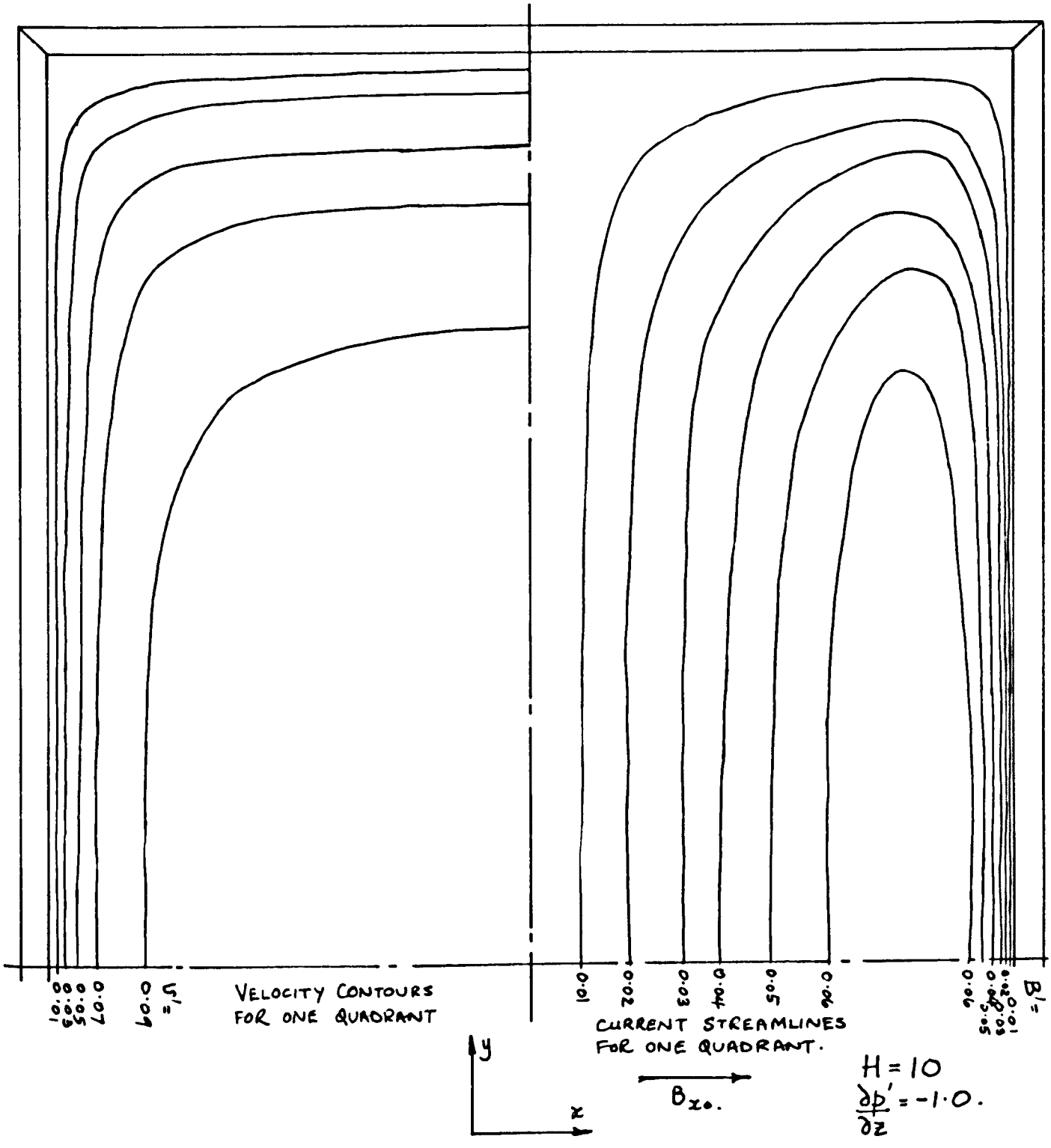

PRESSURE DRIVEN M.H.D. FLOW. - STATIONARY, NON-CONDUCTING WALLS. (COMPUTER SOLUTION) FIGURE 4.4.2.

sufficiently accurate solution was obtained to obtain a contour plot and this was done for some later cases.

Figure 4.4.1 shows a contour pattern which is reminiscent of the classical Poiseuille flow, with modifications to suit the rectangular cross-section of the duct. The M.H.D. version (Figure 4.4.2) shows quite clearly the Hartmann boundary layer (thickness $O(\frac{d_1}{H})$) on the walls perpendicular to the applied magnetic field (B_{x_0}) and the thicker layer $\left(O(\frac{d_1}{\sqrt{H}})\right)$ on the parallel walls. The general shape of the velocity profile is flattened in the core. The contours of B' are also current steamlines, (since $\text{Curl}\,\underline{B}=\mu j$) and show the diffuse flow of current in the core flow (along the $\underline{v}\times\underline{B}$ direction) and the current return within the Hartmann Layer. The $d_1/\sqrt{H}$ layer contains the dispersing transverse current flow.

4.4.2. Rectangular Duct Flow with immersed non-conducting plate

The flow in a duct with an immersed non-conducting thin plate, of half duct height (approx.) and symmetrically placed across the $y=0$ axis is considered in this section. Figure 4.4.3 shows the O.H.D. version of this case. The boundary layer on the immersed plate forces the peak velocity into the region above the tip of the plate.

When the magnetic field is applied, (see Figure 4.4.4) the region adjacent to the plate has a flatter profile - the velocity variation being limited to two Hartmann layers, one on the plate and one on the wall. The peak of velocity still occurs above the tip of the plate and there is a tendency for a greater proportion of the flow to occur in this region. Thus in the M.H.D. flow, the plate is displaying the tendency to lock the flow to itself. Since the plate is non-conducting, as we have already seen in Chapter 3, the limiting locking power of the plate is to reduce the mean core velocity adjacent to the plate to a half of the main stream core velocity - this limit is attained for a semi-infinite plate in an infinite fluid.

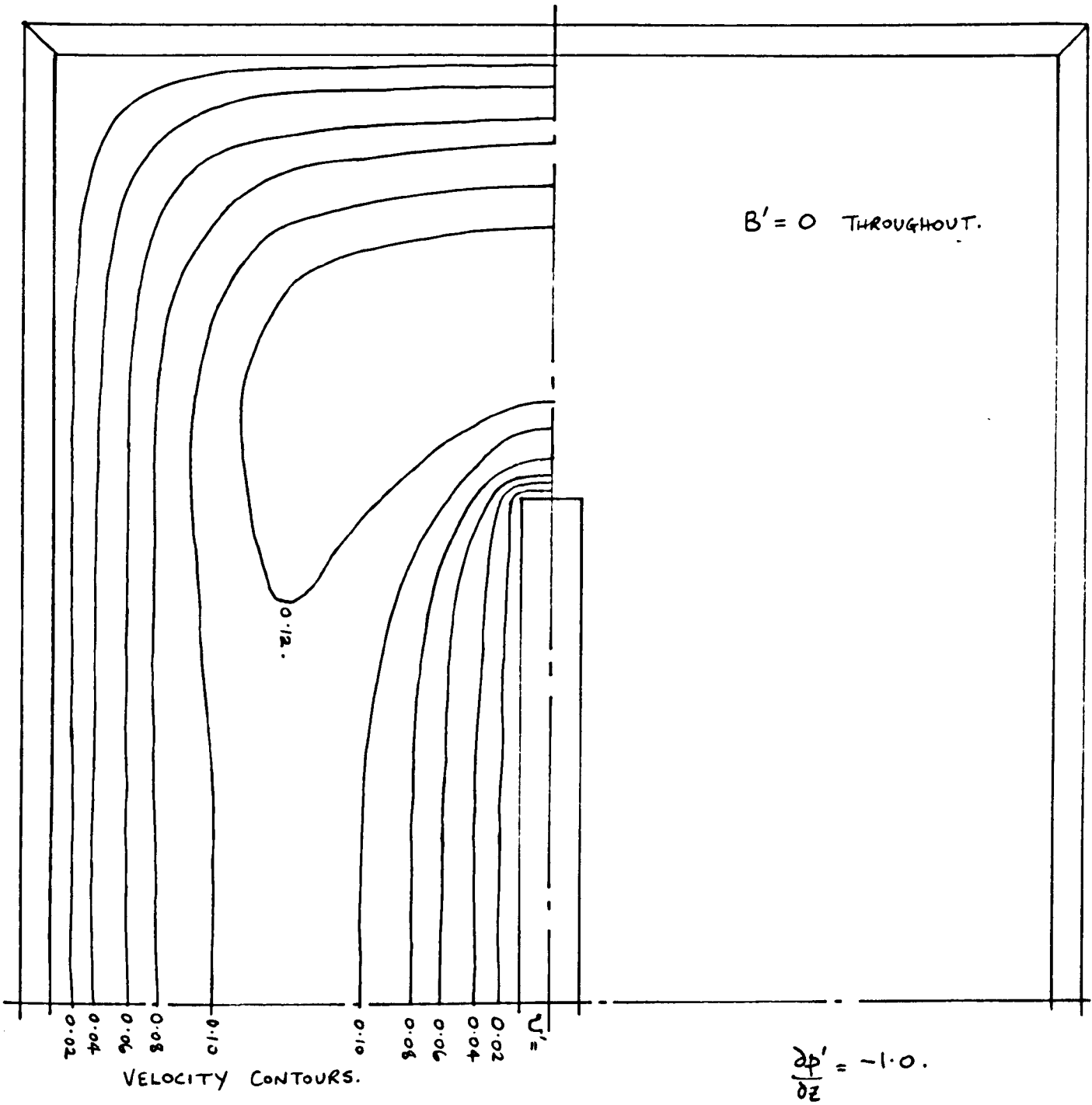

PRESSURE DRIVEN O.H.D. FLOW - WALLS & CENTRE-PLATE STATIONARY. (COMPUTER SOLUTION) FIGURE 4.4.3.

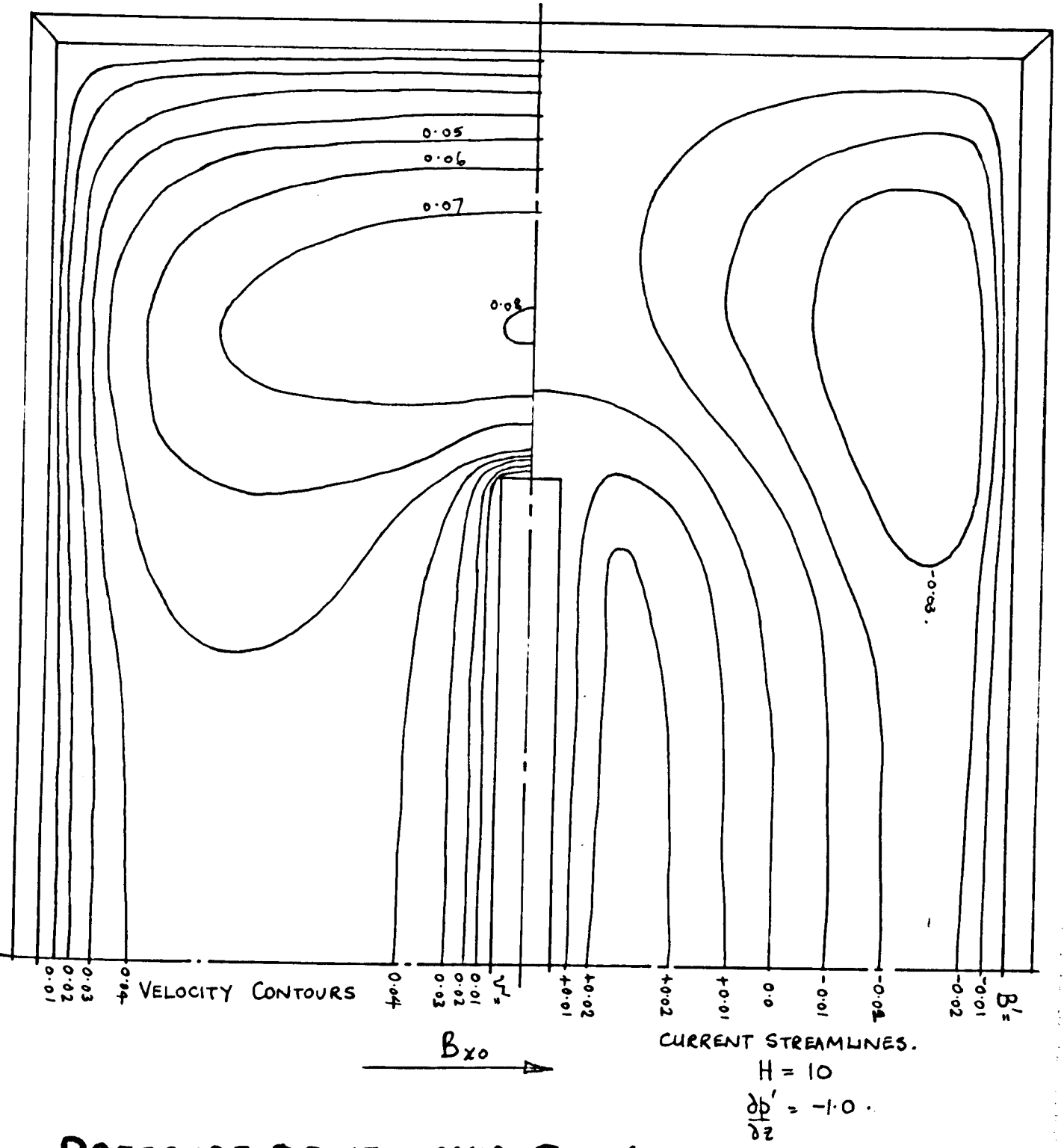

PRESSURE DRIVEN M.H.D. FLOW - WALLS & CENTRE PLATE STATIONARY, & NON-CONDUCTING. (COMPUTER SOLUTION)

FIGURE 4.4.4.

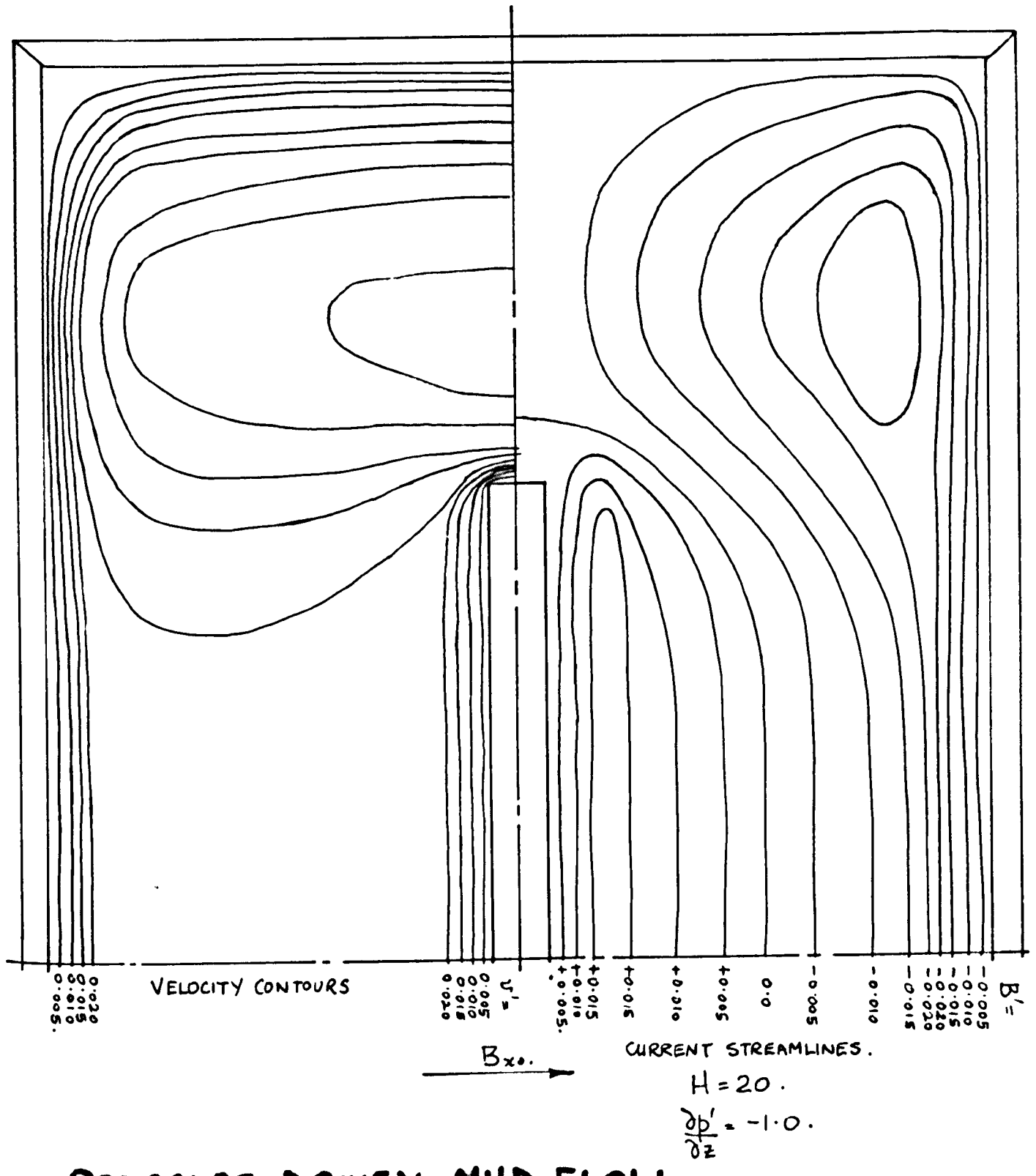

PRESSURE DRIVEN M.H.D. FLOW – WALLS & CENTRE-PLATE STATIONARY, & NON-CONDUCTING. (COMPUTER SOLUTION)

FIGURE 4.4.5.

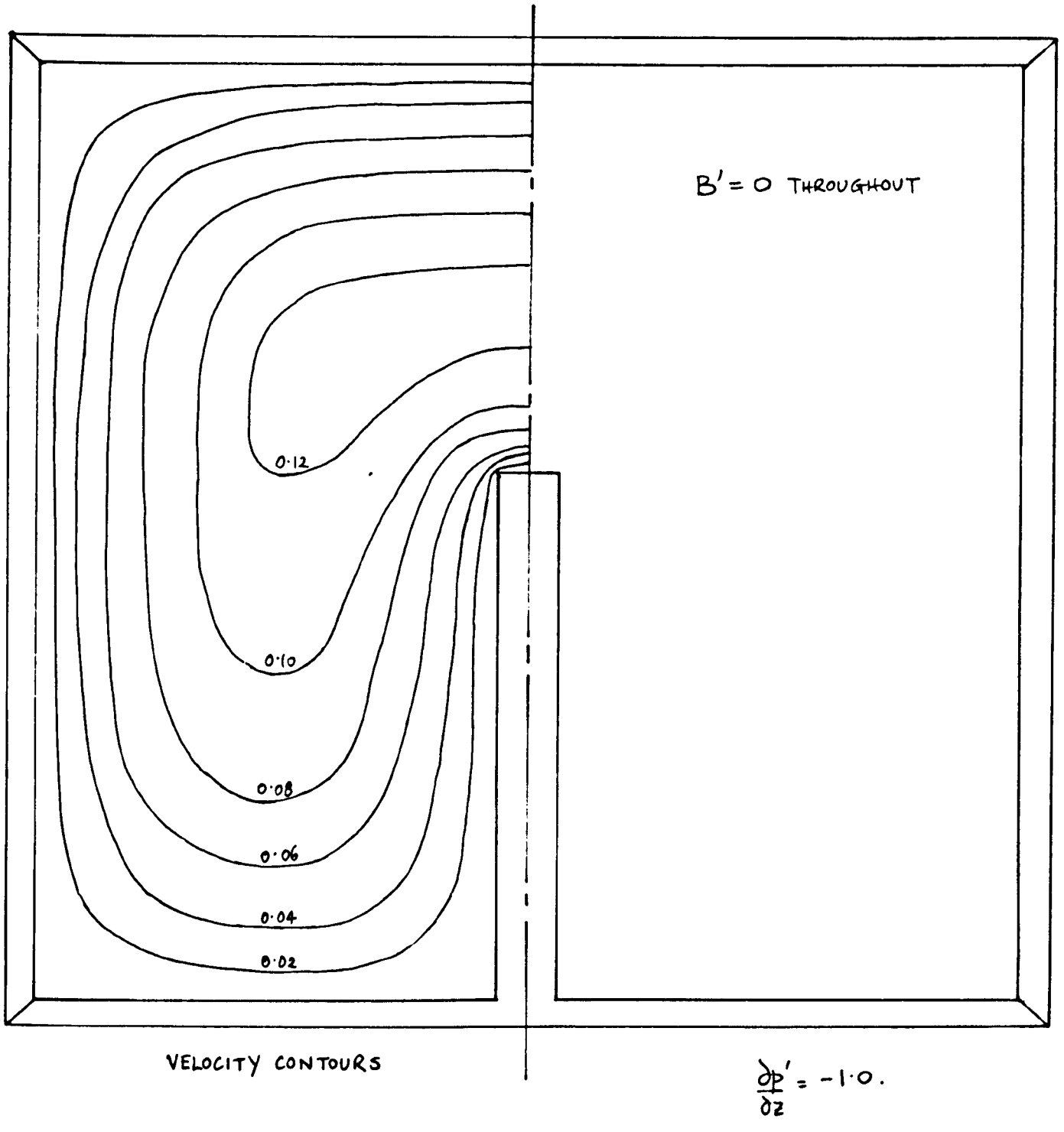

PRESSURE DRIVEN OHD FLOW - WALLS & CENTRE PLATE STATIONARY, WITH SOLID BOTTOM WALL. (COMPUTER SOLUTION)

FIGURE 4.4.6.

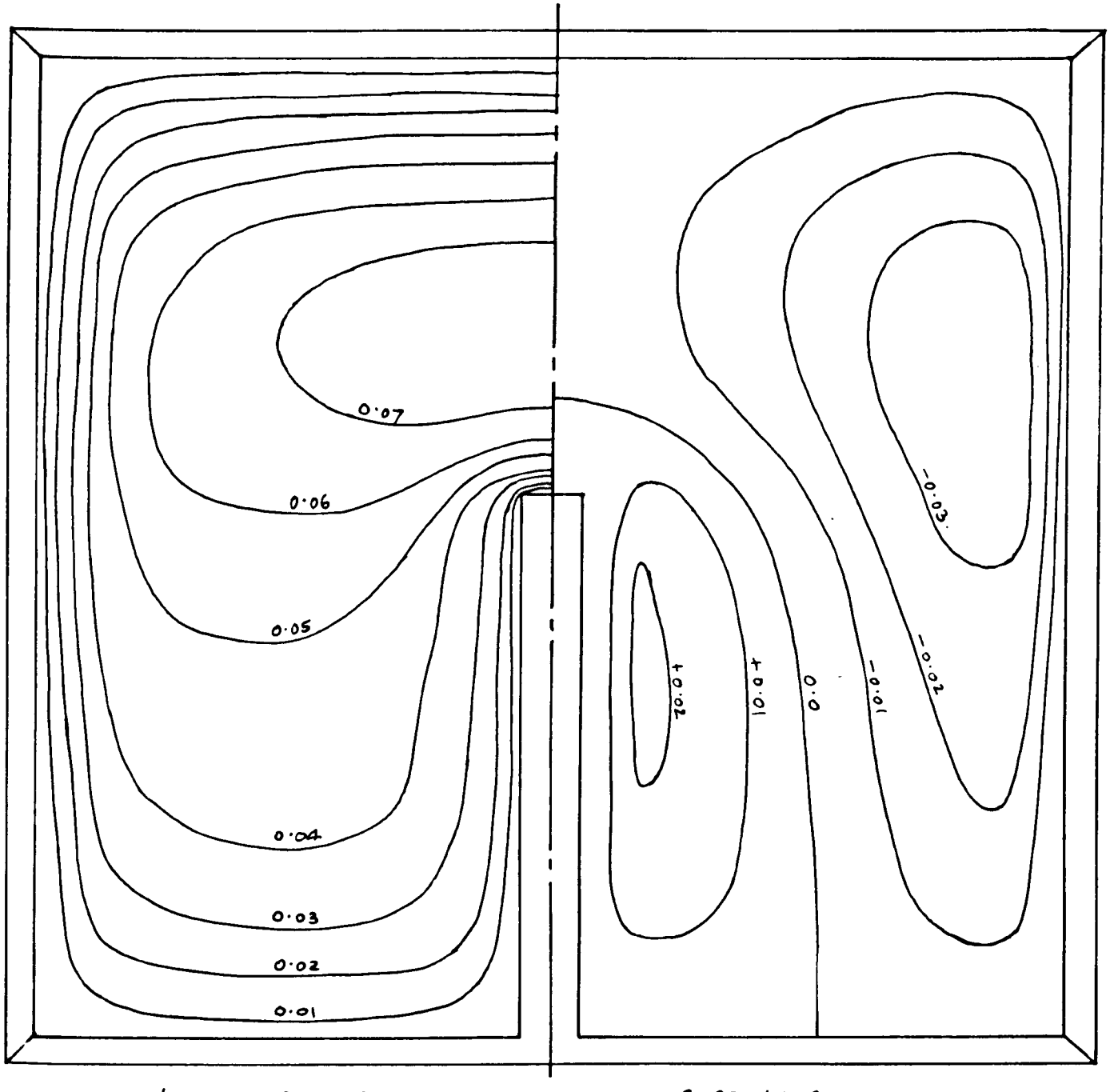

VELOCITY CONTOURS

CURRENT STREAMLINES.

B_{x_0}

$H = 10$

$\frac{\partial p'}{\partial z} = -1{\cdot}0.$

PRESSURE DRIVEN M.H.D. FLOW - WALLS & CENTRE PLATE STATIONARY & NON-CONDUCTING, WITH SOLID BOTTOM WALL. (COMPUTER SOLUTION). FIGURE 4.4.7.

For Figure 4.4.4. $(H=10)$ $\dfrac{\bar{v}_{CORE1}}{\bar{v}_{CORE2}} \approx 0.61$

and for Figure 4.4.5 $(H=20)$ $\dfrac{\bar{v}_{CORE1}}{\bar{v}_{CORE2}} \approx 0.502$

where core 1 is the core adjacent to the plate and core 2 is the 'main-stream' core above the tip of the plate. Therefore the limiting value of this mean velocity is almost achieved at H = 20 with this configuration.

The current streamline patterns (see Figures 4.4.4 and 4.4.5) for this case show again a diffuse current flow through the core which returns both down the Hartmann layer on the immersed plate and also down the Hartmann layer on the wall. This division of return current flow causes a transverse current flow adjacent to the tip of the immersed plate, which coincides with a 'wake' in the velocity profiles between the two core regions.

In Figures 4.4.6 and 4.4.7, the same case is repeated, but with the solid bottom wall condition (non-conducting and stationary). The result is qualitatively very similar, but the locking effect of the plate is attenuated by the existence of the boundary layer on the bottom wall, which effectively reduces the height of the plate. All the current now has to return above the base line of the mesh, and the distribution of current is approximately half flowing left and half right.

4.4.3. Ducts and immersed plates with varying shape factor

A qualitative investigation was made of the effect of varying the shape factor of rectangular ducts with immersed non-conducting plates - maintaining the same geometrical relationship between the plate and the duct. The shape factor was varied by a factor 4 and $\frac{1}{4}$ and the results for C.H.D. flow and M.H.D. flow (H = 10) are shown in Figures 4.4.8, 4.4.9 and 4.4.10, 4.4.11 respectively. (H is based on the actual duct half-width in each case).

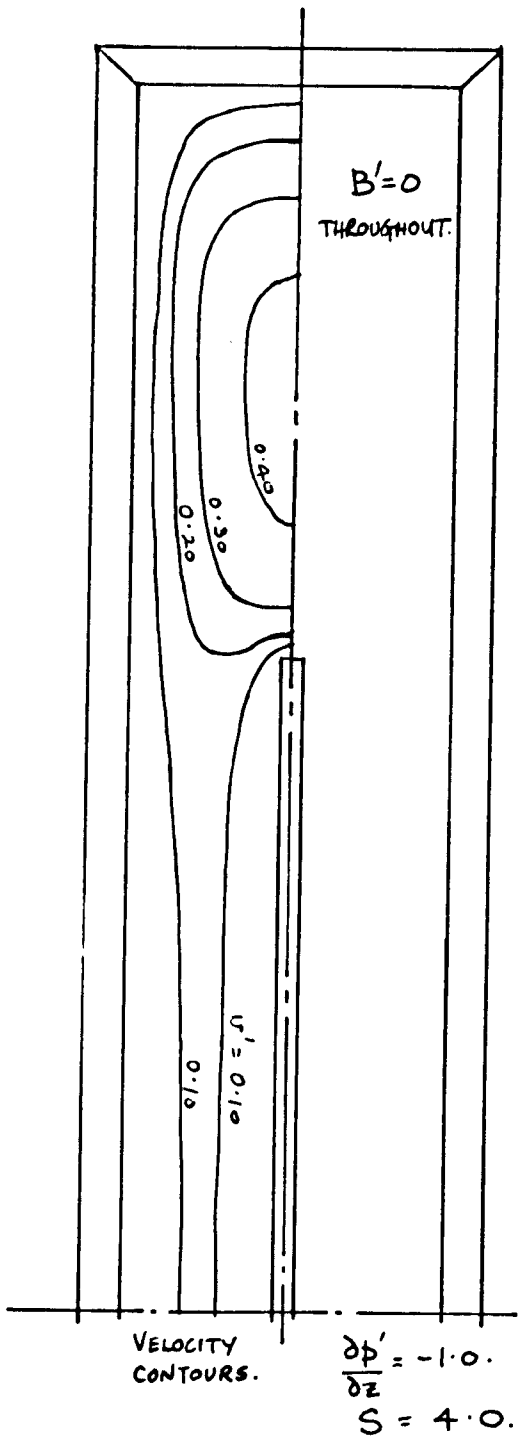

PRESSURE DRIVEN O.H.D. FLOW - STATIONARY WALLS, DUCT LONG ⊥ APPLIED FIELD (COMPUTER SOLUTION) FIGURE 4.4.8.

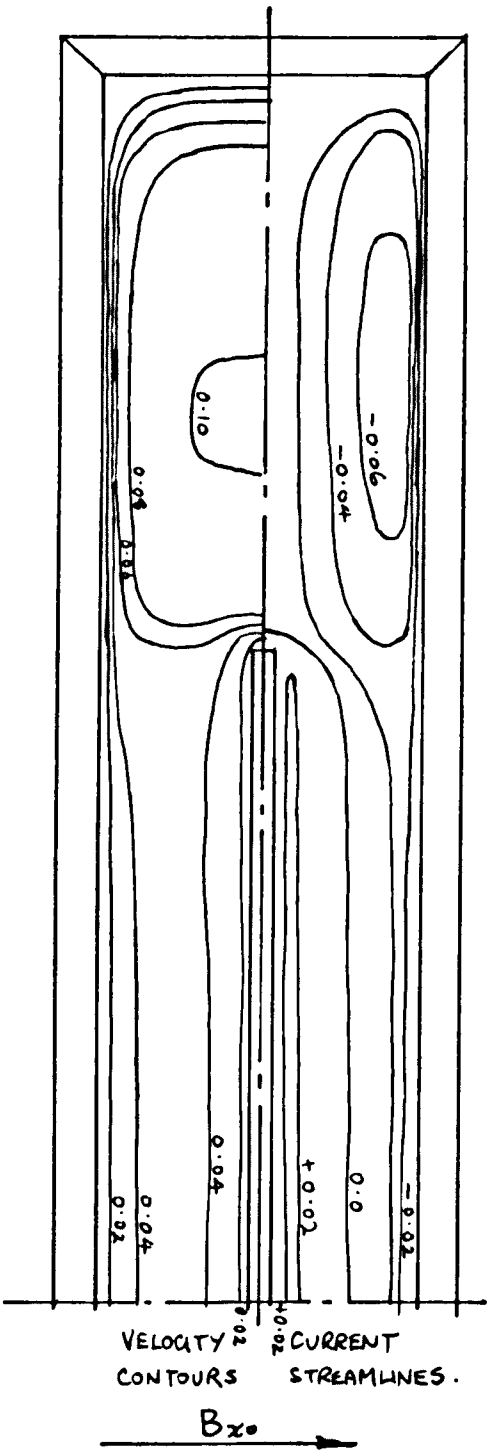

$H = 10$

$\frac{\partial p'}{\partial z} = -1.0$

$S = 4.0.$

PRESSURE DRIVEN MHD FLOW - STATIONARY, NON-CONDUCTING WALLS, DUCT LONG ⊥ APPLIED FIELD. (COMPUTER SOLUTION). FIGURE 4.4.9.

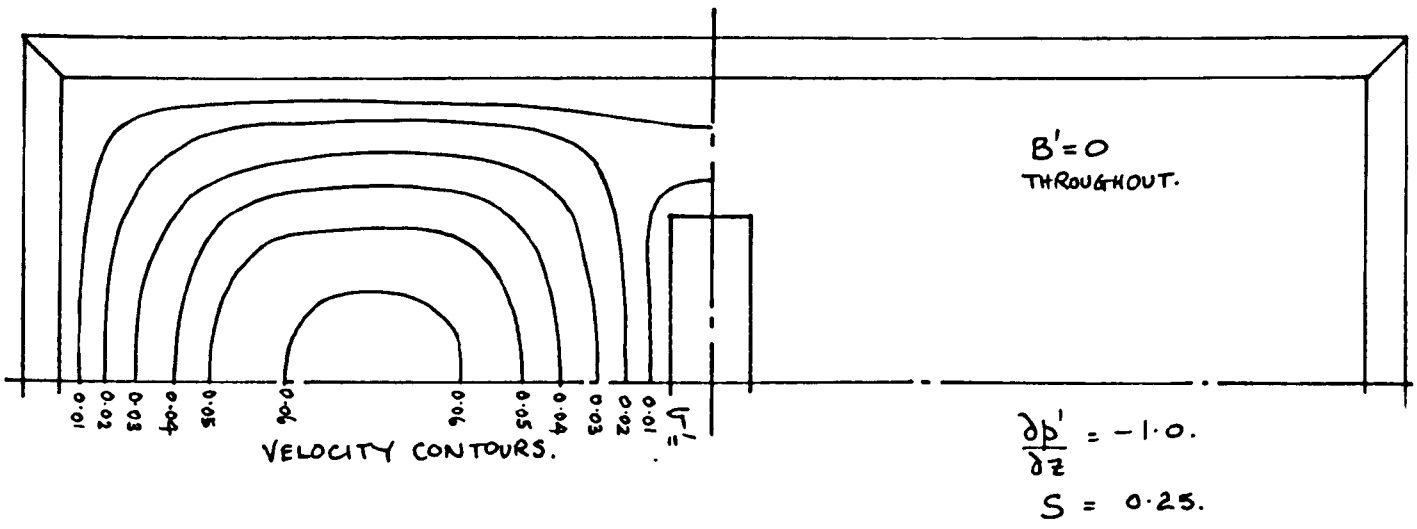

PRESSURE DRIVEN O.H.D. FLOW - STATIONARY WALLS, DUCT LONG // APPLIED FIELD. (COMPUTER SOLUTION) FIGURE 4.4.10.

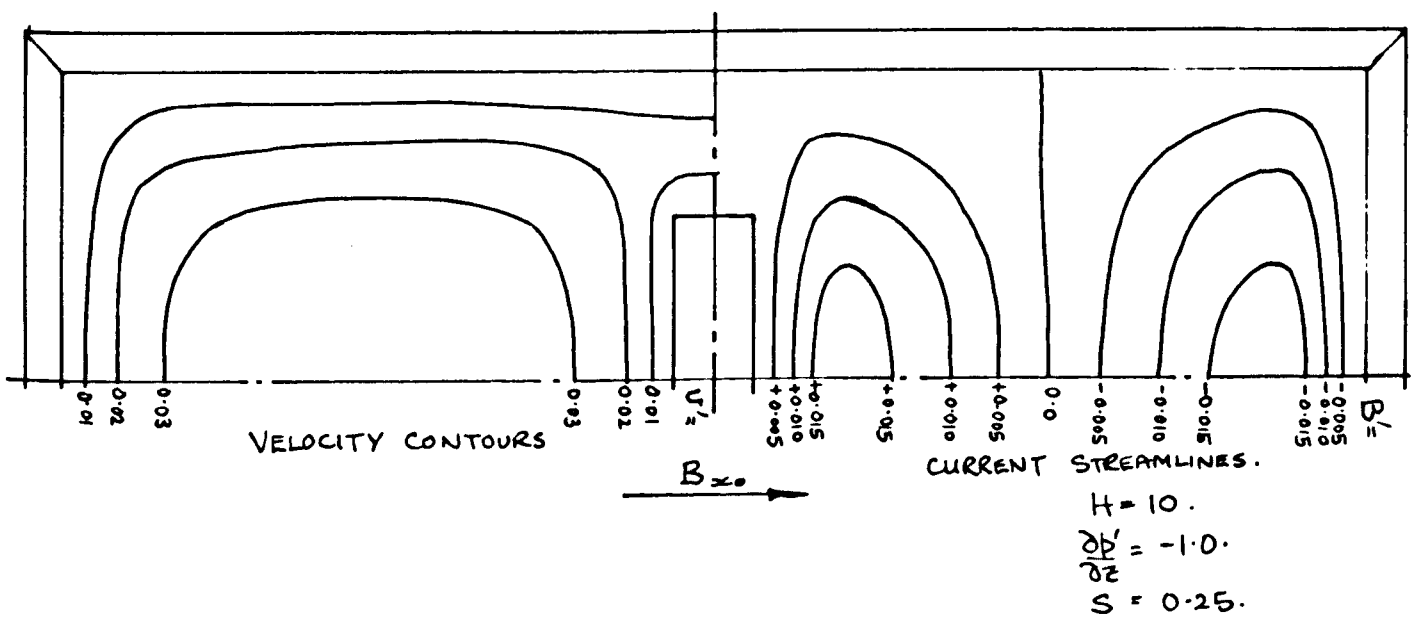

PRESSURE DRIVEN M.H.D. FLOW - STATIONARY, NON-CONDUCTING WALLS, DUCT LONG // APPLIED FIELD. (COMPUTER SOLUTION) FIGURE 4.4.11.

It is interesting to compare Figures 4.4.9 and 4.4.11, (i.e. the two M.H.D. flows at x4 and $x\frac{1}{4}$ shape factor). The first notable feature is the marked difference in current flow pattern. In the case of a duct which is long perpendicular to the applied field (Figure 4.4.9), the transverse current flow adjacent to the tip of the plate is more marked and for a duct which is long parallel to the applied field (Figure 4.4.11) this effect is not detectable. In fact, this latter case behaves very much like a duct with a continuous partition along the whole of the $\chi = 0$ axis (i.e. two separate ducts).

Looking now at the velocity profiles, it can be seen that the effect of the magnetic field in modifying the shape of the contours is much more pronounced in Figure 4.4.9, than in Figure 4.4.11. In Figure 4.4.9, the transverse 'wake', separating the two core regions, is more pronounced than in Figures 4.4.4 and 4.4.5, and does not appear at all in Figure 4.4.11, which just displays a general flattening of the velocity profile compared with the O.H.D. case (Figure 4.4.10).

Increasing the shape factor (increasing the length of the duct perpendicular to the applied field) is seen to give a marked increase in the effect of the immersed plate in M.H.D. interactions on the shape of the profiles, with this particular configuration.

4.4.4. Variation of Normalised Pressure Gradient/Mean Velocity with Hartmann Number

For the Hartmann Number varied over the range 0 - 20, the ratio of Normalised Pressure Gradient/Mean Velocity was evaluated for both a rectangular duct with no obstructions and for a rectangular duct with an immersed plate.

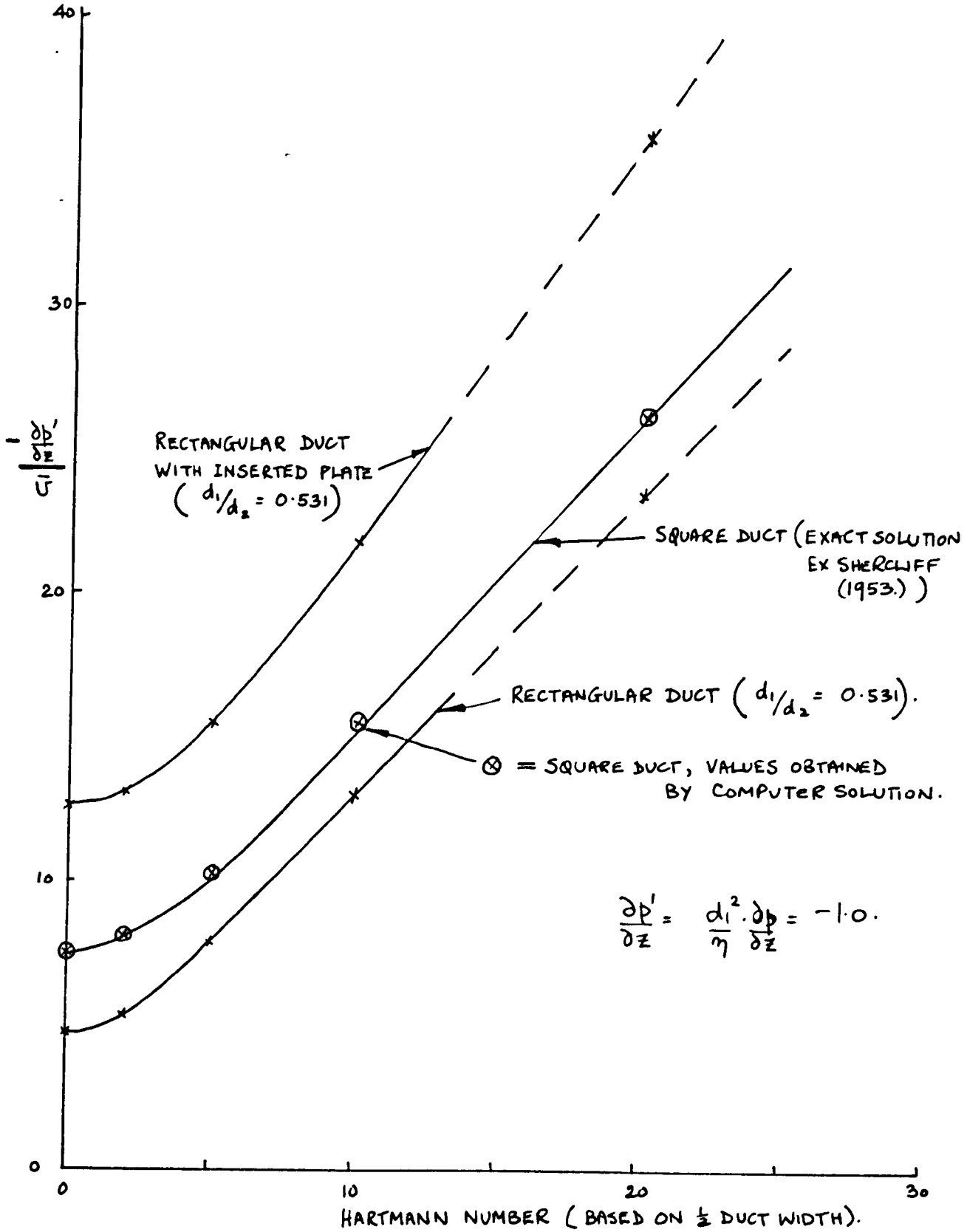

VARIATION OF NORMALISED PRESSURE GRADIENT / MEAN VELOCITY WITH HARTMANN NUMBER.

(FROM COMPUTER SOLUTIONS.) FIGURE 4.4.12.

For comparison with the exact values presented by Shercliff (1953), the values corresponding to a square duct were also evaluated. Figure 4.4.1 shows the excellent agreement obtained between Shercliff's result and the values obtained by numerical analysis.

For the rectangular duct results, the shape factor of the duct was $\frac{d_1}{d_2} = 0.531$, corresponding to a mesh shape factor of 1.0. The result for the unobstructed rectangular duct lies below that for the square duct i.e. a greater mean velocity is obtained for a given value of $\frac{\partial b'}{\partial z}$, since for constant $\frac{\partial b'}{\partial z}$, and constant d_1, the change in shape factor from 1 to 0.531 implies a greater duct cross-section and hence a greater velocity. The effect of introducing the immersed plate is to reduce the mean velocity for the same $\frac{\partial b'}{\partial z}$, even beyond the value for a square duct; this reduction is caused by the extra drag introduced by the immersed plate.

4.5. Results for Cases with Moving Boundaries and no Pressure Gradients

4.5.1 Half-Side Walls Moving

The first case to be studied is of little practical importance, but it illustrates the phenomenon of the transverse wake. Consider a rectangular duct with all non-conducting walls, with a discontinuity in the walls perpendicular to the applied field direction (side walls) (see Figures 4.5.1 and 4.5.2). The centre portion of the side walls is then moved with $v' = 1$, by external excitation.

The resulting O.H.D. flow is shown in Figure 4.5.1 and displays a gradual decrease in velocity when rotating around the discontinuity. However, in the M.H.D. case with H = 10 (see Figure 4.5.2), the variation in velocity is limited to a transverse wake which is symmetrical about the y = const line at the discontinuity in wall velocity, and is of total thickness $O\left(\frac{d_1}{\sqrt{H}}\right)$.

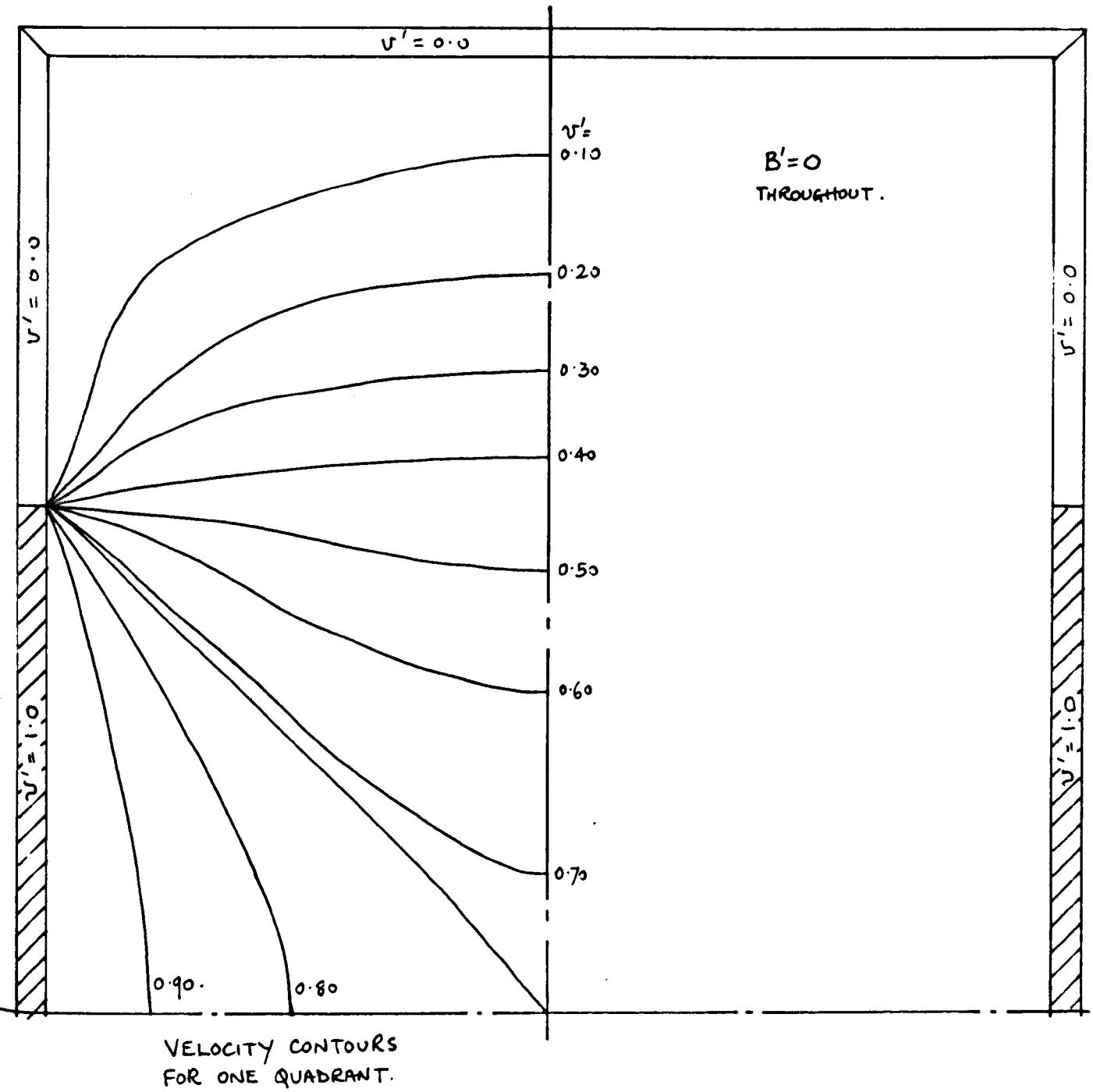

VELOCITY CONTOURS
FOR ONE QUADRANT.

O.H.D. FLOW - ½ SIDE WALLS MOVING (COMPUTER SOLUTION) FIGURE 4.5.1.

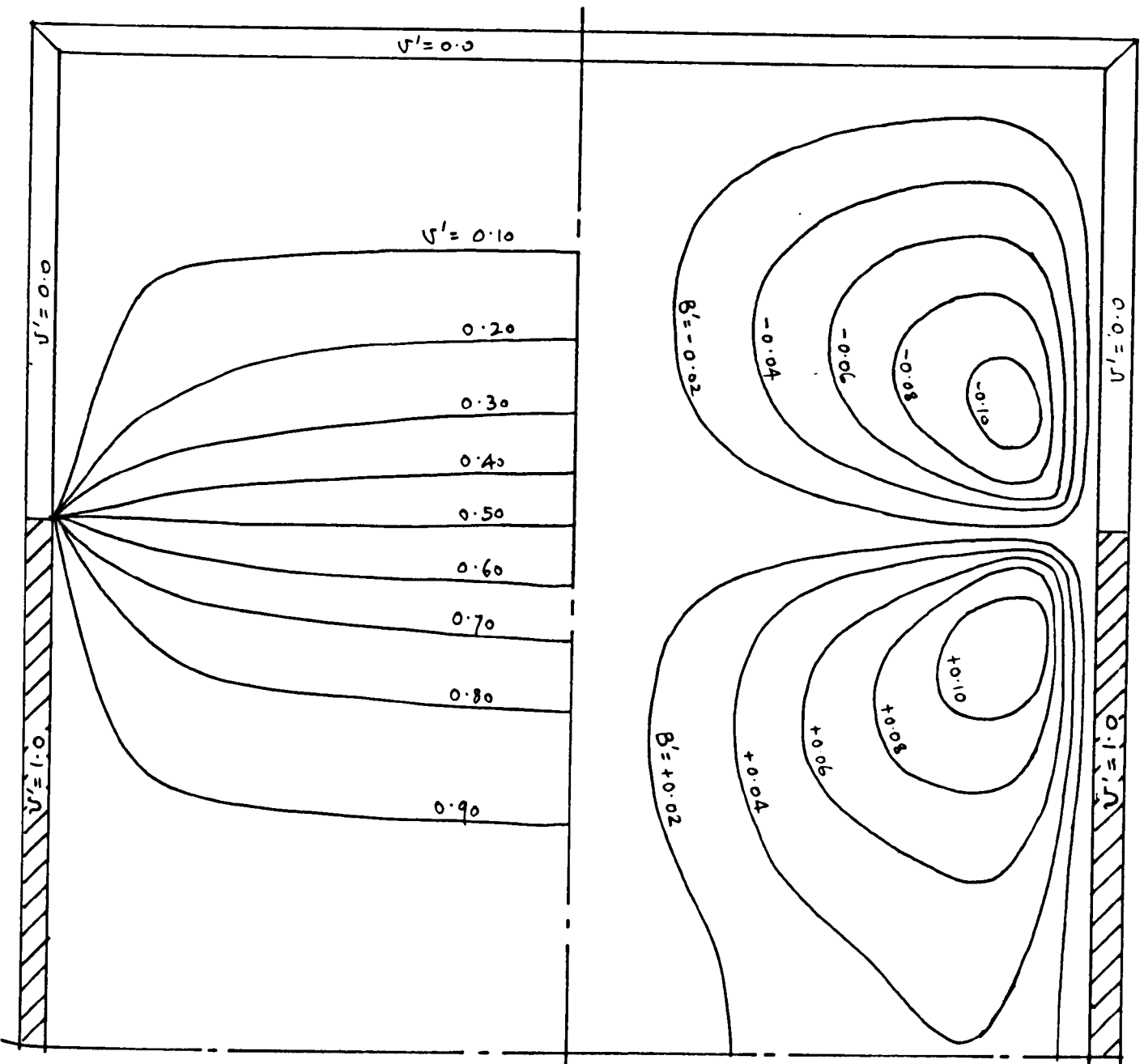

VELOCITY CONTOURS.
FOR ONE QUADRANT

CURRENT STREAMLINES.
FOR ONE QUADRANT.

B_{x_0}

H = 10.

M.H.D. FLOW, NON-CONDUCTING WALLS - ½ SIDE WALLS MOVING (COMPUTER SOLUTION)

FIGURE 4.5.2.

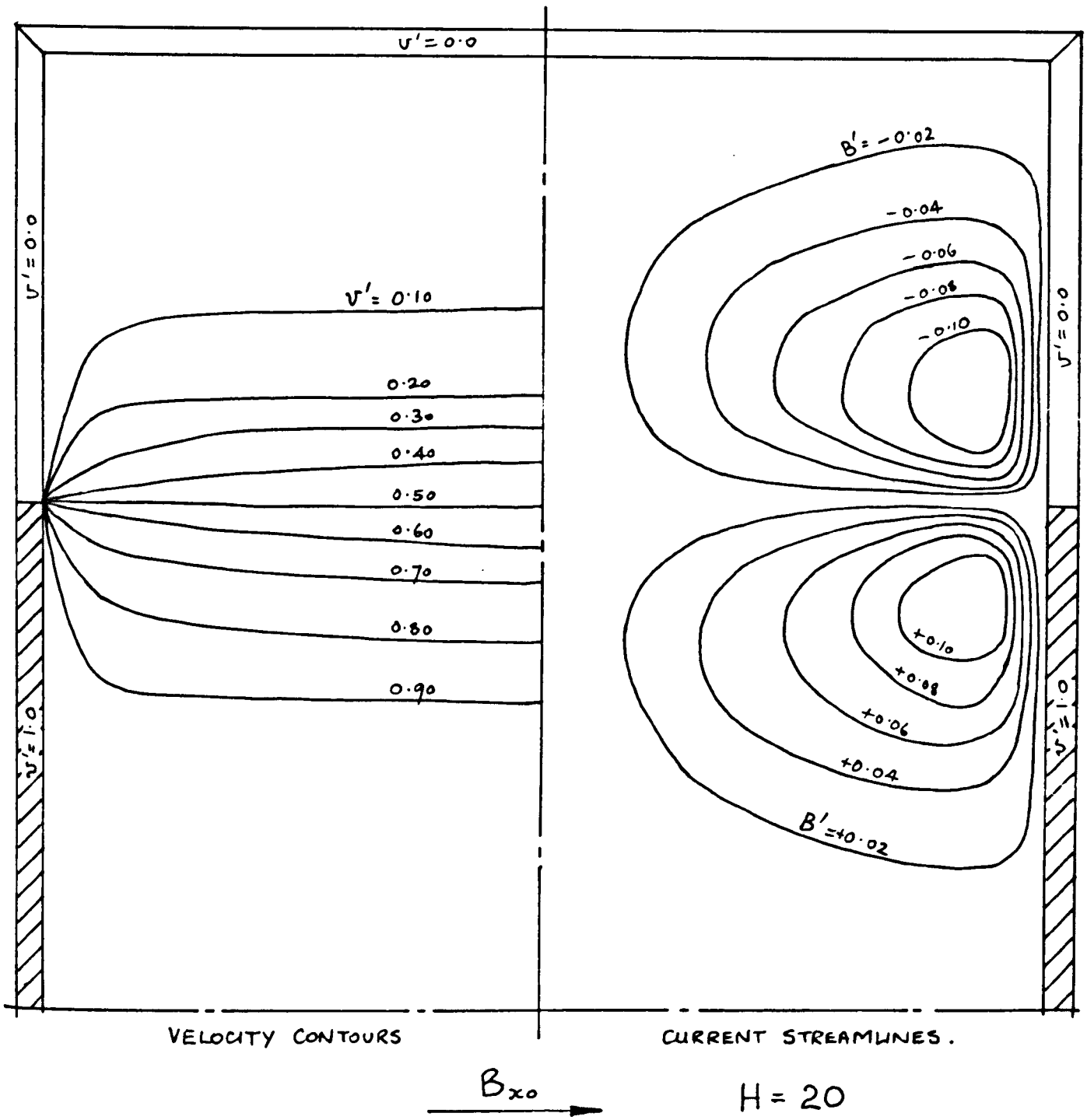

MHD FLOW, NON-CONDUCTING WALLS- ½ SIDE WALLS MOVING (COMPUTER SOLUTION)

FIGURE 4.5.3.

It separates two core regions - the upper region being approximately stagnant and the lower region moving at approximately the same velocity as the excited portions of the walls. This should be contrasted with the pressure driven flows which have semi-infinite inserted plates. Here, the locking effect produced a velocity, in the core adjacent to the plate, equal to half the exciting velocity. The effect of locking the lower core region to the wall velocity in this case is produced by superimposed effects of two moving portions of the walls, one on each side.

The current distribution, as well as the velocity distribution, show the transverse wake effect - especially in Figure 4.5.3 (H = 20 for this case). Considering one quadrant, it can be seen that the current flow is in opposing directions along Hartmann layers on the stationary and moving portions of the side walls. At the discontinuity, the two current streams merge and flow inwards towards the core of the flow within the transverse wake, and continuously feed the core flow with a diffuse current distribution in the $\underline{v} \times \underline{B}$ direction on either side of the wake. Thus a total of three current distribution loops are formed in each half of the duct - one adjacent to the moving part of the side wall and one each to the stationary portions, although a large proportion of the current in the loop adjacent to the moving portion does return before crossing the $y = 0$ axis, so forming two sub-loops.

4.5.2 Non-conducting Moving Immersed Plate

The second dynamically excited case could more easily be achieved in practice, although its main interest is in its comparison with the non-conducting semi-infinite plate case investigated by Hasimoto (1960), and an investigation of the effect of imposing finite limits to the plate and to the volume of fluid. (cf. Figure 2.2.1).

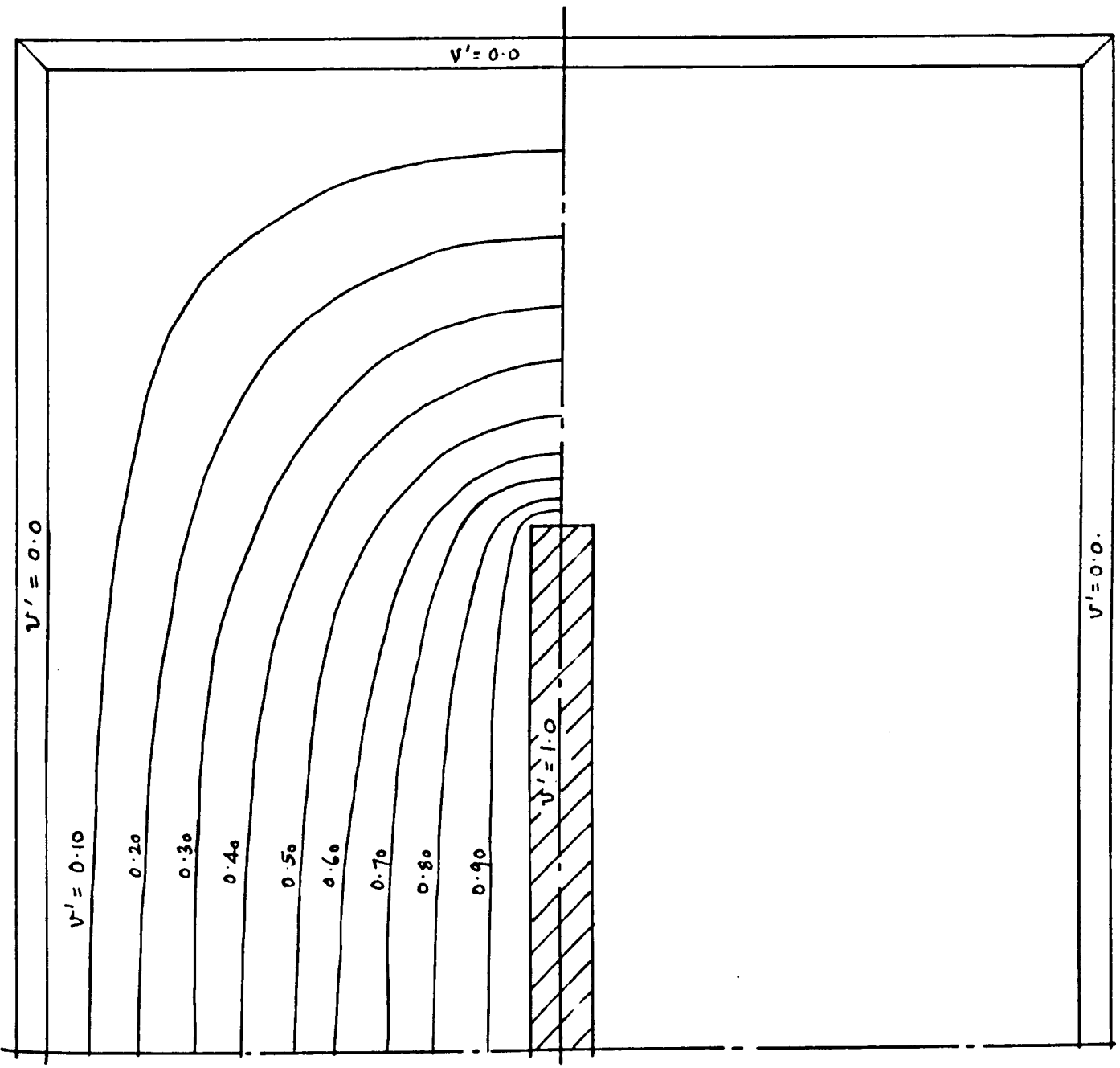

VELOCITY CONTOURS.

O.H.D. FLOW - CENTRE PLATE MOVING.

(COMPUTER SOLUTION) FIGURE 4.5.4.

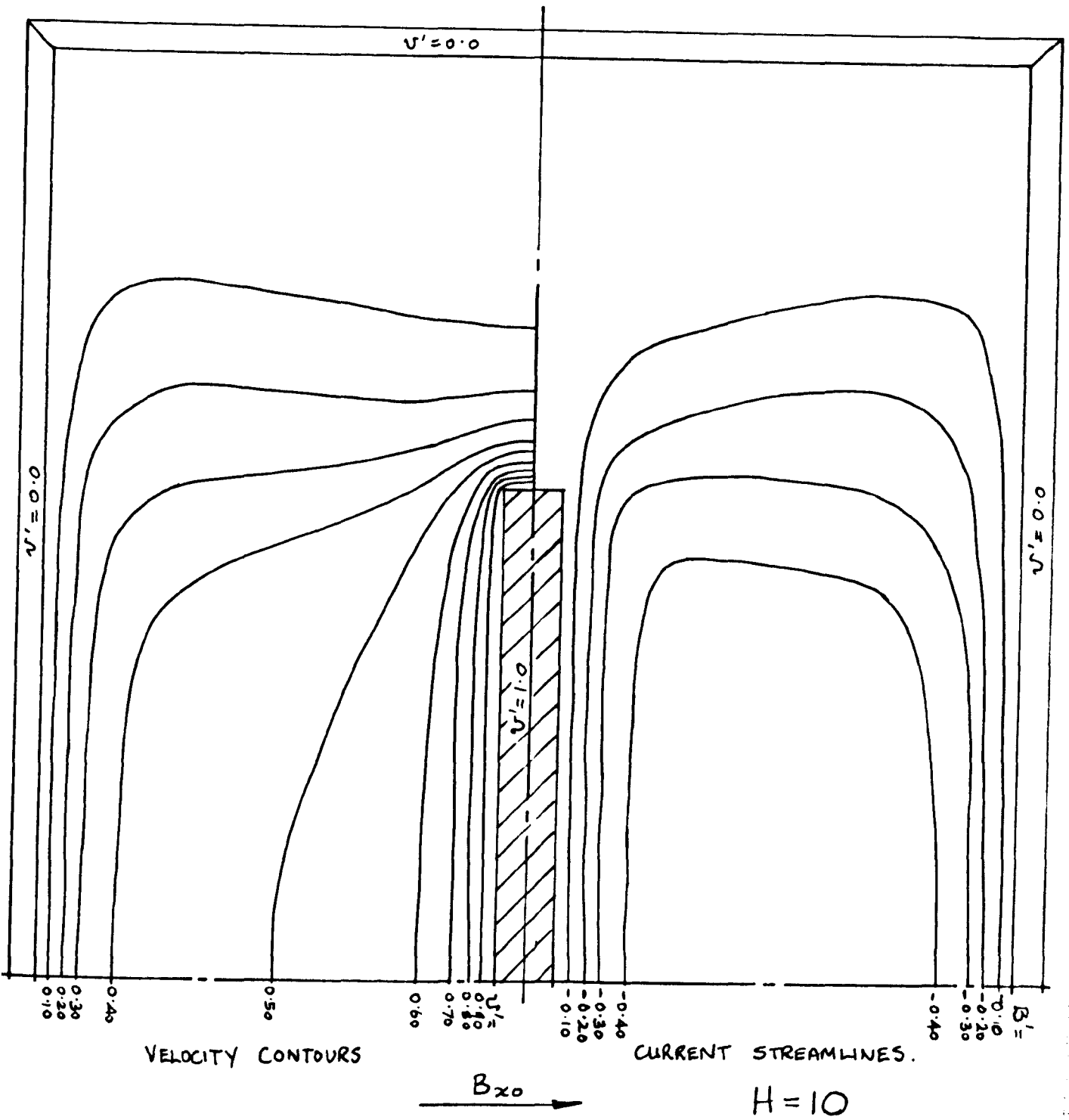

M.H.D. FLOW - CENTRE PLATE MOVING, NON-CONDUCTING PLATE & WALLS. (COMPUTER SOLUTION) FIGURE 4.5.5.

Figures 4.5.4. and 4.5.5 show the O.H.D. and M.H.D. versions of this flow. The shape of velocity contours in the O.H.D. case (Figure 4.5.4) show great similarity to those of pressure driven duct flow with the inserted plate absent (Figure 4.4.1), but when the magnetic field is applied (Figure 4.5.5), there is a striking change in the contour pattern even at H = 10. The flow in each quadrant is now divided into 2 Hartmann layers, on the plate and on the side walls, with a transverse wake emanating from the tip of the plate which diverges as it leaves the plate. This wake divides the core flow into two regions, the one above the wake being stagnant, and the one below the wake moving with a mean velocity equal to half the plate velocity. The current flow is limited to the region adjacent to the plate (i.e. it does not fill the whole duct), and is further limited to the two Hartmann layers and the transverse wake. Very little current flows in the core of the flow adjacent to the plate, and the current forms a closed loop up one Hartmann layer, across the diverging wake and back down the other Hartmann layer.

If this result is compared with Hasimoto's exact solution, great similarity can be seen. The effect of placing a limit on the length of the immersed plate and of imposing the upper wall of the duct makes very little difference to the solution. The side walls (perpendicular to the magnetic field) do have a marked effect,since they introduce the Hartmann layers which terminate the developing wakes and provide current return paths.

4.5.3 Top and Bottom Walls Moving

The third dynamically excited case was primarily investigated since the O.H.D. version of the flow could be compared with an analytical solution (see section 4.3.4), but it does also provide an interesting M.H.D. situation (see Figures 4.5.6 and 4.5.7). The O.H.D. velocity distribution displays a

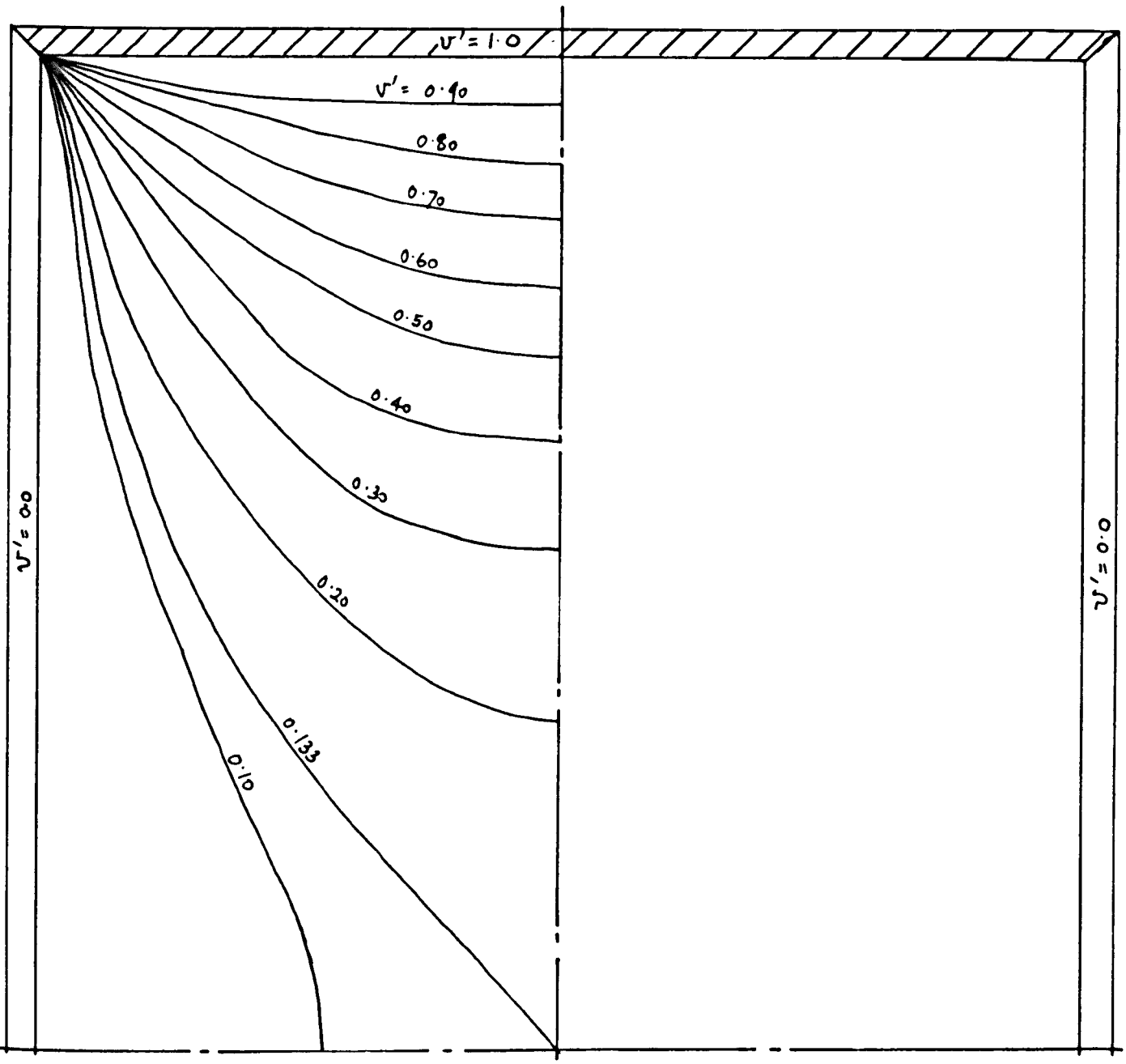

VELOCITY CONTOURS.

O.H.D. FLOW - TOP & BOTTOM WALLS MOVING (COMPUTER SOLUTION) FIGURE 4.5.6.

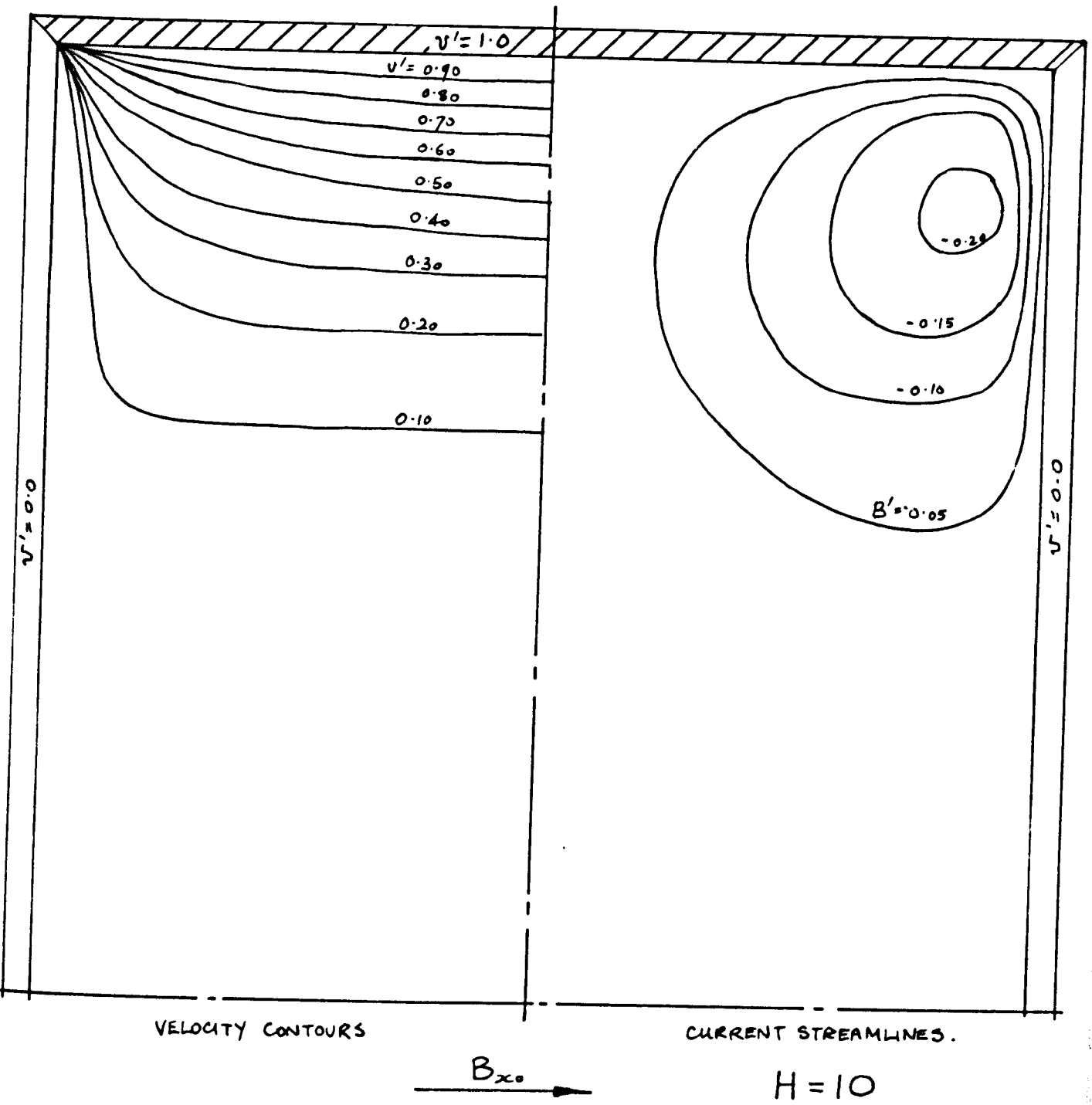

M.H.D. FLOW - TOP & BOTTOM WALLS MOVING (COMPUTER SOLUTION). FIGURE 4.5.7. NON-CONDUCTING WALLS

gradual decrease about the apex at the discontinuity in wall velocity, (cf. Figure 4.5.1), but when the magnetic field is applied, the fluid velocity is limited to a boundary layer on the moving wall of thickness $O\left(\frac{d_1}{\sqrt{H}}\right)$. The current is also limited to this layer and flows diffusely in the core of the layer returning through an abbreviated Hartmann Layer on the side walls; the transverse current flow along the moving wall feeding the core flow. In the limit as $H \to \infty$, the plate would become completely ineffective in exciting any flow in the duct, as the boundary layer thickness tends to zero.

4.5.4. Variation of Mean Velocity with Hartmann Number for Dynamically Excited Cases

Figure 4.5.8 shows the variation of mean velocity with Hartmann Number for the three cases investigated in this Chapter.

(a) Half Side Walls Moving

The mean velocity rises initially with increasing Hartmann Number, but quickly asymptotes to the theoretical $H \to \infty$ limit, which corresponds to the situation when all the fluid adjacent to the moving portion of the walls is moving with the moving wall velocity. The reason for the swift approach to this limit is the symmetry of the transverse boundary layer about the y = const. line, (at the level of the discontinuity in wall velocity).

(b) Immersed Plate Moving

In this case, the mean velocity decreases with increasing Hartmann Number to the limiting value at $H \to \infty$, which corresponds to all the fluid adjacent to the plate moving with half the plate velocity. This trend, which is contrary to that experienced in case (a) may be explained by considering that the plate in case (b) initially influences a large portion

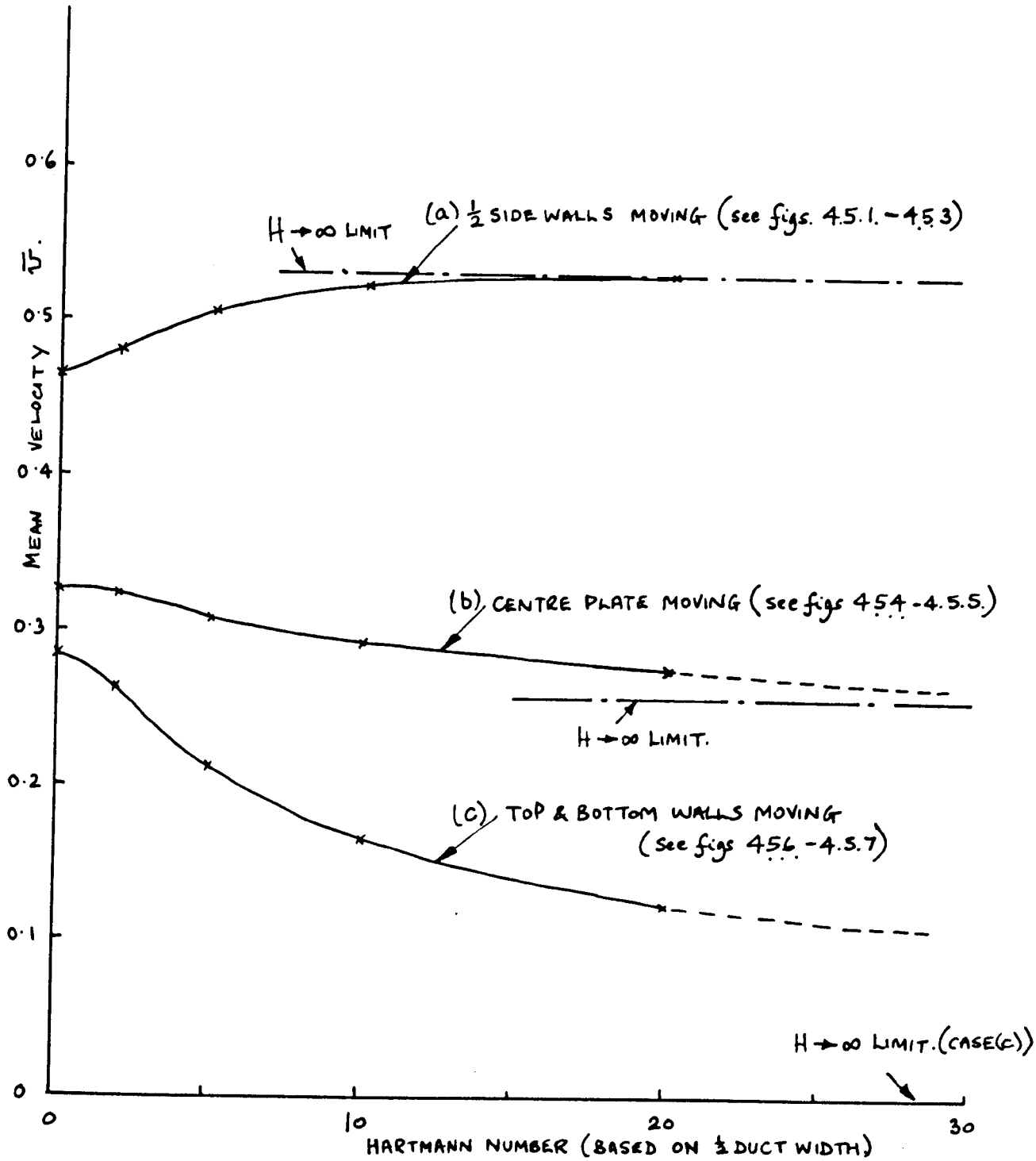

VARIATION OF MEAN VELOCITY WITH HARTMANN NUMBER FOR CASES WITH MOVING BOUNDARIES.
(FROM COMPUTER SOLUTIONS)

FIGURE 4.5.8.

of the central part of the duct cross section and has its effect reduced to the adjacent portions by the application of the magnetic field, whereas in case (a) the O.H.D. flow only shows a small influence on the central portion of the cross section, and this is increased with increasing M.H.D. interaction, e.g. consider the area enclosed between the 0.5 contour and the 1.0 contour for each case and the change that occurs in moving from O.H.D. to M.H.D. flow. Case (a) shows an increase in area, and case (b) a decrease. The slower approach to the $H \to \infty$ limit in this case cf. case (a) is caused by the asymmetry of the profiles about the same y = const. lines.

(c) Top and Bottom Walls Moving

As already stated, the effect of increasing the M.H.D. interaction is to reduce the influence of the moving plate on the flow and this is reflected in the decrease of mean velocity with increasing Hartmann Number; in the limit as $H \to \infty$, the mean velocity will tend to zero (see Figure 4.5.8). The rate of approach to the asymptote after H = 10 is doubtful, since the inaccuracy of the finite difference mesh is particularly pronounced in this situation. The flow is limited to the moving wall boundary layer and so the mean velocity only has contributions from this region, where the accuracy of the finite-difference method is worst. Because of the lower accuracy at H = 20, it is likely that this value of $\bar{U}$ given in Figure 4.5.8 is slightly inaccurate and the extrapolation is dubious. The general trend is, however, as expected.

5. EXPERIMENTAL INVESTIGATION OF COMBUSTION PLASMA M.H.D. FLOWS

5.1 Description of the Problem and the Necessity for an Experimental Approach

The main investigation in this thesis is concerned with magneto-viscous interactions in combustion plasma flows under the influence of transverse magnetic fields. The high Hartmann Numbers which will be produced in M.H.D. generators of any appreciable size suggest that such interactions will be of considerable importance in their design, (e.g. a 25 MW (electrical output) generator will have a Hartmann Number $\sim 10^3$),

The theoretical approach which was pursued in the preceding chapters gives only a limited understanding of the phenomena experienced in generators which employ combustion plasma for the working fluid, since the variation in properties with temperature and the non-scalar conductivity were not included. A complete theoretical treatment would be extremely difficult and in any case the quality of the results may well be masked by the enormous analytical effort required to solve the complete problem.

Earlier experimental work has limited relevance to this particular situation. The large bulk of isothermal experiments in mercury flows have given a clear understanding of many of the basic magneto-viscous interactions (e.g. Alty (1966), Hunt and Malcolm (1968), Alpher et al (1960)), in which transverse wakes appear under the action of transverse fields. Although they cannot give any indication of the magnitude of the effects when they are transposed into the combustion plasma medium, these experiments have demonstrated the validity of the theoretical work and in some cases extended it beyond the bounds of the present analytical solutions.

In the field of combustion plasma M.H.D. flows, most of the experiments carried out so far have been involved with bulk effects in generators e.g. the induced voltage. The experiments of the Stanford Institute for Plasma Research (Olin (1966), Sonju (1968)) were an attempt to open the field of detailed fluid-mechanic investigations of M.H.D. flows in hot gases. Olin actually used internal probes to investigate the turbulence damping effect of a transverse magnetic field, whereas Sonju made accurate skin friction measurements to investigate the effect of variable wall temperature on M.H.D. interactions in duct flow.

The experiments described in this thesis extend the present knowledge of combustion plasma M.H.D. flows in the specific case of pressure driven flows past thin plates which are inserted into rectangular ducts. The particular advantages of using this configuration for experimentation were two-fold:-

(a) it permitted high surface temperatures to be achieved on the surface of the plate (which minimisedthe effects of a cold boundary layer on the M.H.D. interaction).

(b) it enabled transverse boundary layers to be produced under M.H.D. conditions which enabled investigations of M.H.D. interactions to be carried out by velocity profile measurements in the core of the flow - so eliminating the difficulties of wall boundary layer probing.

Although high Hartmann Numbers can only be achieved in combustion plasma flows by utilising large ducts and extremely high gas temperatures to produce high electrical conductivity , these experiments at moderate Hartmann Number aimed to demonstrate the quality of effects which would be produced with greater magnitude in M.H.D. Generators.

The situations in which magneto-viscous interactions may occur in M.H.D. generators are likely to be three-dimensional and not closely comparable to the 2-D cases investigated here. However, several classes of possible interactions can be suggested:-

(a) In Faraday generators, there could be interactions between the main (generated) current flow, as it enters the collection electrodes, and the component of the applied field which is normal to these electrodes (produced by 'barrelling' of field lines). For modular electrodes, a configuration resembling that of Hunt and Malcolm (1968) would be achieved, with a resulting cross-flow.

(b) If a cross-connected generating duct is to be employed, with looped electrodes, (inclined to the axis of the duct) the flow adjacent to the 'insulator' wall (perpendicular to the applied field) will have a component of velocity parallel to a discontinuity in wall conductivity between the electrode loops and intermediate insulators. Thus, transverse wakes, analogous to those produced by a discontinuity in the velocity boundary condition on such a wall, will be produced; providing that the walls are hot.

(c) In Hall generators, in the region in which the longitudinal (induced) current flow enters the collection electrodes, (which envelop the whole cross-section of the duct) there will be a region of current flow into the wall experiencing a normal applied magnetic field, and a situation somewhat analogous to (a) will ensue.

A further complication is that the O.H.D. flow in large generators would be highly turbulent and the magnetic interactions may or may not remove the turbulence from the flow.

5.2. Experimental Conditions Required and Possible

The conditions of flow required in the experiment were:-

(a) $H \gg 1$

(b) $N \sim 1$

(c) $N_H < 1$

(d) $R < 10^3$.

(e) $M \ll 1$

These conditions ensured that M.H.D. effects developed in an acceptably short distance (a few widths of the duct), that the Hall Effect did not predominate (see section 8.2 for further discussion) and that turbulence phenomena did not mask the laminar M.H.D. interactions caused by the boundary layer on the inserted plate. They also ensured that compressibility effects were negligible and that magneto-viscous interactions were significant.

In M.H.D. generators, high gas velocities are desirable since the power density is $\propto \sigma B^2 v^2$. For these experiments, which did not involve net power extraction, much lower velocities were used, which also involved lower flowrates and pressures (and greater ease of experimentation). Lower velocities also assisted in satisfying conditions (b), (d) and (e) above. The critical parameter was H, and the principal variable in the parameter was the electrical conductivity of the gas. This is critically dependent on gas temperature and so a low heat loss gas duct had to be used, together with a combustion chamber with the maximum outlet temperature compatible with containment materials.

The scale of the experiment, which directly affected conditions (a), (b) and (d) was determined solely by economic restraints, and the magnetic field strength (B) was limited to ~ 1 weber/m^2, since highly sophisticated magnets could not be employed. (e.g. superconducting magnets or very high power air-core electromagnets).

It was decided to adopt an open-cycle configuration for the experimental M.H.D. duct, which was very similar to the layout of an open cycle M.H.D. generator, and to use the combustion products of propane and oxygen at atmospheric pressure, as a working fluid. The choice of a gaseous fuel was based on its convenience in control and handling (Propane was preferred to acetylene because of the much lower weight of cylinders/lb of gas and its somewhat safer operational characteristics - even though the flame temperature is 10% lower).

In order to obtain design data on the properties of this working fluid, a computer program, (Grayston (1966)) written to provide information for the C.E.G.B. M.H.D. Generator, was used to provide data for the conditions employed in these experiments.

The data corresponds to a stoichiometric mixture of oxygen and propane at one atmosphere pressure; the effect of varying the amount of 'seed' material in the flow was investigated. The purpose of introducing seed was to enhance the electrical conductivity of the gas with an easily ionised element. An element with low ionisation potential was required, and in common with most open cycle M.H.D. generation experiments potassium was selected and injected in the form of solid K_2SO_4 (Cesium would have been better, but it is extremely expensive. Ionisation Potentials:- Cs = 3.87 volt, K = 4.32 volt). The seed concentration was varied between 0.5 and 1.0 mol % K in the gas, since previous calculations for M.H.D. generators suggested that this seeding level produced the optimum enhancement of conductivity.

Figure 5.2.1 shows the variation of gas conductivity with temperature for varying seed flows and Figure 5.2.2. shows how the optimum seed flowrate can be determined. In this Figure, the adiabatic flame temperature and gas

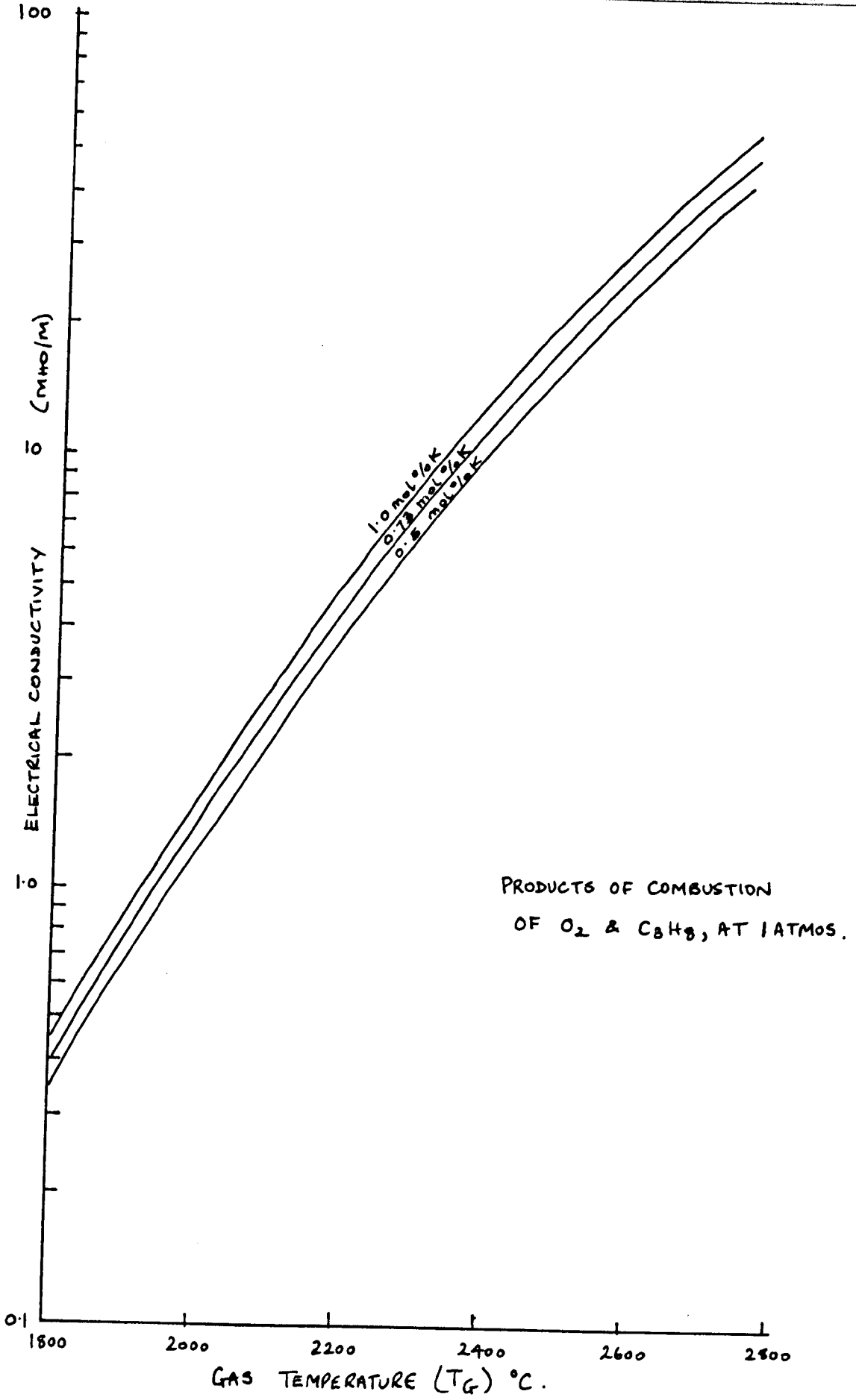

COMPUTED VARIATION OF GAS CONDUCTIVITY WITH TEMPERATURE.

FIGURE 5.2.1.

COMPUTED FLAME TEMPERATURE & CONDUCTIVITY WITH FINITE HEAT LOSS.

FIGURE 5.2.2.

COMPUTED VARIATION OF HALL PARAMETER WITH TEMPERATURE & SEED CONCENTRATION.

FIGURE 5.2.3.

DATA FROM GREEN ON VISCOSITY OF COMBUSTION GASES.

FIGURE 5.2.4.

conductivity are displayed for different heat loss levels (expressed as a percentage of the calorific value of the fuel). As expected, the flame temperature is seen to drop as the seed flowrate increases, because energy is required to vaporise, dissociate and ionise the seed and to bring it into thermal equilibrium with the gas. There are thus two opposing factors; increasing the seed flow gives extra conduction electrons to the gas and it reduces the conductivity of the gas itself by reducing its temperature. It was estimated from Figure 5.2.2 that there was an optimum seed level, at a heat loss of 30%, of 0.73 mol % K.

The Hall parameter was also calculated for the same ranges of seed flow and temperature and the variation is shown in Figure 5.2.3. The parameter lies in the range 0.3 - 0.7 for all the considered variation of properties, and so Hall effects were not likely to be significant in the experiments. (The transverse conductivity of the gas is reduced by a factor $\frac{1}{1+(\omega\tau)^2}$ i.e. $\sim$ 0.8 at 2300°C).

The viscosity of the combustion products was calculated using data by Green (1957) and is presented in Figure 5.2.4.

From the computer results for conductivity and the data for viscosity, it was possible to calculate the Hartmann Number and Interaction Parameter which could be achieved in practice. A possible configuration was selected as a 6" x 2" rectangular channel, which experienced a transverse field of 1 weber/m^2, (the duct was 2" wide in the direction of the magnetic field), and calculations were made for an assumed thermal input of 110 KW (gas velocity $\sim$30 ft/s) with a stoichiometric mixture of propane and oxygen, (these flowrates could conveniently be produced from bottled gas). The results are presented in Figures 5.2.5 and 5.2.6, which show that if a gas temperature of 2200°C could be achieved, then a Hartmann Number of $\sim$ 7 and

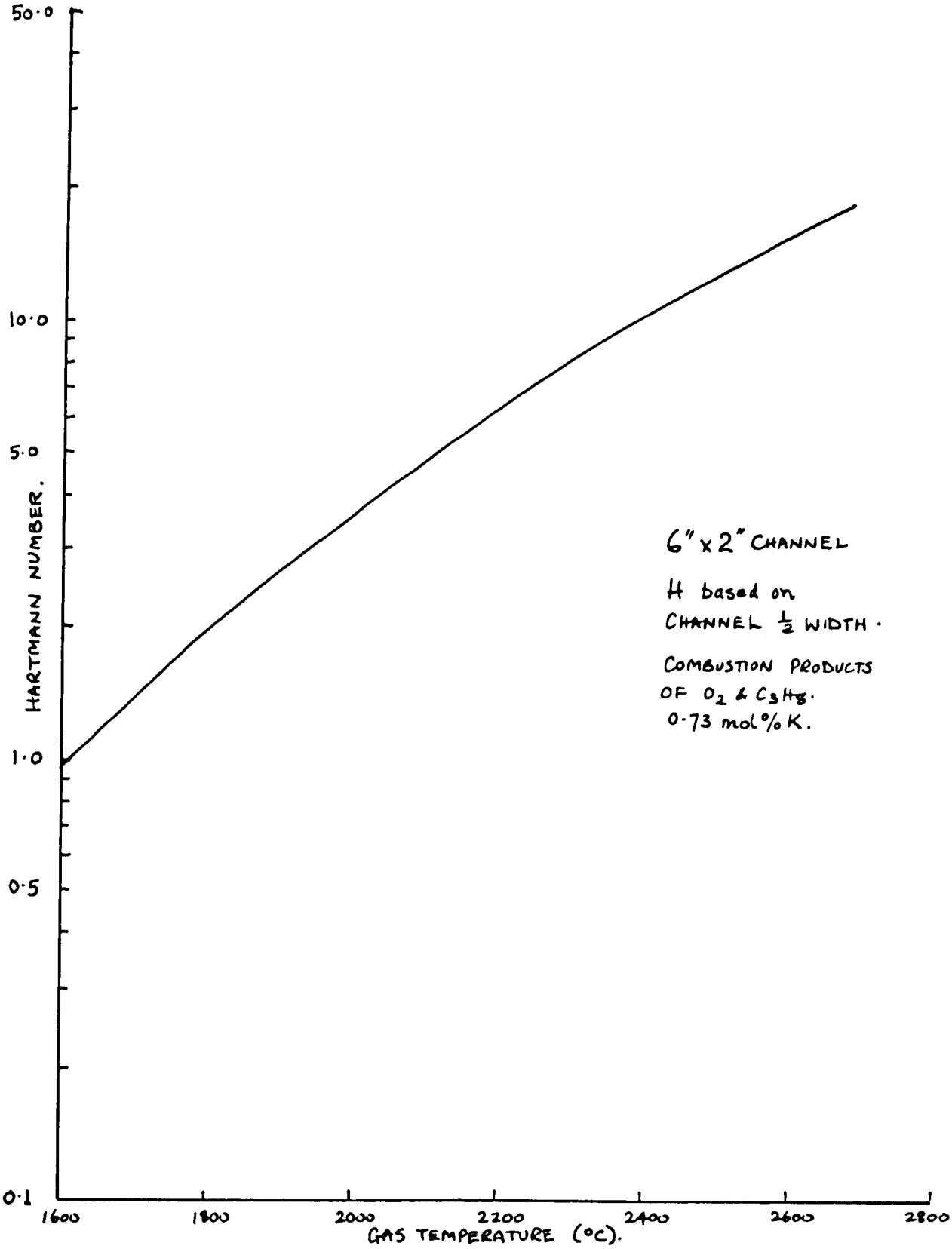

COMPUTED VARIATION OF HARTMANN NUMBER (H) WITH GAS TEMPERATURE.

FIGURE 5.2.5.

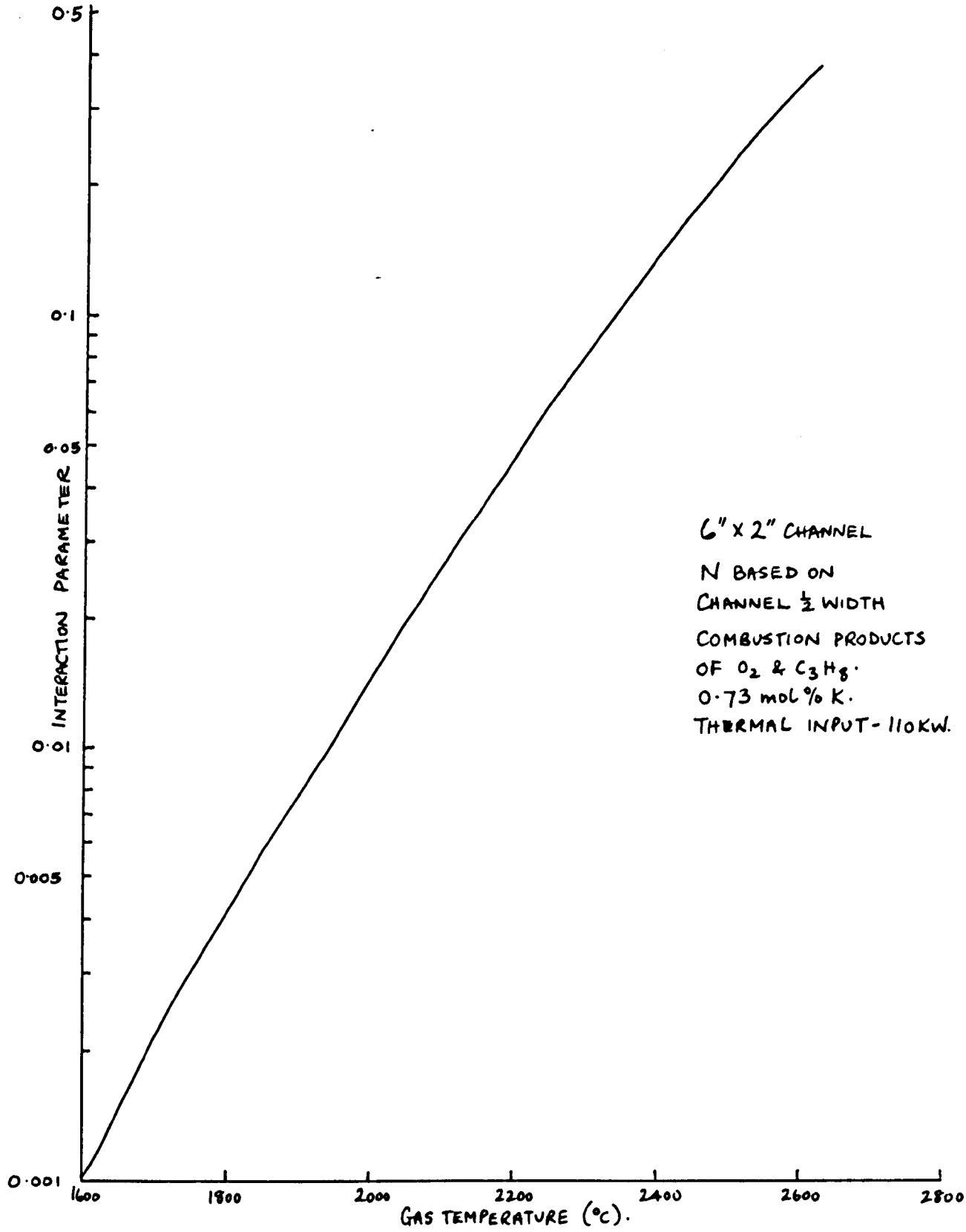

COMPUTED VARIATION OF INTERACTION PARAMETER (N) WITH GAS TEMPERATURE.

FIGURE 5.2.6.

an interaction parameter of ~ 0.05 could ensue, (based on the duct width of 1"). This implies that there would be a significant interaction within a distance equal to 20 times the width of the duct i.e. 20 in.

The Mach Number in the test duct was estimated to be ~ 0.01 for a thermal input of 110 KW; this eliminated the necessity to consider any possibility of significant compressibility effects.

The Reynolds Number (based on the duct half width) was also estimated for the test duct and was found to be $\sim 10^3$, at 2200°C and 110 KW thermal Input. This suggested that although the flow was not indisputably laminar, turbulence phenomena would not be predominant.

Since an adiabatic flame temperature of 2700°C is produced at the optimum seed flowrate (0.73 mol % K), 2200°C was a reasonable assumption for an achievable temperature in the M.H.D. duct. Later calculations and measurements substantiated this assumption and showed that it was probably exceeded in practice.

These calculations showed that if a 12" long magnetic field was employed, then the magneto-viscous interaction would be substantially developed within the length of the M.H.D. duct.

The selection of materials for containment of the high temperature gas stream also provided severe limitations on the scope of the experiment. The best refractory materials to withstand a high temperature gas stream which contain an alkali metal are the high purity oxide refractories. Dickson, Sanders and Tseung (1964) showed that a magnesite brick which has low iron oxide content and a high calcia to silica ratio proved to be most resistant to alkali attack over 1600°C. The melting point of pure magnesia is 2800°C and high purity magnesite is somewhat lower. Although the melting point of zirconia is comparable (2715°C) and its resistance to alkali att

is also good, it was not favoured for use in combustion chamber and duct linings because of its unfortunate behaviour during thermal cycling. (It suffers a structural change in the crystal lattice at about 1000°C). Stabilised zirconias (e.g. with magnesia or calcia) can be used however, and these have reasonable life under cycling conditions, although they do not compare well with magnesia in this mode of operation.

Zirconia is however one of the few refractory materials which can be used as a high temperature electrical conductor, under these conditions of alkali metal vapour attack. The electrical conductivity of magnesia and zirconia (data from Ryshkewitch (1960)) is shown in Figure 5.2.7, from which it can be seen that zirconia has a conductivity which is three orders of magnitude greater than magnesia over a large temperature range. Assuming that the gas conductivity is ~ 10 mho/m, then assuming a refractory temperature of 1800°C, $\frac{\sigma_{ZrO_2}}{\sigma_{gas}} \sim 10$ & $\frac{\sigma_{MgO}}{\sigma_{gas}} \sim 0{\cdot}02$

Thus a duct lining of magnesia would effectively be an electrically insulating duct and zirconia could be considered to be a good conductor with respect to the gas conductivity (although its performance would not match the equivalent performance of copper in mercury flows, when $\frac{\sigma_{Cu}}{\sigma_{Hg}} \sim 50$).

For the combustion chamber, where an adiabatic wall condition would be desirable, the maximum wall surface temperature had to be adopted. If magnesia had been used as a hot face material, then temperatures well in excess of 2000°C could have been allowed. But since the thermal conductivity of magnesite brick is relatively high (~ 20 CHU/ft^{2}hr°C/in) compared with a good insulation refractory such as silica fibre (~ 1 CHU/ft^{2}hr°C/in), and its use would necessitate an excessively thick wall to reduce the external temperature to < 100°C, a composite wall lining had to be adopted, using intermediate insulating refractory materials up to their limiting operating temperature.

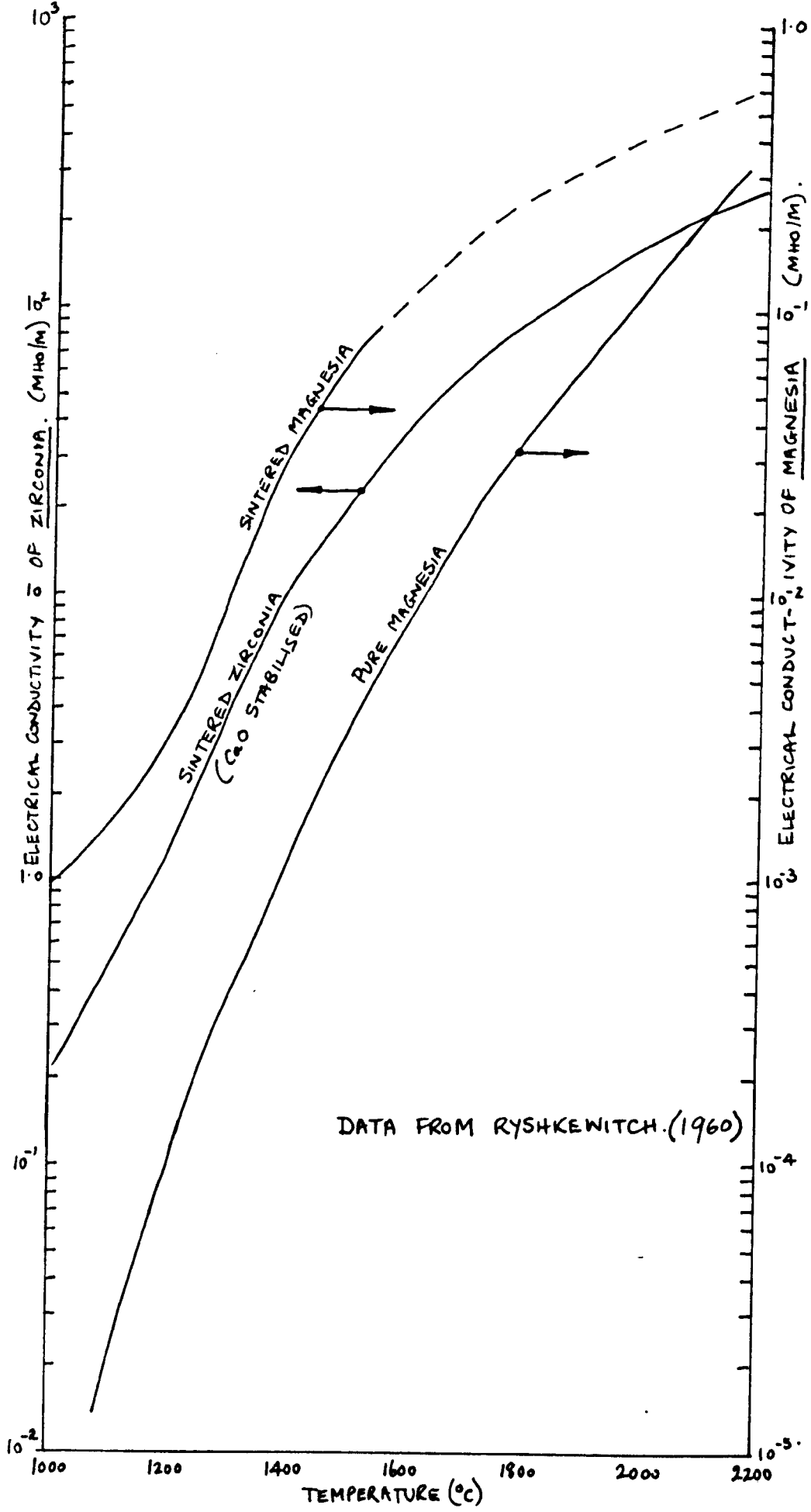

ELECTRICAL CONDUCTIVITY OF MAGNESIA & ZIRCONIA. FIGURE 5.2.7.

In the M.H.D. duct, where the thickness of insulation was limited by the size of the magnet gap, a completely insulated duct would not have been feasible, (this would in any case have wasted a very large proportion of the working volume within the magnet gap). Consequently, a water-cooled duct was adopted, even though this increased the heat losses from the duct. A compromise which employed some refractory insulation within a water-cooled duct was the most satisfactory solution.

A 6" x 2" duct was used as suggested earlier and $1\frac{1}{2}$" of insulation together with $\frac{1}{2}$" for a water-cooling passage was allowed on each side of the duct; thus a 6" gap magnet was required, with a pole face 6" high and 12" long and flux density 1 weber/m^2 across the gap.

The important design feature which needed verification was the ability to produce a mean gas temperature of 2200°C or more in the experimental M.H.D. duct. Discussion of this must wait until a more detailed design of the combustion chamber and duct has been presented. Estimates of heat losses are included in the description of the design of the apparatus in the next chapter.

A wall temperature as near as possible to the gas temperature was required in order to provide a hot (electrically conducting) boundary layer on the walls of the M.H.D. test section. The low temperature of the duct walls produced by water-cooling and limited insulation in the test-section would not have been satisfactory in this respect, and the only method of achieving a higher surface temperature was to immerse a refractory plate into the gas stream where it was able to take up a temperature which was intermediate between the gas temperature and the duct wall temperature.

This implied that any M.H.D. interaction which would be produced by the boundary layers of the duct walls would be small, and the only hope of producing a significant interaction would be to use inserted plates. The estimates of the temperature of the duct wall of the M.H.D. test section are presented in section 6.1.

5.3. Experimental Measurements Required and Possible

5.3.1 Measurement of Gas Velocity

In order to investigate the interactions of a transverse magnetic field on the flow of high temperature gases, a device capable of measuring velocity profiles within the test duct was required. The instrument had to be capable of producing 2-D velocity profiles while withstanding extreme conditions of temperature and deposition from the gas stream. The two instruments considered were (a) water-cooled pitot-static probes and (b) water-cooled hot-film anemometers. Because of the unproven reliability and extreme cost of (b), the pitot static probe was selected for these experiments (see section 6.2 for full description of probe).

Pitot probes have been used before in M.H.D. flows, (East (1964), Hunt (1967), Hunt and Malcolm (1968), Olin (1966)), both in hot gas flows and in mercury flows, and discussion has taken place regarding the corrections which should be applied to the readings of total pressure in M.H.D. flows.

The general result is that a correction factor of $(1 + K.\ N)$ must be applied to the velocity head measured in constant property flows. Experimentally, the value of K was found by East (1964) and Hunt (1967) to be ~ 0.4.

In these experiments the interaction parameter based on the duct $\frac{1}{2}$ width d_1 was ~ 0.1 and so the interaction parameter based on a probe diameter d_p given by $d_p/d_1 \sim 0.1$, (i.e. the maximum tolerable size of probe) would be 0.01 and therefore the correction to the velocity head was $\sim 1\%$.

In practice, the use of a water-cooled probe in a hot gas flow produced non-uniform conductivity effects around the probe and the simple theory was not strictly applicable. However, because of the tendency of a cold boundary layer to exclude the possibility of induced current flow, it was most likely that the effect of water cooling the probe would be to lessen the M.H.D. correction factor even more.

Two further correction terms had to be considered, viz. the viscous term and the density variation term. The former is important when the Reynolds Number (based on the probe diameter) is small. Schowalter and Blaker (1961) showed that for flow over a cylinder this term is small (<5%) for $Re_{\frac{1}{8}} > 20$. For a probe of 1/8" diameter, (cf. 2" wide duct) $Re_{\frac{1}{8}} \sim 70$, and the viscous correction would be very small.

If absolute measurements of velocity were to be made, however, this correction term would have been needed for the actual probe design being used. This calibration would normally be carried out at the same Reynolds Number in cold air in a uniform-velocity calibrated nozzle. However, in order to achieve the Reynolds Number, which was experienced in the hot gas duct, in the cold air flow, an extremely low velocity would have to be used and this would result in a velocity head which would be too small to be measured by available instruments. (The low velocity is caused by the increased density and lower viscosity of cold air cf. hot gas).

The velocity head encountered in the hot gas flow was $\sim$ 0.03 in.w.g., which was measurable using commercially available equipment, but a cold air flow at the same Reynolds Number would produce only $\sim$ 0.0004 in.w.g.

The only way to have overcome this impasse would have been to use a more viscous fluid; in fact the parameter which determines the size of velocity head produced by a fluid at a fixed Reynolds Number is μ^2/ρ

($\because v\alpha \mu/\rho$ at constant Re and constant geometry and velocity head $\alpha \rho v^2$). This parameter was calculated for water at 16°C and 4°C and air at 16°C. Compared with air, water produced velocity heads 5 x and 9x greater at 16°C and 4°C. Thus one way of overcoming the calibration difficulty would have been to use cold water, which would have brought the velocity head to within the range of the most sensitive micro-manometers; even so, the boundary layer adjacent to the probe would not be allowed for.

However, the density correction term posed altogether a more serious problem. It arose because the $\rho v \frac{dv}{dz}$ term in the incompressible equation of motion cannot be integrated along the stagnation streamline simply to give the traditional $\frac{1}{2}\rho v^2$ expression for velocity head. If a fluid with varying density is being considered (in the thermal boundary layer on the probe surface, the gas temperature varied from the free stream temperature of $\sim$2400°C to a surface temperature of $\sim$200°C), a correction term of the form $-\int \frac{v^2}{2} \frac{\partial \rho}{\partial z} dz$ must be applied to the measured differential pressure, (total-static) to determine the true value of the so-called velocity head $\frac{1}{2}\rho v^2$. Because of the extreme difficulty in measuring, or even predicting theoretically, the value of v & $\frac{\partial \rho}{\partial z}$ along the stagnation streamline in order to estimate this term, and because for small M.H.D. interactions the value of the term would not differ appreciably from its value in ordinary hydrodynamic flow, it was decided to make only comparative measurements between O.H.D. and M.H.D. flows and not to attempt absolute measurements of velocity.

Variation in density distributions between equivalent O.H.D. and M.H.D. flows could be caused by changes in local temperature which may, in turn, be caused by

(a) Joule heating effects.

(b) Changes in velocity profiles and turbulence levels, which may affect the convective transfer of heat.

The joule heating effect is discussed further in section 8.1, but it was assumed that for the low M.H.D. interactions expected in these experiments, changes in density distribution produced by joule heating and differences in convection mechanisms would not be appreciable, since the temperature distribution was dominated by radiation to the duct walls.

The decision to make only comparative measurements between O.H.D. and M.H.D. flows (the only experimental parameter which was varied between O.H.D. and M.H.D. flows was the magnetic field - which in turn affected the overall pressure gradient along the duct and the velocity distribution - the total mass flowrate remained constant) eliminated the need for the calibration of the probe to determine the viscous effect.

It was decided to use a pitot-static probe, rather than a simple pitot probe with wall static tappings, to eliminate the possibility of transverse pressure gradients disturbing the measurements of differential pressure. Transverse pressure gradients would occur in regions of developing flow and in the presence of Hall currents, but the effect of the induced (B_z) field in producing transverse pressure gradients would be negligible.

In isothermal measurements using pitot-static probes, the differential pressure between total and static tappings is equated to the velocity head, $h = \frac{1}{2}\rho v^2$, and a knowledge of the fluid density enables the local velocity to be deduced. Because of the difficulty of estimating the local fluid density in this case (no temperature profiles could be measured - see section 3.3.2), it was decided to present the profile measurements as profiles of $\sqrt{h}$, which in the case of isothermal flows would be simply the velocity multiplied by a constant factor. In hot gas flows, with cooled walls, some variation in density is to be expected near the walls, and so the $\sqrt{h}$ profiles are not similar to the true velocity profiles in these regions. But for reasons described

earlier, changes in density distribution between M.H.D. and O.H.D. flows were not expected to be dominant compared with the changes in velocity caused by the magneto-viscous interaction.

5.3.2 Measurement of Gas Temperature

The range of gas temperatures which had to be measured in the experiment (2000 - 2600°C) were in the accepted working range of the Sodium D-line Reversal Technique (see Appendix C for full description) with a tungsten strip lamp used as a light source. Measurements of gas temperature were useful for optimising flow conditions to give the maximum gas temperature (and hence maximum electrical conductivity) in the test duct. The temperature measurement was much simpler than the direct measurement of electrical conductivity and was more suitable for routine measurement during experiments.

The method only produced bulk gas temperatures, however, and no experimental measurements of temperature profiles were obtained.

5.3.3 Measurement of Gas Conductivity

A simple method of measuring gas conductivity is to set up a small conduction cell by immersing two electrodes into the gas flow. If the current-voltage characteristics of the cell are then measured, it is possible to estimate the bulk electrical conductivity of the gases. (Brogan (1962), for example). The effect of the boundary layer on the electrodes is to produce a non-linear I-V curve, but if the slope of the curve is taken in the middle region, i.e. between the low voltage region where the boundary layer is predominant and the high voltage region where current saturation is experienced, then a representative value of bulk conductivity is obtained. This method is useful for approximate measurements of electrical conductivity, and has been applied to measurements in a variety of M.H.D. duct arrangements, e.g. English and Rantell (1968) used the method with a coal-oxygen M.H.D. Combustor.

Olson and Lary (1962) used an R.F. probe technique for measurements of electrical conductivity of high temperature gases, and the method was further developed by Taylor (1967) for measurements in an M.H.D. experiment.

The method is based on measurements of the dissipation of R.F. energy in the medium surrounding a coil which is fed with an R.F. signal from an oscillator/monitor unit. The level of dissipation is dependent on the electrical conductivity of the medium and the resistance of the coil (which may vary if the temperature of the medium varies).

Taylor found that thermal drift was so pronounced when using a sheathed coil, that changes in dissipation caused by the presence of a conducting medium could only be measured if the transient response of the R.F. circuit was measured when the gas flow was shut off.

Both Olson and Lary, and Taylor used gas cooled, refractory sheathed coils in ducts with cool walls. Such probes would not withstand the high heat flux conditions which would be produced by a refractory lined duct and so a water-cooled copper tube had to be used to make the coil for these experiments. This necessitated the use of demineralised water, to remove the possibility of a leakage path across the coil. Because the water cooled coil produced a region of cool non-conducting gas in its own immediate vicinity, there was no possibility of providing an external short circuit to the coil and no sheath was required.

The probe did not give a direct measurement of electrical conductivity and had to be calibrated with fluids of known conductivity (with a sheath over the coil to simulate the cold (non-conducting) boundary layer). Electrolytes (e.g. KCl) have been commonly used for this purpose in the past and the details of the calibration which was carried out with this coil are described in Appendix E. A possible objection to the use of electrolytes is their

vastly different dielectric constant compared with the dielectric constant of gases, which may affect the dissipation level. However, provided that $\sigma \gg \epsilon\omega$, where ω is the frequency of the imposed R.F. signal, and ϵ is the permittivity of the medium, then dielectric effects can be neglected. (This condition can be derived by considering the equation governing the induced magnetic field in the case of a steady sinusoidal response).
In fact this condition is satisfied both in the case of electrolytes and gas flows for an R.F. signal of $\sim$10 mc/s in the range 1 — 10 mho/m, although in the case of electrolytes ($\sigma/\epsilon\omega \sim 20$ at 1 mho/m), some slight dielectric effect is present and if the conductivity is any lower, the effect will no longer be negligible.

6. DESIGN AND CONSTRUCTION OF APPARATUS

6.1 Test Rig

6.1.1. Overall Thermal Design and Specification of Refractories

The rig needed to provide containment for the working fluid with the lowest possible heat losses compatible with safety and protection of ancillary equipment. The combustion chamber also acted as a seed evaporation chamber and delivered fully combusted gases laden with dissociated seed to the experimental M.H.D. duct and its dimensions were governed by seed evaporation rather than combustion.

(a) Combustion Chamber Heat Losses

It was required to reduce the combustion chamber heat losses as much as possible and so it was advantageous to have an extremely high thermal resistance across the wall. Since the rig was not to be run continuously, but only for relatively short test runs, a thermal design based on steady state conduction through the wall was not ideal. This would have necessitated a very large thickness of the hot-face magnesite refractory (high thermal conductivity) to reduce the interface temperature between the hot-face brick and the insulating brick to an acceptable level for the application of low conductivity aluminosilicate refractories. The maximum temperature which could be tolerated was $\sim 1600^{\circ}C$, and for an adiabatic flame temperature of $2900^{\circ}C$, the hot-face temperature would have been well in excess of $2000^{\circ}C$.

Only the transient period was considered, when heat was diffusing into the wall, and so a smaller thickness of magnesite brick could be selected, which would experience a temperature of $1600^{\circ}C$ at its backface after the time taken to pre-heat the chamber and to complete a test-run. A supplementary advantage of using a reduced thickness of hot-face brick was that the surface temperature rose more rapidly during thepre-heating

period, since the greater proximity of the insulating refractory restricted the diffusion of heat away from the surface. The critical thickness required was estimated to be 3", by assuming that if 2 hours were allowed for the diffusion of heat into the walls and the inner wall was maintained at 1600°C, then the characteristic distance to which this temperature level would have diffused would be $\sqrt{\alpha T}$ (where, α is the thermal diffusivity of magnesite (~ 0.03 ft^2/hr) and T is the characteristic time). Since the inner temperature would in fact rise from zero to over 2000°C, during a test run, this estimate of penetration thickness was high, and taking the warm-up period into account, a total test time of ~ 3 hours seemed feasible.

Because of the uncertainty involved in this calculation, and the complexity involved in undertaking a complete transient temperature study of the system, it was decided to build a trial combustion chamber. This exercise also provided useful experience in the construction and operation of high temperature combustion chambers and was used as a preliminary facility for electrical conductivity measurements. (See section 7.1).

The internal dimensions of the combustion chamber were determined by considering the residence time required to evaporate and dissociate the seed material. Assuming plug flow through the chamber with 110 KW thermal input, and assuming that a 6" x 6" cross-section was used, then for a 9" long combustion chamber, the residence time was calculated to be 60 ms. Experiments by Nettleton & Raask (1965) indicated that this would be sufficient for the dissociation K_2SO_4 seed of mean size 60μ at a flame temperature of 2600°C. (Their experiments indicated evaporation times $\sim$ 10 ms).

The cross-sectional dimensions of the chamber were chosen to give a shape which would easily match the required test duct shape and would give an acceptably low velocity in this high temperature region, which would reduce the

attack on the refractories to acceptable rates. (In fact, the rate of attack experienced in practice in this combustion chamber was quite acceptable and was limited to inter-granular attack and a glazing of the surface of the bricks) The results of the preliminary combustion chamber trials which are relevant to the present exercise are displayed in Figure 6.1.1, which shows the transient temperatures at different depths in the refractory lining. (Thermocouples were placed at ½" and 3" from the inner wall of the chamber). For these experiments the 3" magnesite hot face brick was surrounded by a lining of aluminosilicate insulating brick (also 3" thick) and a 2" layer of compressed low temperature and low conductivity insulation. (See Figure 6.1.3.). This composite wall produced an overall thermal resistance which was sufficient to maintain the outside wall temperature less than 100°C.

It can be seen from Figure 6.1.1 that the critical time, i.e. when the aluminosilicate refractory reached its maximum operating temperature of 1600°C, occurred 2 hr.20 min. after light-up. This would have allowed about 1½ hours for measurements to be made on the rig after allowing for an initial pre-heating period. In actual fact, the complete rig was designed to run under slight suction, whereas this trial combustion chamber was slightly pressurised, since the exhaust ran to atmosphere. Lower rates of temperature rise than those experienced in these trials were experienced in the refractory insulation of the rig and a longer period for experimentation was achieved.

The estimates of the required thermal resistance were made by considering the steady state heat flux from the combustion gases to the wall by forced convection and by radiation, for a variable inner wall temperature, and also by considering the heat flux by conduction through the wall, again with variable inner wall temperature (calculated by assuming linear heat flow). The inner wall temperature, and hence the actual heat flux, was

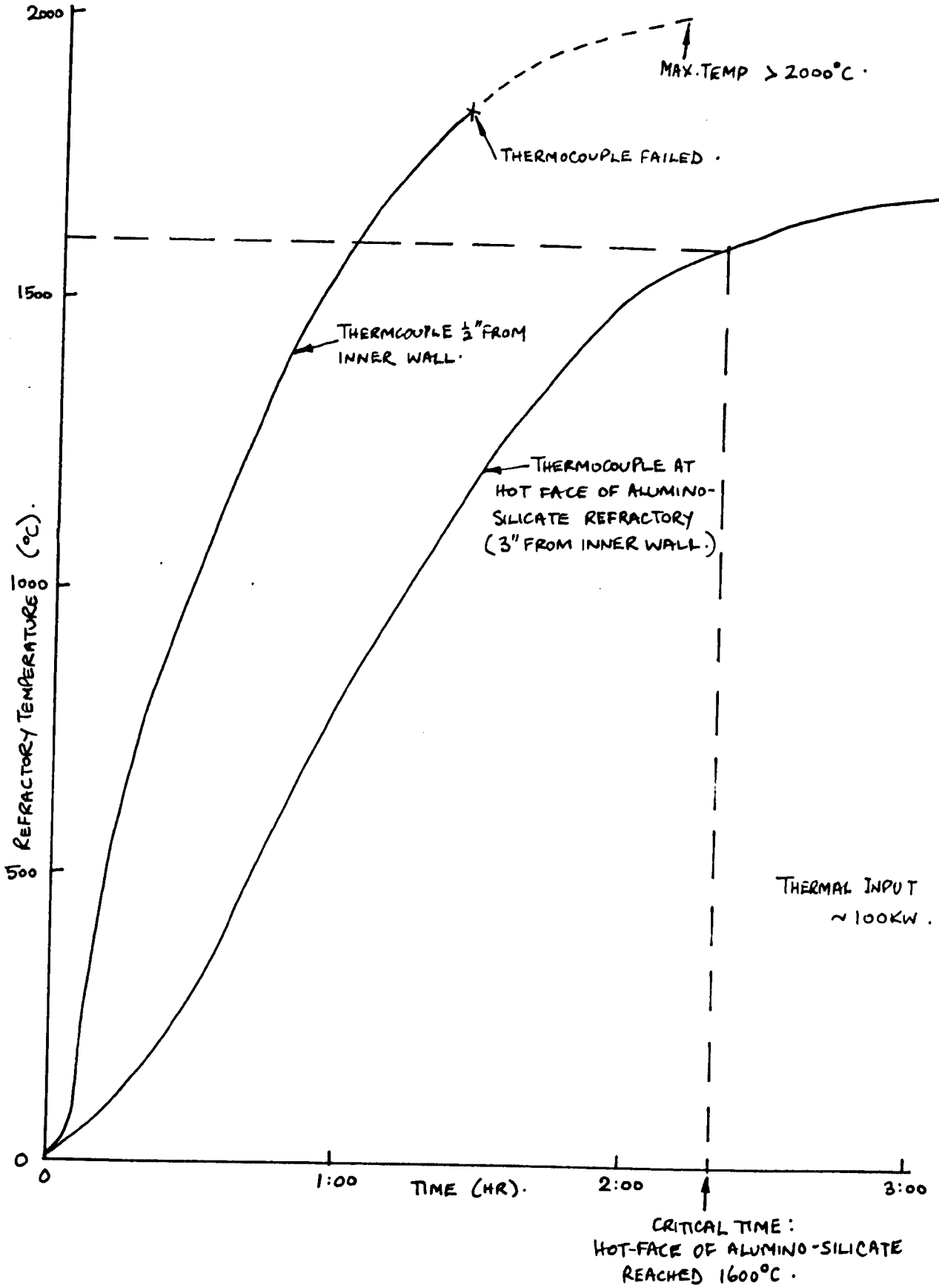

VARIATION OF REFRACTORY TEMPERATURES WITH TIME - COMBUSTION CHAMBER TRIAL.

FIGURE 6.1.1.

found by equating these two expressions (see Figure 6.1.2). The radiative and convective components of the heat flux were determined as follows:-

(i) Radiative Heat Flux from Gases

The gas emissivity was estimated by calculating the non-luminous emissivity of the CO_2 and H_2O in the flame. The increase in emissivity caused by the visible line emission of the seed material was neglected. The method of McAdams (1954) was used and indicated that a total emissivity of 0.008 would be achieved at 2500°C. This rather low value was attributed to the low beam length of the gas (6") and the absence of any particulate matter in the flame. To allow for possible luminous radiation an emissivity of 0.01 was assumed for the gas. Data for the emissivity of refractory bricks is unreliable, and a figure of 0.5 was assumed.

The radiative component of the heat flux was then calculated using the equation

$$q_r = \sigma \varepsilon_g \left(\frac{\varepsilon_w + 1}{2}\right)\left(T_g^4 - T_w^4\right) \qquad \ldots.6.1.1.$$

where the subscripts w and g refer to the conditions at the wall and in the core of the gas respectively.

(ii) Convective Heat Flux from Gases

An empirical relationship was developed by Bohm (see Schofield et al (1963)) for combustion gas flow in the refractory lined passages of brick regenerators and this was used to give an estimate of the convective component of the heat flux.

The heat transfer coefficient given by Bohm is:-

$$h_c = \frac{C_1 \cdot W_0^{0.8} \cdot T^{0.25}}{d^{0.333}} \qquad \ldots.6.1.2.$$

where W_0 = S.T.P. gas velocity and C_1 is a constant.

(b) M.H.D. Test Duct

The cross-sectional dimensions of this water-cooled duct were determined by considerations of the values of the Hartmann Number and Interaction Number, (see Chapter 5) and considerations of the maximum size of magnet which could be obtained. (see section 6.1.5). A 6" x 2" duct was considered to be the optimum design, which allowed for $1\frac{1}{2}$" of insulation at each side of the gas passage. It was found that if any thickness of magnesite less than 1" was used for the duct side walls, it was liable to collapse after a few runs because of cracks produced by thermal shock. Consequently, the side walls were made of 1" magnesite brick, with $\frac{1}{2}$" of compressible low conductivity silica fibre between the water-cooled external wall and the back of the brick. (See Figure 6.1.3). On the top and bottom walls, where there was no restriction on the thickness of insulation, $1\frac{1}{2}$" thick magnesite was used, together with $1\frac{1}{2}$" alumino-silicate insulating brick, to give a reduced heat loss from the duct compared with the side walls.

With these designs of combustion chamber and duct, the heat losses from the gas flow were estimated in order to estimate the gas temperature (and hence electrical conductivity) which would be obtained in the test duct. The surface temperature at the hot faces of the combustion chamber and duct linings was estimated from Figure 6.1.2 to be 2200°C and 1550°C (for side walls) respectively - this assumed mean gas temperatures of 2500°C in the combustion chamber and 2200°C in the duct. (Ideally, the calculations of duct gas temperature should have been done iteratively - but this approximate method was sufficient for our purposes).

CALCULATIONS FOR HEAT LOSSES THROUGH WALLS OF COMBUSTION CHAMBER & DUCT. FIGURE 6.1.2.

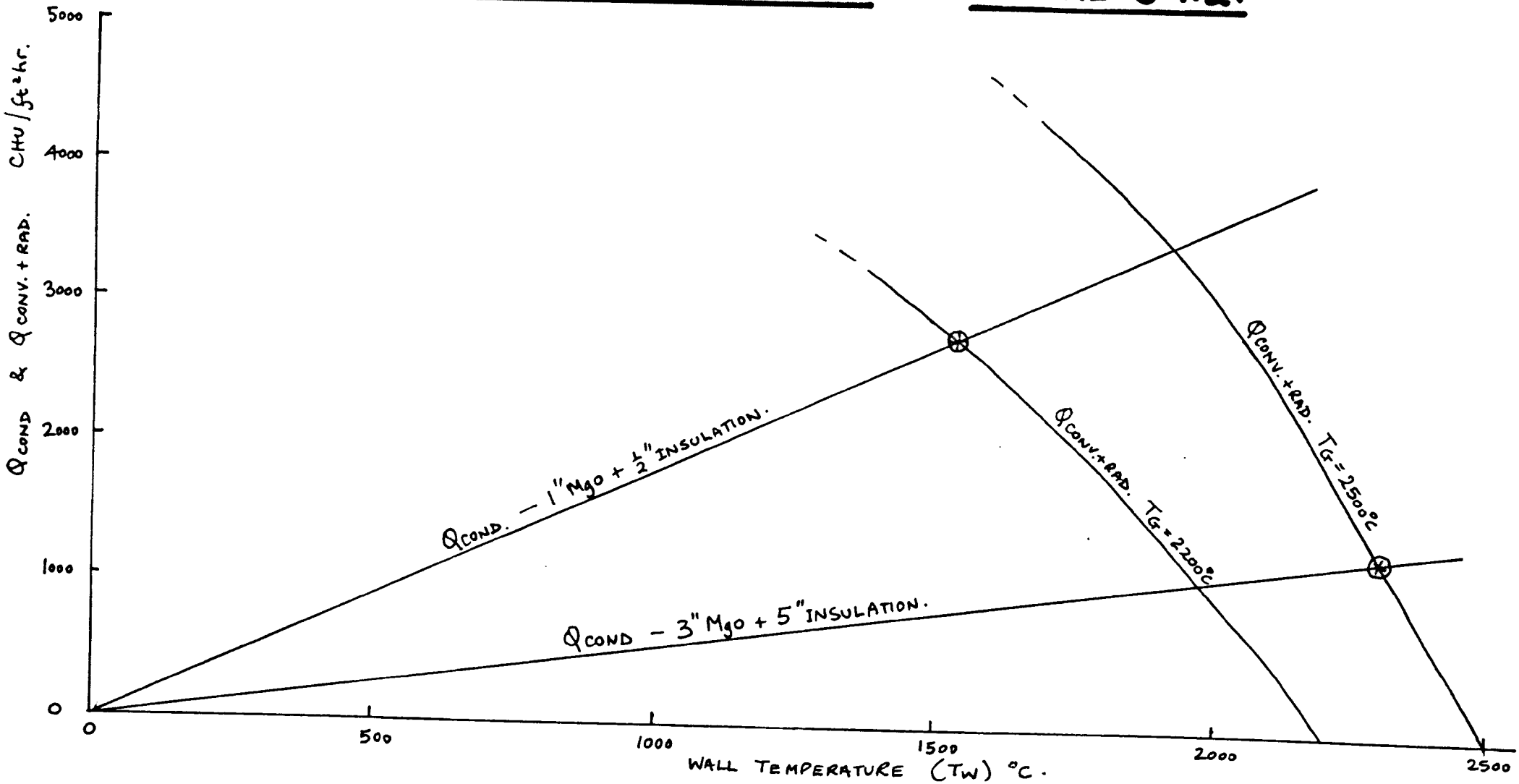

The heat lost to the refractory walls in the combustion chamber was estimated to be ~1.6 KW and in the test duct up to the end of the experimental section (assumed to be 2 ft long) ~ 3.9 KW. In addition, there were radiative losses through port-holes and along the exhaust duct (see Figure 6.1.3). Thus for a thermal input of 110 KW, which was assumed in Chapter 5, the total heat loss to the refractory walls was estimated to be 5% of the input. Assuming that the adiabatic flame temperature is 2780°C as predicted in Figure 5.2.2, then an approximate estimate of the gas temperature at a position 2 ft along the duct (assuming C_p is constant) gave T_g = 2640°C. This was a highly optimistic estimate; with random radiation losses included, together with combustion inefficiency and entrainment of air (since for practical purposes it is usual to run atmospheric ducts at pressures slightly less than atmospheric), then a rather lower exit temperature was expected.

The thermal performance of the complete rig was investigated during the commissioning trials and the results of gas temperature measurements made on the rig are presented in section 7.1.

6.1.2. Design and Construction of Combustion Chamber and Duct Work

(see Figures 6.1.3 and 6.1.4 and 6.1.5 and Plates 1 and 2)

Since no cooling was required for the combustion chamber, the refractory insulation was merely held in a rigid box, which gave access for the burner. Two port-holes at the exit end of the chamber were provided as a sight-path for optical measurements of gas temperature.

The flange plate at the junction between the combustion chamber and duct was provided with water-cooling since it was not fully insulated (see Figure 6.1.3) and similarly the test section and the exhaust section were provided with water-cooled walls.

SIDE VIEW OF RIG, SHOWING COMBUSTION CHAMBER & MAGNET

PLATE 1.

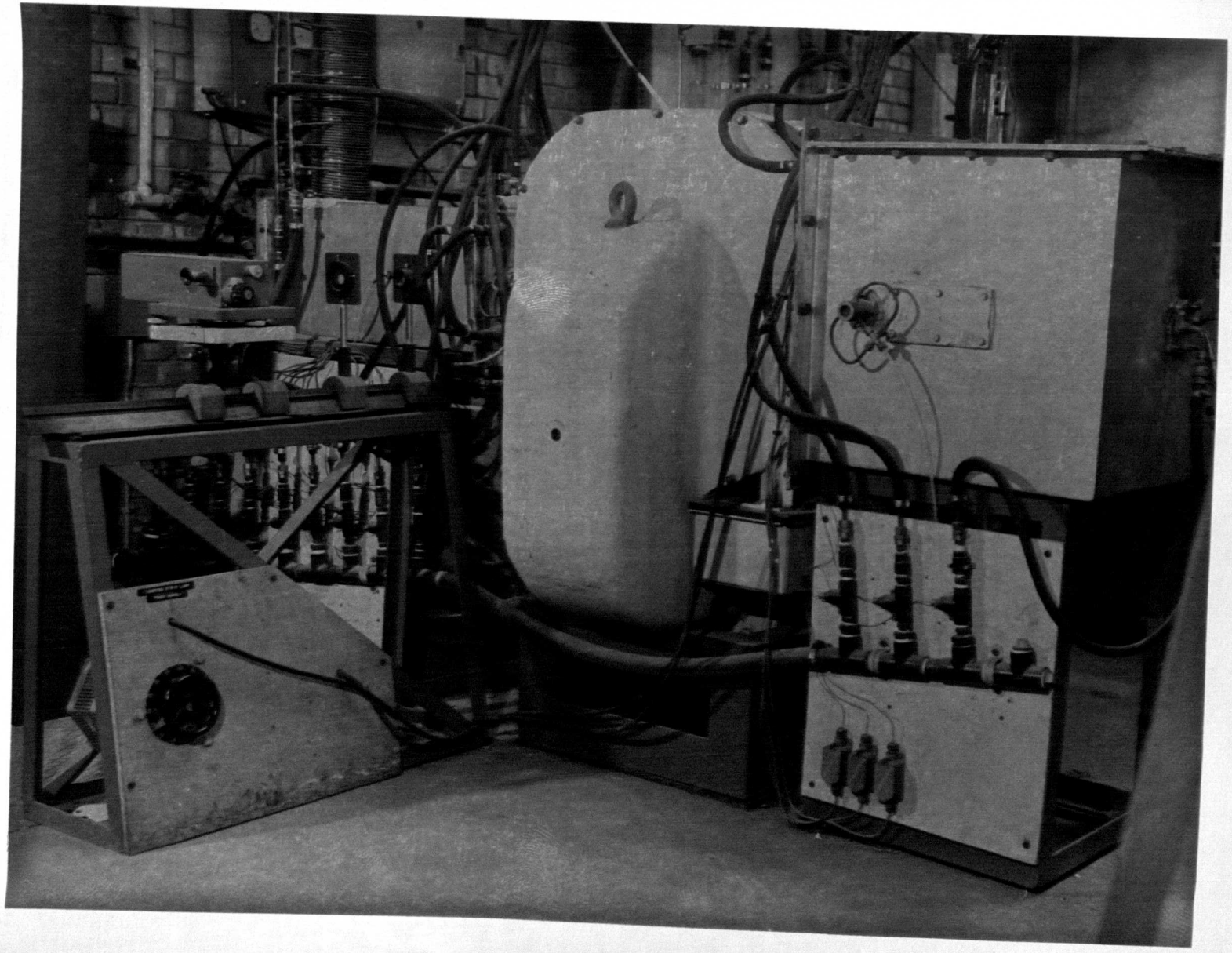

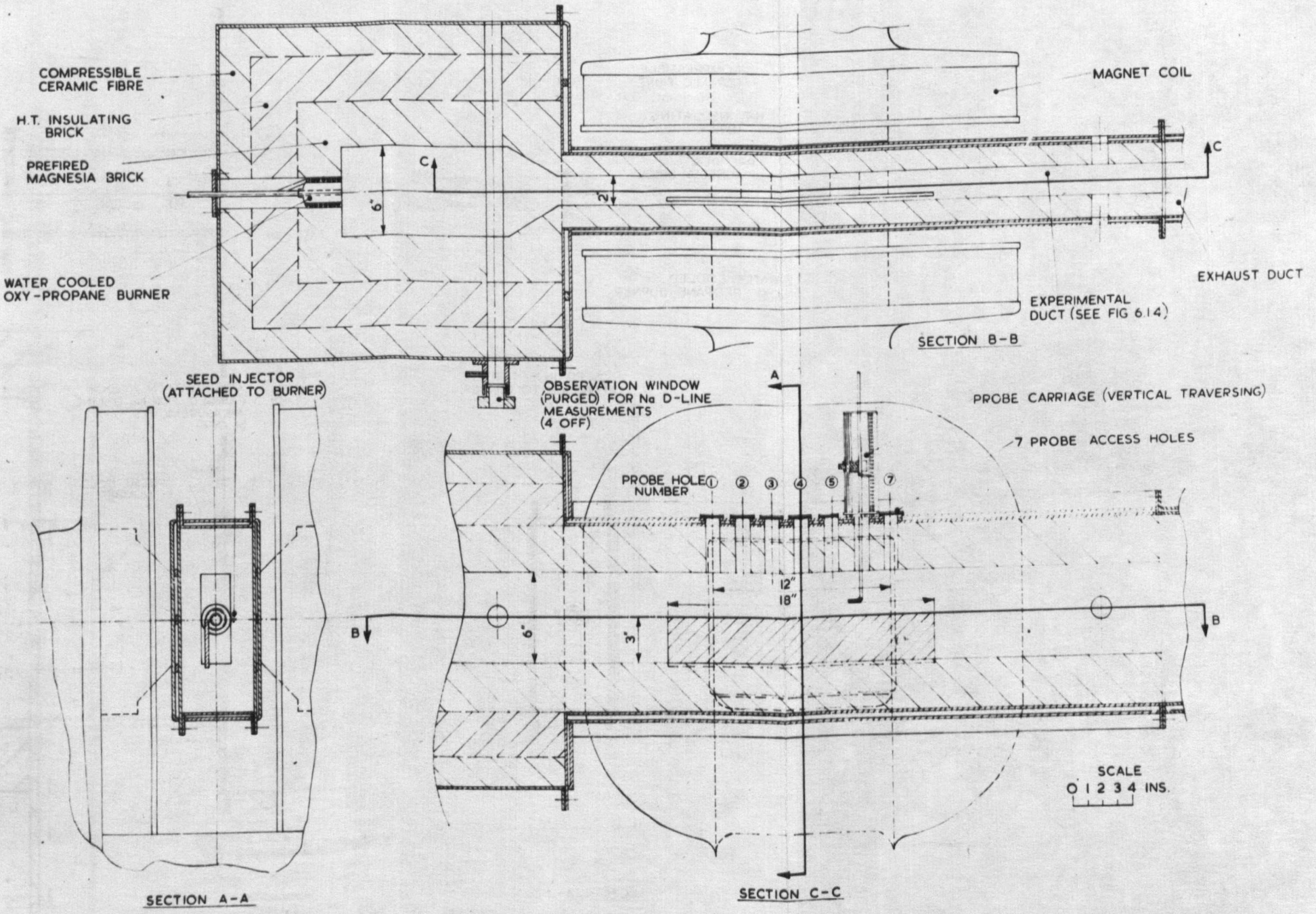

GENERAL ARRANGEMENT OF TEST RIG (DUCT AND COMBUSTION CHAMBER IN SECTION) FIG. 6.1.3

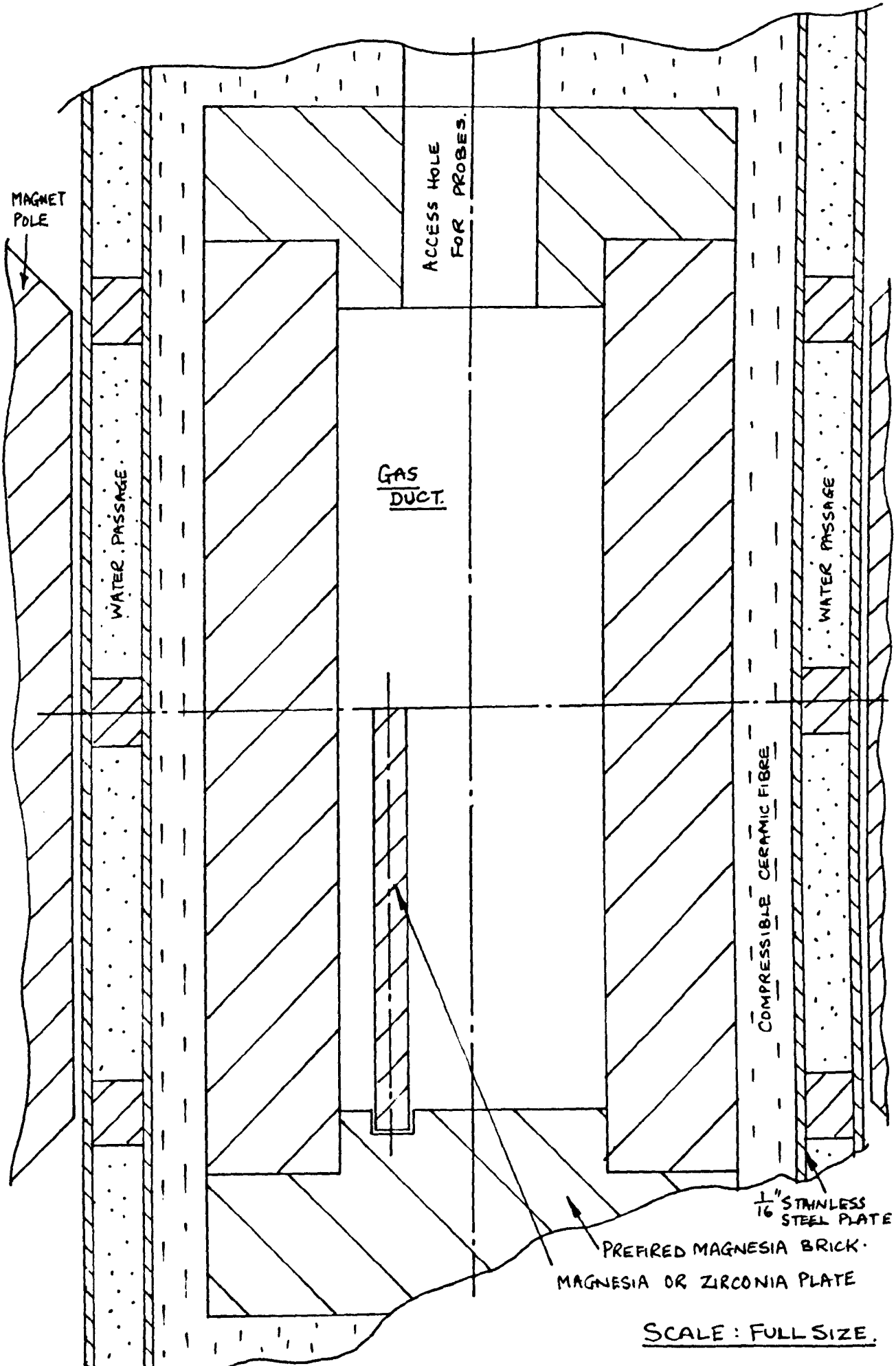

SCALE : FULL SIZE.

CROSS-SECTION OF EXPERIMENTAL DUCT . FIGURE 6.1.4.

The cooling system was a double-skin wall with water flowing around baffles, which also acted as spacers between the two skins.

Non-magnetic stainless steel was used for the test duct which was situated within the magnetic field and mild steel was used elsewhere.

The water flowed longitudinally along the test section and exhaust section and was divided into separate flows for each panel of the ductwork. The test section was designed so that the top and bottom covers could be removed easily for inspection and access to the test duct, for the installation of refractories.

The roof of the test duct was provided with 7 probe holes (1" diameter) for the insertion of traversing probes, and two further port-holes were provided at the end of the test section for the measurement of the gas exit temperature. The entry length of the test duct was determined by the size of the magnet coils, but it was large enough to suggest that the flow at entry to the M.H.D. section (i.e. the section within the magnet poles) was free from any large scale turbulence produced by mixing and swirl in the combustion chamber. The acceleration through the contraction at entry to the nozzle was beneficial in this respect. No measurements of turbulence levels in the duct were, however, attempted.

6.1.3. Burner System and Seed-Feeder

The burner which was selected for use in the combustion chamber was a B.O.C. "Sapphire" Burner which was adapted by attaching a water-cooling coil around its nozzle, together with an injection pipe for the seed material.

A mixing valve was incorporated upstream of the control valves in the burner unit and this fed premixed fuel and oxygen to the stabilising nozzle. The individual flows of oxygen and propane were produced by manifolds of gas bottles and reached the burner via a solenoid valve, flowmeter and non-return valve (see Figure 6.1.5).

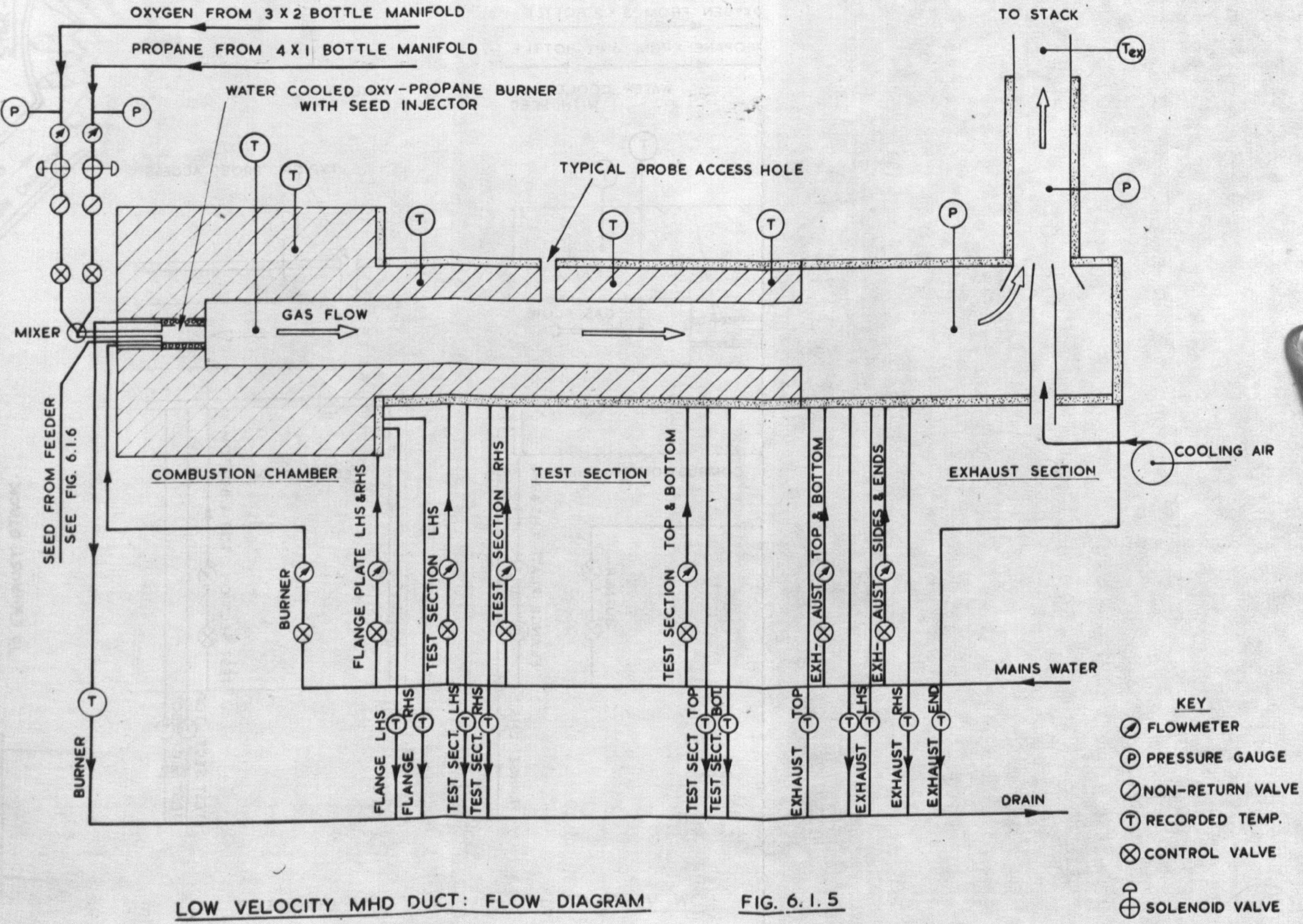

LOW VELOCITY MHD DUCT: FLOW DIAGRAM

FIG. 6.1.5

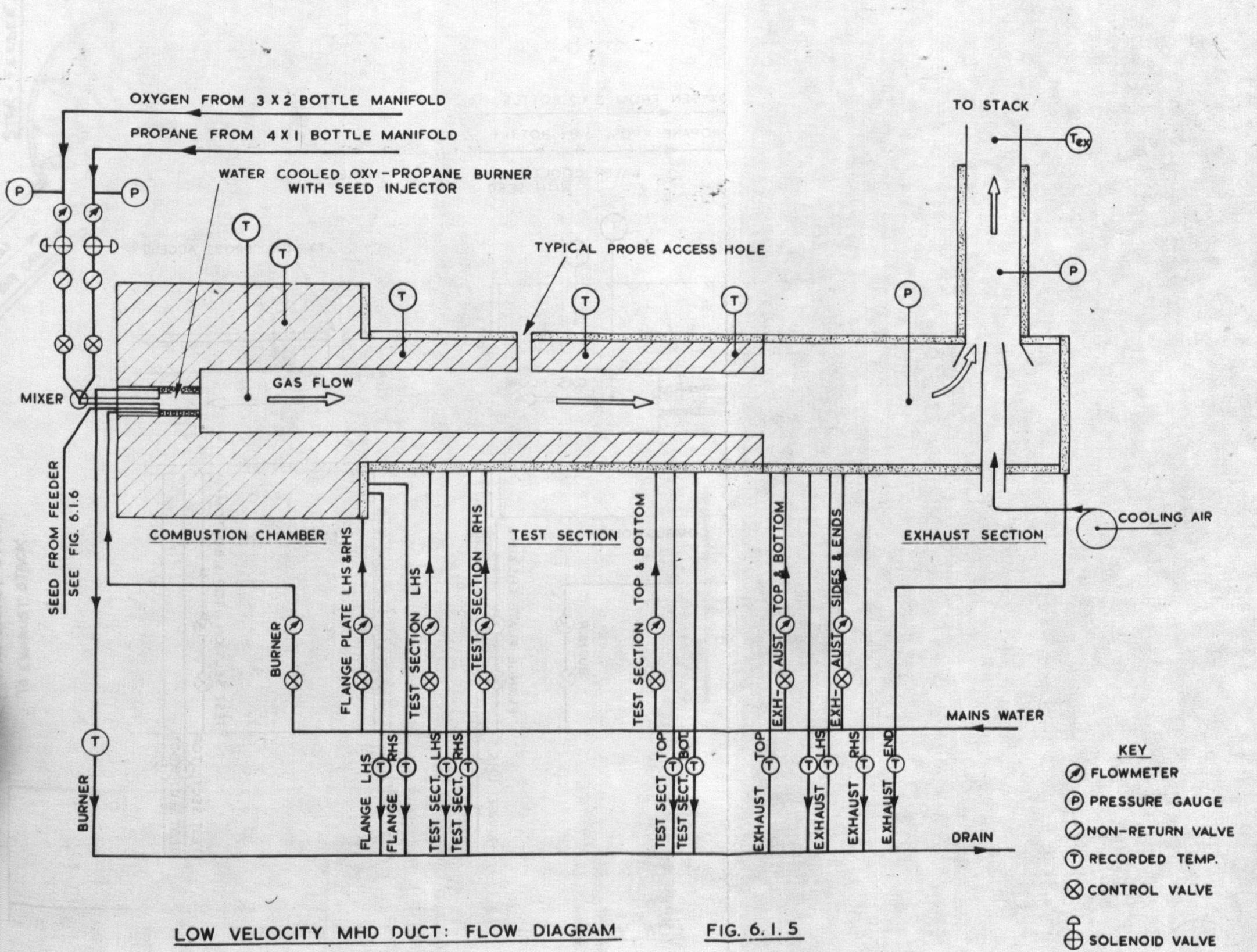

LOW VELOCITY MHD DUCT: FLOW DIAGRAM

FIG. 6.1.5

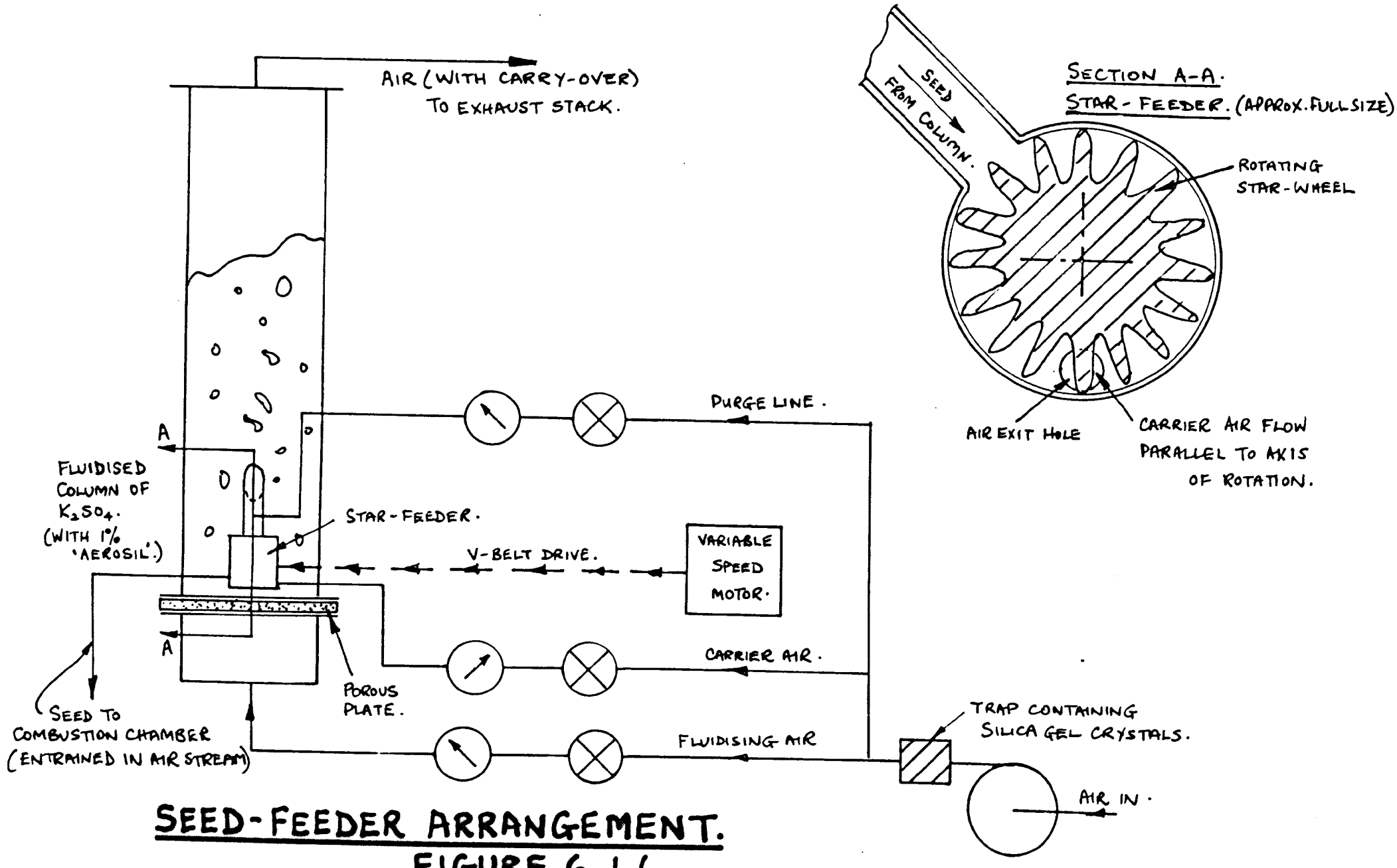

SEED-FEEDER ARRANGEMENT.
FIGURE 6.1.6.

The seed-feeder (see Figure 6.1.6), which supplied seed along a pneumatic line to the combustion chamber, consisted of a 6" diameter fluidised column of seed (K_2SO_4) which enabled the granular material ($\sim 60\mu$) to be transported and metered as a fluid. From the column, the seed fell under gravity down a feed pipe (at 45° to the vertical) into a star-feeder, which consisted of a rotating star-wheel within a cylindrical chamber. This transferred the seed to the carrier air line and thence to the combustion chamber.

It was found necessary to dry the fluidising air flow to prevent the column of seed from clogging. Also, following the recommendation of Cranfield (1966), 1% "Aerosil" by weight was added to the K_2SO_4 in order to improve its flow properties. (Aerosil is finely divided - sub-micron - silica, and reduces the inter-granular friction).

The calibration of the seed-feeder in terms of mass flow rate of seed is described fully in Appendix B.

6.1.4. Exhaust System (See Figure 6.1.5)

The flow of gas at exit from the test section entered an exhaust section which was water cooled with no additional insulation. This section contained an air ejector which provided sufficient dilution to reduce the temperature of the final gas flow to $\sim 200^{\circ}C$ and also provided $\sim$ 1" w.g. suction. The ejector was designed using the principles described by Kastner and Spooner (1950). The diluted exhaust then passed through a damper, which was used to give fine control of the differential pressure between the test section and atmosphere, and finally through a diffuser and an exhauster fan to atmosphere.

6.1.5. Control Instrumentation for Combustion Chamber and Ducts

(See Plate 2.)

Figure 6.1.5 is a flow diagram for the whole rig except for the magnet and probing instrumentation. The instrumentation shown on this diagram was necessary for the safe operation of the rig and the production of reproducible running conditions.

The flowrates of the oxygen and propane supplies were metered with conventional rotameters, and rotameters were also used for the monitoring of water flows to the various sections of the water cooled duct work. Chromel-Alumel thermocouples were used to monitor the water exit temperatures from these water cooled sections, and platinum/platinum 13% Rhodium thermocouples were installed to monitor the temperature in the refractory lining of the combustion chamber and test duct.

Pressures were monitored in the oxygen and propane delivery lines and also in the exhaust duct above and below the ejector. The gas temperature at exit from the rig was also monitored, but measurements of gas temperature in the hot zone were only undertaken intermittently using a manually operated sodium D-line technique (see Appendix C for a full description of this technique).

6.1.6. Magnet Specification

The electromagnet, which was designed and constructed by Lintott Engineering Limited, satisfied the specification that it must produce(within 5%) magnetic flux density of 1 weber/m^2 over a pole-face which was 12" x 6", with a pole gap of 6", using an available power supply, (motor-generator set) producing 500A at 80V. Appendix D describes the calibration of the magnet and a determination of the flux distribution. The Lintott design incorporated 288 turns (i.e. 144,000 AT at 500A) in 4 double pancakes in each of two coils.

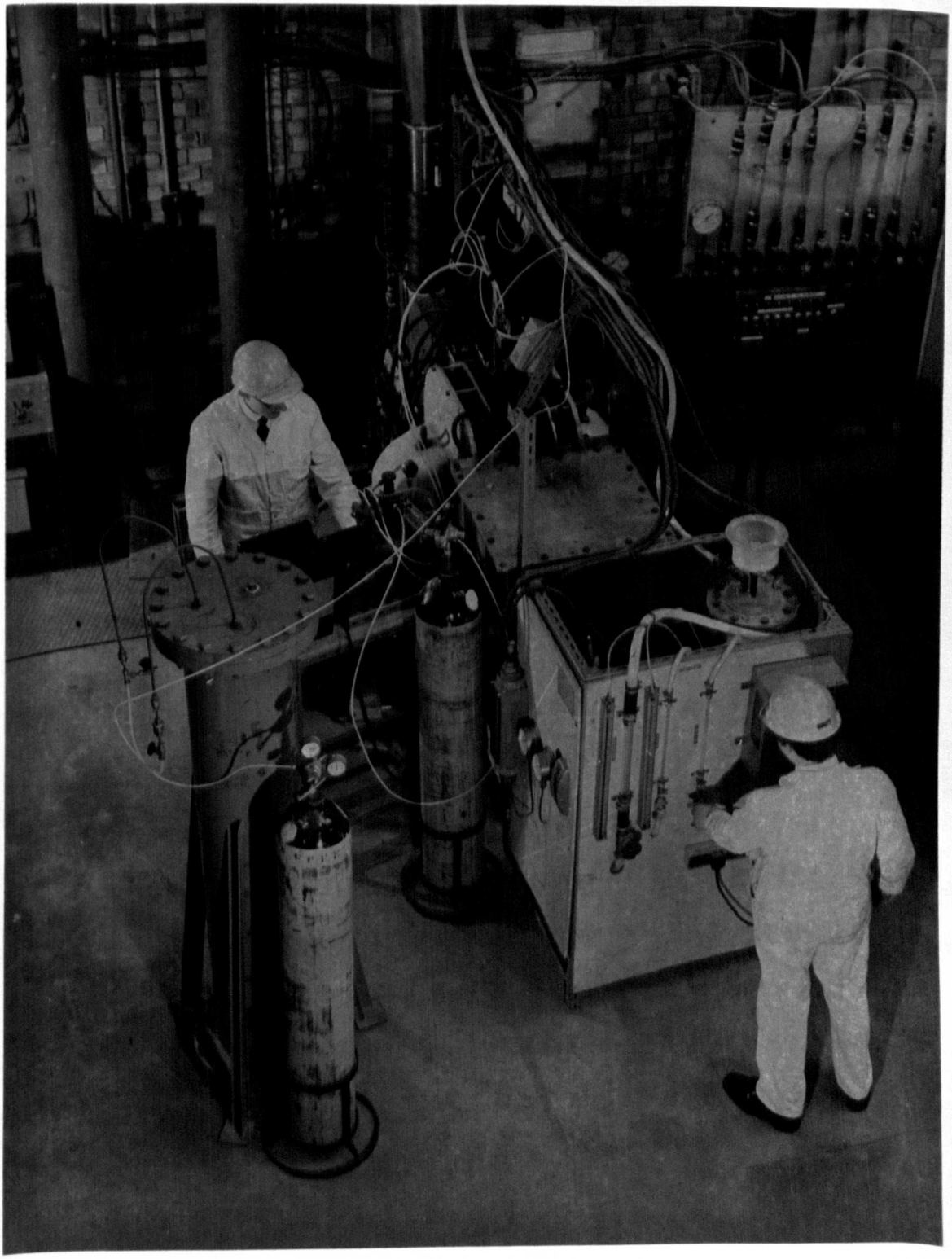

AERIAL VIEW OF RIG, SHOWING ANCILLARY EQUIPMENT.

PLATE 2.

It required a water supply of $\sim$3 gall/min at 80 p.s.i. (An interesting feature of the magnet was discovered:- although the stored energy was $\sim 4.10^5$ Joules (and in any case one would normally expect that it would be inadvisable to open circuit on an apparently inductive load), it was found possible to employ a simple D.C. switch in the power circuit for emergency shut-down since the effective magnet inductance was found to be negligible. This was caused by the use of a large aluminium clamping plate to retain the coils against the iron-yoke. The currents induced in this plate during any change of current flow in the coils were sufficient to dissipate the stored energy safely).

6.1.7. Magnet Supplies and Control Instrumentation

Figure 6.1.7 shows the arrangement of the supplies and instrumentation which were installed for the magnet.

An 80 p.s.i. pump, operating in a closed circuit, was used to provide a water supply of guaranteed pressure. (Mains pressure varied from 50 p.s.i. to 100 p.s.i.) The cooling flow for the magnet came from this circuit and passed through a filter.

The generator of the power supply had variable field excitation which gave a range of delivery current from 400 - 500A. (400A was the minimum level of self-excitation).

The cooling water flowrate was not metered, but a low flow alarm switch was incorporated into the circuit. Again, the exit water temperature was not measured continuously, but a high temperature switch was installed at the exit from each double pancake. The alarms for low flow and high cooling water temperature were all monitored in a relay operated alarm circuit which incorporated an alarm bell and indicator lights. The details of the circuitry are shown in Figure 6.1.7.

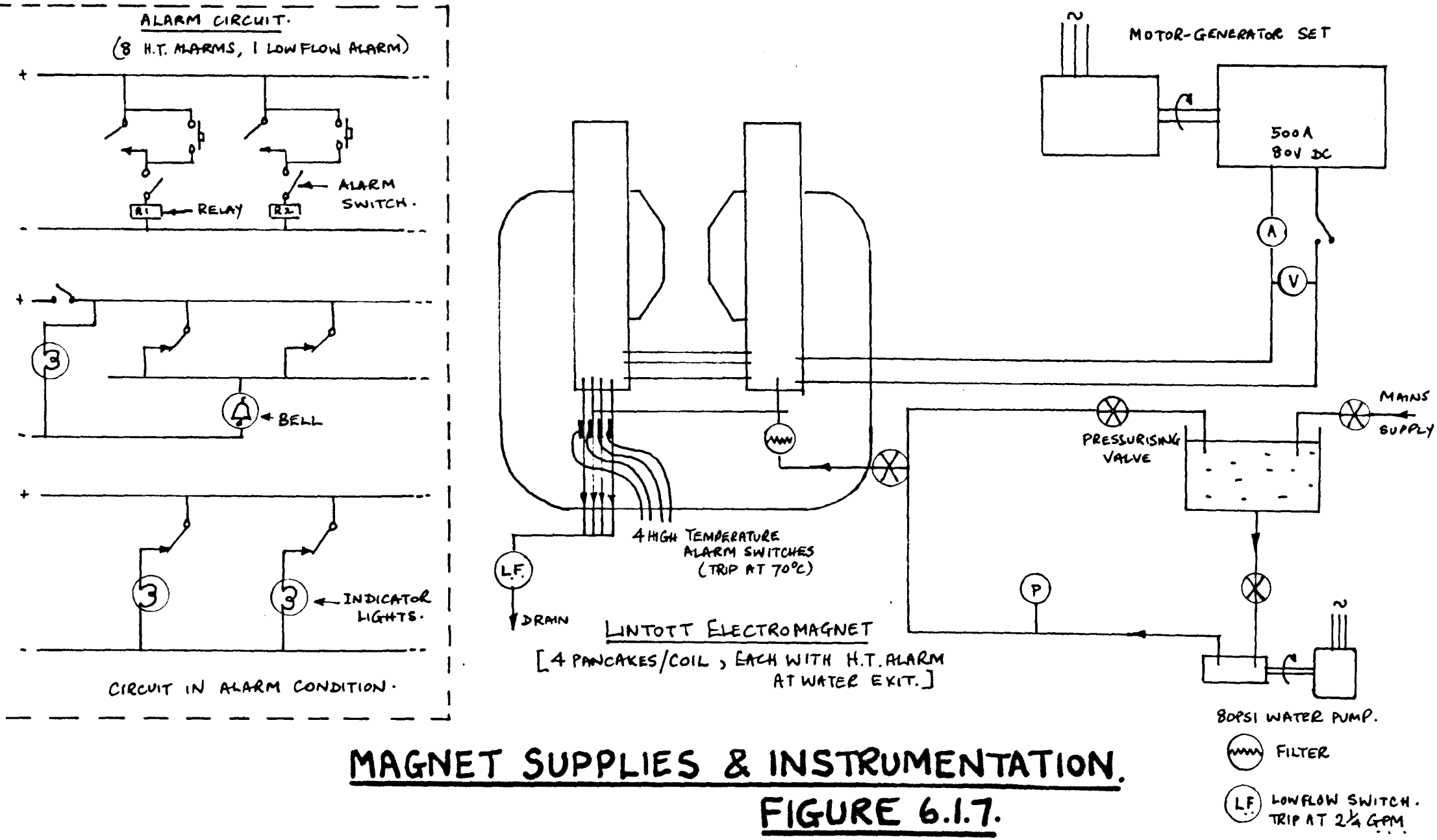

MAGNET SUPPLIES & INSTRUMENTATION.

FIGURE 6.1.7.

6.2 Probes and Associated Instrumentation

6.2.1 Water-Cooled Pitot-Static Probe (See Figure 6.2.1 and Plates 3 and 4)

Olin (1966) used a miniature water-cooled pitot-static probe to investigate turbulence damping effects in high temperature M.H.D. gas flows. The design which was adopted for use in these experiments was originally based on Olin's probe, (which was designed and supplied by Thermo-Systems Inc.) although a different configuration for the water-cooling tubes was adopted for convenience in manufacture.

The probe design incorporated a water-cooled main stem in which water flowed in concentric annuli (cold water being fed down the inner annulus to the tip of the probe) and a tip section which was separately cooled. Because of the difficulties of incorporating pressure tappings, the tip section was constructed by winding a helical coil of hypodermic tube around the pressure tapping tubes and then silver-soldering the whole cluster of tubes together. Details of the final design of the 1/8" O.D. probe are shown in Figure 6.2.1 - this design was evolved during a series of development trials.

The initial design was found to be susceptible to blockage of the total head pressure tapping with both freezing seed and refractory vapour, (an analysis of the deposit formed on the probe without seed flow indicated that its metal composition was mainly magnesium) and so a solid copper tip was manufactured which had a bore which was much larger than the bore of the hypodermic tube itself. The copper tip was cooled simply by conduction into the water jacket. Whereas the initial hypodermic tube blocked in only a few seconds, the copper tip enabled measurements to be taken for over 2 minutes without blockage, even when the probe was experiencing the full seed flowrate.

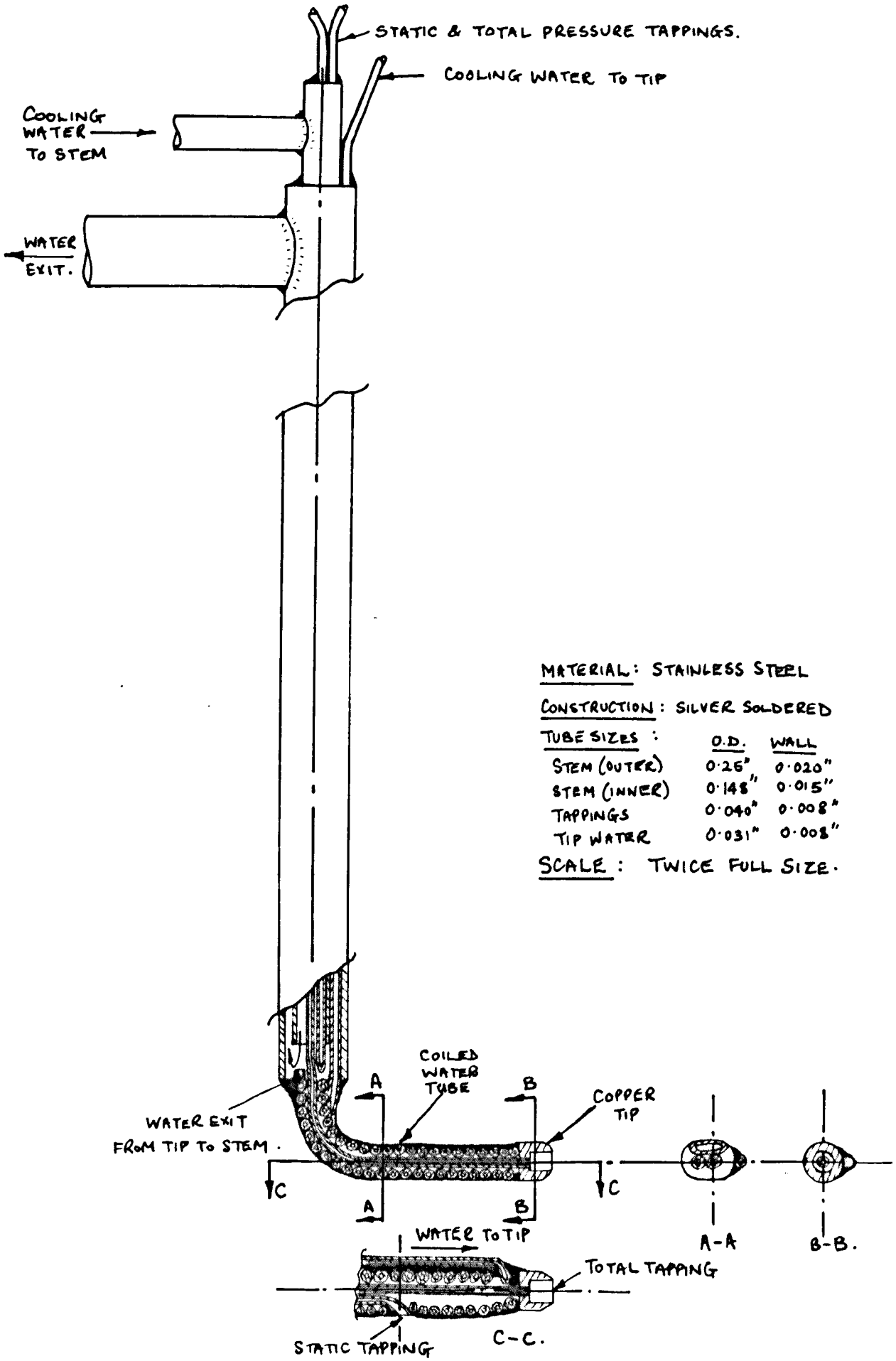

WATER-COOLED PITOT-STATIC PROBE

FIGURE 6.2.1.

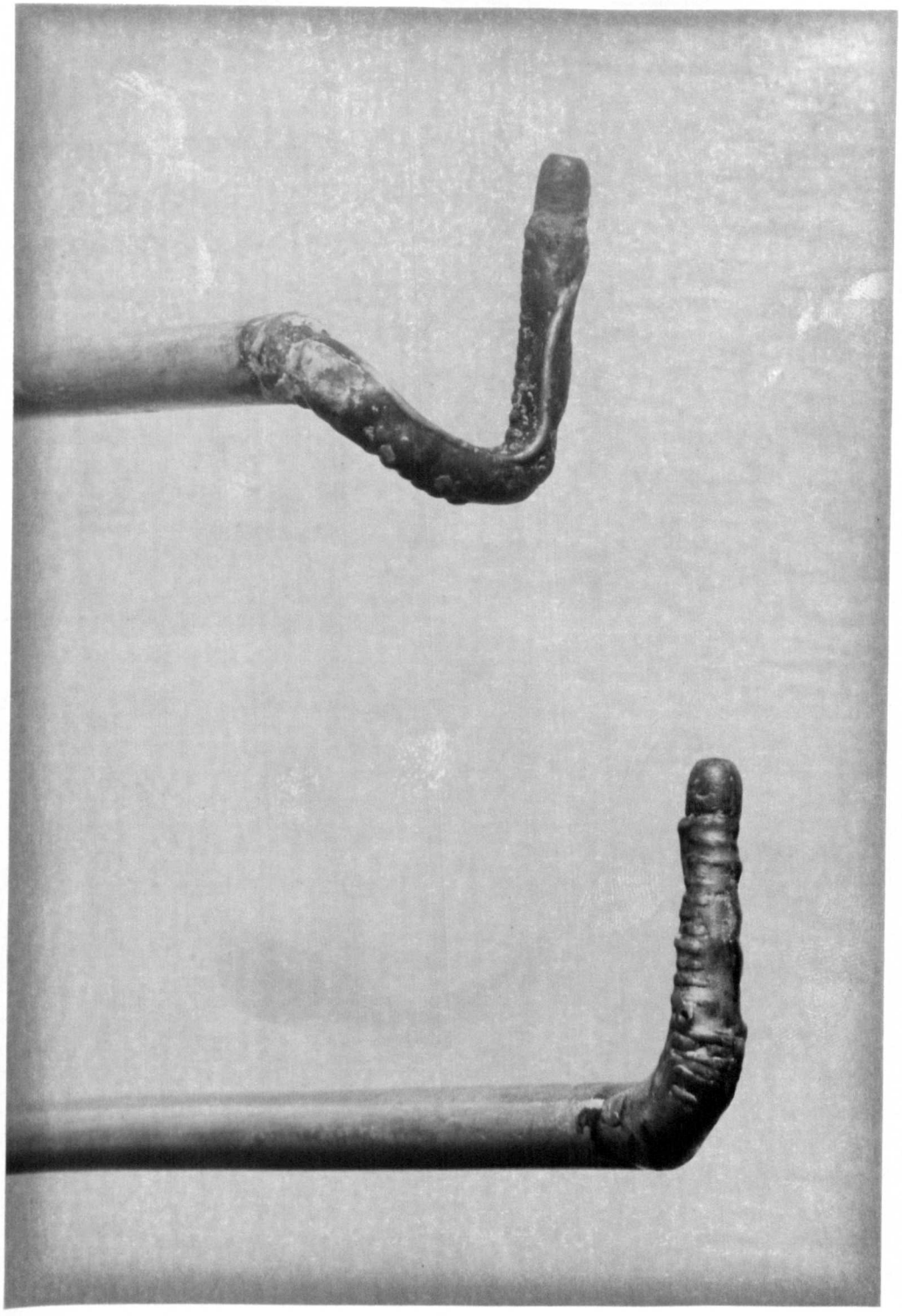

TIP SECTIONS OF PITOT-STATIC PROBES, STRAIGHT & CROOKED VERSIONS.

PLATE 3.

The cooling water supply for the main stem of the probe was mains water at mains pressure, and the supply for the tip (500 p.s.i.) was provided by a pressurised blowdown tank. Initially, mains water was used to fill up this tank, and on two occasions, after at least an hour's continuous insertion in the gas stream, sudden failure of the water jacket was experienced. Since the water was carefully filtered, these incidents were attributed to the deposition of the mineral content of the water in the passage. De-mineralised water was used thereafter for the tip-section, and no further failures were experienced.

Only one static pressure tapping was provided, and although this did not suffer from blockage by deposits, it was susceptible to blockage by condensation which was formed on the outside of the cool probe when it was inserted into the gas steam. Fortunately, it was found that condensation was not formed when the rig had been fully preheated; radiation from the hot walls in the test section was able to raise the surface temperature of the probe above the dew point.

A second probe was made which had an offset tip for traversing in a plane 3/8" off the duct centre line.

6.2.2. Services for Pitot-Static Probe (See Figure 6.2.2. and Plate 4)

As mentioned in section 6.2.1, a source of high pressure water was required to supply a sufficient flowrate to the tip section of the probe. Instead of using a multi-stage high pressure pump, the small flowrates required for the probe were more conveniently produced by a pressurised blowdown tank with sufficient capacity to produce the required flowrate for a complete test run.

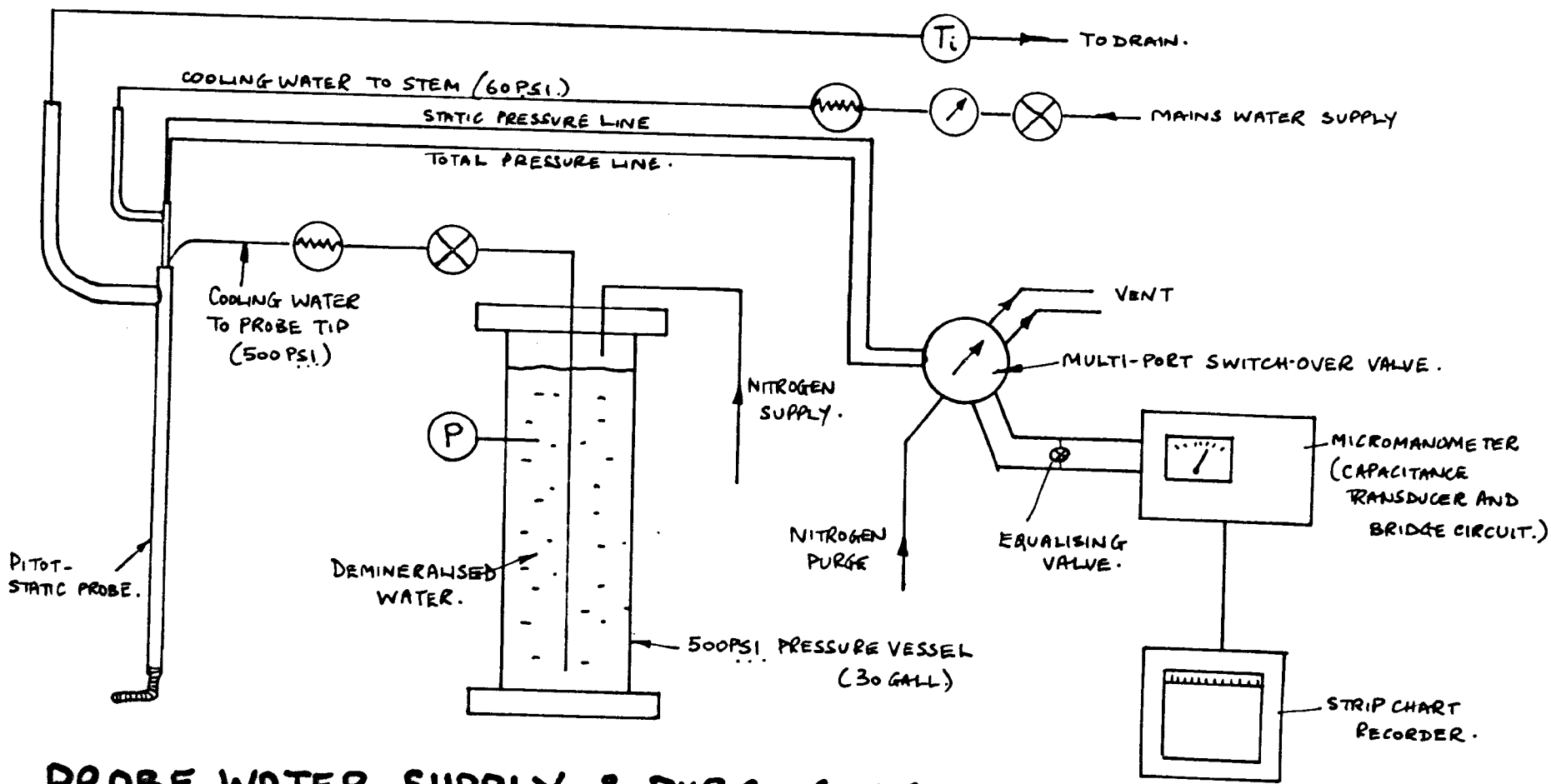

PROBE WATER SUPPLY & PURGING ARRANGEMENT.

FIGURE 6.2.2.

(Ti) = TEMPERATURE INDICATOR.

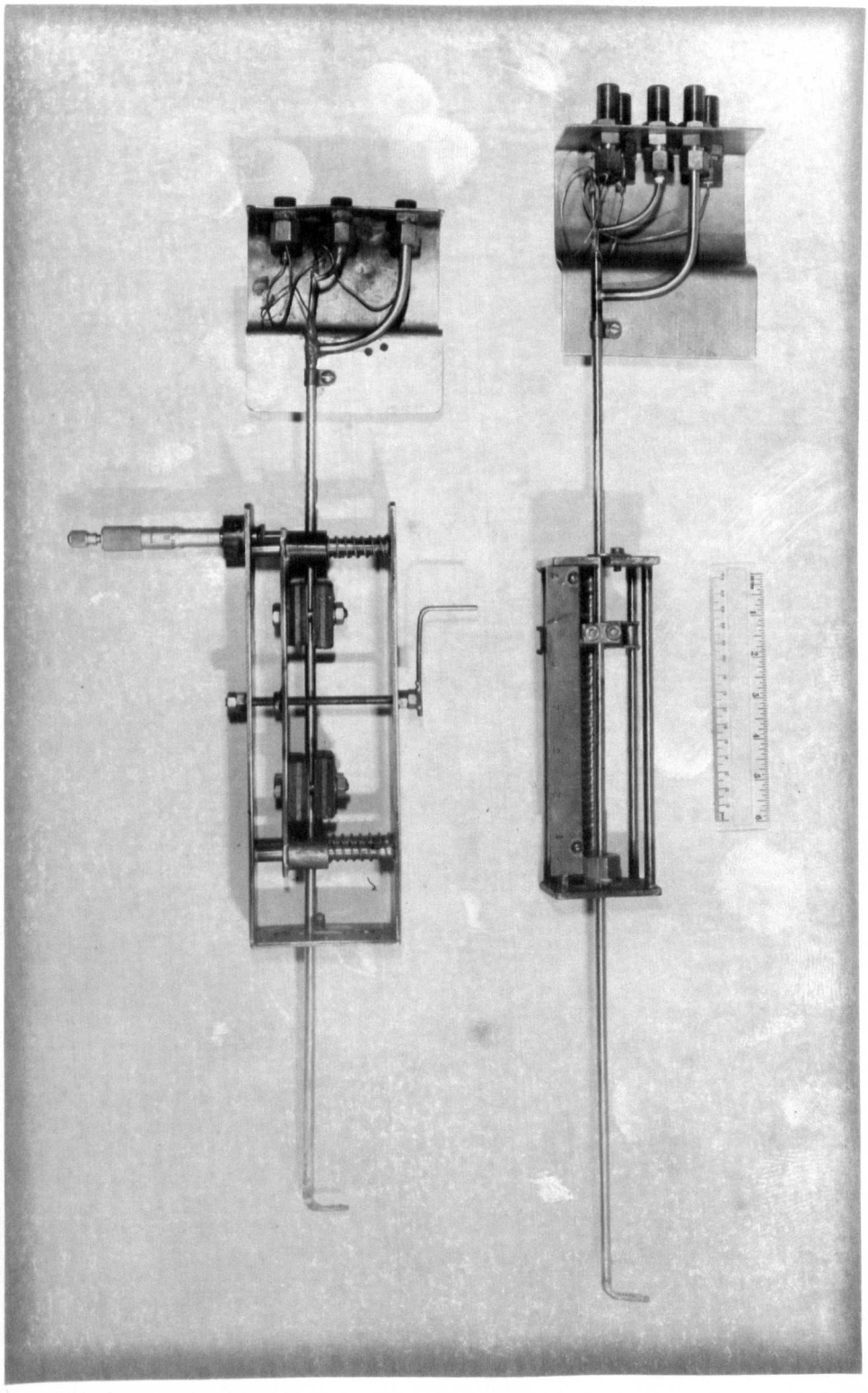

VERTICAL & HORIZONTAL TRAVERSING UNITS, WITH PITOT-STATIC PROBES.

PLATE 4.

(NOTE : DURING OPERATION OF THE HORIZONTAL TRAVERSING UNIT (LEFT) THE PROBE WOULD BE ROTATED THROUGH 90° FROM THE POSITION SHOWN IN THIS PLATE.)

The flowrate through the tip section of the probe was not metered continuously, but a flowrate-pressure calibration was carried out. Since the exit temperature from the tip section could not be measured, (the exhaust flow is ejected into the main stem of the probe) an estimate of the required flow was made by assuming a uniform heat flux density to the probe and calculating the heat flux to the stem. This indicated that for a water temperature rise of 15°C, a water flow of ∿2 ml/sec was required through the tip and this required an inlet pressure of 500 p.s.i. (a 15°C rise was very cautious, but allowed for the possibility of partial blockage by deposits etc). Figure 6.2.2 shows the arrangement of the high pressure water system, and also the purge-system and pressure measuring equipment.

The probe was equipped with a multi-port rotary valve, so that an intermittent nitrogen purge could be applied to both pressure tappings, in order to clear any deposits or condensation from the tappings. The three positions of the valve (a) produced a purge, (b) vented all the lines to atmosphere and (c) connected the probe to a differential manometer. The purge was applied before all measurements of differential pressure and the pressure equalising valve was always open until the purge and vent operations had been completed.

An I.R.D. Micromanometer (capacitance transducer and bridge circuit) was used to measure the differential pressure (and hence velocity head). The range of the manometer was 0 - 1" w.g. with an accuracy of better than 3%, for readings ∿ 0.1" w.g. It was found advantageous to feed the micromanometer through a constant voltage transformer to minimise drift.

The output from the micromanometer was recorded on a strip chart recorder so that a record of signal fluctuations with time was obtained. It was found that fluctuations were experienced as seed deposits built up on the outside surface of the probe and changed its geometry.

Two probe carriages were constructed to support and traverse the probe across the duct in the vertical plane and the horizontal plane. (See Plate 3). Vertical positioning could be achieved to within ~0.030", and horizontal positioning to within ~0.005".

6.2.3. R.F. Conductivity Probe and Associated Instrumentation

The circuitry for the R.F. generator and dissipation level monitor was a replica of that described and used by Taylor (1967). The coil was similar to his in electrical design, but differed in thermal and mechanical aspects since it was a water cooled, non-sheathed design. The probe is shown in detail in Figure 6.2.3; the coil was wound by hand from 1/8" O.D. copper tube and was supported in a plug of 'autostik' ceramic cement. It was found that if water spillage or leakage was allowed to penetrate this cement then the short circuit to the R.F. signal caused the generator to become overloaded, so a layer of 'araldite' was placed over the ceramic plug. The probe was fed from the same demineralised water supply as the pitot-static probes - which limited the operation of the probe to a thermal input to the rig of 85 KW, at which the outlet temperature of the probe was 70°C. (500 p.s.i. inlet pressure). The calibration of the probe is described in Appendix E.

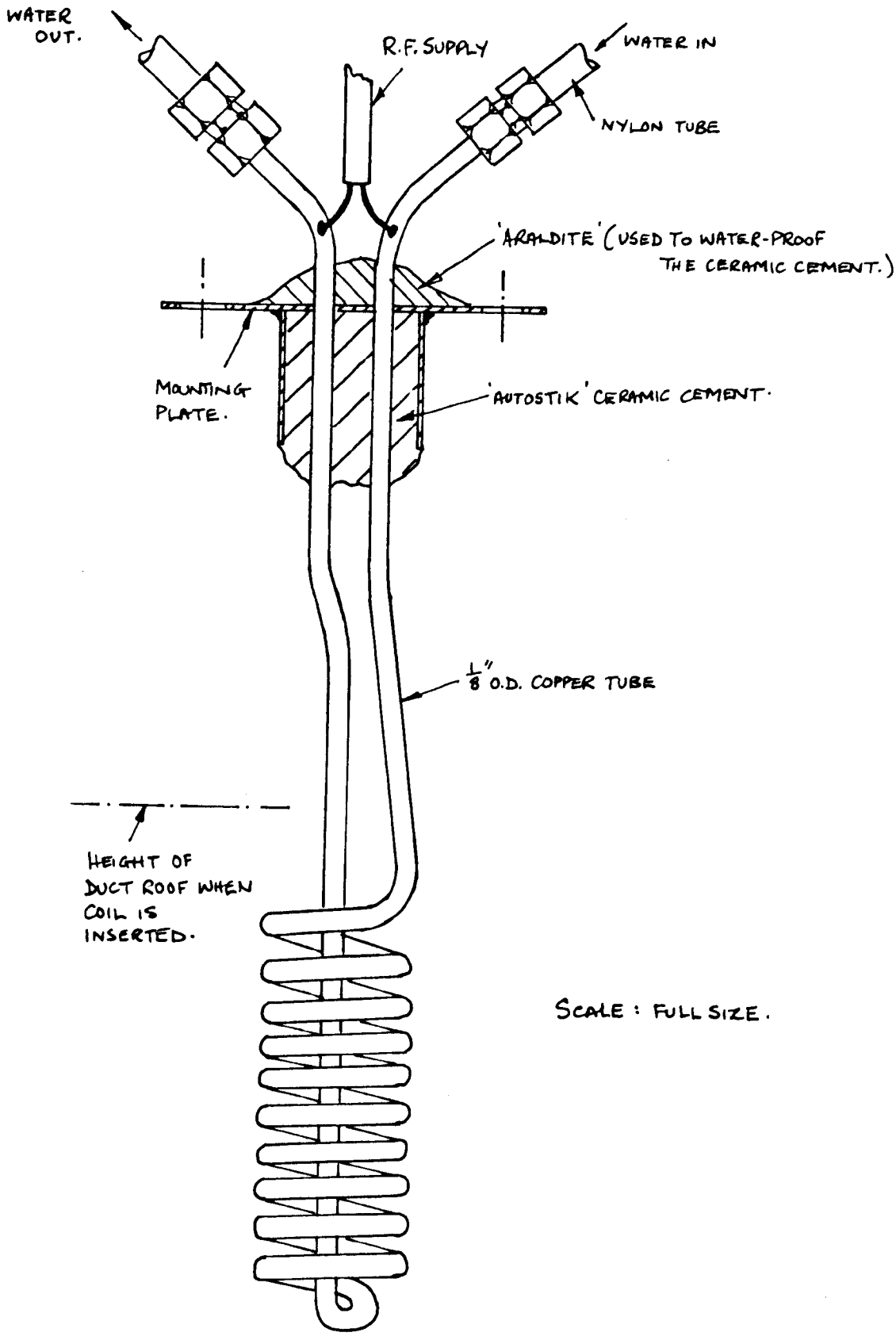

R.F. CONDUCTIVITY PROBE.

FIGURE. 6.2.3.

7. EXPERIMENTAL RESULTS

7.1 Measurements of Electrical Conductivity and Gas Temperature

7.1.1 Initial Measurements of Electrical Conductivity and Gas Temperature. (See Figures 7.1.1 and 7.1.2).

The trial combustion chamber (see section 6.1) was used to obtain initial measurements of the electrical conductivity of the gas at exit from the combustion chamber, when loaded with approximately 1 mol % K. In these experiments the gases issued as a free jet from the exit port of the combustion chamber and two carbon electrodes were placed within the jet. A small D.C. supply was used to drive current across the electrode gap at voltages up to 40 V.

The gas temperature was measured by the Na D-line technique (see Appendix C) through a port-hole in the exhaust tube of the combustion chamber. (See Figure 7.1.1). Since the gas temperature was measured a considerable distance upstream of the conductivity cell, heat losses to the refractory walls of the exhaust tube of the chamber, and entrainment of ambient air into the exhaust jet, reduced the actual gas temperature in the cell several hundred degrees below the measured value. However, this measurement served as a means of standardising conditions and gave a measure of the performance of the combustion chamber.

At a thermal input of 100 KW, the gas temperature was measured to be 2500°C and a typical I-V characteristic is displayed in Figure 7.1.2. This shows a non-linear region at low applied voltages, and a linear portion at voltages above about 10V. Following the accepted practice (e.g. Brogan (1962)), the slope of the linear portion of the characteristic was measured in order to give the resistance of the conductivity cell. The intercept of the straight line at zero current gave a measure of the voltage drop across the boundary

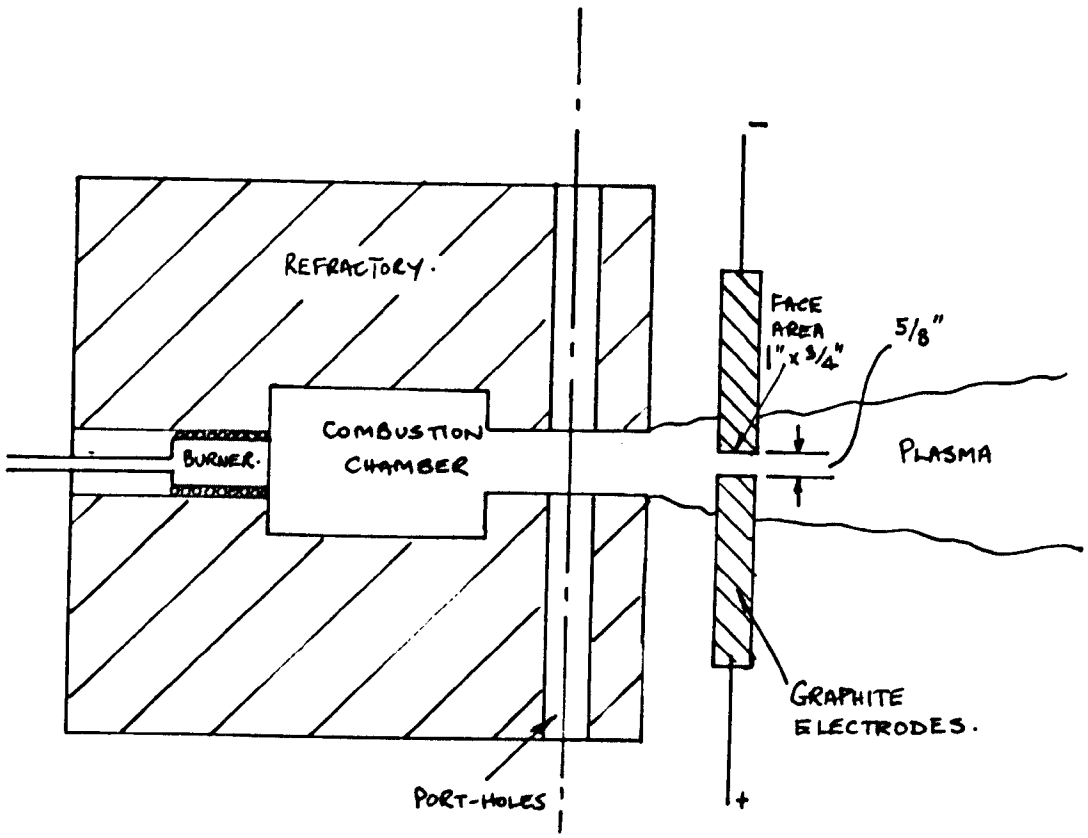

℄ OF LIGHT PATH FOR Na D-LINE TEMPERATURE MEASUREMENT.

0 1 2 3 4 5 6

SCALE (IN).

LAYOUT FOR EXPERIMENTS TO DETERMINE GAS CONDUCTIVITY & TEMPERATURE WITH TRIAL COMBUSTION CHAMBER. FIGURE 7.1.1.

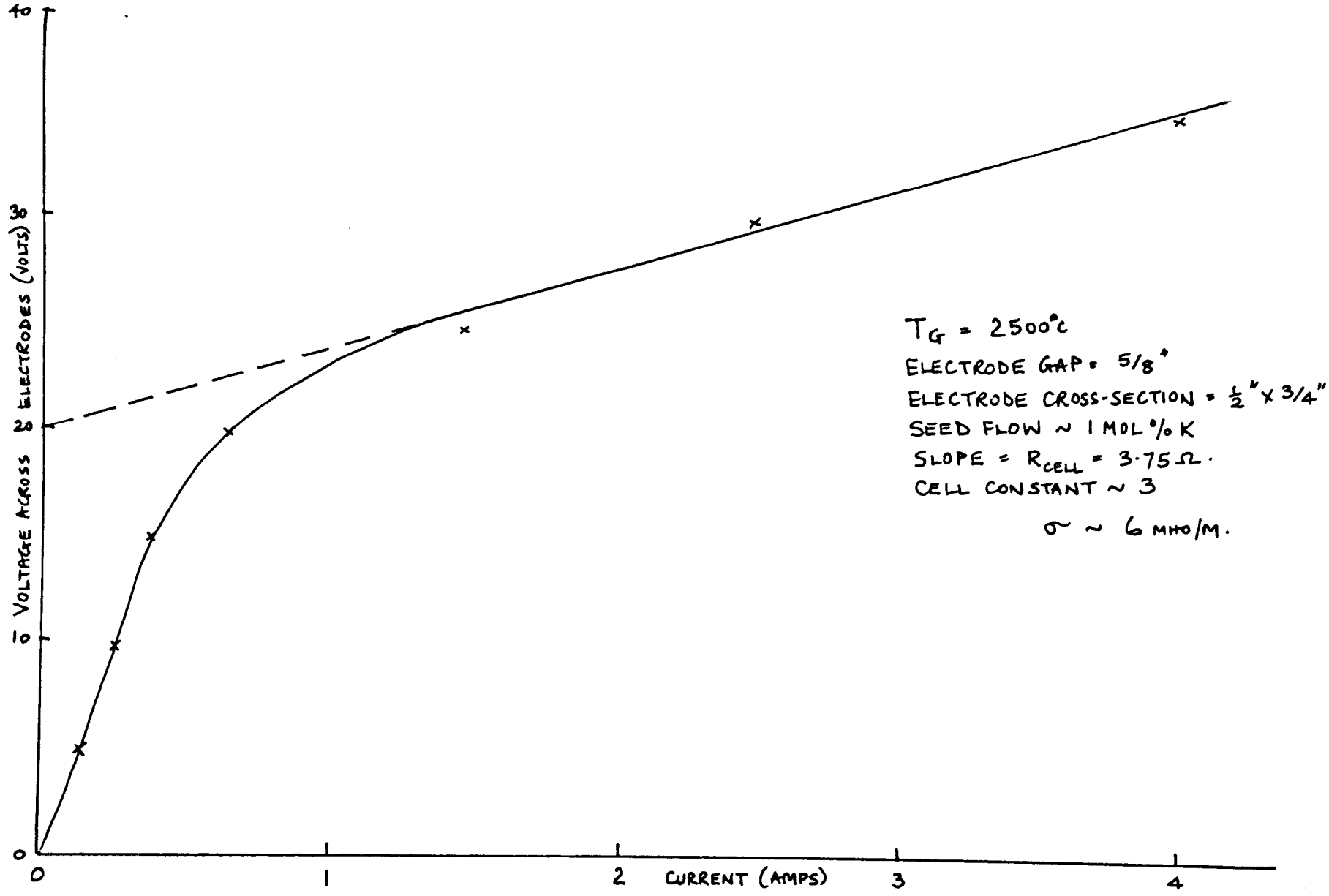

ELECTRICAL CONDUCTIVITY MEASUREMENTS ON TRIAL COMBUSTION CHAMBER. FIGURE 7.1.2.

layer on the electrodes. This voltage drop (~10V) was lower than that experienced in water-cooled conduction cells, where ~ 80V drop was often recorded.

The conductivity of the gas, calculated assuming parallel flow of electrons across the gap, was 17.6 mho/m. If an allowance is made for fringing of the current path, estimating a correction factor of ~ 3 for resistance from the electrolyte tests of Gray and Smith, (1967) this estimate of conductivity is reduced to ~ 6 mho/m.

If this value of conductivity is compared with the computed values in Figure 5.2.1, it is seen to correspond there to a gas temperature of 2200°C. The exact gas temperature at the position of the electrical conductivity measurement was not measured accurately, but it would be approximately in the range 2200 - 2300°C for a combustion chamber temperature of 2500°C and so the agreement with theory is quite good. One can, at least, be assured that the seed had been substantially evaporated, and contributed, as expected, to enhance the electrical conductivity of the gas stream.

One difficulty which was experienced in these experiments was the oxidation of the graphite electrodes - even in slightly rich flames. The gap between the electrodes had to be measured before and after the I-V characteristic had been determined, and in fact, the graphite electrodes were only inserted for the limited period during which I-V measurements were actually being made.

7.1.2. Gas Temperature Measurements during the Main Experimental Programme on Test Rig. (See Plate 5).

Gas temperatures were measured during experiments on the complete test rig (see Figure 6.1.3) both at exit from the combustion chamber and at exit from the test section, so that an estimate could be made of the mean gas temperature in the M.H.D. test section (and hence an estimate made of the gas electrical conductivity and Hartmann Number).

SIDE VIEW OF RIG
SHOWING INSTRUMENTATION
FOR VELOCITY &
TEMPERATURE
MEASUREMENT.

PLATE 5.

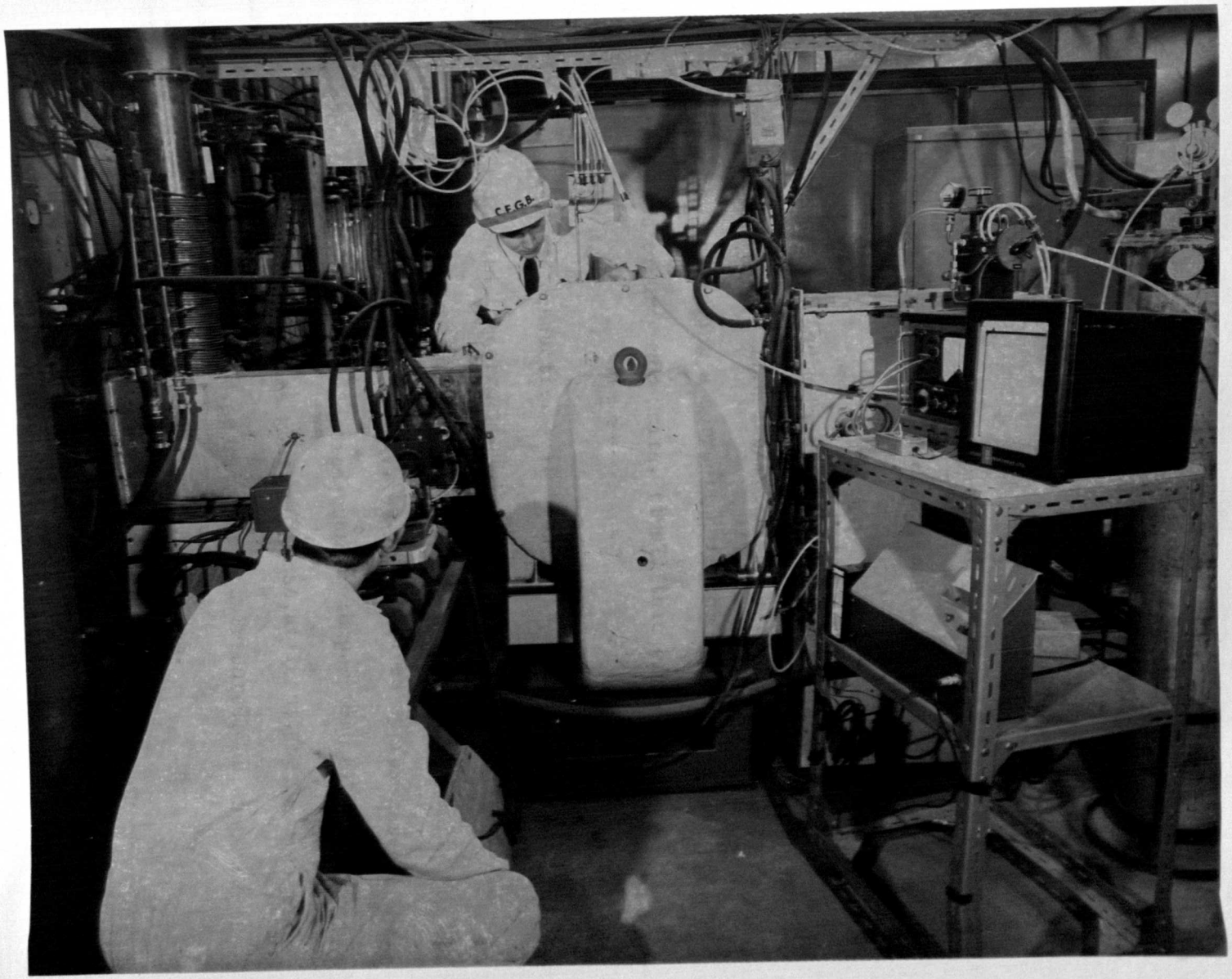

At all flowrates above 85 KW (Thermal Input), the gas temperature at exit from the combustion chamber was near the upper limit of the available range of operation of the Na D-line apparatus.

At a thermal input of 100 KW the gas temperature at exit from the combustion chamber was 2650°C (corrected according to Figure A.7) and at exit from the test section was 2020°C. These temperatures were measured after 1½ hours of operation, when the refractory thermocouples showed that all the refractories in the test section had reached thermal equilibrium.

Thus it was estimated that at 100 KW (Thermal Input) the mean gas temperature in the test section was 2350°C, corresponding to a predicted electrical conductivity of 10 mho/m and a Hartmann Number (based on the duct ½ width) of 9.5 and Interaction Parameter of 0.11.

At 85 KW (Thermal Input), the exit temperature from the test section dropped to 1800°C and so the mean gas temperature in the test section would have fallen to 2225°C, indicating an electrical conductivity of 5.3 mho/m, a Hartmann Number of 7 and Interaction Parameter of 0.07.

7.1.3. Gas Conductivity Measurements with R.F. Probe

The R.F. probe technique (for description of calibration see Appendix E) was used to measure the electrical conductivity of the gas stream in the test section. The probe was inserted through the central probe hole (No. 4) and measurements were made of the dissipation from the coil under transient conditions when the gas flow was switched off. The output signal from the R.F. generator-monitor circuit (which indicated the power delivered to the coil) was displayed on a storage oscilloscope which enabled a detailed investigation of the transient behaviour of the probe to be made. Several phenomena were identified; firstly the transient behaviour was found to consist of two regions, a fast transient which lasted between 0.5 and 1.0 seconds and a slow transient lasting up to a minute. The fast transient was attributed to fast thermal

effects (i.e. diffusion through the copper;time constant ~ 0.1 second) and electrical effects caused by the removal of the conducting medium. The shut-down was not instantaneous since the contents of the combustion chamber took a short time to be exhausted. The slow transient was caused by the slow thermal effect of the cooling of the water inside the probe as new water was fed from the reservoir. (See Figure 7.1.3 for sketches of typical transients). The form of the transient was studied for a range of water temperatures at exit from the probe (this was achieved by having "shots" of combustion gas of varying length between 1 second and several minutes) in order to distinguish between fast thermal effects and electrical effects in the initial fast transient. It was found that an increase in the probe cooling water temperature changed the form of the transients significantly (again see Figure 7.1.3). The magnitude of the first transient was reduced and the magnitude of the second transient increased, although the overall change in dissipation level, between the probe in the steady state gas flow and the probe in the duct with no gas stream, remained constant. The initial fast transient could, however, be further subdivided to give an almost instantaneous (~ 0.01 seconds) transient which could be attributed to the electrical effect of removing the conducting medium from the vicinity of the probe, and the magnitude of this transient was found to be insensitive to changes in the probe cooling water temperature.

This may be explained as follows:-

When the gas flow was interrupted, the temperature in the gas surrounding the coil fell from the initial steady state temperature to the relatively low temperature of the terminal slug of gas. This fall of temperature resulted in a much more rapid fall of gas conductivity to a level which was equivalent to negligible conductivity because of the exponential nature of the conductivity-temperature relationship.

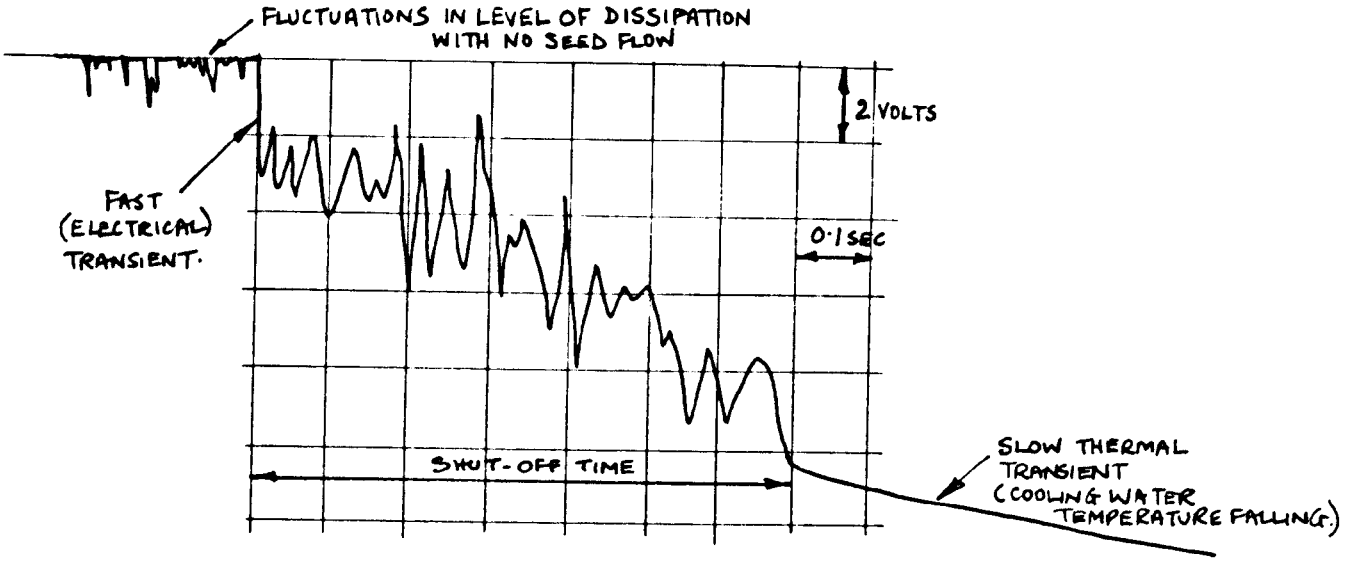

CASE (i): RESPONSE TO SHUT-DOWN AFTER SHORT 'SHOT' OF COMBUSTION GAS i.e. PROBE COOLING WATER TEMPERATURE HAD NOT REACHED EQUILIBRIUM.

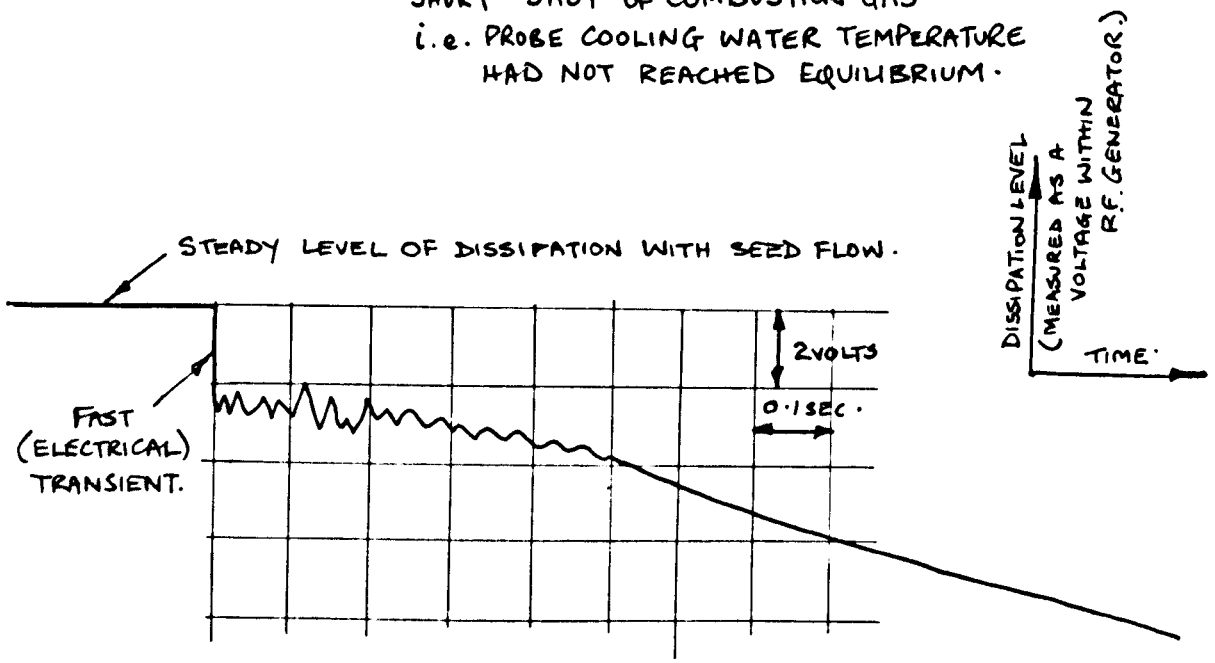

CASE (ii): RESPONSE TO SHUT-DOWN AFTER STEADY-STATE FLOW OF COMBUSTION GAS.

R.F. CONDUCTIVITY PROBE - TYPICAL TRANSIENTS MEASURED DURING SHUT-DOWN OF GAS FLOW

FIGURE 7.1.3.

Consequently, although a non-instantaneous shut-down was experienced, this only affected the thermal behaviour of the probe. The electrical performance of the probe (i.e. its sensitivity to the conductivity of the surrounding medium) was only affected at the instant of shut-down.

The magnitude of the initial transient was found to be 3 volts ($\pm \frac{1}{2}$ volt), with a thermal input of 85 KW. Using the electrolyte calibration this would indicate a mean gas conductivity in the test section of 2 - 5 mho/m. When compared with the temperature measurements of section 7.1.2 and the theoretical predictions of electrical conductivity of section 5.2., reasonable agreement can be shown to exist. (At the measured steady state mean temperature of 2225°C, the predicted conductivity is 5 mho/m).

Another interesting point emerged from the examination of the time variation of dissipation. If no seed was injected, then a fluctuating level of dissipation was observed, (magnitude of fluctuation ~ 1 volt), but when the seed flow was introduced, the dissipation level became steady at the upper level of the fluctuations. Since some seed was still present in the gas stream even when the main feed flow was not operating, (this was produced by seed which had been absorbed into the refractory lining of the chamber) an intermittently conducting gas stream was produced. This fact could be appreciated by visual inspection of the gas stream through one of the windows of the combustion chamber. When the seed flow was switched off, a lilac colouration was seen (characteristic of potassium), which fluctuated in intensity, whereas with the full seed flow, a continuous strong lilac colouration was visible. The magnitude of the fluctuation of dissipation with no imposed seed flow gave an approximate indication of the increase in conductivity gained by adding seed flow, viz. 3 mho/m.

Although these measurements of conductivity have uncertain accuracy, because of difficulties encountered both (a) in the calibration of the device and (b) in its operation at high temperatures, they do give results which agree approximately (within a factor of 2) with the theoretical predictions and measurement using I-V characteristics. This method could not, however, be used for standardising M.H.D. experimental conditions, because of the uncertain accuracy and difficulty of operation, and measurements of gas temperature were used for this purpose (since conductivity is highly dependent on temperature and fairly insensitive to seed flow).

7.2 Results for Rectangular Duct Flows with no obstructions

The first internal investigation of the character of flows of combustion plasma in rectangular ducts with transverse magnetic fields was a simple measurement of the interaction of the field with the shape of the velocity profile in the duct, (measured perpendicularly to the direction of the applied field).

The miniature water-cooled pitot-static probe (see section 6.2), was used in conjunction with a vertically traversing carriage which allowed the probe to move along the vertical centre-line of the duct from the top to the bottom walls. The central probe hole (No. 4) was used for these traverses (see Figure 7.2.1). The probe operating procedure was developed during the initial attempts to make these measurements, which provided a basis for experiments with more complex situations,(section 7.3) when plates were inserted into the rectangular duct.

7.2.1 Probe Operating Procedure (See Plates 5 and 6)

The operating procedure which was adopted for the water-cooled pitot-probe was to apply the nitrogen purge at all times other than the short time taken to obtain a differential pressure measurement and to insert the probe only when the duct walls had been pre-heated (and were able to offer radiant

VIEW OF TOP OF TEST-SECTION SHOWING PROBE-TRAVERSING UNIT.

PLATE 6.

PROBE IS INSERTED INTO PROBE-HOLE NO. 6.

heating to the outside of the probe) - this eliminated problems caused by deposition of solids and condensation on the pressure tappings. The differential pressure (~ 0.1 in. w.g.) was recorded at intervals of 1" across the duct and the time-mean reading (after the manometer had reached equilibrium) was noted for each position of the probe (in section 7.3, more detailed traverses-intervals of $\frac{1}{4}$"-were made). On a few occasions, stray readings were obtained when large deposits became attached to the body of the probe - this trouble was usually cleared by removing the probe from the duct for a thorough cleaning.

7.2.2. Measurements of Velocity Profiles

The duct had a 6" x 2" cross-section, with an inner lining of magnesite refractory (essentially non-conducting). A sequence of traverses were made with a thermal input of 100 KW to measure h; firstly with no seed flow, then with 1 mol % K seed flow and a nominal magnetic field strength of 1 weber/m^2. Finally, the O.H.D. condition was repeated. As discussed in section 5.3.1, the velocity profiles were presented as profiles of $\sqrt{h}$.

The O.H.D. profiles measured after the M.H.D. profiles were essentially the same as the original O.H.D. profiles within the experimental error. Slight variations in total flowrate and temperature occurred, (caused by small changes in the supply pressure of oxygen and propane) and small changes in pressure gradient occurred between M.H.D. and O.H.D. flows; for these reasons it was decided to normalise all profiles of $\sqrt{h}$ with respect to the mean value of $\sqrt{h}$ over the traverse. $(= \overline{\sqrt{h}})$

Figure 7.2.2 shows a graphical summary of 6 traverses in the form of normalised values of $\sqrt{h}$ $(\sqrt{h}/\overline{\sqrt{h}})$ - the O.H.D. traverses (2 before and 2 after the M.H.D. traverses) and the M.H.D. traverses were averaged separately.

There is seen to be very little change in the shape of the M.H.D. and O.H.D. profiles, and all that can be said is that there was a slight flattening of the profile when the M.H.D. interaction was introduced. This effect could have been caused by either:-

(a) The Hartmann effect

or (b) The circulating currents in the region of changing magnetic field, at the leading edge of the pole-faces. (See Shercliff (1965)).

Both (a) and (b) could act to produce flattening of the velocity profiles in the direction transverse to the applied magnetic field.

In uniform conductivity M.H.D. duct flow (rectangular), the Hartmann Effect (a) would produce boundary layers on the walls parallel to the magnetic field of thickness $O\left(\frac{d}{NH}\right)$ - see Figures 4.4.1 and 4.4.2 for the fully developed solution to this case. The streamwise component of the circulating currents would react with the streamwise varying transverse field to alter the vorticity of the flow, with the net effect of accelerating the flow in the regions near to the top and bottom walls - effect (b).

It is not clear from this result which of these effects is causing the small M.H.D. interaction, but a negative conclusion can be drawn i.e. that the Hartmann Effect was not appreciable. This is attributable to the low duct wall temperature ($\sim 1600^{\circ}C$), which resulted in very low gas electrical conductivity in the thermal boundary layer adjacent to these walls. (From Figure 5.2.1 it can be seen that the conductivity falls by two orders of magnitude in reducing the gas temperature from the core value of $\sim 2300^{\circ}C$ to the wall value of $\sim 1600^{\circ}C$).

Thus the boundary layer on the duct walls would have a complex structure, comprising a hydrodynamic sub-layer adjacent to the walls with an electrically conducting (M.H.D.) outer layer. Because of the exponential

conductivity-temperature relationship, the division between these two parts of the boundary layer would be quite distinct and a step-function for the conductivity profile would be a good first approximation (see Cramer (1967)). The situation is also similar to a pressure driven M.H.D. flow in which slip occurs at the non-conducting walls - this analogy is discussed further in Chapter 8.

The qualitative effect of M.H.D. turbulence damping would be to make the profiles appear more like the fully laminar profiles i.e. with more pronounced peaks. The fact that the opposite trend was noticed suggests that turbulence damping did not predominate the M.H.D. interaction - although it may have slightly attenuated the result of effects (a) and (b), mentioned earlier. (In the following section, which deals with a configuration which was asymmetric about the y = o axis, an antisymmetric M.H.D. interaction was discovered, which could only be originated by magneto-viscous effects, since turbulence effects, Hartmann effects and disturbances produced by effects at entry to the magnetic field would all produce symmetric interactions).

7.3 Pitot-Static Probe Measurements in Rectangular Ducts with an Immersed Plate (Long in flow direction and half duct height)

The duct configuration used in this section is shown in Figure 7.2.1. The internal dimensions of the duct were unchanged from the configuration used in section 7.2, but a long plate ($\frac{1}{4}$" thick) was inserted into the duct. The plate was 'long' in the flow direction and extended 3" beyond the edges of the magnet poles both upstream and downstream. The plate was only 3" high, however, and so provided a discontinuous hydrodynamic condition in the vertical plane, (reminiscent of the semi-infinite plate discussed in Chapter 3 and very similar to the computer solutions of section 4.4.). Because of the limited width of the duct, it was decided to offset the inserted plate so that the

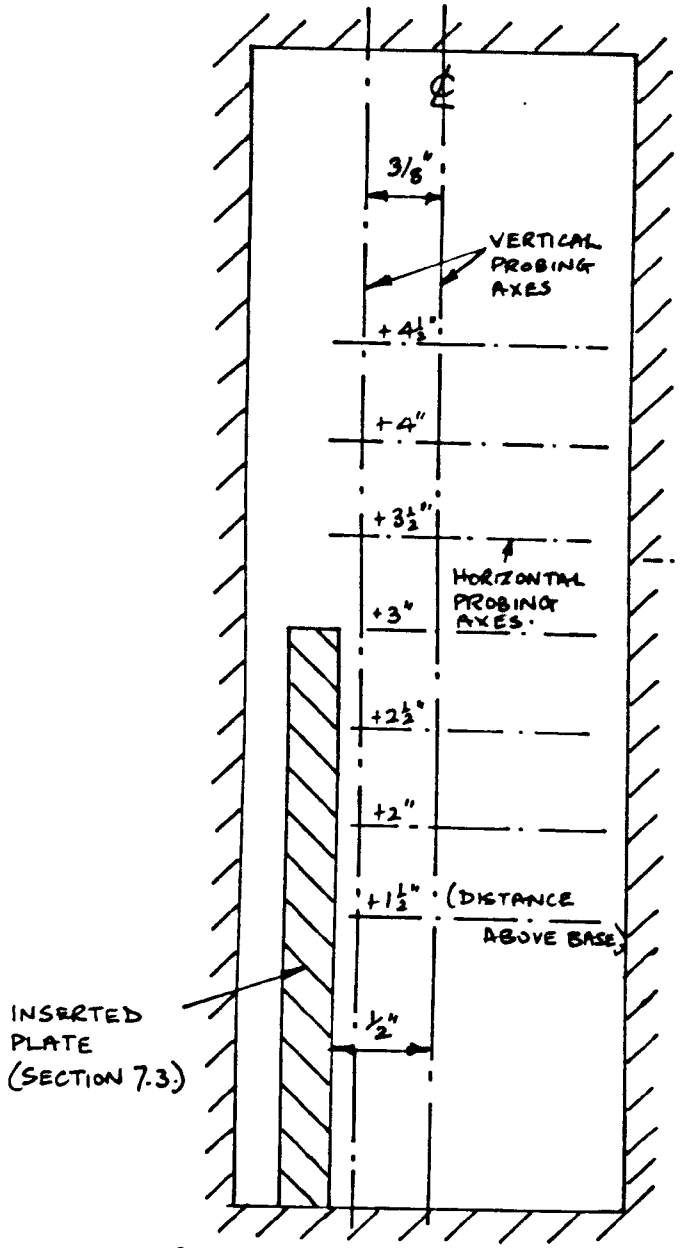

CROSS-SECTION OF TEST-DUCT. (FULL SIZE)

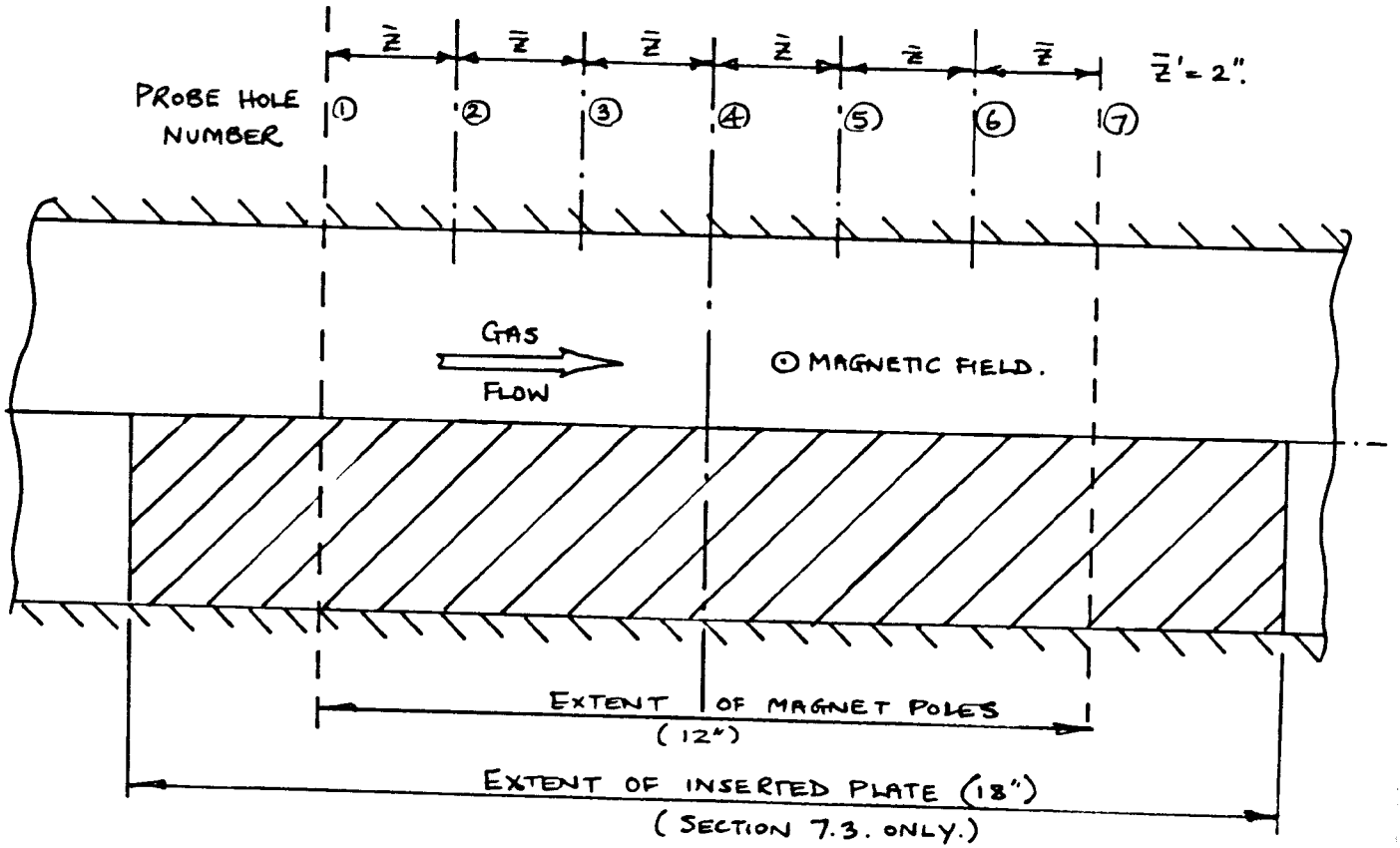

ELEVATION OF TEST DUCT (⅓ FULL SIZE).

AXES OF PROBING USED FOR RESULTS IN SECTIONS 7.2 & 7.3

FIGURE 7.2.1.

plate centre-line was 5/8" from the duct centre-line. Although this destroyed the symmetry of the situation about the $\chi = o$ axis, the results of section 7.2 indicated that the M.H.D. interaction caused by the duct walls alone was insignificant and so the M.H.D. interaction caused by one side of the plate was obtained in this instance - the side nearer the wall being adjacent to a region where no M.H.D. interaction was possible because of the low gas temperature.

The investigation of this particular configuration, which aimed to establish the existence of transverse wakes emanating from the tip of the immersed plate, with the M.H.D. interaction extending over the bulk of the core flow and not limited merely to the plate boundary layer, was subdivided into the following self-contained exercises:-

(a) An investigation of the effect of varying the conductivity of the plate, using magnesia and zirconia plates.

(b) An investigation of the effect of varying the gas conductivity, by varying the thermal input to the rig.

(c) An investigation of the streamwise development process of the O.H.D. and M.H.D. flows.

(d) A detailed investigation of the 2-dimensional variation of velocity over the cross-section of the duct for O.H.D. and M.H.D. flows.

The miniature water cooled pitot probe was again used for these measurements, and apart from the investigation of the development process, all profiles were measured at probe hole No. 6 - i.e. the last probe hole within the uniform magnetic field, which was 11" from the leading edge of the magnet pole. The M.H.D. interactions for each case were monitored by again measuring O.H.D. and M.H.D. profiles of $\sqrt{h}$ along the vertical centre-line of the duct, and for the 2-D investigation, horizontal traversing

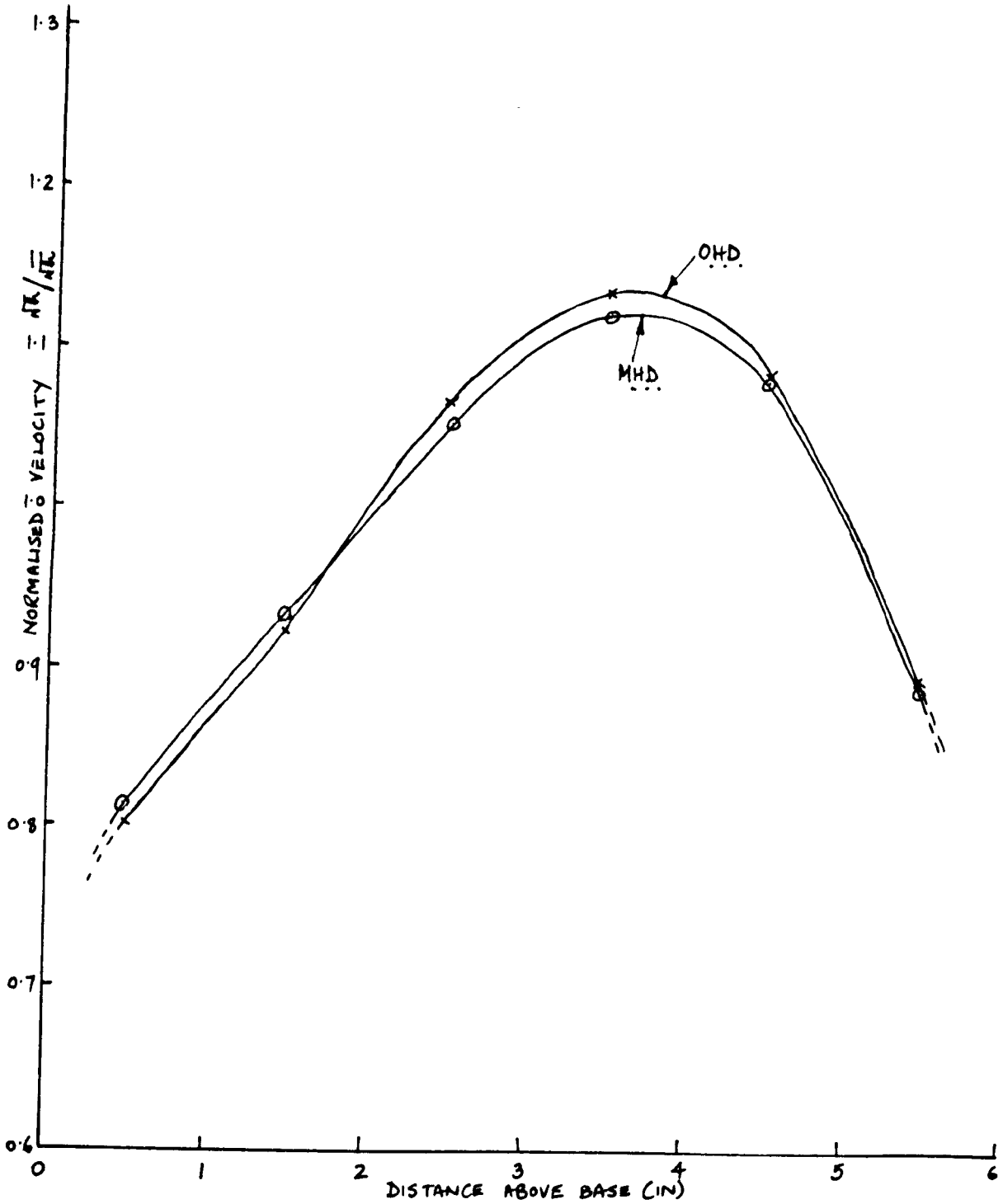

RUN 29 : RESULTS AVERAGED OVER 4 O.H.D. & 2 M.H.D TRAVERSES
THERMAL INPUT 100 KW.
PROBE ON ℄ OF DUCT & IN PROBE-HOLE 4.

VERTICAL TRAVERSES IN UNOBSTRUCTED RECTANGULAR DUCT. FIGURE 7.2.2.

was also introduced, together with a special crooked-probe (with an offset tip).

7.3.1 The Effect of Plate Conductivity

Although the theoretical studies presented in Chapters 3 and 4 were limited to cases which employed non-conducting plates, it is known from the results of Hasimoto (1960) that the effect of a perfectly conducting plate on the M.H.D. flow of uniformly conducting fluids is more severe than a non-conducting plate, (for the semi-infinite stationary plate, the core velocity adjacent to the plate will be zero for a perfectly conducting plate and half the free-stream velocity for a non-conducting plate; both when the flow is fully developed. - See Figure 2.2.1). Two materials were used for the plate; magnesia and zirconia, which gave approximations to the non-conducting and perfectly conducting cases, (See Section 5.2).

Figure 7.3.1 shows the normalised $\sqrt{h}$ profiles measured along the vertical centre-line of the duct, (i.e. $\frac{3}{8}$" from the centre-line of the plate) for the case with the non-conducting magnesia plate. A thermal input of 100 KW was used again, and the optimum seed flowrate of 0.73 mol % K was imposed for the M.H.D. flow, in which the magnetic field strength was nominally 1 weber/m^2. The corresponding results for the flow past a geometrically identical zirconia plate (electrically conducting) are shown in Figure 7.3.2, which also includes a comparison between O.H.D. flow with and without seed. This latter comparison shows that there is no significant change when the seed flow is applied to O.H.D. flow, although it was found that when the seed was flowing, the scatter of the results was rather greater than with no seed flow - this was explained by the disturbance of the aerodynamics of the flow around the tip of the pitot-static probe by deposits of seed. The duplicate sets of readings obtained for the M.H.D. and O.H.D. cases indicate the scatter which was encountered in the experimental measurement.

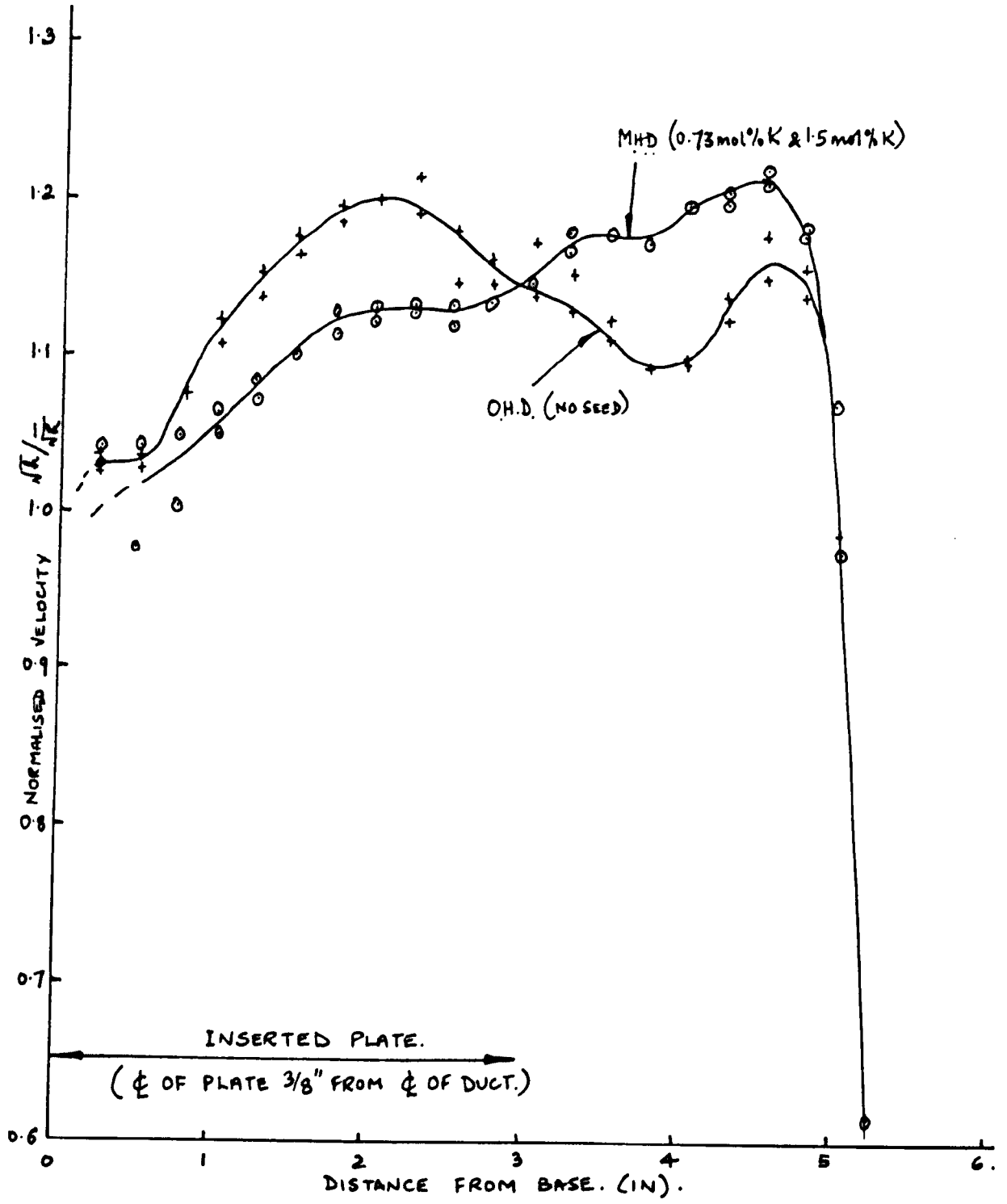

RUN 36: THERMAL INPUT 100KW
PROBE ON ℄ OF DUCT & IN PROBE HOLE 6.

VERTICAL TRAVERSES WITH INSERTED MAGNESIA PLATE.

FIGURE 7.3.1.

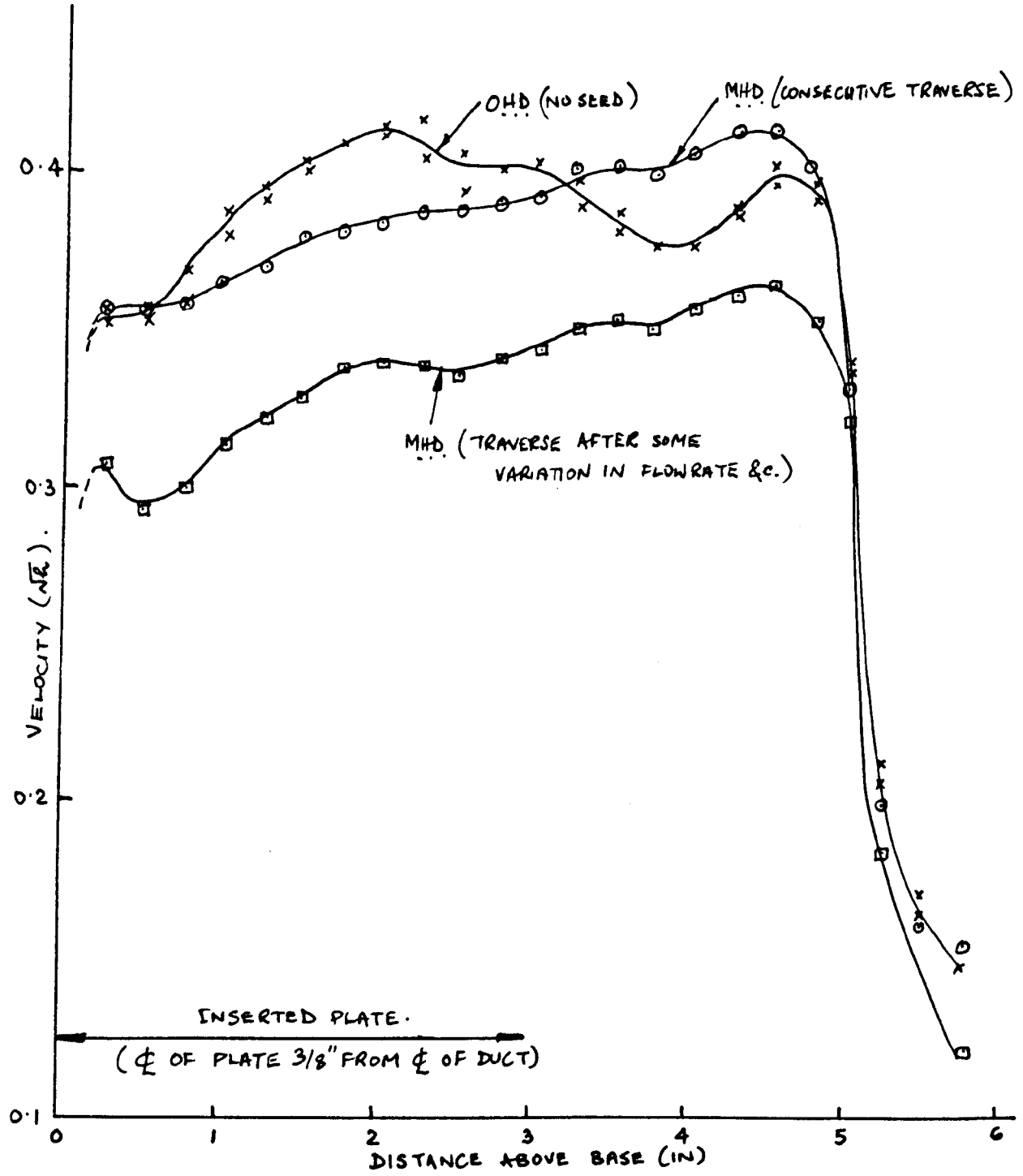

RUN 36 : THERMAL INPUT 100 KW.
PROBE ON ℄ OF DUCT & IN PROBE HOLE 6.
MEASURED VALUES OF $\sqrt{R}$ DISPLAYED WITHOUT NORMALISATION.

VERTICAL TRAVERSES WITH INSERTED MAGNESIA PLATE.

FIGURE 7.3.1.A.

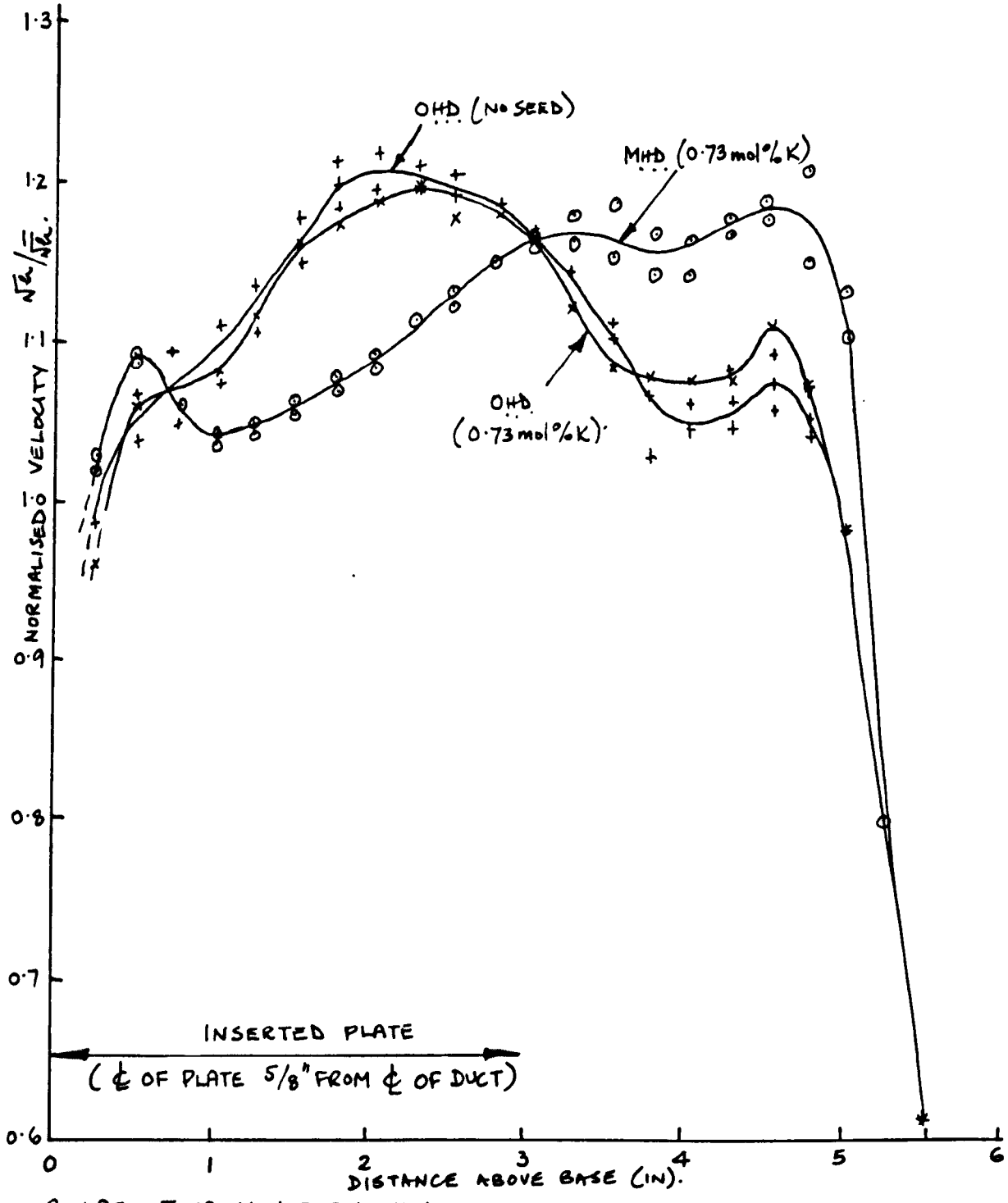

RUN 38: THERMAL INPUT 100KW.
PROBE ON ℄ OF DUCT & IN PROBE-HOLE G.

VERTICAL TRAVERSES WITH INSERTED ZIRCONIA PLATE

FIGURE 7.3.2.

Figure 7.3.1.A is included to show the measured profiles of $\sqrt{h}$ before normalisation. The lower profile was obtained after some small variation in total flowrate and although it has the same shape as the other M.H.D. profile it is a confusing presentation of the basic M.H.D. interaction. This interaction is antisymmetric about the edge of the immersed plate and so the shape of the M.H.D. profile is distinctly different from the equivalent O.H.D. profile - the normalisation in terms of mean values over the cross-section does not obliterate this change of shape.

The sets of results for both the magnesia and zirconia plates show the same type of M.H.D. interaction. When the transverse field is applied, the core region adjacent to the plate is decelerated (cf. this result with Figures 4.4.3, 4.4.4 and 4.5.4, 4.5.5, and see discussion in Chapter 8).

In order to make a comparison between the results for the two plates, the ratio between the profiles for the M.H.D. and O.H.D. cases was calculated. This has the effect of eliminating the basic shape of the O.H.D. profile from the results and displays the variation of the magnitude of the M.H.D. interaction on the velocity profile across the traversing axis. This is somewhat similar to the M.H.D. profile that would be produced by the plate in an originally uniform O.H.D. flow - and displays the transverse wake effect with clarity. Figure 7.3.3. shows this presentation of the results, from which it can be seen that there is an increased interaction in the case of the zirconia plate (electrically conducting) compared with the magnesia plate (non-conducting). The M.H.D. and O.H.D. traverses which were measured successively were used to calculate these ratios, so eliminating time variations as far as possible.

The interaction is not so great as may have been expected for a fully developed flow with either plate under uniform conducting conditions. It is shown later that we are not dealing with fully developed flows (see section 7.3.3.), and the known non-uniformity of electrical conductivity tends to

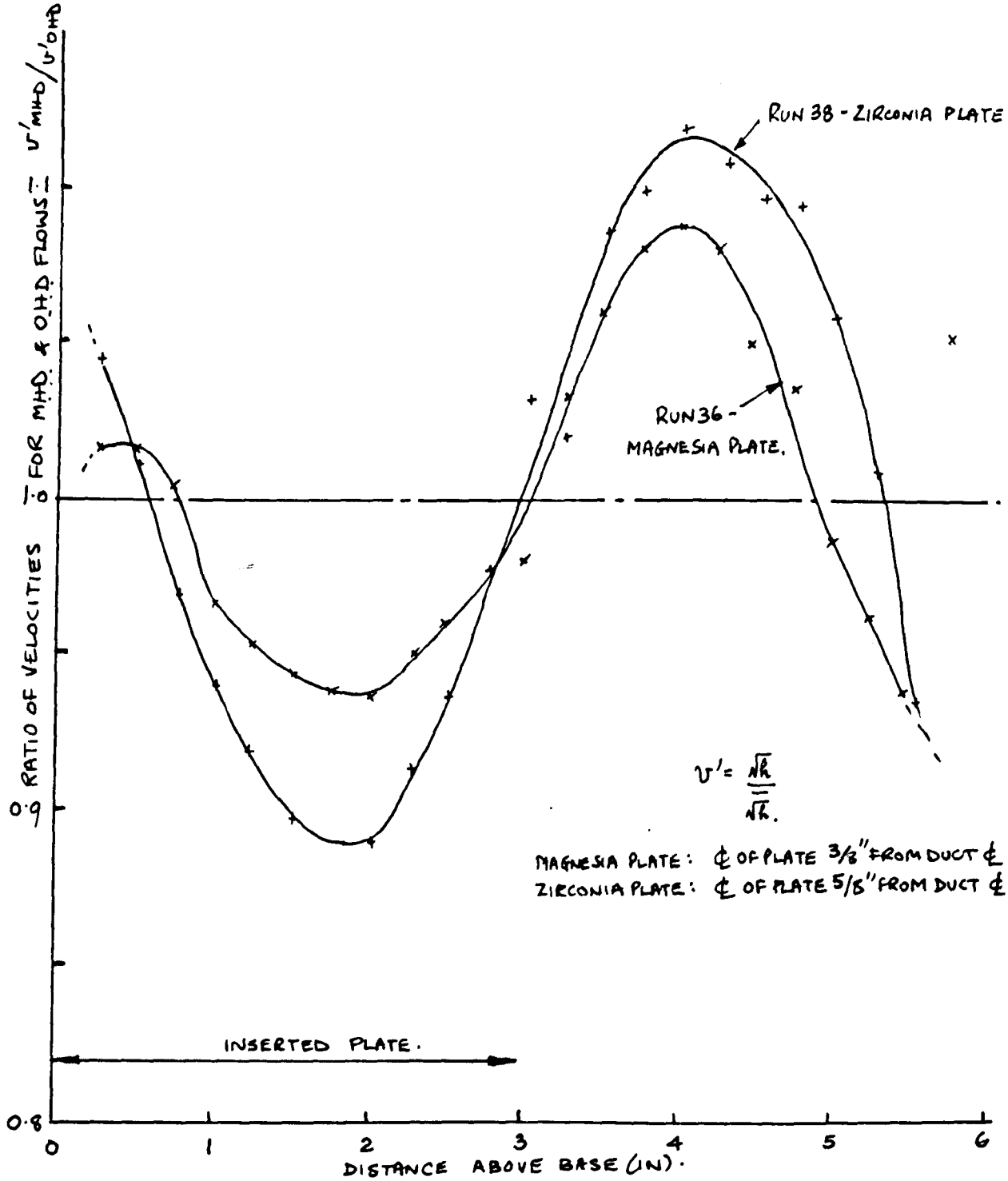

RUNS 36 & 38: THERMAL INPUT 100KW.
PROBE ON ℄ OF DUCT & IN PROBE HOLE 6.

RATIO OF VERTICAL VELOCITY PROFILES FOR O.H.D. & M.H.D. FLOWS - COMPARISON BETWEEN MAGNESIA & ZIRCONIA PLATES.

FIGURE 7.3.3.

reduce the magnitude of the interaction even further as it did in the results of section 7.2. The conductivity of the gas immediately adjacent to the plate was less than the conductivity in the core, but since the temperature of the plate was intermediate between the duct wall temperature and the gas temperature, there was a much thinner layer of low conductivity gas adjacent to the plate than on the duct walls, (it was estimated that the plate temperature was ~ 2000°C cf. duct wall temperature of ~1600°C) and so the attenuation of the magneto-viscous interaction was not so great at the plate compared with the duct wall.

The non-uniform shape of the O.H.D. profiles of $\sqrt{h}$ cannot be explained simply, but it is likely that the complex variations of density within the duct caused by the inserted 'hot' plate and the partially cooled walls are partly the cause. The O.H.D. flow is far from its fully developed state and the shape of the profiles may also be influenced by development effects.

The increase in M.H.D. interaction produced by the zirconia plate compared with the magnesia plate was not as great as may have been expected from Hasimoto's result. In fact, the difference in position of the plate between the two cases (the magnesia plate was 3/8" from the duct centre-line and the zirconia plate was 5/8") could account for all of the difference between the two results.

The fact that there was so little difference between the performance of the two plates may be explained by the existence of the cold (poorly conducting) sub-layer on the plate. The sub-layer acted as a barrier to the flow of current into the plate and so the conducting zirconia plate behaved almost as a non-conducting plate.

In the regions near the top and bottom walls of the duct, the ratio of M.H.D./O.H.D. profiles (Figure 7.3.3) showed a random behaviour. These regions were cool, conductivity was low and the M.H.D. interaction was either weak or non-existent.

7.3.2. The Effect of Gas Conductivity

The effect of variations in gas conductivity on the M.H.D. interaction in this configuration was investigated by varying the total flowrate through the rig (which also altered the total thermal input). This had two effects; (a) it altered the mean gas temperature in the test section, and hence the conductivity, (b) it altered the mean gas velocity. Effect (a) varied the Hartmann Number alone, and (b) varied the Hartmann Number and the Interaction Parameter. Table I shows the conditions which were used for the two sets of measurements.

	Thermal Input (KW)	Mean Gas Temperature (^{o}C)	Mean Gas Conductivity (mho/m)	Hartmann* Number	Interaction* Parameter
Case (a)	85	2225	5.3	7.0	0.07 ~~0.70~~
Case (b)	100	2350	10.0	9.5	0.11

TABLE I

* based on $\frac{1}{2}$ duct width and Transverse Magnetic field = 1 weber/m^2

In Figure 7.3.4 the normalised profiles for a thermal input of 85 KW and a zirconia plate are displayed and Figure 7.3.5 shows a comparison between these results and the results shown in Figure 7.3.2; (zirconia plate at 100 KW Thermal Input) again the comparison is framed in terms of the ratio of M.H.D. and O.H.D. profiles. The magnitude of the M.H.D. interaction will depend on the interaction parameter and the Hartmann Number - and one may postulate that

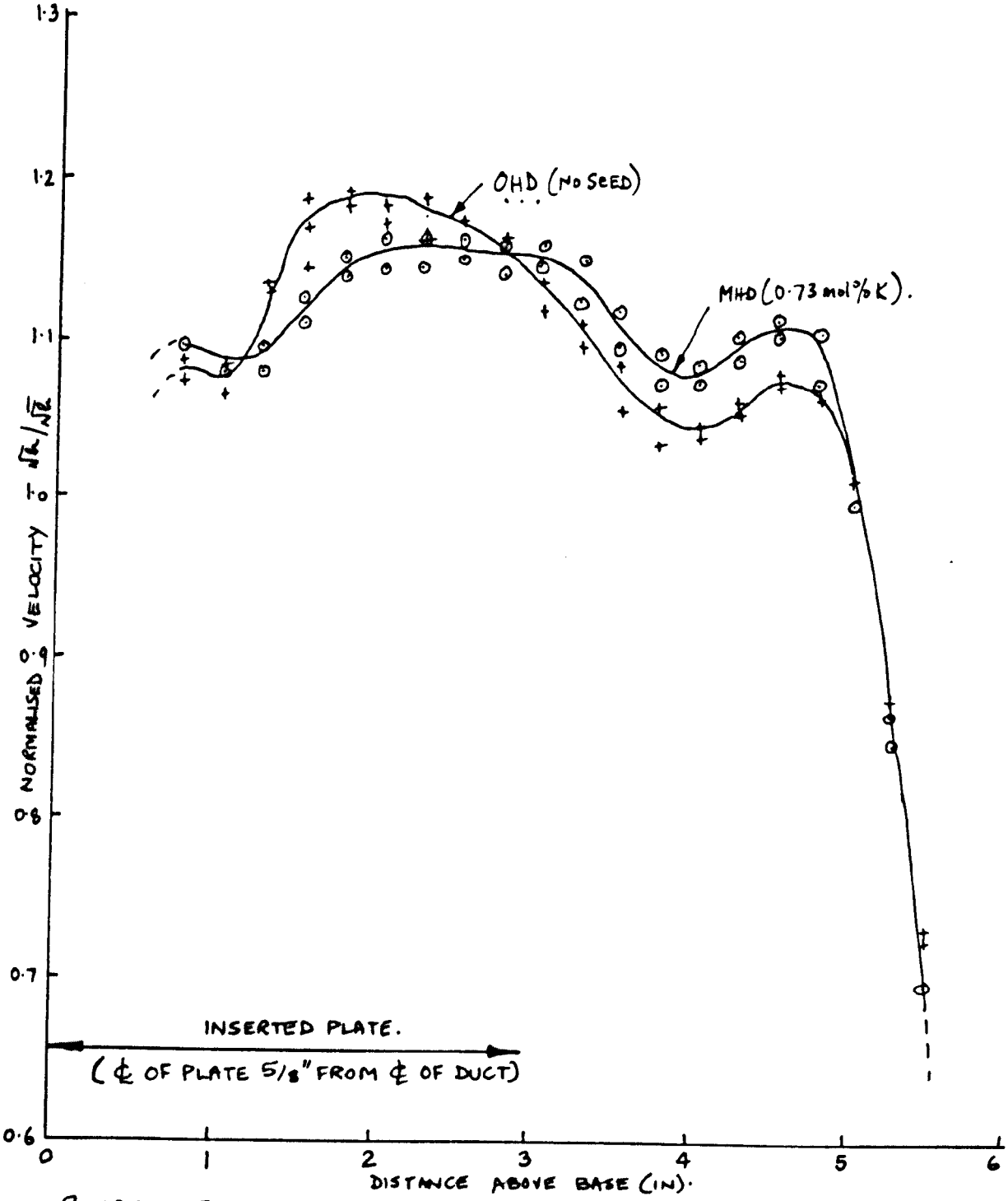

RUN 37: THERMAL INPUT 85 KW
PROBE ON ℄ OF DUCT & IN PROBE HOLE 6.

VERTICAL TRAVERSES WITH INSERTED ZIRCONIA PLATE

FIGURE 7.3.4.

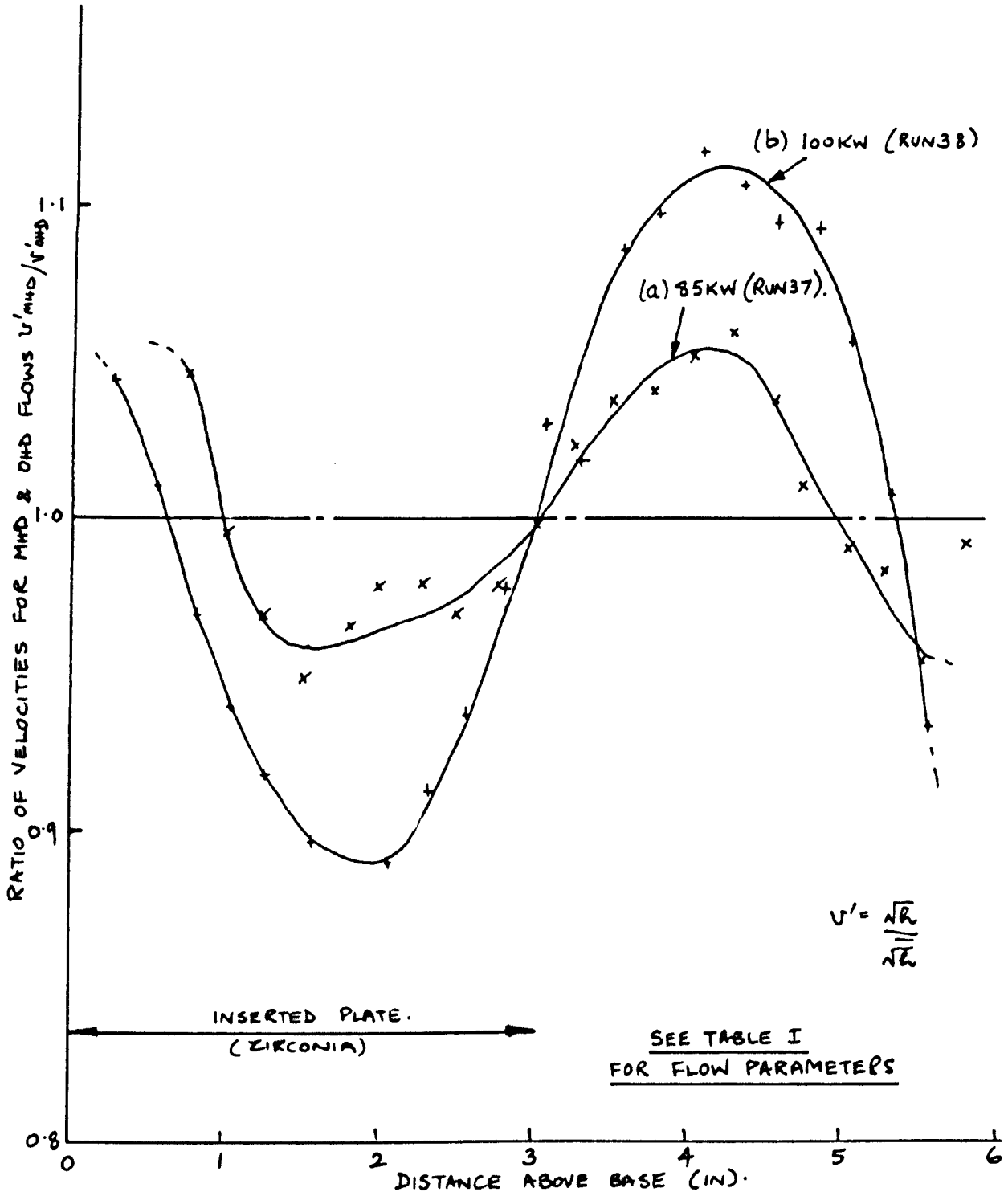

RUNS 37 & 38 : THERMAL INPUTS 85KW & 100KW RESPECTIVELY

RATIO OF VERTICAL VELOCITY PROFILES FOR OHD & MHD FLOWS - COMPARISON BETWEEN CASES WITH DIFFERENT THERMAL INPUT.

FIGURE 7.3.5.

the M.H.D. interaction ought to be proportional to the product of the interaction parameter and the Hartmann Number in a developing M.H.D. flow, since the depth (measured in the field direction) of the region adjacent to the plate which is affected by the M.H.D. disturbance based on the plate is $O(Hd_1)$. (Section 3.2 showed that the width of the transverse wake is $O\sqrt{\frac{d_1 x}{H}}$ and thus for the width to be $O(d_1)$ the value of x must be $O(Hd_1)$).

The ratio $\frac{H_a N_a}{H_b N_b} = 0{\cdot}47$ (using values from Table I), and the ratio of the peaks of the interaction curves of Figure 7.3.5, (a measure of the magnitude of the M.H.D. interaction) is 0.48, which shows somewhat fortuitous agreement with the theoretical postulate.

7.3.3. The Development Process

In order to investigate the development of the profiles, traverses were made at three probe-holes (Nos. 2, 4 and 6 - see Figure 7.2.1) along the length of the test section. Because of variations in temperature distribution between different positions along the duct and changes in conditions between the runs during which the various probe-holes were used, (caused by slight movements in the refractory lining and variations of flow conditions), it was impossible to make a direct comparison between the profiles measured at each traversing station. Instead, the ratio of the M.H.D. to O.H.D. profiles was again calculated and Figure 7.3.6 shows the variation in the shape of these profiles along the duct. Because the O.H.D. profile is very slow to develop, (in our case the hydrodynamic entry length is ~80 times the $\frac{1}{2}$ width of the channel i.e. ~7 ft, and the total length of the test section is only 1 ft) and the M.H.D. development distance is relatively short, (~10 times the $\frac{1}{2}$ width of the duct i.e. ~ 10 in) the variation in the ratio of the M.H.D. to O.H.D. profiles along the stream-wise direction will give an indication of the development of the M.H.D. interaction. Figure 7.3.6 shows this variation,

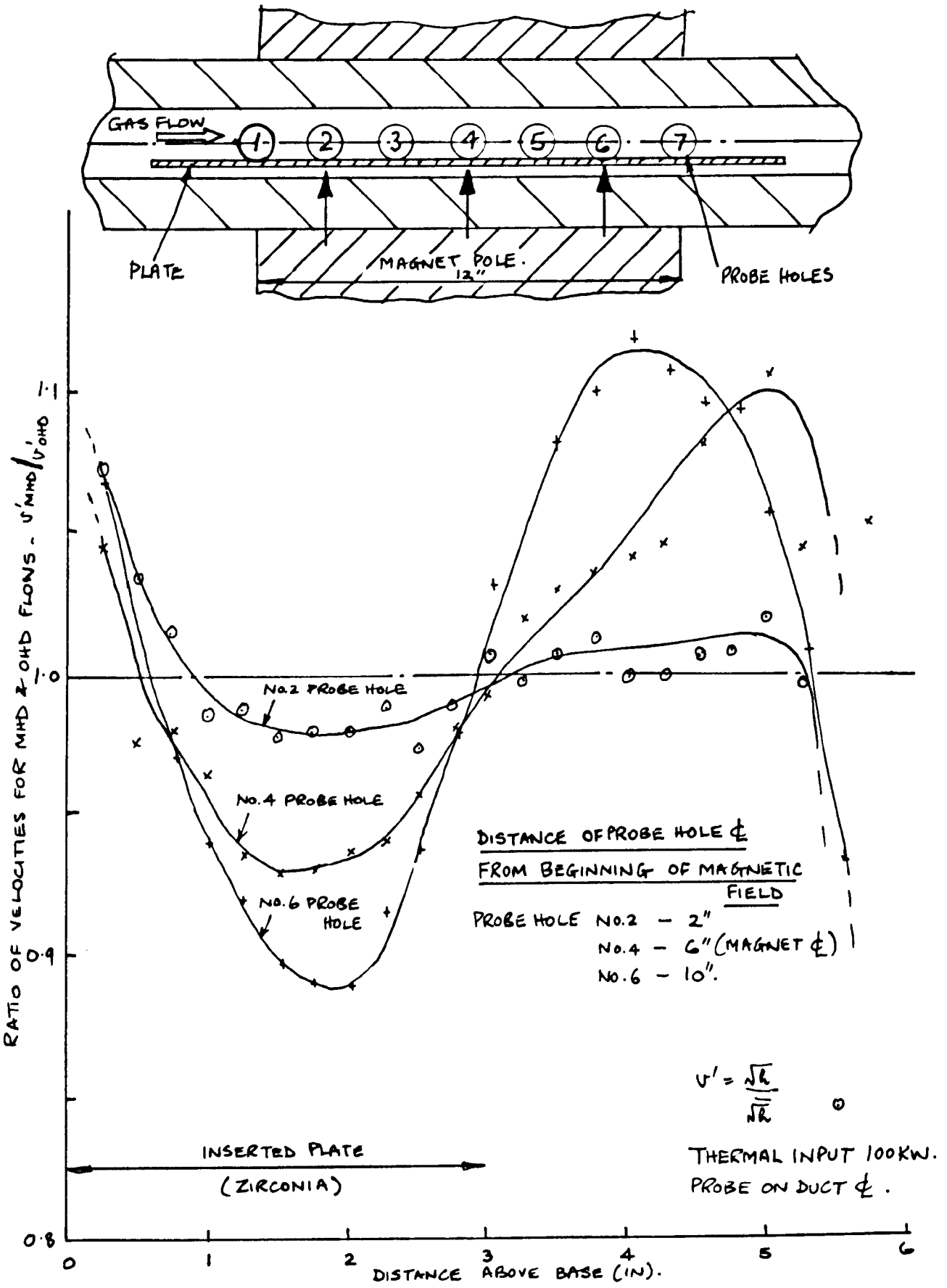

RATIO OF VERTICAL VELOCITY PROFILES FOR O.H.D. & M.H.D. FLOWS - PROBE AT THREE AXIAL POSITIONS ALONG DUCT.

FIGURE 7.3.6.

although no conclusions about the degree of approach to the fully developed M.H.D. flow can be made. (Section 7.4 describes a study of the development process of the O.H.D. and M.H.D. boundary layers on a flat plate).

All the other measurements of velocity profiles which are described in this section were carried out at probe hole No. 6, at which there was the maximum M.H.D. interaction before the downstream fringe field began to affect the flow.

7.3.4. 2-D Profiles over the Cross-section of the Duct

In order to investigate the properties of this flow configuration more fully, it was decided to probe over the 2-D cross-section of the duct at port hole 6. Figure 7.3.7 shows a vertical traverse result, for an axis displaced 3/8" off the centre-line of the duct towards the plate (see Figure 7.2.1) i.e. only 1/8" from the edge of the plate. These measurements were made with a crooked probe, with its tip offset 3/8" from the stem.

The results are presented in the form of the ratio between M.H.D. and O.H.D. profiles again in Figure 7.3.8, and the profile measured on the vertical centre-line of the duct is also presented for comparison. It can be seen that the interaction adjacent to the plate was reduced more than the interaction above the plate, when moving from the centre-line to the axis which was only 1/8" from the plate. This may be attributed to the cooling effect of the plate on the flow adjacent to the plate.

Two sets of horizontal traverses were also made, one at 100 KW and the other at 85 KW thermal input. These results, which are shown in Figures 7.3.9 and 7.3.10, were obtained at different heights above the base of the duct, and by using a combination of the straight probe and the crooked probe it was possible to traverse from the edge of the plate to 0.8" into the core and also above the plate.

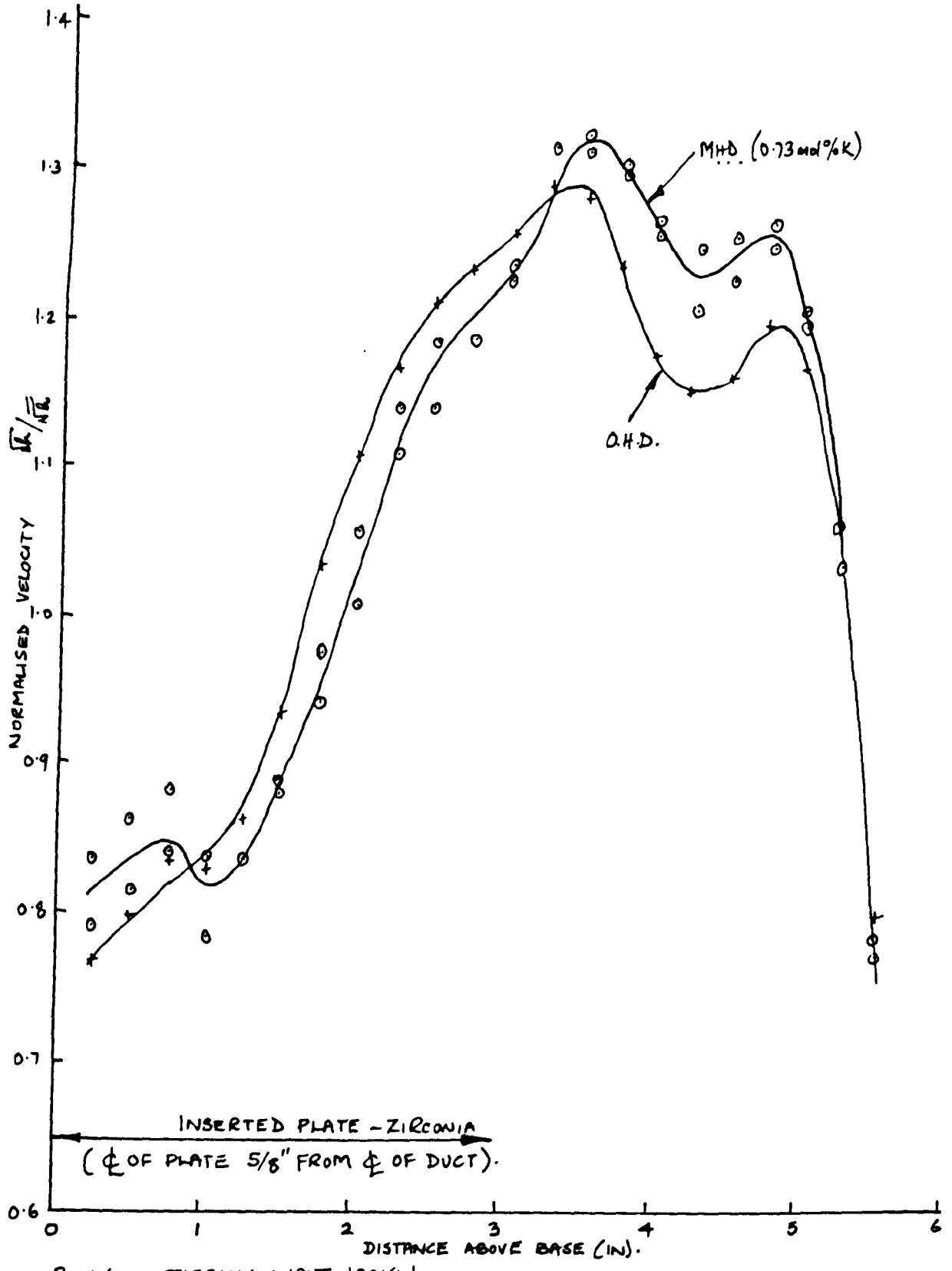

RUN 40 : THERMAL INPUT 100KW
PROBE OFFSET BY 3/8" (i.e. 1/8" FROM EDGE OF PLATE)
& IN PROBE HOLE 6.

VERTICAL TRAVERSES WITH INSERTED ZIRCONIA PLATE

FIGURE 7.3.7.

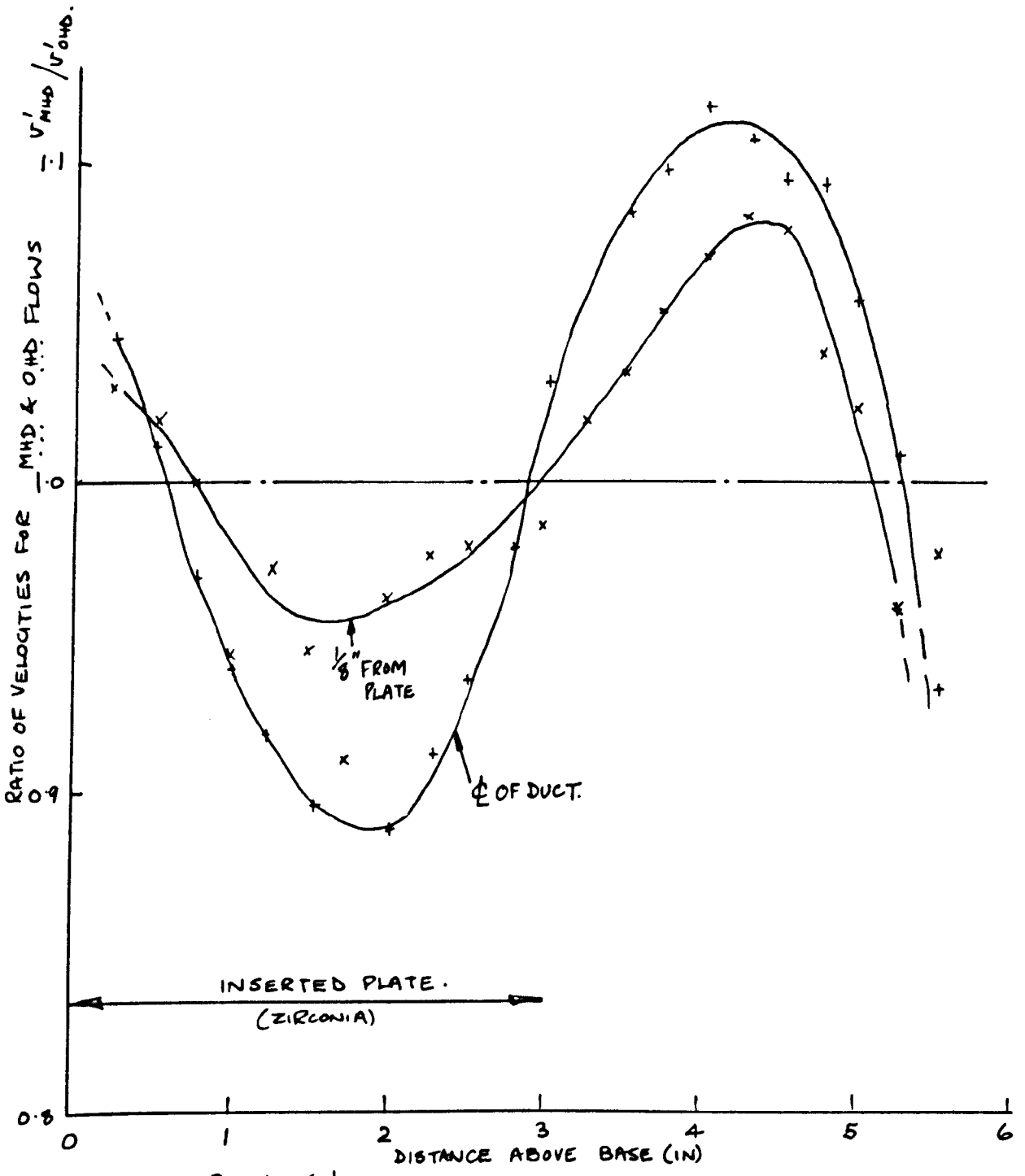

THERMAL INPUT 100KW.
PROBE ON CENTRE-LINE OF DUCT & OFFSET BY 3/8" (i.e. 1/8" FROM PLATE)
PROBE-HOLE 6.

RATIO OF VERTICAL VELOCITY PROFILES FOR OHD & MHD FLOWS. FIGURE 7.3.8.

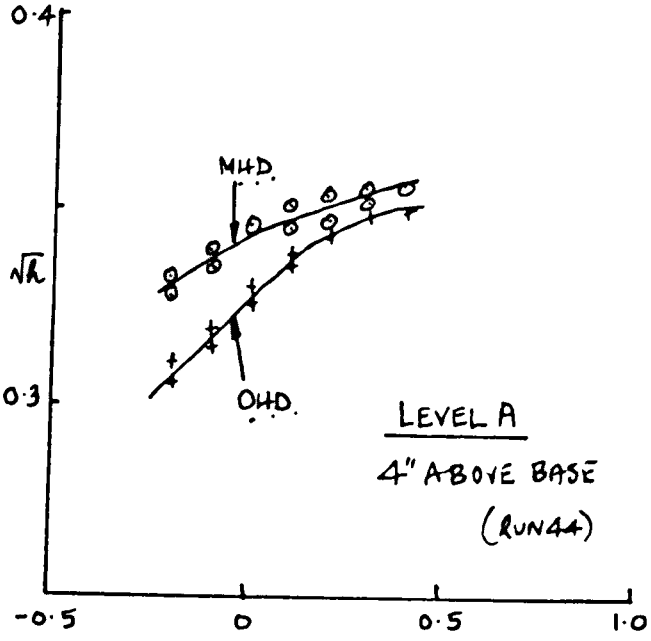

LEVEL A

4" ABOVE BASE

(RUN 44)

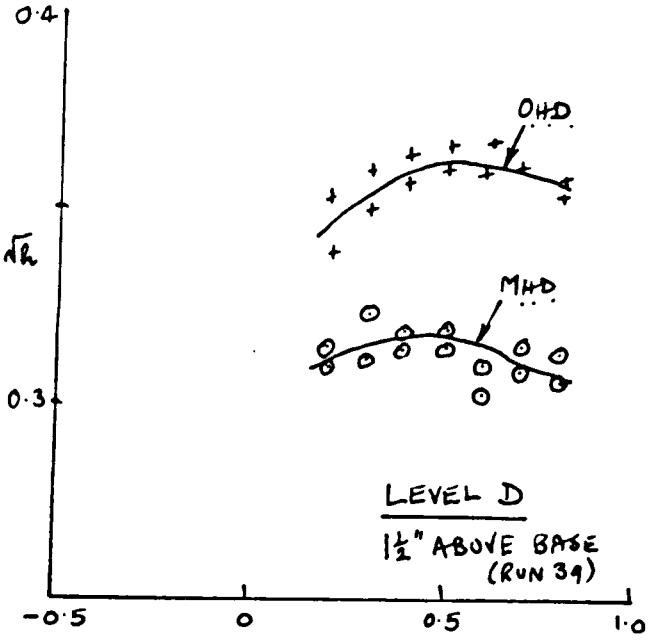

LEVEL D

1½" ABOVE BASE

(RUN 39)

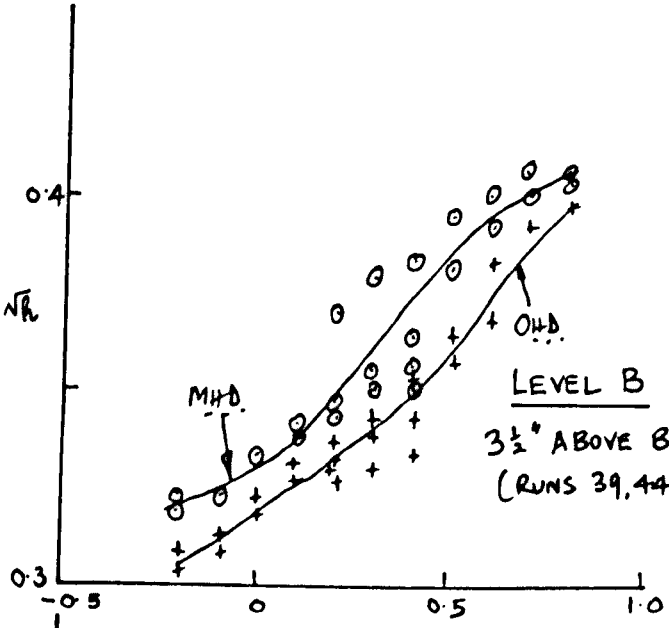

LEVEL B

3½" ABOVE BASE.

(RUNS 39, 44)

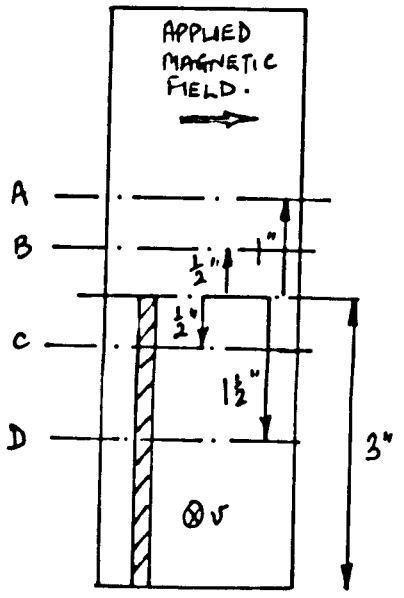

DUCT CONFIGURATION.

THERMAL INPUT 100 KW.

PROBE HOLE 6.

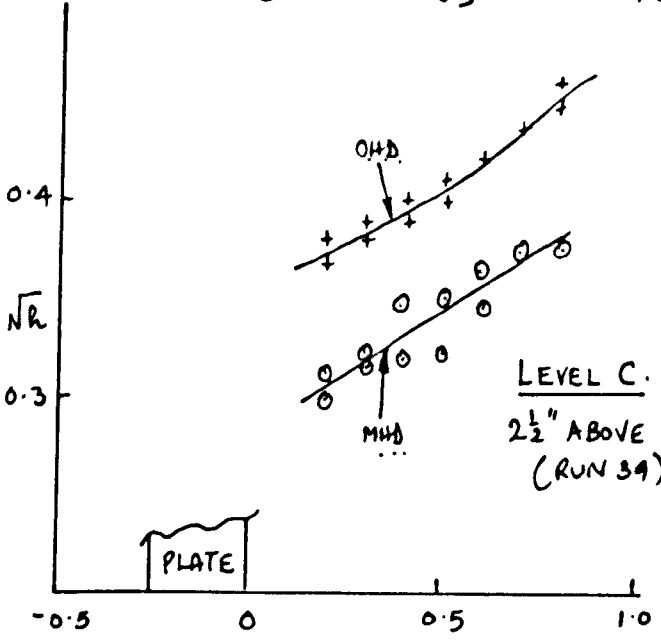

LEVEL C.

2½" ABOVE BASE

(RUN 39).

HORIZONTAL TRAVERSES WITH INSERTED ZIRCONIA PLATE.

FIGURE 7.3.9

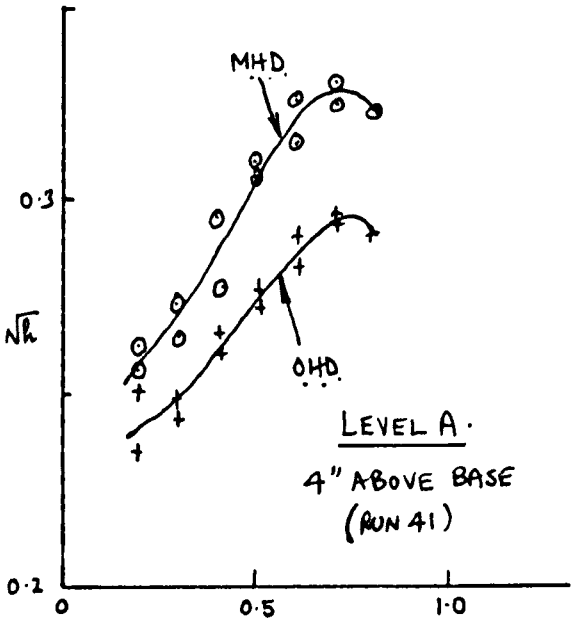

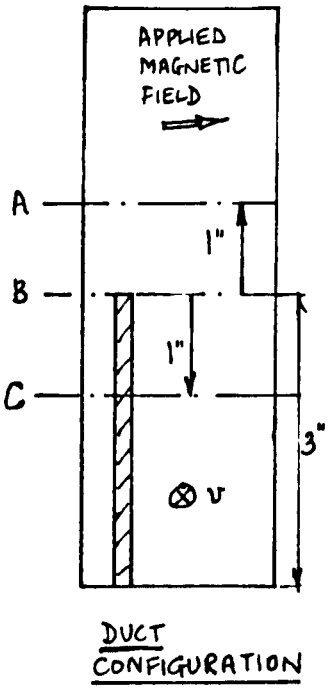

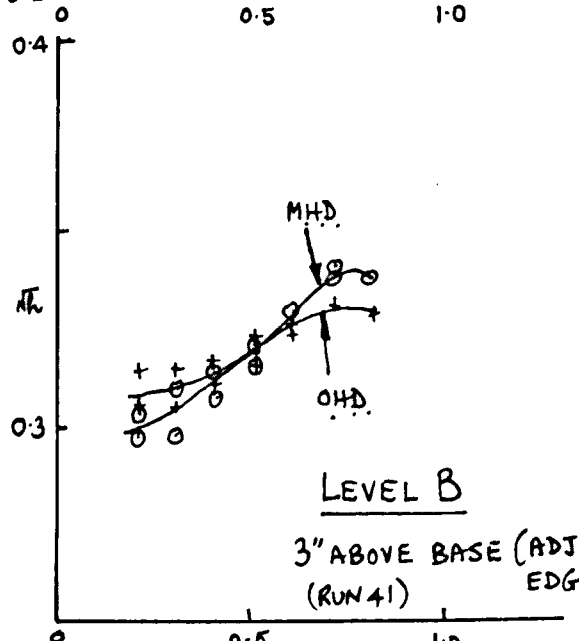

THERMAL INPUT 85KW
PROBE HOLE 6.

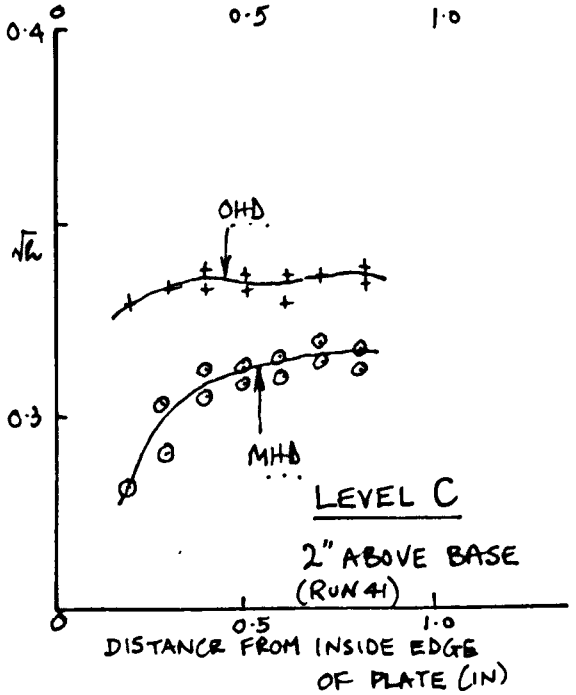

HORIZONTAL TRAVERSES WITH INSERTED ZIRCONIA PLATE. FIGURE 7.3.10.

It was possible to complete a set of these measurements much more quickly than the more extensive vertical traverses and generally, no variation in flow conditions was experienced during the period of measurement. Hence, there was no need to normalise the profiles as before - in any case it was found that the transverse (horizontal) M.H.D. and O.H.D. profiles did not differ significantly in shape at these low Hartmann Numbers since the transverse wake was not traversed. However, the actual values of $\sqrt{h}$, measured by the probe, display the same trends as the vertical traverses - the velocity above the plate being accelerated and the velocity below being decelerated. These traverses enabled the continuity of the interaction in the transverse direction (the direction of the applied field) to be verified and the existence of the transverse wake to be established. This can be seen from Figure 7.3.10 which shows measurements adjacent to the edge of the plate and 1" above and below the edge.

The M.H.D. profile is seen to be above the O.H.D. profile at the position 4" above the base, and below the O.H.D. profile at 2" above the base. At 3" above the base (adjacent to the edge of the plate) the M.H.D. and O.H.D. profiles are almost indistinguishable. These results are shown in Figure 7.3.11 in the form of ratios of M.H.D. and O.H.D. traverses for comparison with the ratio plots for the vertical traverses.

In Figure 7.3.9, the measurements which extended over the top of the plate show that the acceleration of the flow extended into that region from the central core.

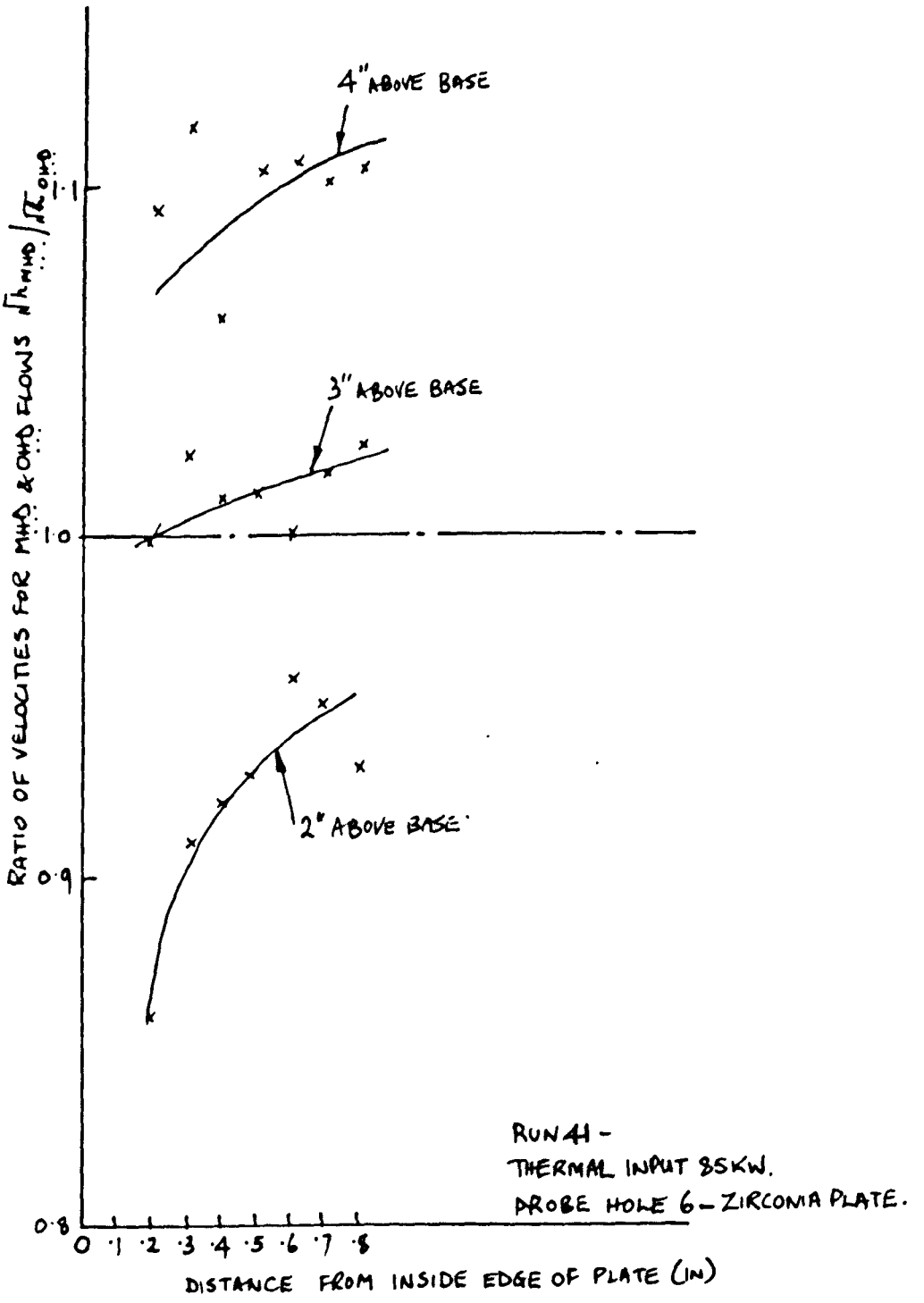

RATIO OF HORIZONTAL TRAVERSES FOR O.H.D & M.H.D FLOWS.

FIGURE 7.3.11.

7.4. Pitot-static Probe Measurements in a Rectangular Duct with an Immersed Plate. (Study of Boundary Layer Development).

Figure 7.4.1 shows the configuration of the duct which was adopted for this series of measurements. The plate configuration was similar to that used by Dix (1962), except that the flow was confined to a duct of finite dimensions. The plate was effectively 'long' in the vertical direction (and perpendicular to both the flow and the applied magnetic field) and 'semi-infinite' in the flow direction. The purpose of the measurements was to study the development of the boundary layer on the plate downstream from its leading edge (which was blunt), during both O.H.D. and M.H.D. flow conditions. A zirconia plate was used, although from the experience of 7.3, it was expected that the high conductivity of the plate would only slightly exaggerate the non-conducting case.

The water cooled pitot-static probe was used again to measure profiles of $\sqrt{h}$ in the transverse direction (i.e. perpendicular to the plate) at a height of 3" above the base of the duct (on the horizontal centre-line). With a thermal input of 100 KW, the probe was inserted at probe holes 3, 4, 5 and 6 in turn and $\sqrt{h}$ profiles were measured in each case under O.H.D. and M.H.D. conditions - the latter at a Hartmann Number of 9.5 (see Table I - section 7.3.2). Probe hole No. 3 was 1" upstream of the leading edge of the plate, and the other positions were 1", 3" and 5" downstream from the leading edge. Figure 7.4.2 shows the profiles which were obtained.

Upstream of the leading edge, there was only a slight modification in the shape of the O.H.D. profile when the M.H.D. interaction was introduced. Both O.H.D. and M.H.D. profiles are almost flat over the extent of the traverse. However, downstream of the leading edge, there is a marked difference between the O.H.D. and M.H.D. profiles. The O.H.D. profile initially shows an increase in $\sqrt{h}$ near to the plate (this is probably caused by the blockage effect of the

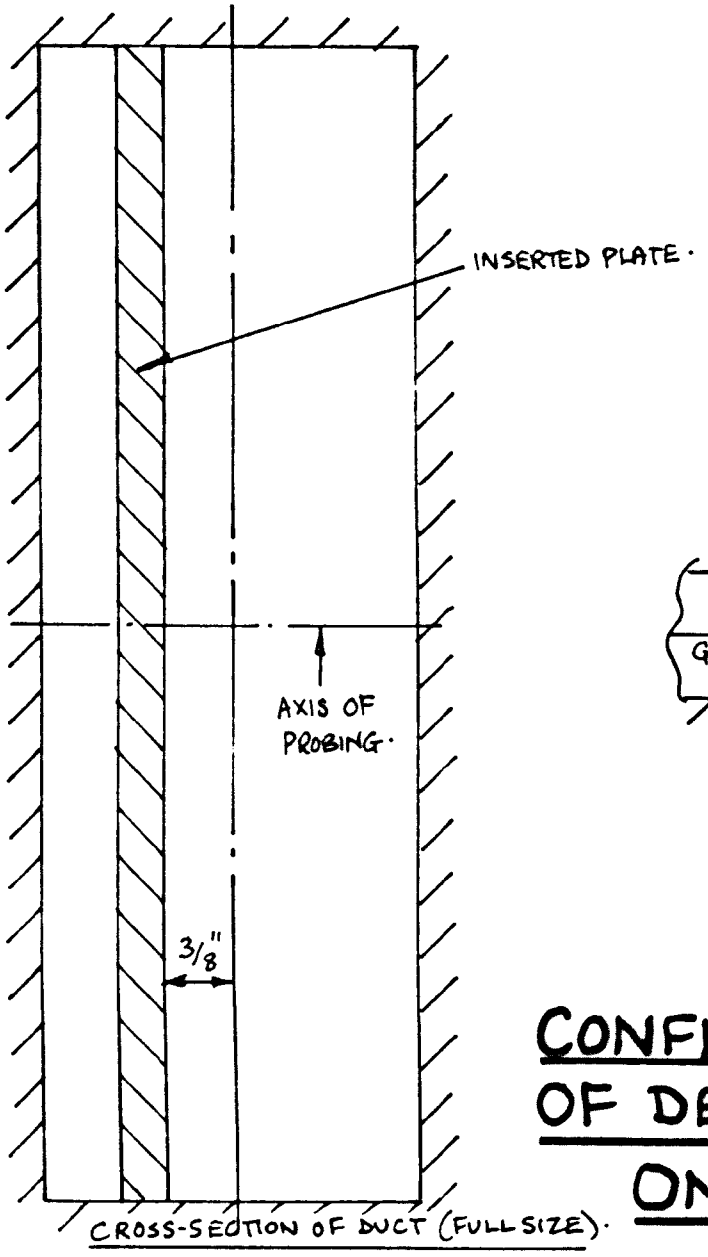

CROSS-SECTION OF DUCT (FULL SIZE).

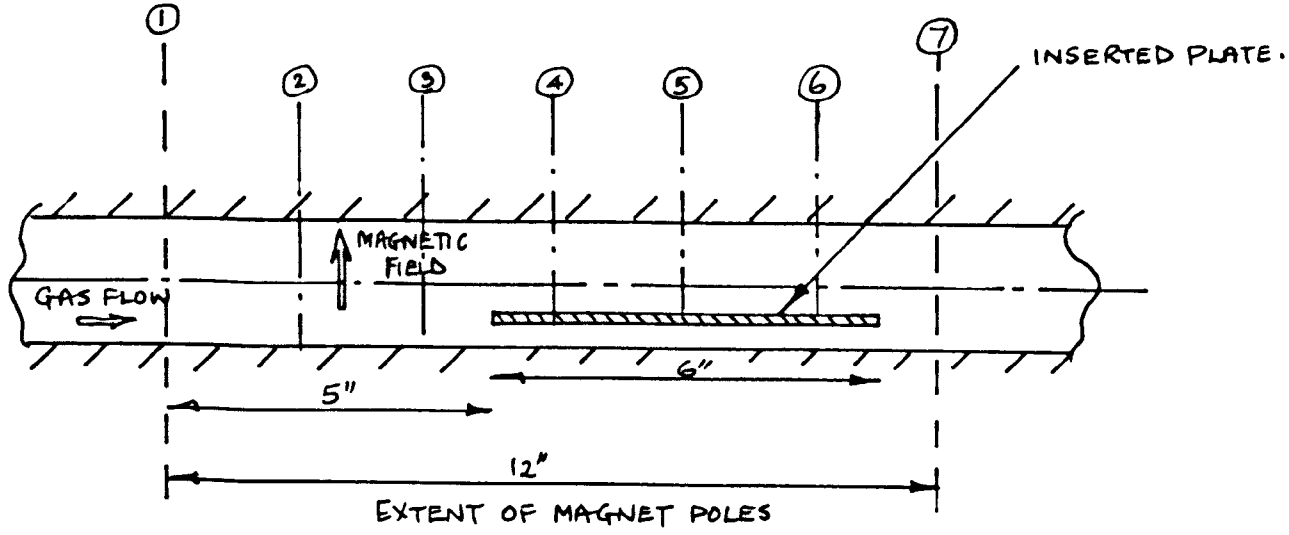

PLAN OF DUCT (1/3 FULL SIZE)

CONFIGURATION OF DUCT FOR INVESTIGATION OF DEVELOPMENT OF BOUNDARY LAYERS ON A FLAT PLATE. FIGURE 7.4.1.

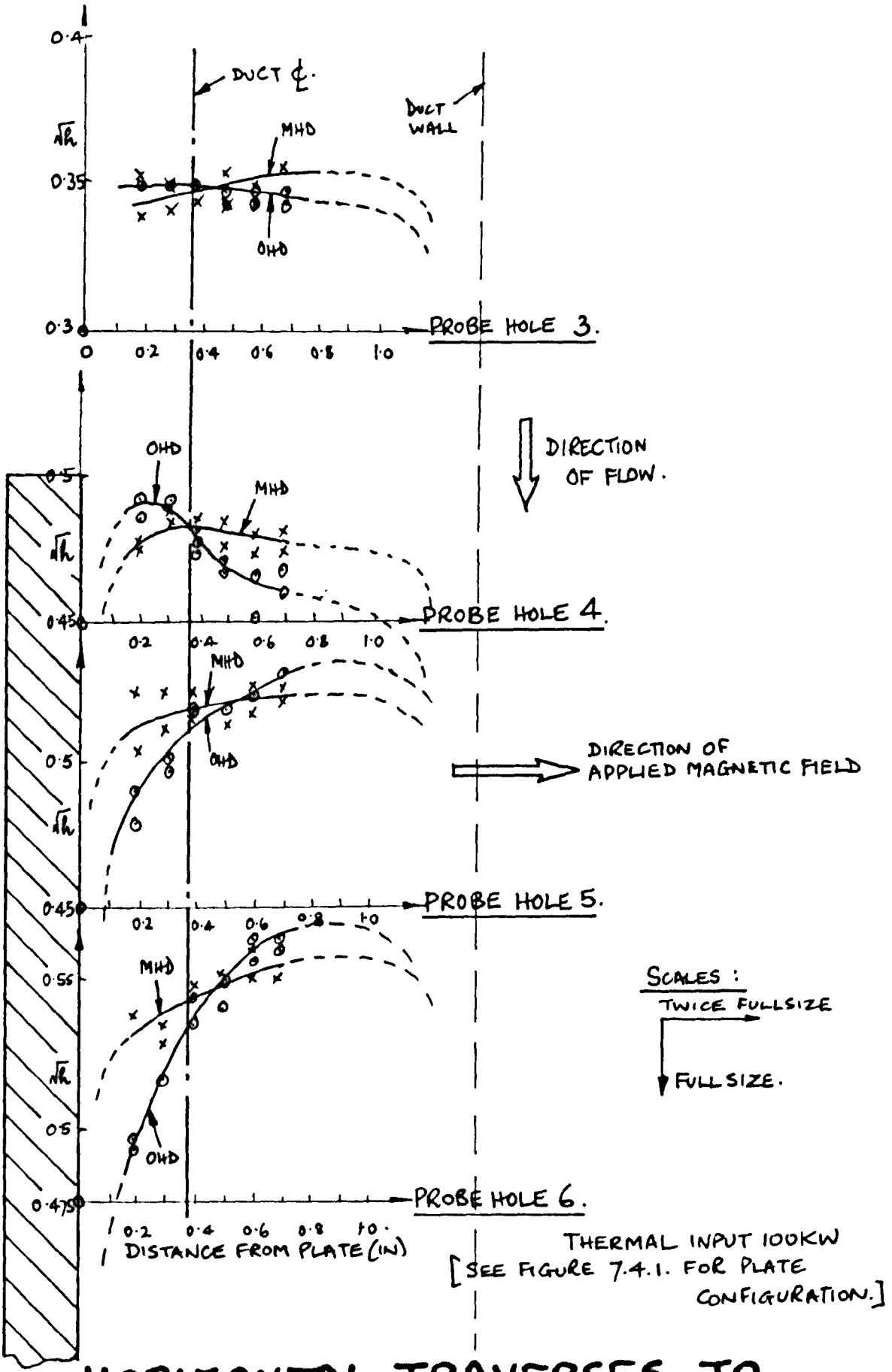

HORIZONTAL TRAVERSES TO DEMONSTRATE DEVELOPMENT OF BOUNDARY LAYERS ON A FLAT PLATE. FIGURE 7.4.2.

plate in the duct), but at the position of probe hole No. 5, the more conventional O.H.D. boundary layer shape can be seen to have appeared, and the slope of the profile near the plate has further increased at probe hole No. 6. The M.H.D. profiles are generally much flatter; the initial increase in $\sqrt{h}$ near the plate at No. 4 probe hole is not so marked and the Hartmann type profile develops quite quickly. There is very little difference in the shape of the M.H.D. profiles between probe holes 5 and 6, and the Hartmann layer thickness would appear to be $\sim 0.1"$ (i.e. $\sim \frac{d_1}{H}$), which agrees with the order of magnitude prediction of the simple isothermal theory. Thus the difference in temperature between the inserted plate and the gas flow cannot be great enough to provide a significant ordinary hydrodynamic sub-layer as experienced on the duct walls.

Although the traverses did not measure the velocity ($\sqrt{h}$) distribution across the full width of the duct, and so the mean velocity could not be determined accurately, the measurements made indicate that there is no significant change in the mean velocity between O.H.D. and M.H.D. cases at each station. By comparison, Figure 7.3.9 shows a change in the mean velocity between O.H.D. and M.H.D. cases in the region adjacent to the plate which is only half the height of the duct.

This comparison gives experimental evidence which complements the discussion by Hunt and Ludford (1968) on the differences between the solutions presented by Dix (1963) and Hasimoto (1960), for plates which are semi-infinite in the stream direction and semi-infinite perpendicular to the stream, respectively.

8. DISCUSSION OF RESULTS

8.1. Joule Heating Effects

In order to confirm that Joule Heating effects were not a predominant factor in the M.H.D. interaction, a simple order of magnitude analysis was carried out.

Power dissipation caused by joule heating = j^2/σ per unit volume. Assuming a gas velocity of 10 m/s and a transverse magnetic field of 1 weber/m^2, the open circuit electric field, assuming uniform flow, would be $\underline{U} \times \underline{B}$ = 10 volt/m. Assuming a conductivity of 10 mho/m (typical value for the core flow), the current density would be $\sim$100 amp/m^2.

$\therefore$ Power dissipation $\sim$1 KW/m^3, as a result of Joule heating.

The energy transferred from the gas to the walls of the duct by convection and radiation at the mid-point of the duct is $\sim$ 700 KW/m^3 (i.e. nearly three orders of magnitude greater than Joule heating). Even allowing for the fact that Joule heating will be greater in regions of lower conductivity near to the walls, (the conductivity only drops by 2 orders of magnitude and thus for the same current density, the joule heating will increase by only two orders), it is not likely to have a dominant effect on the density or velocity distributions.

8.2. Hall Currents - Effect on Velocity Distributions

Fay's work (1959) gives a guide to the effect of non-scalar conductivity on velocity distributions in our experiments. Fay considered a simple uniform property Hartmann Layer, and established the existence of a transverse flow (perpendicular to the core flow direction and the imposed magnetic field), and a thickening of the boundary layer at large values of the Hall parameter ($\omega\tau$).

The Hall parameter was $\sim$0.5 in these experiments , and Fay's analysis indicates that a transverse velocity of $\sim$14% of the core velocity would be induced in the Hartmann layer and the Hartmann layer itself would be

broadened by $\sim$10%.

It would be extremely difficult to carry out a complete analysis of duct flow with inserted plates in the presence of Hall currents, but this simple consideration of the interaction of the Hall Effect on the Hartmann boundary layer indicates that although some transverse flow in the Hartmann layers and some broadening of the layers may be expected, the overall change in velocity profiles as a result of the Hall Effect (with $\omega\tau \sim 0.5$) is only likely to be $\sim$10%. Hence, the theoretical solutions (Chapter 4) give a reasonable approximation to the non-scalar conductivity case experienced in practice. However, the omission of non-uniform conductivity from the theory is more serious.

8.3 Comparison between Velocity Profiles measured in the Experimental Programme and those predicted by Theory - Flows past long plates of half the duct height.

The experiments based on flows past long, thin plates, (section 7.3) which were only half the duct height, produced velocity profiles along a vertical axis (parallel to the plate and transverse to the flow direction) which in general indicated that with the M.H.D. interaction, the flow was decelerated in the region adjacent to the plate and accelerated in the core region above the plate. This result agrees qualitatively with the conclusions of Chapter 3, which described the similarity solutions for flow induced by a stationary semi-infinite plate in an infinite fluid with uniform velocity at large distances from the plate. Here, it was found that the M.H.D. solution showed that the velocity in the region adjacent to the plate was half the free-stream velocity and so a normalised profile which traverses the transverse wake ($v' = v/\bar{v}$, where $\bar{v}$ = mean value across traverse) produces a curve similar to the sketch shown in

Figure 8.3.1, (assuming that the profile does not include the Hartmann layer on the wall). If the profile is measured far enough away from the plate in O.H.D. flow, the effect of the plate on the uniform free-stream velocity distribution is not great, and Figure 8.3.1 also represents the form of the profile of U'_{MHD}/U'_{OHD}. This is similar in form to the profiles of U'_{MHD}/U'_{OHD} produced in section 7.3 - see Figure 7.3.3 for example.

However, it was expected that the walls of the duct would interfere with the 'infinite fluid' solutions of Chapter 3 and so numerical solutions (Chapter 4) of duct flow with inserted plates were produced. Velocity profiles of the same form as before (i.e. U'_{MHD}/U'_{OHD}) were produced from the pressure driven flows (section 4.4) at the vertical axis which was midway between the plate and the wall, and these are presented in Figures 8.3.2 and 8.3.3. Four duct shape-factors were employed, which demonstrate that no simple relationship between the M.H.D. and O.H.D. flows exists, with a Hartmann Number of 10 for the M.H.D. cases. The interference between the M.H.D. effects produced by the plate and the effects produced by the duct walls themselves is highly dependent on the duct shape factor, and the ratio of M.H.D. to O.H.D. normalised velocity profiles shows that a simple relationship such as that shown in Figure 8.3.1 cannot be applied to the case of flows which are limited by finite ducts. In fact the same relationship only holds for cases with $S \sim 1$. For high values of S, the shape of the curve is reversed, and for low values, the curve displays the characteristics of a rectangular duct flow in which the centre plate acts as a complete wall, see Figure 8.3.3. Thus the proximity of both the top and bottom walls have a severe effect on the ratio U'_{MHD}/U'_{OHD} at this value of the Hartmann Number.

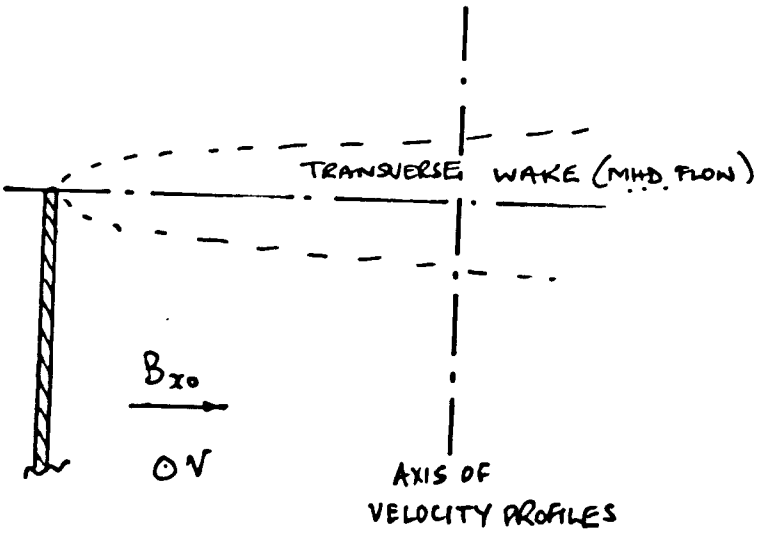

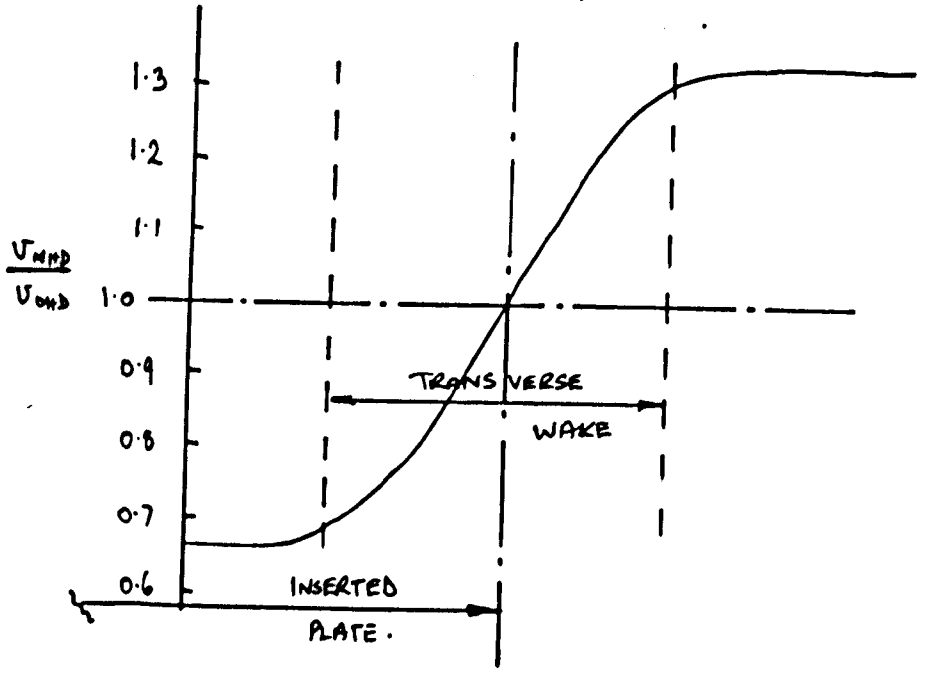

~ UNIFORM OHD VELOCITY DISTRIBUTION - AT LARGE DISTANCE FROM PLATE

RATIO OF VELOCITY PROFILES FOR STATIONARY, SEMI-INFINITE PLATE IN AN INFINITE FLUID. FIGURE 8.3.1.

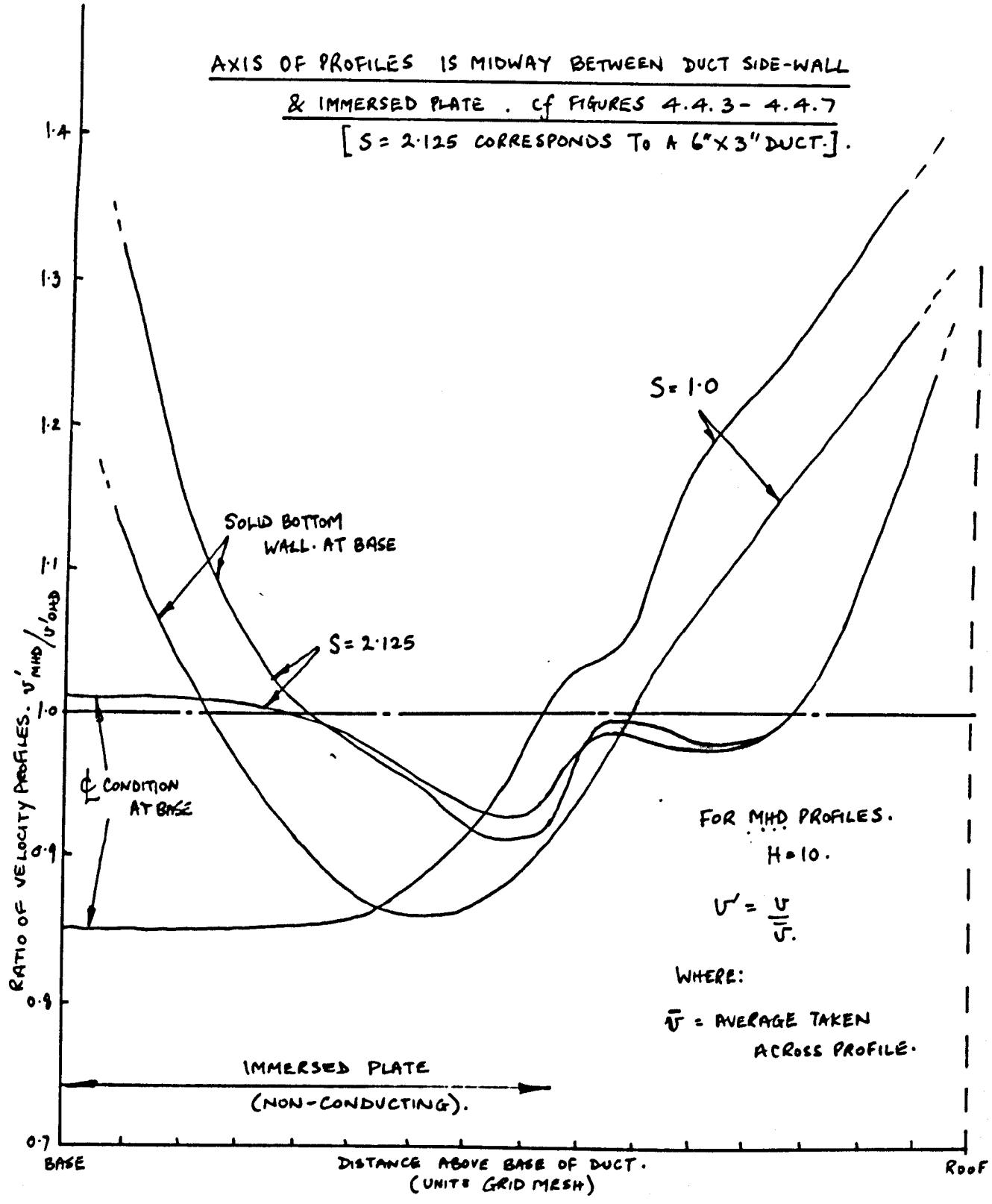

RATIO OF VELOCITY PROFILES - PRESSURE DRIVEN FLOWS IN RECTANGULAR DUCTS WITH IMMERSED PLATES. (COMPUTER SOLUTION). FIGURE 8.3.2.

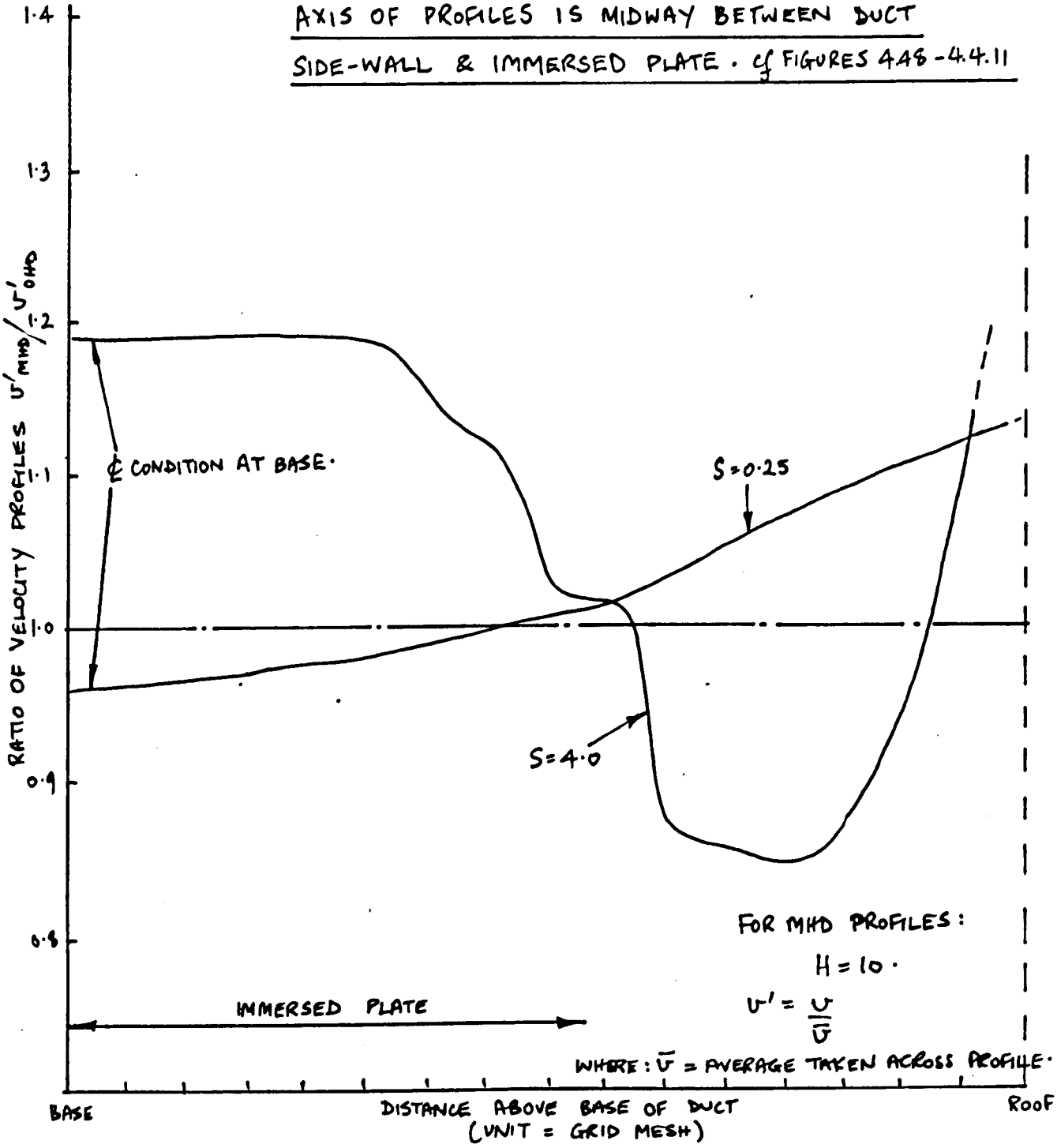

RATIO OF VELOCITY PROFILES - PRESSURE DRIVEN FLOWS WITH VARYING SHAPE FACTOR. (COMPUTER SOLUTION)

FIGURE 8.3.3.

The results of section 7.2 - flows in a rectangular duct with no immersed plates - showed that there was negligible M.H.D. interaction when the duct walls alone were the source of boundary layers in the flow. This was attributed to the low temperature ($\sim 1600^{o}C$) of the walls. When the immersed plate experiments were carried out with an identical duct construction, no Hartmann layer formation could therefore be expected to occur on the duct walls. The immersed plate, which was several hundred degrees hotter than the walls, would be able to sustain a Hartmann layer, however, (the results of section 7.4 demonstrated this) and so the flow in the duct would behave like an M.H.D. flow throughout the core and near the immersed plate, but not near the duct walls. The boundary condition on the perimeter of the effective M.H.D. region would then approximate to a moving insulating wall condition - i.e. the boundary would be a layer of non-conducting, moving gas. Hence the velocity distribution is not likely to show close similarity to the pressure driven theoretical cases, in which a stationary wall condition was used.

The actual situation achieved in the experiments of section 7.3 was therefore an addition of an M.H.D. flow excited by a moving wall condition with a stationary plate and a pressure driven M.H.D. flow within the region bounded by the limit of the electrically conducting fluid, i.e. a mixture of Figure 4.5.5 and Figure 4.4.4. Surrounding this region there would be a region of cooler, non-conducting gas which provided slip between the M.H.D. region and the duct walls. It is impossible to make any quantitative conclusion from this hypothesis, since the position of the limit of electrical conductivty is not known and this would affect the resulting situation quite critically. For this reason also, it was decided not to attempt to model the situation using the computer.

It would also be very difficult to apply the method of Kieffer (1965) to make even qualitative conclusions about the effect of non-uniform conductivity, since a precise knowledge of the spatial variation of conductivity is required in his method. (Step-functions and continuous functions of conductivity were used). The only way of providing a complete solution to the non-uniform conductivity case would be to solve the momentum equation, electrodynamic equation and the energy equation simultaneously, i.e. by coupling the conductivity variation with temperature variations. This poses a considerable problem for computation in all but the simplest cases, and was beyond the scope of the present project.

The theoretical work described in Chapter 4 was undertaken before the results of any experiments were available and it could be argued that in the light of experimental results, it was not the most suitable study for producing a greater understanding of the experimental results. However, it was the nearest approximation to physical reality which could be modelled by numerical methods with the available resources. Having accepted its major limitation of uniform conductivity, it still gives an increased understanding of uniform property M.H.D. flows in the range of geometries studied and indicates some of the effects which may be expected to arise in more complex situations where the conductivity is variable - especially if hotter duct walls could be produced.

9. SUMMARY OF CONCLUSIONS

(a) Similarity solutions were obtained for the fully developed M.H.D. flow induced by the movement of a semi-infinite non-conducting flat plate, moving along its own length with a transverse magnetic field. (The plate was semi-infinite in the direction perpendicular to the field and flow). These results gave a clear indication of the qualitative nature of transverse wakes which emanate from the edge of such plates, although the solution was not so complete as that given by Hasimoto (1960).

(b) Numerical solutions (by computer) were obtained for ordinary hydrodynamic and M.H.D. duct flows, both with and without immersed plates. Fully developed flows in rectangular ducts were considered for fluids of uniform properties and two-dimensional variations of velocity and current stream-lines across the cross-section of the duct were produced. Solutions for simple cases were compared with exact analytical solutions and showed good agreement.

The effect of inserting a plate (long in flow direction) of half duct height (perpendicular to the applied field) was investigated in the case of pressure driven flow and the transverse wake phenomenon was again demonstrated. Several cases of flows excited by moving parts of the duct wall or an inserted plate were investigated and compared with the similarity solutions and Hasimoto's solutions.

(c) Experiments were carried out on combustion plasma flows to determine the form of the interaction of a transverse magnetic field on the velocity distribution. It was found that a magneto-viscous interaction could be produced using a high temperature, refractory plate which was immersed in the flow. This interaction was investigated with a water-cooled pitot-static probe which was used to measure two-dimensional

velocity distributions over a cross-section of the duct near the end of the region of transverse magnetic field.

(d) In the case of an inserted plate which was half duct height and long in the flow direction (and perpendicular to the applied field), the experimentally determined interaction was shown to be qualitatively the same as the similarity solutions for a semi-infinite plate in an unbounded flow. It did not, however, correspond closely to the numerical solutions for duct flows with inserted plates. This discrepancy was attributed to the fact that the duct walls were much cooler than the inserted plate and the gas in the boundary layers on the duct walls was not electrically conducting. An attempt to produce an M.H.D. interaction in the rectangular duct without an inserted plate was not successful for the same reason.

(e) Using an inserted plate which was the full duct height and perpendicular to the applied field, but semi-infinite in the flow direction, the development of boundary layers was studied for O.H.D. and M.H.D. conditions. The M.H.D. layer (Hartmann type) was found to be thinner and to develop more quickly than the viscous O.H.D. layer.

(f) A miniature water-cooled pitot-static probe and an R.F. conductivity probe were successfully developed for use under conditions of 2300°C, 1 atm, seeded combustion gases.

(g) The magnitude of the magneto-viscous interactions produced in these experiments at a Hartmann Number of ~10 was sufficiently substantial to warrant a more detailed study of the configurations to be used in open cycle M.H.D. Generators where Hartmann Numbers of $\sim 10^3$ may well be experienced.

10. RECOMMENDATIONS FOR FUTURE WORK

(a) The technique used for the computer solutions could be extended to deal with electrically conducting wall conditions by introducing a short iterating routine which would enable boundary conditions of the form $v' = 0$, $\frac{\partial B'}{\partial n} = 0$ to be simulated by successive approximations from an initially guessed solution on the boundary. This extension was not pursued here because (i) it would have involved too much computer time and (ii) all the experiments dealt effectively with non-conducting walls.

(b) The possibility of solving non-uniform conductivity situations by a direct simultaneous solution of the momentum, energy and electrodynamic equations should be explored for some simple boundary layer configurations. This exercise would involve considerable computing effort.

(c) The development process of the transverse wake produced in Hasimoto's configuration should be investigated further. Again, numerical (computerised) methods may prove useful at moderate Hartmann Numbers.

(d) The experimental programme could best be extended by using a larger apparatus - particularly a larger magnet. This would allow higher wall temperatures to be achieved (by allowing the inclusion of more effective duct wall insulation within the magnetic field) and higher Hartmann Numbers (achieved by increasing the scale of the experiment and/or by decreasing the heat losses by better insulation, so preserving high gas temperatures and conductivity). Also, if a longer magnetic field is combined with a low heat loss duct, flows which are more nearly fully developed could be produced.

(e) If very high wall temperatures were achieved ($\sim$ gas temperature), then the other interesting class of transverse M.H.D. wake could be investigated, viz. that produced by a discontinuity in wall electrical conductivity.

11. REFERENCES

Alpher R.A. Hurwitz H., Johnson R.H., and White D.R., 1960, Rev. Mod. Phys. 32. 4. 758.

Alty C.J.N., 1966, 'Magnetohydrodynamic Duct Flow', Ph.D. Thesis, Cambridge University.

Bleviss Z.O., 1960, J. Fluid Mech. 9. 49.

Braginskii S.I., 1960, Soviet Physics JETP. 37. (10). 5. 1005.

Brogan T.R., 1962, in 'Gas Discharges in the Electricity Supply Industry, Ed. Forrest, Butterworths, p. 571.

Bugden et al, 1964, Proc. O.E.C.D. Int. Symp. M.H.D. Elect. Power Gen. Paris, 3. 1105.

Butterfield P., Schofield J., and Young P.A., 1963, J. Iron and Steel Inst. 201.

Cramer K.R., 1965, 'Variable Conductivity M.H.D. Couette Flow'. Office of Aerospace Research Report (U.S.A.F.). No. ARL 65 - 13.

Cranfield R.R., 1966, C.E.G.B. Report No. RD/M/N172.

Dickson D.J., Sanders R.W., and Tseung A.C.C., 1964, Proc. O.E.C.D. Int. Symp. M.H.D. Elect. Power Gen. Paris. 3. 1127.

Dix D.M., 1963. J. Fluid Mech. 15. 449.

East D.A., 1964, 'The Pitot Tube in Magnetohydrodynamics', Ph.D. Thesis, Mass. Inst. Tech.

English P.E. and Rantell T.D., 1968, 'The Determination of the Electrical Conductivity of the Gases in a Pitot-Scale Coal-Fired M.H.D. Combustor'. B.C.U.R.A. Research Report M.H.D. 36.

Fay J.A., 1959, 'Hall Effect in Laminar Hartmann Boundary Layers'. Avco-Everett Research Report No. 81.

Gaydon A.G. and Wolfhard H.G., 1960, 'Flames, their Structure, Radiation and Temperature', Chapman and Hall.

Goodwin E.T., (Senior Editor), 1960,'Modern Computing Methods'. 2nd Ed. Notes on Applied Science No. 16. H.M.S.O.

Gray W.A. and Smith J.L., 1967, J. Inst. Fuel, May '67. 186.

Grayston A.M., 1966, 'A Computer Program for the analysis of combustion products used in M.H.D. Generation'. C.E.G.B. Research Report No. RD/L/N52/66.

Green S.W., 1957, 'Viscosity and Thermal Conductivity of Rocket Gas Mixtures', R.A.E. Tech. Memo. R.P.D. 132.

Grieg J.R., 1964, 'The Sodium D-line Reversal Method of Temperature Measurement'. C.E.G.B. Research Report No. RD/L/R1253.

Hale F.J. and Kerrebrock J.L., 1964, J.A.I.A.A., 2. 3. 461.

Hasimoto H., 1960, J. Fluid Mech. 8. 61.

Hartmann J. and Lazarus F., 1937, Math-fys Medd. 15. 7. 1.

Henderson F.M., 1960, 'Elliptic Functions with Complex Arguments', Univ. of Michigan Press.

Heywood J.B., 1965, A.I.A.A.J., 3. 9. 1752.

Heywood J.B. and Womack G.J. (Editors), 1969, 'Open Cycle M.H.D. Power Generation. (Pergamon).

Hunt J.C.R., 1967, 'Some aspects of Magnetohydrodynamics', Ph.D. Thesis, Cambridge University.

Hunt J.C.R. and Leibovitch S., 1967, J. Fluid Mech. 28. (2). 241.

Hunt J.C.R. and Ludford G.S.S., 1968, J. Fluid Mech. 33. (4). 693.

Hunt J.C.R. and Malcolm D.G., 1968, J. Fluid Mech. 33. (4). 775.

Hunt J.C.R. and Stewartson K., 1966, J. Fluid Mech. 23. (3). 533.

Hunt J.C.R. and Williams W.E., 1968, J. Fluid Mech. 31. (4). 705.

Kastner L.J. and Spooner J.R., 1950, Proc. Instn. Mech. Engrs. London, 162. 149.

Kerrebrock J.L., 1961, J. Aero. Sci. 28. 8. 631.

Kieffer P.C., 1965, 'Variable Conductivity Fully Developed M.H.D. Channel Flow'. M.S. Thesis. Air Force Institute of Technology, Air University.

Langlois W.E., 1964, 'Slow Viscous Flow', MacMillan.

McAdams W.H., 1954, 'Heat Transmission'. McGraw-Hill.

Moffatt H.K., 1964, Proc. 11th Int. Appl. Mech. Cong. (Munich), p.946.

Moffatt W.C., 1964, A.I.A.A.J., 2. 1495.

Nettleton M.A. and Raask E., 1965, 'Measurements of the Rate of Evaporation of Potassium Sulphate Droplets'. C.E.G.B. Research Report RD/L/N121/65.

Olin J.G., 1966, 'Turbulence Suppression in Magnetohydrodynamic Flows'. Report No. 85, Stanford University, Insitute for Plasma Research.

Oliver D.A. and Mitchner M., 1967, J.A.I.A.A., 5, 3. 1424.

Olson R.A. and Lary E.C., 1962, Rev. Sci. Insts. 33. 1350.

Ryshkewitch E., 1960, 'Oxide Ceramics - Physical Chemistry and Technology'. Academic Press.

Sato H., 1961, J. Phys. Soc. Japan. 16. 7. 1427.

Schowalter W.R. and Blaker G.E., 1961, J. Appl. Mech., March '61. 136.

Shercliff J.A., 1953, Proc. Camb. Phil. Soc. 49. 1. 136.

Shercliff J.A., 1956, J. Fluid Mech. 1. 6. 644.

Shercliff J.A., 1965, 'A Text-book of M.H.D.'. Pergamon.

Sonju O.K., 1968, 'Viscous Magnetohydrodynamic Flows'. Report No. 245. Stanford University Insitute for Plasma Research.

Tani I., 1962, J. Aero. Sci. 29. 3. 297.

Taylor D.S., 1967, 'Gas Conductivity Determinations using Radio Frequency Energy Dissipation Techniques'. University of Sheffield, Dept. of Fuel Tech. and Chem. Eng., Report No. FTCE/4/DST.

Thomas D.L., 1967, 'Application of the Sodium D-line Reversal Method of Temperature Measurements to M.H.D. Flames'. C.E.G.B. Research Report No. RD/L/R1486.

Todd, L., 1967, J. Fluid Mech. 28. (2). 371.

Todd, L., 1968, J. Fluid Mech. 31. (2). 321.

Waechter R.T., 1966, 'Asymptotic Methods for Large Hartmann Number in Magnetohydrodynamics'. - Ph.D. Thesis. Cambridge University.

Waechter R.T., 1968, Proc. Camb. Phil. Soc. 64. 871.

Yakubenko A.Ye., 1963, Zh. Prikl. Mekh. Tekh. Fiz. 6. - N.A.S.A. Trans. TTF-241, 1964.

Yen J.T., 1964, Phys. Fluids. 7. 5. 723.

APPENDIX A

DETAILS OF COMPUTER PROGRAM USED IN NUMERICAL ANALYSIS

A.1 FORMATION OF MATRIX EQUATION FROM FINITE DIFFERENCE MESH

In order to adapt the finite difference technique to a direct method of solution suitable for computation, the set of simultaneous linear equations obtained by writing the governing equation

$$\left[\nabla'^2 + H\frac{\partial}{\partial x'}\right]\phi'_+ = \frac{\partial b''}{\partial z} \qquad \ldots.A.1.1.$$

in terms of finite differences for each point ($\phi_{0,0}$) on the mesh,

$$\phi_{1,0}\left(1+\frac{H'}{2}\right) + \phi_{-1,0}\left(1-\frac{H'}{2}\right) + \phi_{0,1}\cdot\frac{1}{S^2} + \phi_{0,-1}\cdot\frac{1}{S^2} - 2\phi_{0,0}\left(1+\frac{1}{S^2}\right) = \frac{\partial b''}{\partial z} \qquad \ldots.A.1.2.$$

is written in the form of a matrix equation.

$\underline{A}\underline{\phi} = \underline{b}$ (see section 4.2 for derivation of the finite difference equation).

If equation A.1.2 is rewritten in the form:-

$$C_2\phi_{1,0} + C_3\phi_{-1,0} + C_4(\phi_{0,1}+\phi_{0,-1}) + C_1\phi_{0,0} = P \qquad \ldots.A.1.3.$$

then the form of the matrix $\underline{A}$ can be shown by considering the points on the first few rows of the mesh. (See Figure A.1).

The size of the matrix will be determined by the size of the mesh; the side dimension of the matrix will be equal to the total number of points in the mesh and the matrix will be square.

The leading diagonal of the matrix contains the coefficient (C1) relating to the nodes of the mesh ($\phi_{0,0}$) and each row of the matrix contains the coefficients relating to the neighbouring nodes to that specified in the same row of the vector $\underline{\phi}$. Since the mesh is numbered row-wise, the coefficients corresponding to $\phi_{1,0}$ and $\phi_{-1,0}$, occur in the adjacent diagonal rows to the leading diagonal, and the coefficients for $\phi_{0,1}$ and $\phi_{0,-1}$ are separated from the leading diagonal by a number of elements equal to the width of the finite

difference mesh. A total of 5 diagonal rows of coefficients completes the matrix; all other locations being zero.

The right hand side vectors of the equation A.1.1have contributions firstly from the pressure gradient (source) terms, and secondly from the boundary condition terms whenever a mesh point adjacent to a boundary is involved. To illustrate the form of the matrix equation, the first few rows of the equation are shown in Figure A.1. for the case of a 16 x 16 mesh with boundary regions as shown in Figure 4.1.1 (c).

In order to incorporate the symmetry condition on the bottom wall, the term C4 ($\phi_{0,1} + \phi_{0,-1}$) in equation A.1.3is replaced by 2 C4 ($\phi_{0,-1}$) for the nodes on the line of symmetry. For the immersed plate case (Figure 4.1.1 (d)), the leading diagonal coefficient is replaced by 1.0 and all other coefficients omitted for all nodes which coincide with the plate; the boundary condition then appears in the right hand side vector.

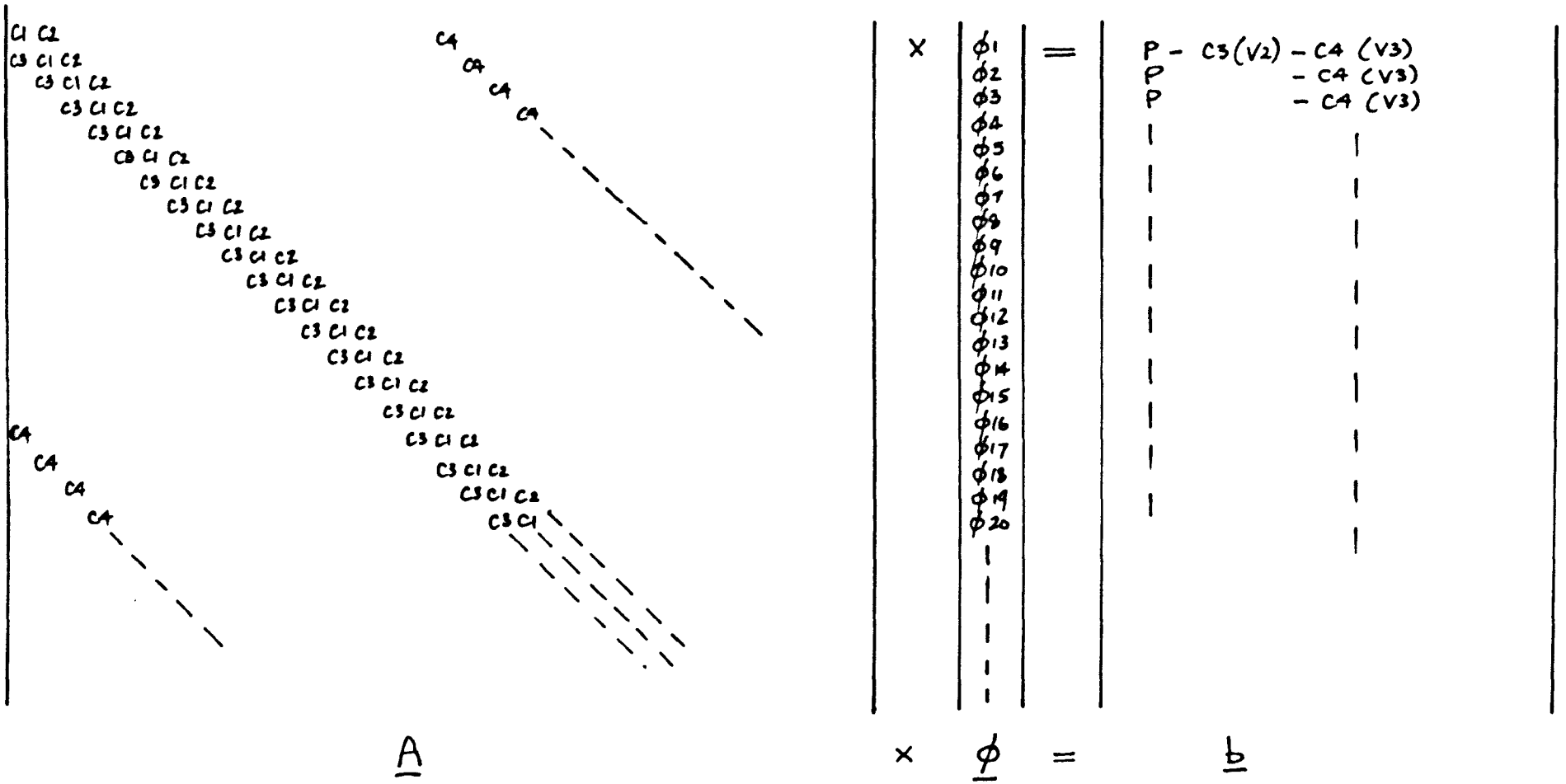

LAYOUT OF FIRST FEW ROWS OF MATRIX EQUATION

FIGURE A.1.

A.2. C.E.G.B. LIBRARY PROGRAM 'BAND'

The Library program BAND is able to solve a band matrix equation with a set of right hand side vectors of the form

$$\underline{A}.\underline{\phi} = \underline{b}_1 , \underline{b}_2 , \underline{b}_3 \ldots\ldots \qquad \ldots\ldots A.2.1.$$

The procedure first reduces the band matrix $\underline{A}$ into the product of an upper triangular matrix (with leading diagonal elements unity) and a lower triangular matrix.

i.e. $$\underline{A} = \underline{L}.\underline{U}_1 \qquad \ldots\ldots A.2.2.$$

However, if: $$\underline{y} = \underline{U}_1.\underline{\phi} \qquad \ldots\ldots A.2.3.$$

then, $$\underline{L}.\underline{y} = \underline{b}_1 , \underline{b}_2 \ldots\ldots \qquad \ldots\ldots A.2.4.$$

Equation A.2.1 is then solved by the successive solution of equation A.2.4 and then equation A.2.3, which is achieved by back-substitution, since the matrices are both triangular (the inversion of $\underline{L}$ and $\underline{U}_1$ is avoided). Thus, for one reduction of the band matrix to triangular form ($\underline{L}.\underline{U}_1$), any number of right hand side vectors may be used to provide different solutions.

In order to feed the program with the matrix of coefficients $\underline{A}$, the coefficients must be rearranged into a vector such that $\underline{A}_{I,J}$ becomes $\underline{B}_{(L-1)(3J-1)+I}$, where $\underline{B}$ isthe vector of the L.H.S. matrix and (2L-1) is the bandwidth of this matrix, i.e. L is the width of the finite difference mesh.

A.3. FORMULATION OF COMPUTER PROGRAM (HART)

The use of the Library program BAND in solving M.H.D. flow problems involves the writing of a main program which will handle input data in the form of boundary conditions, pressure gradient and the other parameters defining the problem - Hartmann Number and shape factor - and which will convert this data into a set of coefficients of the band-matrix $\underline{A}$ and a set of vectors $\underline{b}_i$. Since the size of the matrix is 256 x 256 and the size of the vector is 256, (actually the matrix only contains 256 x 5 non-zero coefficients) there is a considerable data management problem.

The program HART is written with two options which deal with (a) unobstructed rectangular duct flows and (b) rectangular duct flows with inserted plates. The selection between cases (a) and (b) is made by setting the parameter N PLATE equal to 0 or 1 respectively. An additional specification parameter N SOLN is used to denote the number of R.H.S. vectors $\underline{b}_i$ to be used with any one matrix formulation, (i.e. the number of sets of boundary conditions and pressure gradient definitions for one definition of Hartmann Number and shape factor).

Two main subroutines are included in each option of the program to formulate the vector of the matrix (MAT 1 and MAT 2) and to formulate the R.H.S. vectors (VECT 1 and VECT 2). Tables II and III summarise the input data to these two routines, and the flow diagram for the main program is shown in Figure A.2., also the flow diagrams for MAT 1 and VECT 1 are shown in Figure A.3. (MAT 2 and VECT 2 follow the same pattern, although the ordering of the coefficients and vector components differs).

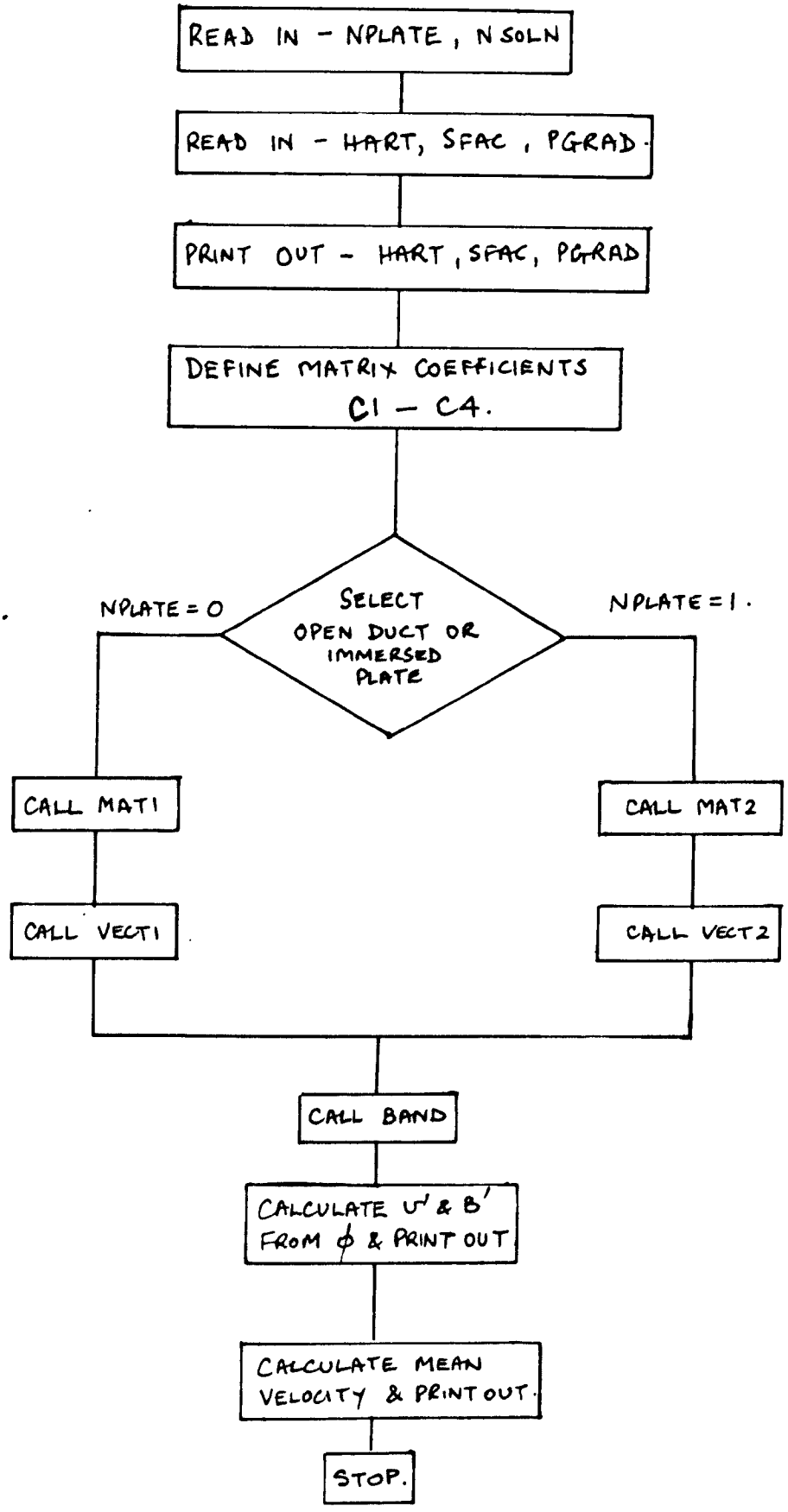

FLOW DIAGRAM FOR PROGRAM 'HART.'

FIGURE A.2.

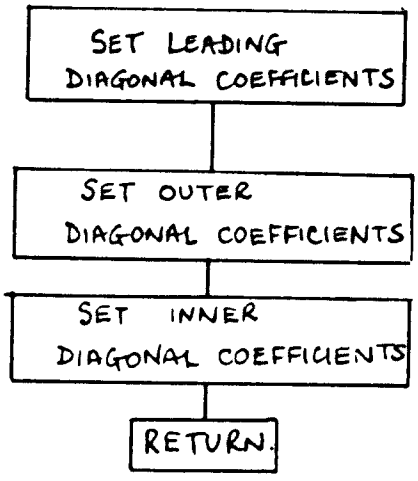

SUBROUTINES MAT 1 & MAT 2.

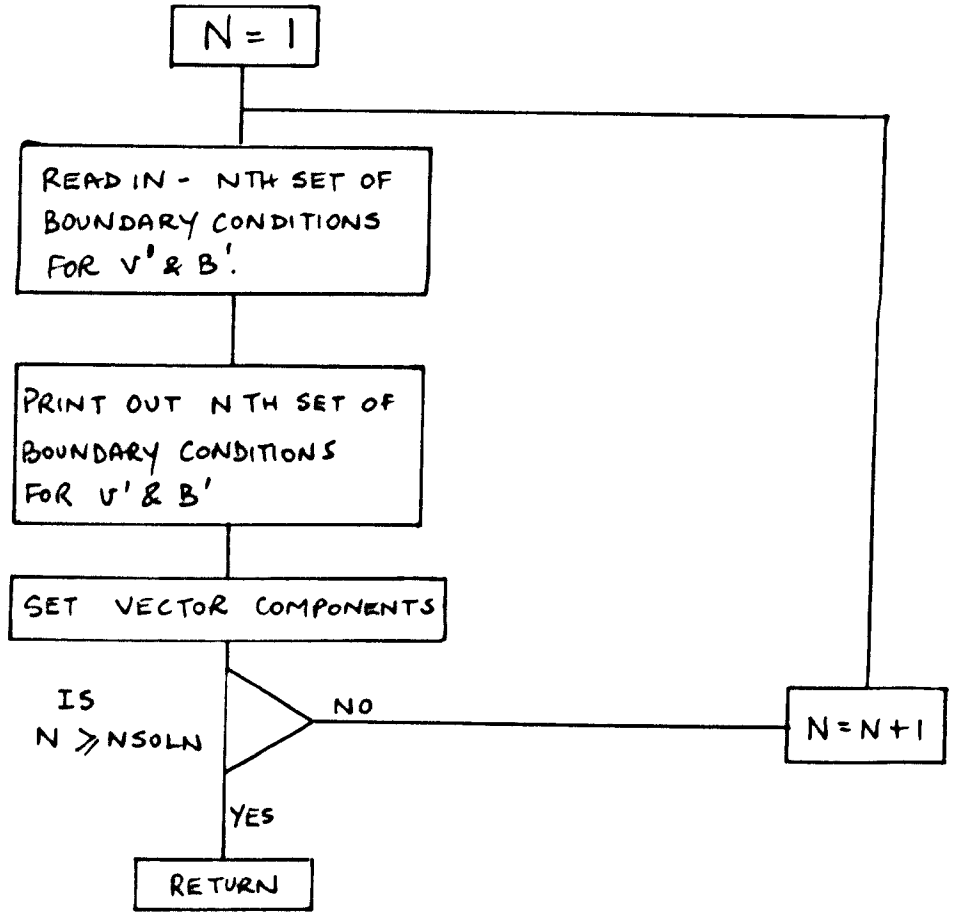

SUBROUTINES VECT1 & VECT2.

FLOW DIAGRAM FOR SUBROUTINES 'MAT1', 'MAT2', 'VECT1', 'VECT2'

FIGURE A.3.

INPUT TO MAT 1 AND VECT 1 FOR 16 x 16 MESH

MAT 1 COEFFICIENTS

J	I = J-16	I = J-1	I = J	I = J+1	I = J+16
1)	0	0	C1	C2	C4
2-15)	0	C3	C1	C2	C4
16)	0	C3	C1	0	C4
17)	C4	C3	C1	C2	C4
18-31)	C4	C3	C1	0	C4
32)	C4	0	C1	C2	C4
Repeat to 225) 226-239) 240)		- ditto -			
241)	2.C4	0	C1	C2	0
242-255)	2.C4	C3	C1	C2	0
256)	2.C4	C3	C1	0	0

VECT 1 COMPONENTS

(Values of Coefficients of PGRAD and Boundary Conditions)

J1,J2	PGRAD	FIB(1)	FIB(2)	FIB(3)	FIB(4)	FIB(5)	FIB(6)	FIB(7)
1,1)	1	0	-C3	-C4	0	0	0	0
2,1 - 15,1)	1	0	0	-C4	0	0	0	0
16,1) (top)	1	0	0	-C4	-C2	0	0	0
1,2 - 1,7)	1	0	-C3	0	0	0	0	0
1,8 - 1,16) (LHS)	1	-C3	0	0	0	0	0	0
16,2 - 16,7)	1	0	0	0	-C2	0	0	0
16,8 - 16,16) (RHS)	1	0	0	0	0	-C2	0	0
All other values	1	0	0	0	0	0	0	0

J = Row number of Matrix
I = Column number of Matrix
(J1,J2) = Coordinates of mesh point
FIB(n) = Value of $\upsilon' + \beta'$ on region (n) of boundary.

TABLE II

INPUT TO MAT 2 AND VECT 2 FOR 16 x 16 MESH

MAT 2 COEFFICIENTS

J	I = J-16	I= J-1	I = J	I = J+1	I = J+16
1)	0	0	C1	C2	C4
2 - 15)	0	C3	C1	C2	C4
16)	0	C3	C1	0	C4
17)	C4	0	C1	C2	C4
18 - 31)	C4	C3	C1	C2	C4
32)	C4	C3	C1	0	C4
Repeat to 97)					
98 - 111)		- ditto -			
112)					
113)	C4	0	C1	C2	C4
114 - 119)	C4	C3	C1	C2	C4
120,121)	0	0	1	0	0
122-127)	C4	C3	C1	C2	C4
128)	C4	C3	C1	0	C4
Repeat to 225)					
226 - 231)		- ditto -			
232,233)					
234 - 239)					
240)					
241	2.C4	0	C1	C2	0
242 - 247	2.C4	C3	C1	C2	0
248,249	0	0	1	0	0
250 - 255	2.C4	C3	C1	C2	0
256	2.C4	C3	C1	0	0

VECT 2 COMPONENTS

(Values of Coefficients of PGRAD and Boundary Conditions)

J1,J2	PGRAD	FIB(1)	FIB(2)	FIB(3)	FIB(4)	FIB(5)	FIB(6)	FIB(7)
1,1	1	0	-C3	-C4	0	0	0	0
2,1 - 15,1	1	0	0	-C4	0	0	0	0
16,1 (top)	1	0	0	-C4	-C2	0	0	0
1,2 - 1,7	1	0	-C3	0	0	0	0	0
1,8 - 1,16 (LHS)	1	-C3	0	0	0	0	0	0
16,2 - 16,7	1	0	0	0	-C2	0	0	0
16,8 - 16,16 (RHS)	1	0	0	0	0	-C2	0	0
8,8 - 8,16	0	0	0	0	0	0	0	1
9,8 - 9,16 (PLATE)	0	0	0	0	0	0	1	0
All other values	1	0	0	0	0	0	0	0

TABLE III

(See Table II for nomenclature)

A.4. OPERATION OF THE PROGRAM

A.4.1 Data Input

The data deck is made up of the following cards

(1) N PLATE (0 or 1)

(2) N SOLN (Less than 5)

(3) HART, SFAC, PGRAD (Hartmann Number and pressure gradient based on half duct width).

(4) Boundary Conditions for v' and B' on all 7 regions.

(4) contains N(=N SOLN) sets of boundary conditions to provide N separate solutions.

The card format is as follows:-

(1) and (2); Integer 0 or 1 punched within 1st five locations.

(3) Each variable punched within a field of ten locations each - in order from L.H.S. of card.

(4) One card for v', followed by one card for B'.
Each boundary condition punched within a field of ten locations - in order from L.H.S. of card.

((3) and (4) both used fixed-point arithmetic).

A.4.2. Output

The printed output gives the parameters and boundary conditions defining the solution, together with a tabulation of values of v' and B' at every point on the finite difference mesh. Finally, the mean velocity is printed.

A.4.3. Operation

The program deck is committed to magnetic disk to reduce the compilation time, and then the time taken to produce each set of solutions (based on each set of parameters HART and SFAC) is approximately 0.25 min with one or two sets of boundary conditions. The program is available in modified form to produce a bottom wall condition.

APPENDIX B

CALIBRATION OF SEED PUMP

The construction of the seed pump was described in section 6.1 (see Figure 6.1.6) and here the calibration of the pump, in terms of mass flowrate of seed, is described.

It was found to be most convenient to vary the flowrate of seed by adjusting the carrier air flowrate, while the screw feeder speed and fluidising air flow were both kept constant.

The effect of increasing the carrier air flow is to increase the back-pressure on the screw feeder. The mass flowrate through the feeder is a function of its speed and the pressure difference across it. So if the inlet pressure is held constant, by maintaining the fluidising air flowrate and the height of the column both constant, then a unique calibration should be possible of the form

mass flowrate = f(carrier air flowrate)

This calibration was attempted, initially with some difficulty, since the physical condition of the seed powder seemed to vary from one run to the next. Improvements were made by introducing bags of drying crystals (silica gel) to the inlet air line and to the fluidising column itself and drying the potassium sulphate seed material before loading it into the column. This improved the repeatability, and when aerosil powder (finely divided silica sub-micron) was added to the powder as 1% by weight, (suggested by Cranfield (1966)) the flow properties of the powder were greatly improved and a satisfactory calibration was obtained.

The seed flow was measured by collecting the delivered seed in porous glass-fibre bags which allowed the air to pass with negligible carry-over of seed. The carrier air was measured by a rotameter, and the resulting calibration curve is shown in Figure A.4. As the carrier air flow was

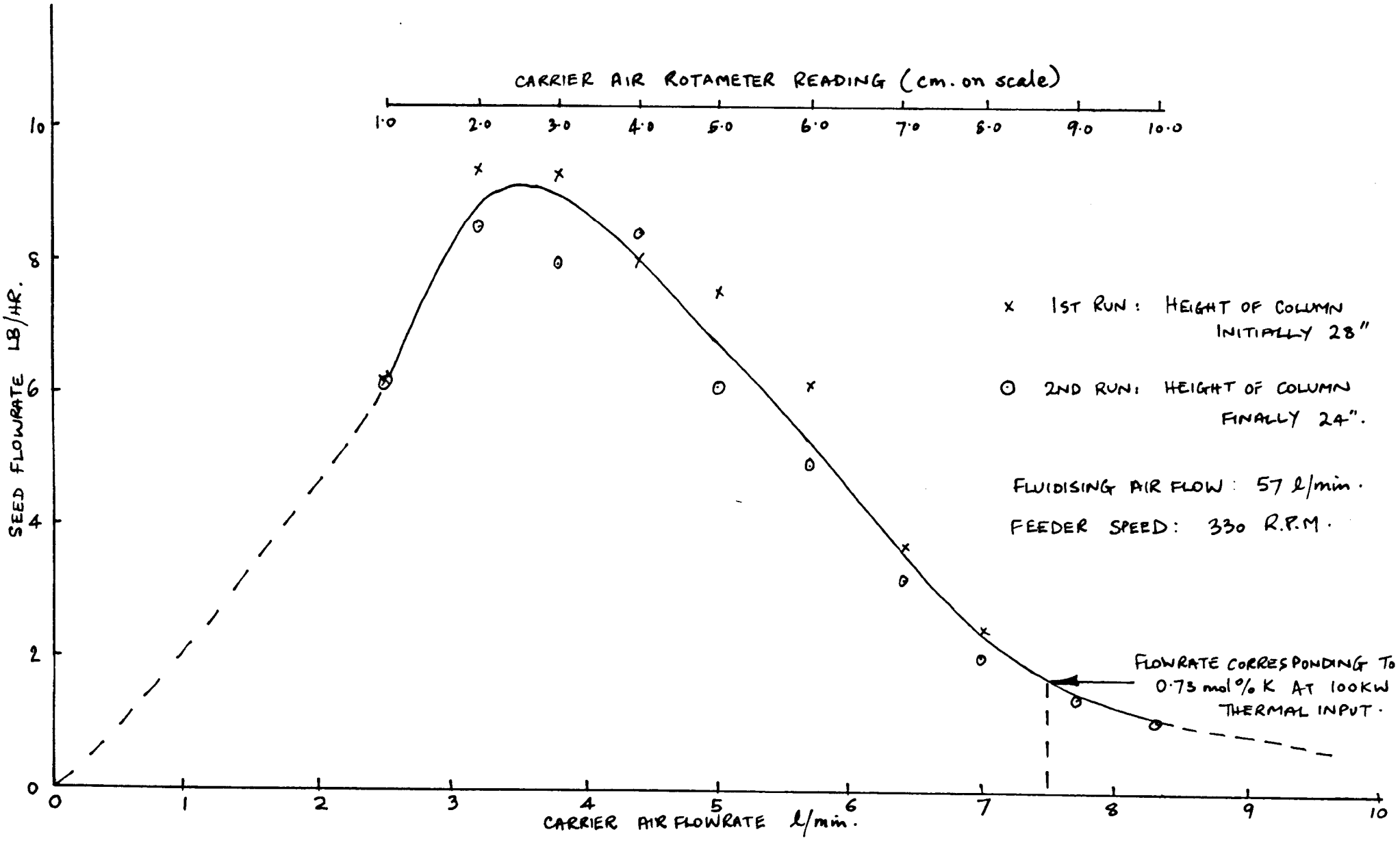

SEED - FEEDER CALIBRATION. FIGURE A4.

increased a little from zero, a very low flowrate, which was highly unstable, was produced. In this condition, the air flowrate was not sufficiently high ~~enough~~ to maintain the seed in suspension in the delivery line (bore = 8 mm) and much of the seed rotating in the screw feeder was not passed into the delivery line. As the air flowrate was increased up to about 3 l/min, the maximum flowrate of seed occurred. Here, the seed was just carried in suspension by the carrier air (air velocity = 1 m/sec) and there was the maximum differential pressure across the feeder. When the air flowrate was further increased, the seed flowrate was gradually reduced, as the back pressure on the screw feeder increased.

The operating range of the pump was actually in this region of well-behaved flow, and a carrier air flowrate of 7.5 l/min gave a seed flowrate corresponding to 0.73 mol % K for 700 s.c.f./hr of oxygen input or 100 KW thermal input.

Two calibration runs were completed consecutively, with the height of the column starting at 28" and finishing at 24". Within this range, there was no appreciable change in calibration within the accuracy of the measurements.

Some fluctuation in seed flowrate was experienced because of the intermittent nature of the delivery from the screw feeder compartments. This was partially eliminated by the provision of a vertical limb in the delivery line in which the bore changed three times between 4mm and 6 mm. The acceleration effect caused by these changes in cross-section, together with the stabilising effect of upwards vertical flow reduced the fluctuations considerably and the mixing experienced in the combustion chamber also reduced the effect.

APPENDIX C

SODIUM D-LINE TEMPERATURE MEASUREMENT

C.1 INTRODUCTION

The method of gas temperature measurement used on the rig was the line-reversal method using Sodium D-line emission. This technique has become the generally accepted standard of gas temperature measurement over the range 1000°K to 4000°K where its accuracy is claimed to be about 1%. In M.H.D. experiments on hot gas flows, this technique has almost invariably been used.

C.2 GENERAL PRINCIPLES

The principle of line reversal techniques have been described by many authors (e.g. Gaydon and Wolfhard (1960)) but a summary of the general principles may usefully be given here. If a source of light emits a continuous spectrum of radiation at a brightness temperature T_B, then at a wavelength λ, the radiant energy emitted by the source will be $f(\lambda, T_B)$, where f is the black body radiation function. $\left[f(\lambda,T_B) = \frac{2\pi h c^2/\lambda^5}{exp\left[hc/kT_B - 1 \right]} \right]$

If λ is an emission frequency of the sodium atoms which are present in the gas whose temperature is to be measured (one of the D-lines for instance) and α_λ is the absorptivity of these atoms at the same frequency λ, then the amount of radiant energy transmitted through the gas will be

$$f(\lambda, T_B).(1 - \alpha_\lambda)$$

If the emissivity of the gas is ε_λ at the same wavelength, the flame will emit radiant energy equal to $\varepsilon_\lambda . f(\lambda, T_F)$, where T_F is the flame temperature, so that the total energy viewed by the observer will be $f(\lambda,T_B)(1-\alpha_\lambda) + \varepsilon_\lambda f(\lambda,T_F)$.

If Kirchhoff's Law is applied for the gas (at equilibrium)

$$\varepsilon_\lambda = \alpha_\lambda$$

and therefore the Radiant energy viewed by an observer

$$= f(\lambda,T_B) + \varepsilon_\lambda \left[f(\lambda,T_F) - f(\lambda,T_B) \right]$$

At a wavelength differing very slightly from the D-line frequency, the absorptivity and emissivity of the sodium atoms will be negligible and thus the radiant energy observed will be purely that from the light source $= f(\lambda+\Delta\lambda, T_B)$.

If the observer can view the continuous spectrum in the region of the sodium D-lines, then a continuous variation of wavelength, with no abrupt change in intensity, will be observed only if $T_F = T_B$. If $T_F > T_B$, then the lines will appear bright against the background of the continuous emission, i.e. flame radiation will augment the background radiation at these wavelengths. If $T_B > T_F$, then dark lines will be seen against the continuous variation of the background source.

It should be noted that the measurement is independent of gas emissivity and also that at the reversal point, i.e. when the D-lines are indistinguishable from the continuous spectrum, the brightness temperature of the source (i.e. the actual temperature of a black body which would produce an equivalent intensity of radiation) is equal to the actual temperature of the gas, assuming thermal equilibrium between the emitting sodium atoms and the gas molecules. This makes the measurement of gas temperature relatively straightforward since the brightness temperature of the source can be measured readily with a standard optical pyrometer (disappearing filament type).

C.3 APPLICATION TO IONISED GAS TEMPERATURE MEASUREMENT

In partially ionised gases, there is a possibility that the sodium atoms, which are used to produce the D-line emission, receive their excitation not from collisions with gas molecules but with electrons, which will have a temperature different from that of the gas in general. (T_e, the electron temperature). However, Grieg (1964) has shown that for gases with a partial

pressure of Nitrogen of 0.5 atmospheres (or more) or for mixtures of gases containing gases with an equivalent collision cross-section to 0.5 atmos. of Nitrogen, the molecular collisions dominate over the electron collisions even when the electron concentration is enhanced by the usual seeding methods, and so the radiation emitted by the sodium atoms during de-excitation will correspond to the temperature of the gas molecules. For gases with much lower molecular collision cross-sections, it may be possible to measure electron temperature in the gas.

Thomas (1967) has studied the corrections which must be applied to reversal temperatures measured under the conditions of the Marchwood 25 MW duct, to account for self-absorption effects in the cool boundary layers adjacent to the port holes. Since the experiments described in Chapter 7 involve a hot-walled duct, the effects should be much less important (wall temperatures in the region of the port holes will be 2000°C, (for the combustion chamber window) compared with 200°C in the 25 MW Duct) and in fact corrections for this effect are ignored here. The effect of particulate matter in the gas stream should have negligible effect in this case since when a gaseous fuel is being considered, the seed particles will all be fully vaporised by the time they reach the measuring station.

C.4. CORRECTIONS FOR WAVELENGTH AND FOR REFLECTIVE LOSSES

Two important corrections must be made to the actual measurements made by the optical pyrometer before the actual gas temperature can be found. Firstly, the brightness temperature of the light source (a tungsten strip lamp is usually used for this purpose) is measured at the red frequency of of the filter in the optical pyrometer (6550Å) and the emission and absorption

of the sodium atoms in the flame occurs at the D-line frequencies (5890Å and 5896Å), so that a correction must be made for the variation of the emissivity of the tungsten strip between these two temperatures. Secondly, a correction must be made for the fact that the flame is viewed through just one lens, whereas the background source is viewed through two lenses. (If the flame is enclosed by a chamber with windows on either side, then the flame will be viewed through one lens and one window and the background source through two lenses and two windows). Thus there will be a differential loss of radiant energy between the optical paths from the filament and from the flame itself, and a correction must be made for the increased filament brightness temperature needed to produce a reversal under these conditions.

These two corrections are displayed in Figures A.5 and A.6. The data for Figure A.5 was taken from Gaydon and Wolfhard, and that for the reflective loss correction in Figure A.6,was determined experimentally. The limit of accuracy of the pyrometer was $\pm$ 6°C (manufacturer's claim), but allowing for other errors, such as variations in mains voltage during measurement, an accuracy of $\pm$ 10°C could reasonably be claimed for these measurements. This accuracy is displayed on the graph, and a straight line relationship which falls within the accuracy limits is superimposed for the purpose of the calibration. A combined correction curve is plotted in Figure A.7. This is to be subtracted from the measured values of brightness temperature - (The negative correction necessary for reflective losses is greater than the positive correction for wavelength change).

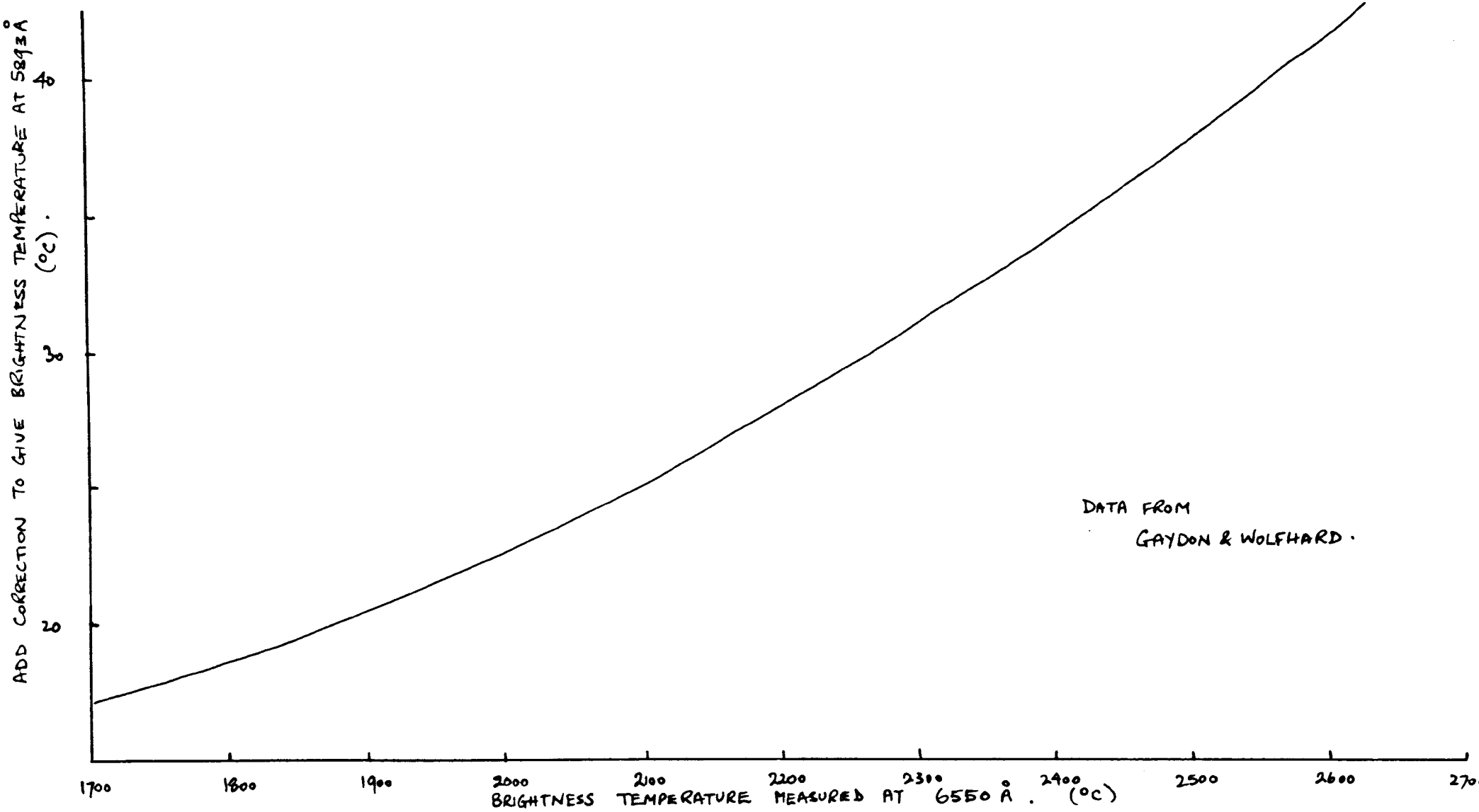

WAVELENGTH CORRECTION FOR SODIUM D-LINE APPARATUS

FIGURE A5.

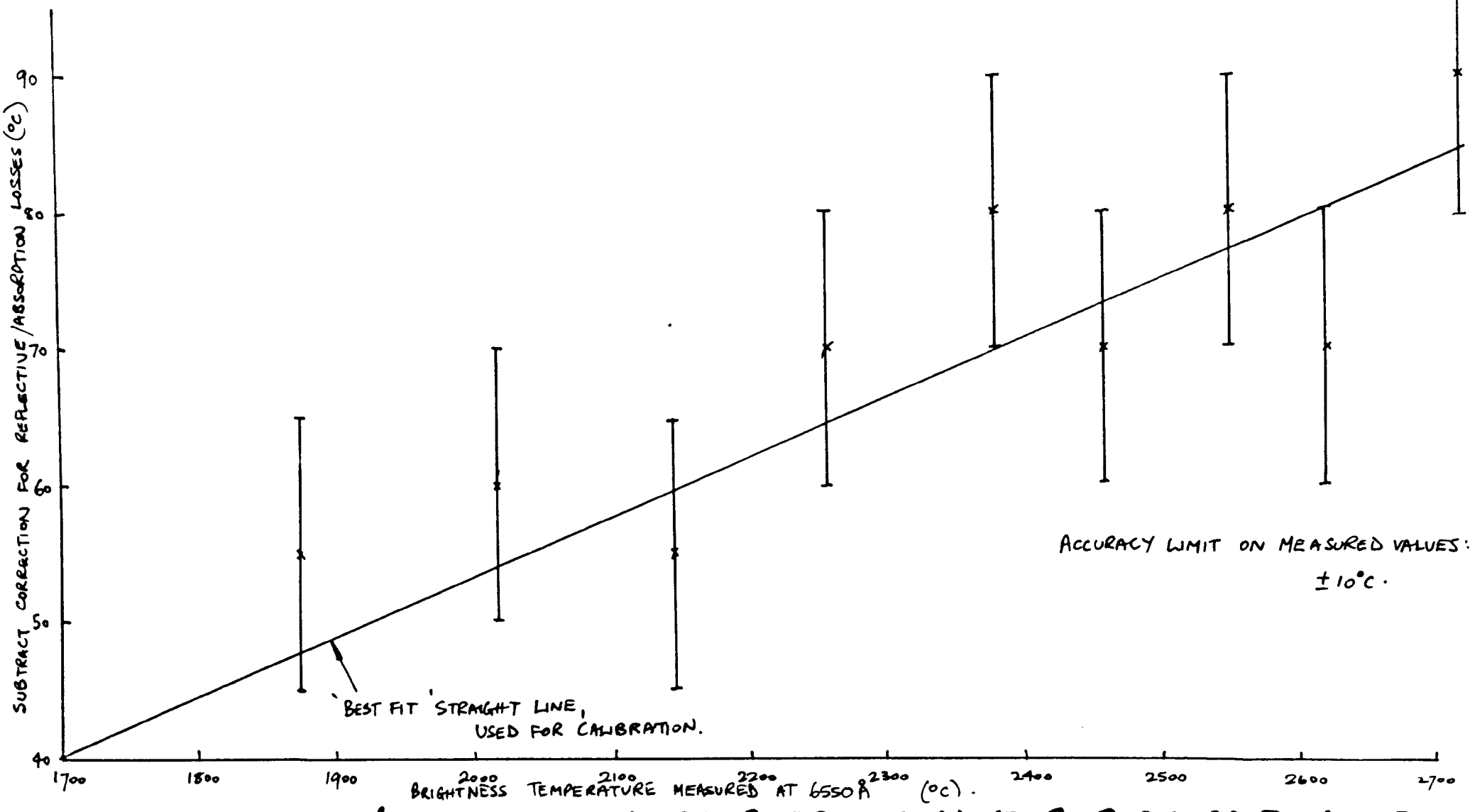

REFLECTIVE/ABSORPTION LOSS CORRECTION FOR SODIUM D-LINE APPARATUS. FIGURE A6.

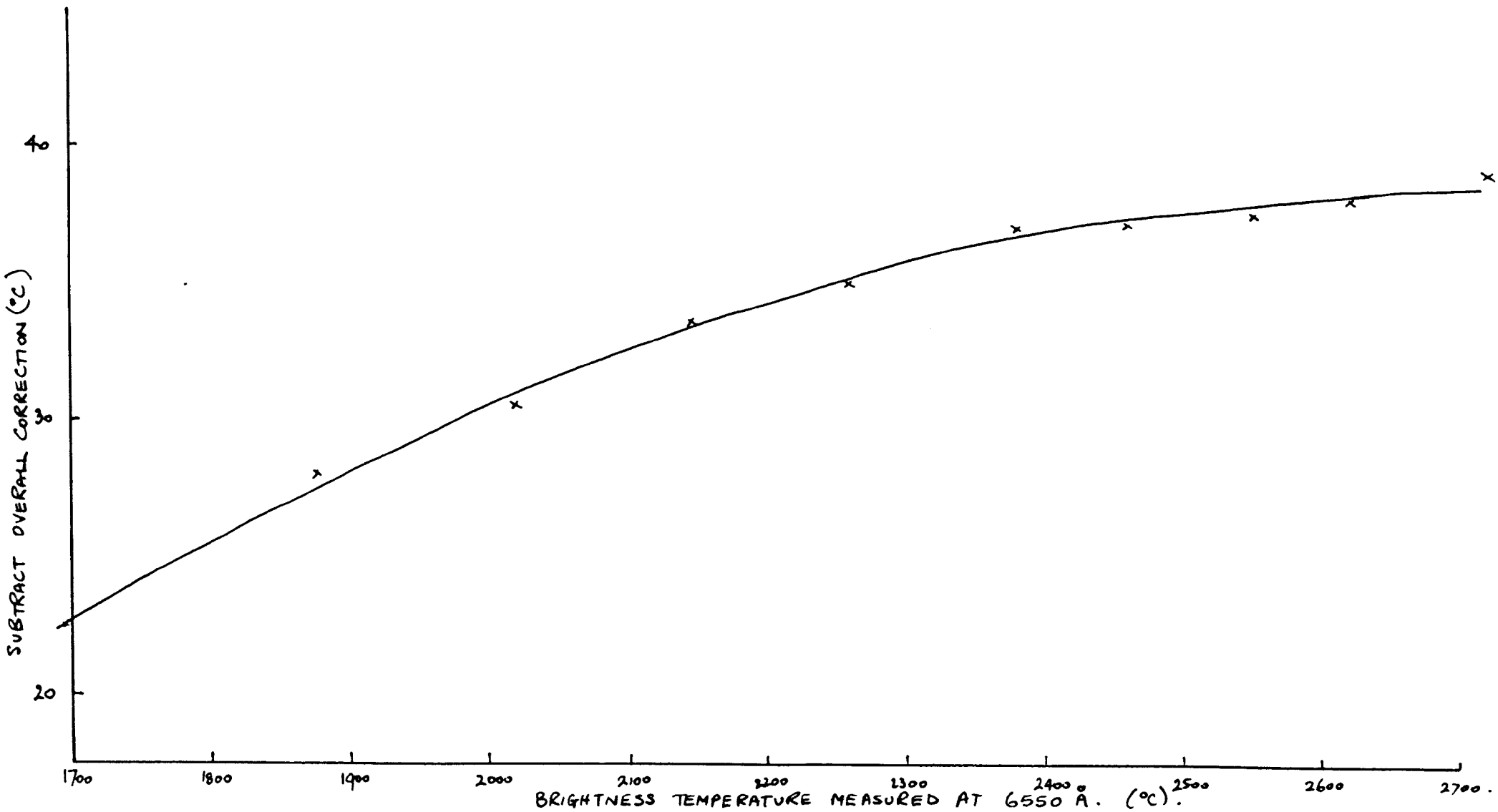

OVERALL CORRECTION FOR BRIGHTNESS TEMPERATURE — SODIUM D-LINE APPARATUS.

FIGURE A.7.

C.5. EXPERIMENTAL ARRANGEMENT (See Figure A.8)

The optical arrangement was assembled on two 1-metre optical benches on either side of the combustion chamber and the gases leaving the chamber were viewed through 1" port holes through the refractory lining. The port holes were covered at each side with silica windows which were continuously purged with a small flow of air to keep them free from condensation and seed. The layout of the lenses was the familiar equal magnification system where object to lens and lens to image distances are all 2f (f = focal length of lenses ≈ 20 cm, + 5 dioptres). An iris diaphragm was inserted into the optical path so that any stray radiation would not be incident on the monochromator i.e. all the incident radiation came from the background source, with interference along the optical path by the flame. A standard Mazda projector lamp with a vertical tungsten strip filament was used for the background source, and the actual brightness temperature of the filament was not in fact measured. Only the effective brightness temperature as measured by the optical pyrometer through the glass of the bulb was measured, but since this temperature was the effective temperature which was seen by the flame also, (when the known corrections for reflective losses at the lens and window had been applied) the actual brightness temperature of the filament was immaterial.

The optical pyrometer used was a Leeds and Northrup self-balancing pyrometer which was equipped with a special close-up objective lens assembly and the monochromator was the Hilger and Watts Model D292, which was modified slightly to enable both D-lines and the adjacent bands of the spectrum to be viewed at the same time - this greatly improved the ease with which the reversal point could be detected.

The benches were aligned carefully with the axis of the port holes and then a check was made to ensure that no extraneous losses were incurred in the transmission of the background source through the chamber. A brightness

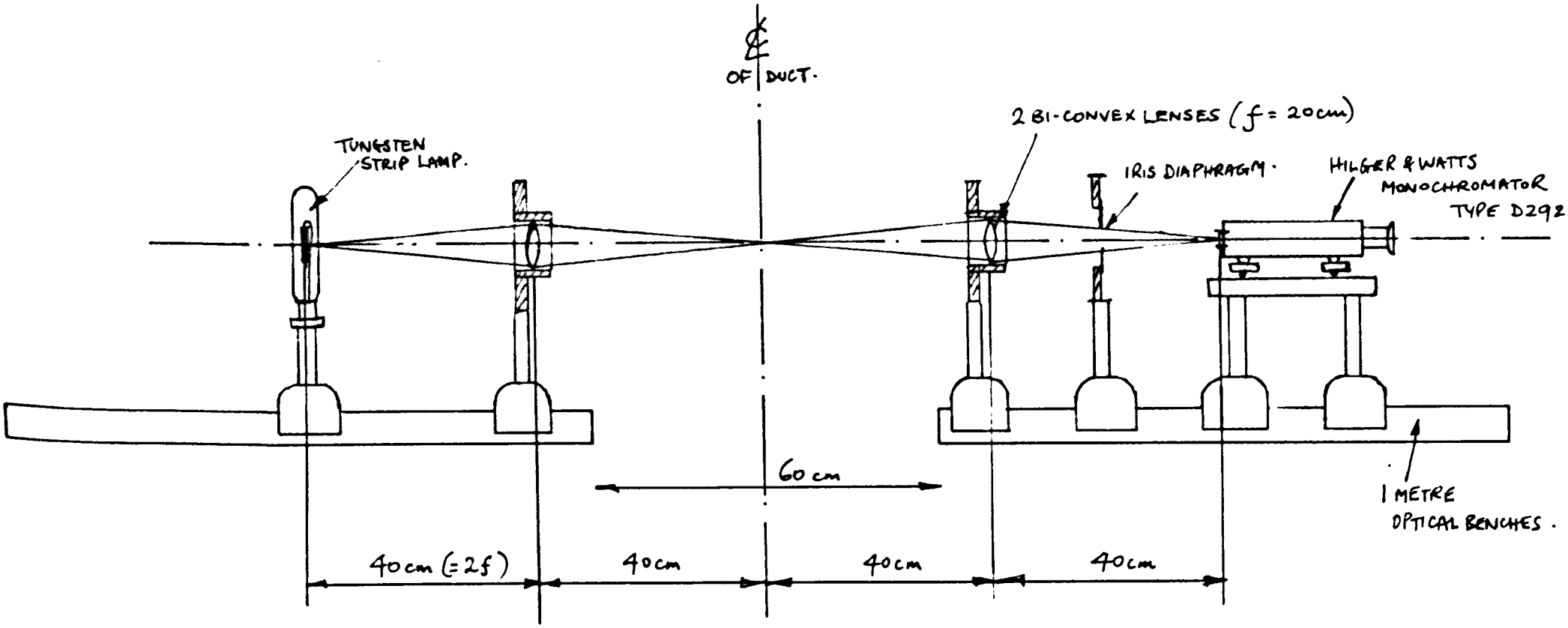

LAYOUT OF SODIUM D-LINE APPARATUS. - FIGURE A8.

temperature of 1920°C, measured adjacent to the tungsten strip lamp, produced an effective brightness temperature at the site of the monochromator slit of 1800°C, i.e. a loss of 120°C; this compared with a loss of 100°C predicted from the correction curve (X2 since 2 lenses and 2 windows are involved). To within the accuracy of $\pm$ 10°C, this confirmed that the alignment was satisfactory, although a regular check had to be made to ensure that all lenses and windows and the glass of the projector lamps were kept clean, so that the correction curves could be applied with certainty.

APPENDIX D

MAGNET CALIBRATION

The magnet was calibrated using both a conventional Cambridge Fluxmeter and also a Hall Probe. Figure A.9 shows the transverse magnetic field strength (B_{x_o}) measured at the centre of the magnet gap, using both instruments. The range of current was limited to 400 - 500A, since the D.C. generator of the motor-generator set which was used to drive the magnet was not self-exciting below 400A (and 500A was the maximum rating of the magnet and the M-G set). Good agreement between the two instruments was found and no saturation of the core was noticeable up to 500A.

Figures A.10 and A11 show the magnetic field distribution measurements which were obtained using the Hall Probe with the current at 500A. The magnetic field was assumed to be symmetrical about the $z = 0$ and $x = 0$ planes, since the coils and core both have symmetry about these planes. However, there was asymmetry of the core about the y = 0 plane and this was reflected in the symmetry in the magnetic field measured by the probe. The contours in the z-y plane were measured at $x = 0$ (centre line) and $x = 1$ (edge of gas duct) and thus cover the range of B_{x_o} over the whole of the 12" test section of the 6" x 2" duct.

Apart from the 1" border region around the pole pieces, there is a very satisfactory uniformity of magnetic field strength. Thus all the probing for velocity perturbations was carried out in the middle 10" length of the pole pieces, and in any case the top and bottom regions of the duct (within 1" of the top and bottom walls) are relatively cold and the M.H.D. interaction is greatly reduced by the consequent fall in electrical conductivity.

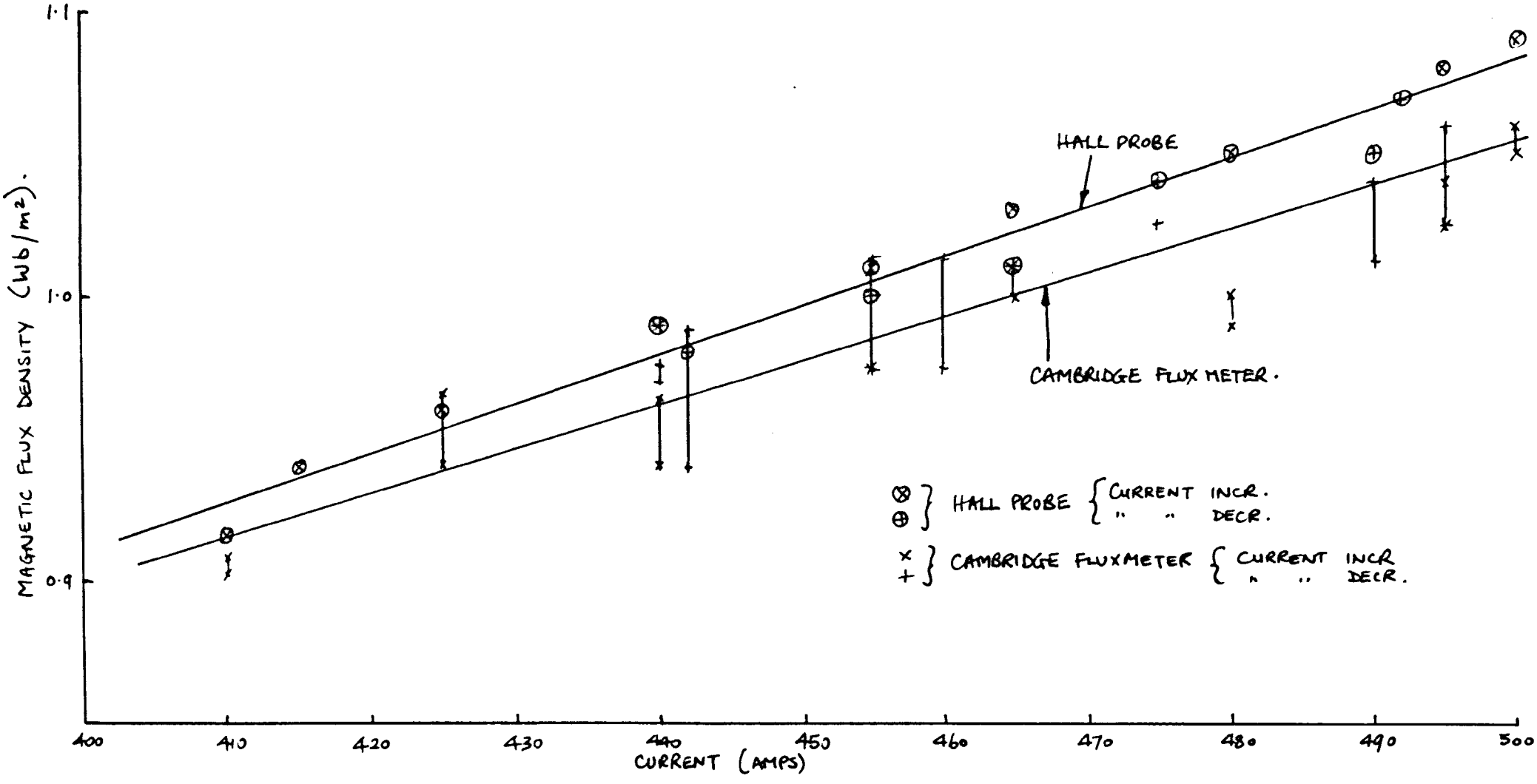

MAGNET CALIBRATION. FIGURE A.9.

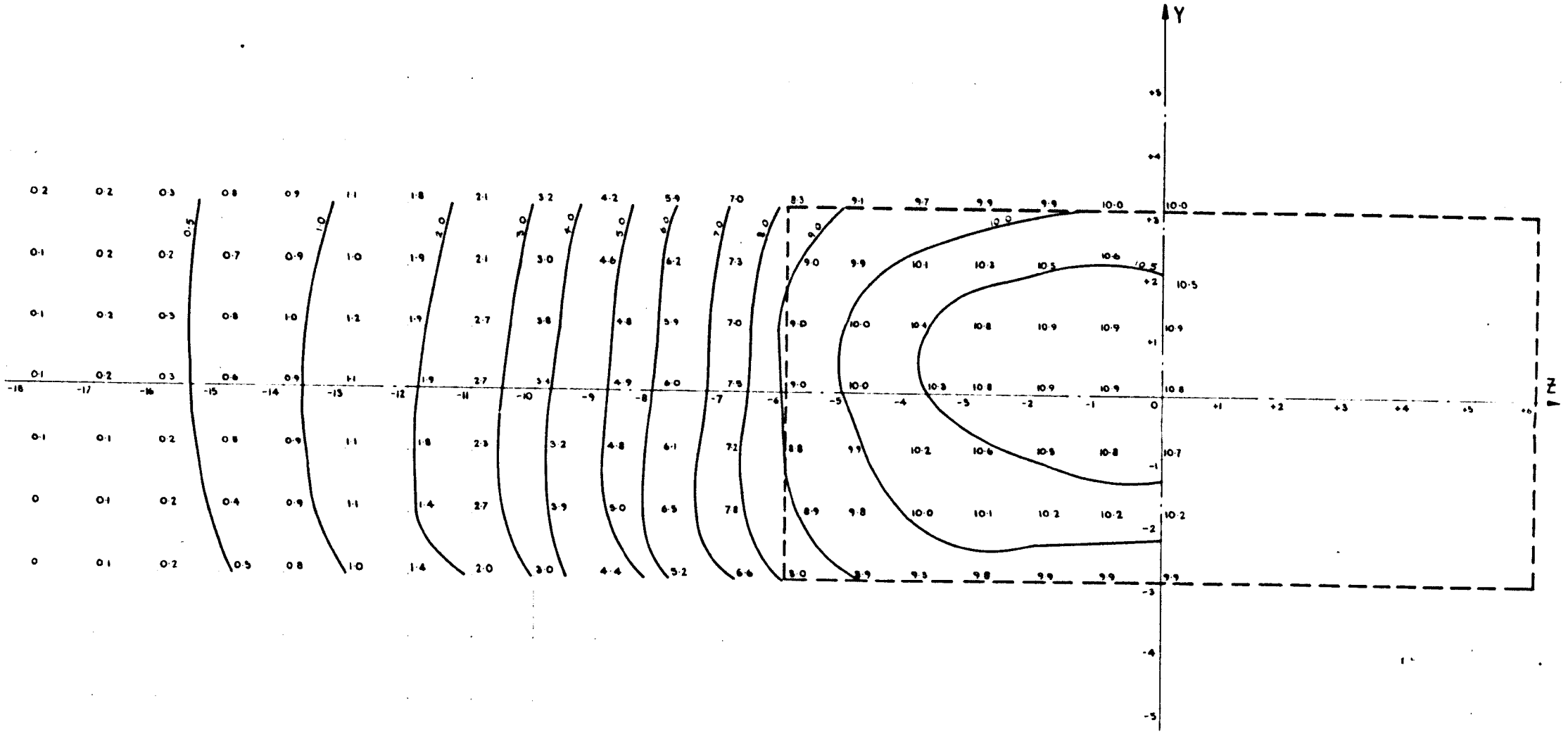

MAGNET CURRENT – 500A

LINES OF CONSTANT MAGNETIC FLUX DENSITY (B_{XO}, KILOGAUSS)

MAGNETIC FIELD DISTRIBUTION

FIG. A 10

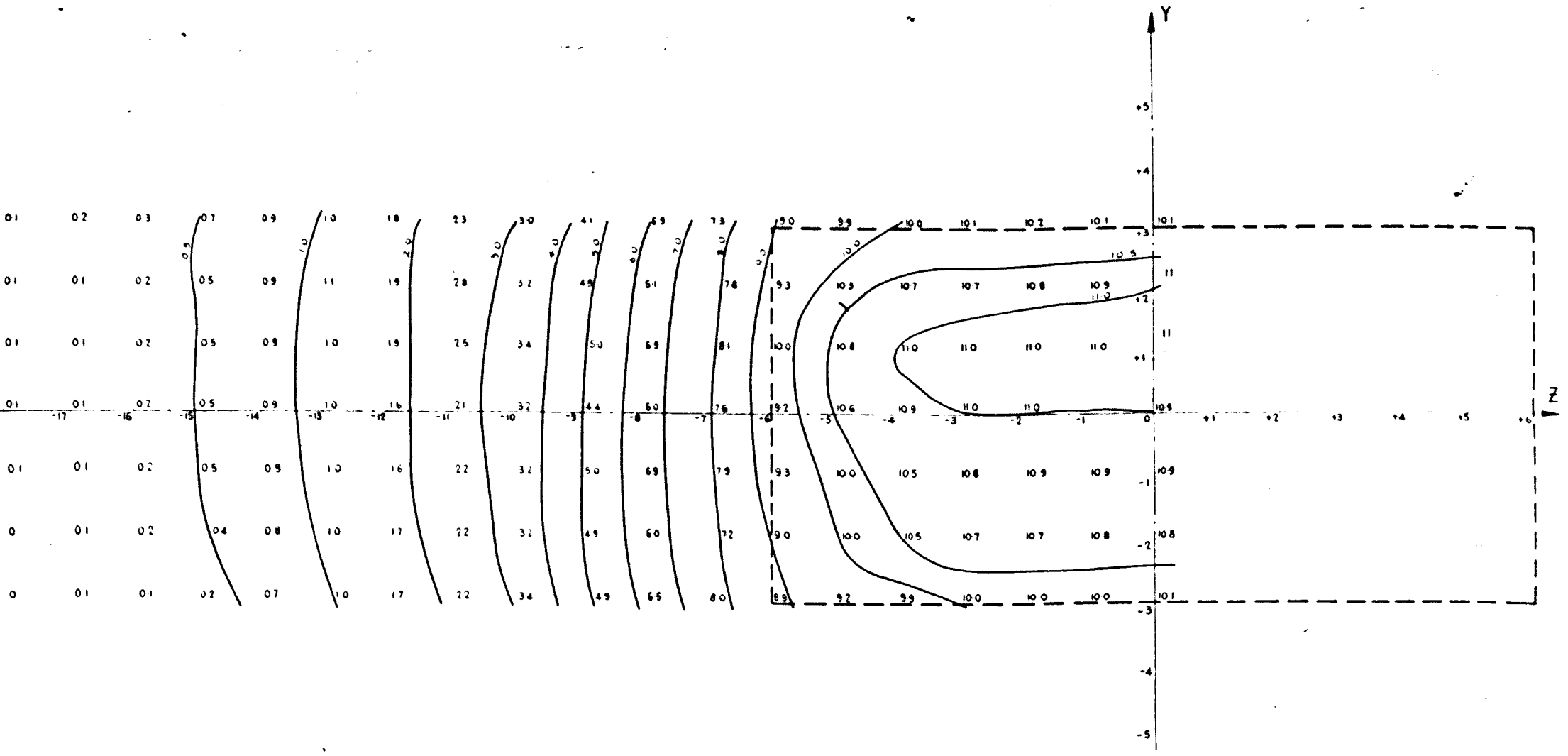

MAGNET CURRENT = 500A $X_{\text{零}} = +1$

LINES OF CONSTANT MAGNETIC FLUX DENSITY (B_{X0}, KILOGAUSS)

MAGNETIC FIELD DISTRIBUTION

FIG. A 11

APPENDIX E

CALIBRATION OF R.F. CONDUCTIVITY PROBE

Solutions of KCl between N/100 and N were found to give a suitable range of conductivity (data of conductivity of standard solutions is well documented) for calibration (0.1 - 10 mho/m). The datum level of dissipation was measured using a 1ℓ beaker containing 800 ml of de-mineralised water. The coil was covered with a thin glass sheath and immersed into the liquid so that it was covered by 1" of liquid. The KCl solutions were then used in turn to measure the variations in dissipation from the coil. The results of three separate attempts at these measurements are shown in Figure A.12.

The absence of any electrolyte from the inside of the coil and from the region outside the coil which was occupied by the sheath was fairly representative of the conditions in the hot gas flow, when the thermal boundary layer around the water cooled coil produced a very similar effect.

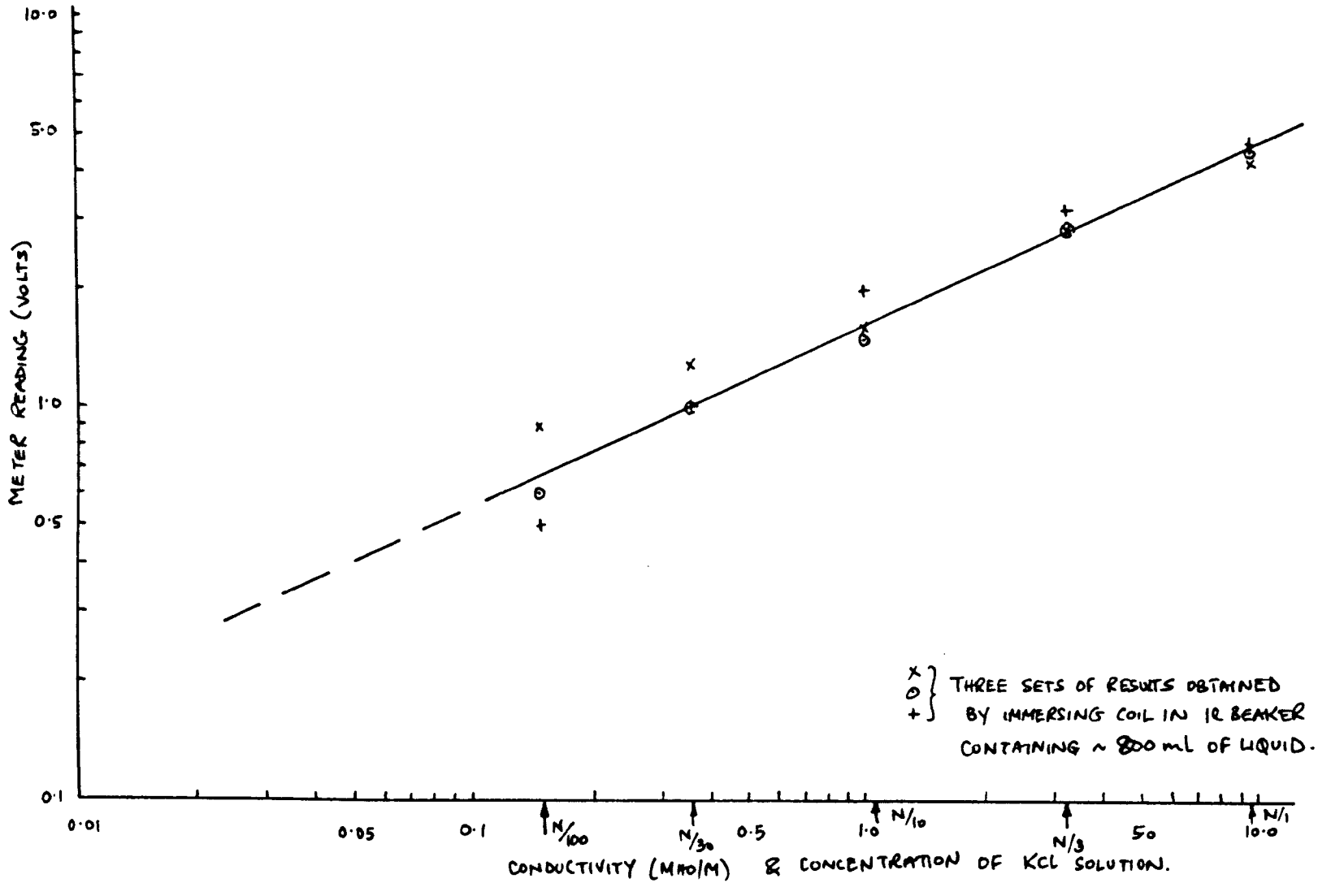

CALIBRATION OF R.F. CONDUCTIVITY PROBE . FIGURE A.12.